NEW DESIGNS AND DETECTION STRATEGIES FOR GLOW DISCHARGE AS AN ALTERNATIVE SPECTROCHEMICAL SOURCE

Michael R. Webb

Submitted to the faculty of the University Graduate School
in partial fulfillment of the requirements
for the degree
Doctor of Philosophy
in the Department of Chemistry,
Indiana University
July 2007

Accepted by the Graduate Faculty, Indiana University, in partial fulfillment of the requirements for the degree of Doctor of Philosophy.

Doctoral Committee

_____

Gary M. Hieftje, Ph.D.

_____

Stephen C. Jacobson, Ph.D.

_____

Milos V. Novotny, Ph.D.

_____

Dennis G. Peters, Ph.D.

June 12, 2007

"*In nostris furnibus legimus, non esse in natura certius sciendi genus, ad cognoscendum per causas radicales, ac constituvas rerum; quam dum scitur quid, quantumque in re quaque, sit contentum.*"

"In our furnaces we read that there is no more certain genus of acquiring knowledge for the understanding of things through their root and constitutive causes, than when one knows what is contained in a thing, and how much of it there is."

- Joan Baptista van Helmont, 16^{th} – 17^{th} century Flemish chemist and "philosopher by fire", in *Opuscula Medica Inaudita*.

(Translation from *Alchemy Tried in the Fire*, W.R. Newman & L.M. Principe)

Acknowledgements

Of course, a Ph.D. is not a solitary effort; It takes the work of many people.

Most directly, I must thank all the people involved in this last stage: Gary Hieftje, for giving me the opportunity, freedom, and guidance to pursue this research; my co-workers in the Hieftje lab,[†] for camaraderie, collaboration, and commiseration - particularly George Chan, for insightful discussions, and James Barnes, for getting me started; Susan Hieftje and Lee Ann Mobley, for all that they do to keep the lab running smoothly; Anna Kertser, whose overconfidence aided me through many frustrations; members of my committee and all the chemistry department faculty at IU, for their various contributions to my education; and the department staff, particularly those in Electronic and Mechanical Instruments Services.

No less credit belongs to many who helped me on my path to graduate school. In particular, my parents, Steve Webb and Dottie Halligan, deserve my thanks for providing all the opportunities I needed, along with the encouragement, advice, and examples to bring those opportunities to fruition. Among the opportunities they provided were education at McQuaid Jesuit High School and Union College; I owe a great debt to my teachers at both. In particular, I must express my gratitude to the Union chemistry and

---

[†] Including Francisco Andrade, James Barnes, José Broekaert, George Chan, Tim Danielson, Carsten Engelhard, Gerardo Gamez, Ole Grøn, Volker Hoffmann, Scott Lehn, Denise McClenathan, Rob McCrindle, Radislav Portyrailo, Steve Ray, Duane Rogers, Amy Rosen, Greg Schilling, Brad Shaw, Jake Shelley, Andrew Szumlas, Bill Wetzel, and Josh Wiley.

physics departments for giving me a solid, hands-on grounding science; to Mike Hagerman, for showing me the fun side of a scientist's life; to Mary Carroll, for guiding me through my research at Union and for her concern with and advice for my career since then; and to the overall faculty of both institutions, for instilling in me the value of a broad education. In addition, I must thank my fellow Union students, chemistry and otherwise, for a lasting network of support and friendship.

Finally, I must thank Katherine Alben for mentoring my first research at the New York State Department of Health and any I have neglected to mention in this brief space.

Abstract

New Designs and Detection Strategies for Glow Discharge As an Alternative Spectrochemical Source

Michael R. Webb
Department of Chemistry
Indiana University
Bloomington, IN 47405

Powerful instrumentation exists for the determination of elemental concentrations in a range of samples, but all such instruments are the product of compromises among desirable properties. Sensitivity, accuracy, precision, portability, expense, sample size, speed, and other aspects of analysis are balanced based on the nature of a problem and the available resources. Opportunities exist for new instruments that strike a different balance from existing methods, particularly if these new techniques offer advantages over existing ones. Glow discharge (GD) is a flexible and potent platform from which to develop new spectrochemical methods, including those for elemental analysis. The methods described here seek to improve upon areas where GD falls short of other methods and to exploit the areas where GD excels, particularly speed and cost.

Glow discharge has predominately been used for the analysis of solids, and it offers high sensitivity and depth resolution at a comparatively low cost in this application. However, it has historically lacked lateral (in the plane of the sample surface) resolution. This

document describes a new method, making use of pulsed GD and monochromatic imaging, that adds lateral resolution better than 100 μm.

Traditionally, glow discharges have found little use in the analysis of solutions, largely due to their inefficiency in vaporizing the solvent. Two glow discharges, both operated at atmospheric pressure to improve desolvation, are described and characterized here.

The solution-cathode glow discharge (SCGD) is a simplified and improved version of the electrolyte-cathode glow discharge. A high voltage is applied across a gap between a sample solution and an electrode, forming a plasma that directly samples the solution and produces atomic emission that is used to identify and quantify the solution's elemental constituents. Several studies on the SCGD are described, including characterization and improvement of the source.

The annular glow discharge (AGD) is another glow discharge for the analysis of solutions. Unlike the SCGD, it is operated between two metal electrodes and the solution does not form a fundamental part of the plasma, which allows greater flexibility in solution composition. Both methods offer competitive analytical performance at low cost and with the potential for portability.

Gary M. Hieftje, Ph.D.	Stephen C. Jacobson, Ph.D.
Milos V. Novotny, Ph.D.	Dennis G. Peters, Ph.D.

Table of Contents

Chapter 4. Spectroscopic and Electrical Studies of a Solution-Cathode Glow Discharge.

Chapter 5. Spectroscopic Characterization of Ion and Electron Populations in a Solution-Cathode Glow Discharge.

Chapter 9. The Annular Glow Discharge: a Small-Scale Plasma for Solution Analysis.

Chapter 10. Future and Ongoing Research.

List of Figures

Chapter 1:

Chapter 2:

Chapter 3:

Chapter 4:

Chapter 5:

Chapter 6:

Chapter 7:

Chapter 8:

Chapter 9:

List of Tables

Chapter 4:

Chapter 5:

Chapter 6:

Chapter 7:

Chapter 8:

Chapter 9:

Chapter 1

Background and motivation.

1.1 AAS, ICP, AND THE NEED FOR ALTERNATIVE SOURCES

"With tongue in cheek," it was once predicted that atomic absorption spectrometry (AAS) publications, and perhaps even atomic absorption instrument sales, would drop to zero before the year 2000.[1] Although the prediction was offered in jest, it might be interesting to examine what trend has played out. The AAS publication rate continues to grow (see Figure 1-1), and the number of AAS publications in recent years appears to be comparable to the combined number of inductively coupled plasma (ICP) atomic emission spectrometry (AES) and ICP mass spectrometry (MS) publications.[†] A great deal of caution should be taken against treating any such literature search results too seriously (an admonition highlighted by the different numbers of records returned with the different literature search services), but it is clear that AAS continues to find a significant level of use. Indeed, other metrics indicate the same. For example, in monetary terms, AAS has been estimated to account for nearly as much (20% vs. 26%) of the atomic spectroscopy market as ICP,[2] despite the higher per-instrument cost of ICP.

Despite the facetiousness of the original prediction, considering why AAS remains

---

[†] Using ISI Web of Knowledge for the year 2005:
"atomic absorption" AND (spectrometry OR spectroscopy) resulted in 1007 hits.
"inductively coupled plasma" AND ("mass spectrometry" OR emission) resulted in 973 hits

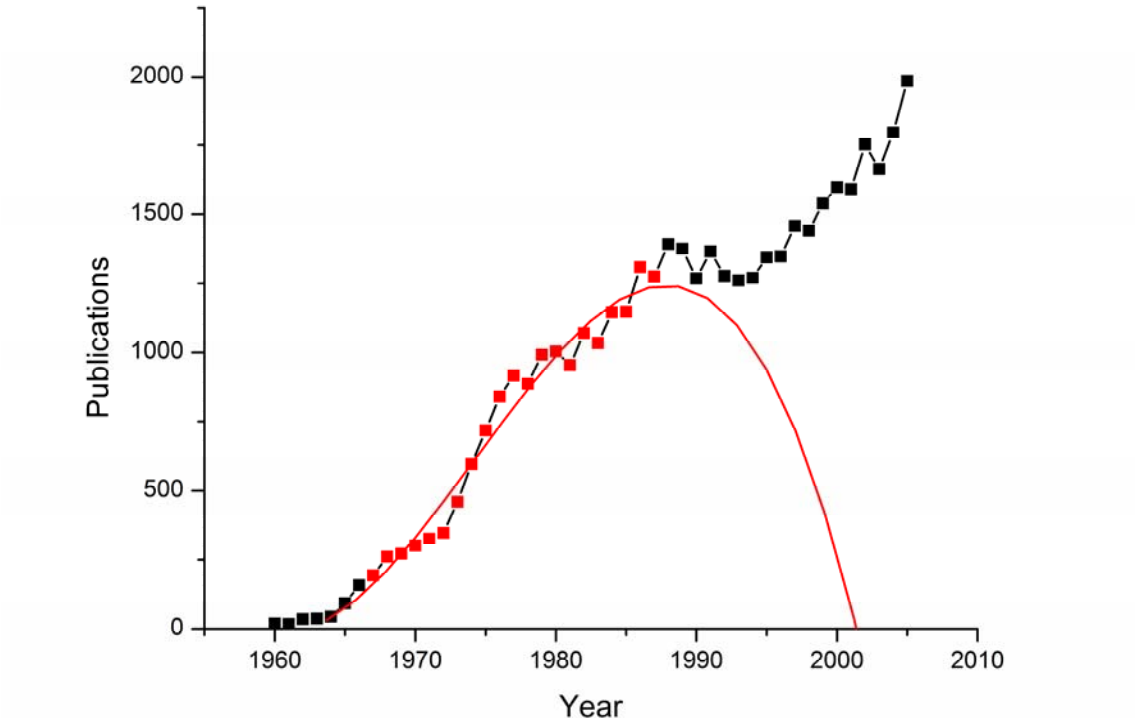

Figure 1-1. Publications per year "containing the concept "atomic absorption spectrometry" or "atomic absorption spectroscopy"" found using SciFinder Scholar. Red line shows a 3rd order polynomial fit to the red data points (1967-1987) suggesting a drop to zero by 2002.

popular in the presence of other, seemingly superior techniques (such as the aforementioned ICP-AES and ICP-MS) is a worthwhile exercise. Comparing detection limits, linear range, matrix effects, and speed of analysis, ICP-AES seems the clear winner against flame (F) AAS. Although graphite furnace (GF) AAS offers lower detection limits for some elements than ICP-AES, the latter method prevails on every other count (in fact, interferences and speed of analysis are even worse for GFAAS than for FAAS), and ICP-MS can be used to achieve detection limits below even GFAAS levels.

What, then, accounts for the continued use of AAS? Since ICP methods are its direct competitors, it might be equivalent to ask: what are the weaknesses of ICP methods that are not shared by AAS methods or are less significant in AAS methods? Detection limits, linear range, matrix effects, and speed of analysis seem to be eliminated as potential answers. Precision using ICP methods is not substantially different from that using FAA and is notably better than that using GFAAS, so that does not account for it.

Ease of use is a viable possibility, and has been given in the past.[2] It would seem, though, that the most significant advantage is cost, particularly because ease of use can be considered an aspect of running cost in the sense that more experienced or more highly trained (and therefore more highly paid) operators are required for ICP. Purchase, running, and maintenance costs are significantly lower for AAS than ICP instruments (particularly if the ICP instruments use MS detection).

Admittedly, there is also a degree of inertia. Absorption methods were established first and became the accepted methods for some analyses. There is little incentive to go

through validation requirements for new methods when old ones are adequate. The adequacy, of course, is based on the factors that have been discussed here.

A less frequently exploited advantage of AAS is its potential for use as a field instrument. ICP is not practical as a field instrument due to its large size, high power requirements, and high gas usage. AAS instruments are comparatively more portable, particularly if they use a tungsten coil or other low power atomizer in place of a graphite furnace or flame.[3] However, such things as the added space typically required for one or more narrow-band light sources place limits on this portability. Expressed somewhat awkwardly in terms of disadvantages, as the discussion has been framed, it could be said that AAS instruments can be less immobile than ICP instruments.

Obviously, neither AAS nor ICP methods are ideal; each represents a compromise prioritizing different factors. This suggests that there may be room for other compromises offering some combination of detection limits better than AAS, cost lower than ICP, linearity better than AAS, etc. In fact, some new source might have certain advantages over *both* AAS and ICP. For example, such a source might be more portable than AAS, or it might have higher throughput than ICP. At the same time, compromises might have to be made in other aspects.

All of the above detection types (AAS, AES, and MS) require that the sample be transferred to the gas phase. This remains an issue in flame, graphite furnace, and ICP methods for the analysis of liquids, and new sources might make gains by incorporating different sample introduction methods. It is also an issue in the analysis of solids. One approach is to dissolve the solid, and then to analyze it as a solution. For some samples,

this can be time consuming and difficult, and spatial information is typically lost. Other strategies offer more direct sampling. For example, lasers can be used to ablate the sample, resulting in small particles and in gas-phase atoms. The converted sample can then be introduced into a flame or plasma for further atomization and for ionization or excitation. Laser ablation (LA)-ICP-MS, for example, offers low detection limits along with spatial resolution in all three dimensions. However, such instruments are expensive and are not free of other disadvantages. For example, poor shot-to-shot precision limits depth resolution,[4] and matrix effects can be substantial.

One type of source has potential as an alternative in these applications and more: the glow discharge (GD). It might seem odd to think of GD as an alternative source because it is actually over 100 years old and it has now been 40 years since the invention of the Grimm lamp,[5] still one of the most common GD designs. Indeed, "modern" analytical GD (roughly, from the introduction of the Grimm lamp) is little more than a decade younger than "modern" FAAS (dated from work of Alan Walsh in the 1950s), and is even closer in age to GFAAS. However, in the decades since, new twists on GD have repeatedly expanded its versatility. By one count, GD was already in its fifth generation 15 years ago.[6] Thus, although an established source in some applications, GD has time and again been introduced to other applications as an alternative source.

1.2 GLOW DISCHARGE OPERATING PRINCIPLES

Before exploring this further, it is necessary to briefly describe the fundamental principles of GD spectrometry. In a simple version of its typical form, GD consists of

two electrodes separated by a low-pressure (0.1-10 Torr) gas, typically argon. A high voltage (several hundred volts to single kilovolts) between the two electrodes accelerates electrons towards the anode and positive ions towards the cathode. As they travel, these charged particles collide with neutral atoms. With high enough collisional energy, the neutrals can be ionized. This creates further ions and electrons, which are also accelerated towards the electrodes and can also undergo collisions with neutrals, creating still more ion-electron pairs. Ions can strike the cathode directly, or neutrals that have gained kinetic energy through collisions with ions can strike the cathode. The kinetic energies of these species knock atoms and electrons free. The erosion of the cathode surface is referred to as sputtering.

Cathode atoms introduced into the GD plasma can undergo collisions with ions, electrons, and neutrals. Through these collisions, cathode atoms can be excited, ionized, or both. Detection is usually accomplished though MS or AES, but other methods, including AAS and atomic fluorescence spectrometry, can also be used. In this relatively simple, traditional form, GD is useful as a source for the elemental analysis of conductive solids, where those solids are used as the cathode.

1.3 GLOW DISCHARGE AS AN ALTERNATIVE SOURCE

As suggested earlier, GD applications do not stop there. With modification, GD has been used for applications including elemental analysis of solid nonconductors;[7] depth-resolved analysis;[8] atomic, structural, and intact molecular analysis of gases;[9-10] and desorption-ionization of solids (for molecular analysis).[11]

The majority of this thesis describes further developments of GD as an alternative source for various purposes. The exception is Chapter 2, which describes a previously undiagnosed distortion in a system used for acquisition of two-dimensional monochromatic images (a monochromatic imaging spectrometer, or MIS). After explanation of the source of distortion, both an instrumental and a mathematical correction are evaluated. The instrumental correction involves the addition of a second monochromator and repairs the distortion with a slight loss in spatial resolution. The mathematical method is also effective in repairing the distortion. Based its origin, the distortion was expected to affect only the vertical axis of the two-dimensional image, and experiments supported this prediction. Thus, when linear slices of an image are what is truly of interest, correction for the distortion is unnecessary, provided that the object being imaged is properly oriented. This result was important moving forward to the experiments described in Chapter 3.

In Chapter 3, a glow discharge optical-emission spectrometry source was evaluated for use in imaging elemental surface distributions. There, GD-AES is offered as an alternative to other elemental analysis methods offering spatial resolution, such as LA-ICP. A 1.8 cm^2 area of a nickel-chromium alloy was sampled and copper emission was observed directly above the surface of a copper inclusion. This emission was imaged using a MIS. By pulsing the glow discharge, the resolution was improved greatly over measurements using direct-current powering. Ranges of gas flows, pulse frequencies, pulse potentials, pulse widths, and pressures were explored to determine their effects on spatial resolution and were related to atom transport in the glow discharge cell. Pressure,

pulse width, and pulse frequency were all found to have significant effects on resolution.

Chapters 4-9 focus on novel glow discharges operated at atmospheric pressure and used for the analysis of liquid samples. These discharges are alternatives to ICP-MS, ICP-AES, FAAS, and GFAAS. Chapters 4-6 are studies of the solution-cathode glow discharge (SCGD), which is a greatly simplified version of the electrolyte-cathode discharge (ELCAD). In both systems, the sample solution is the cathode of the glow discharge.

In Chapter 4, the SCGD design is introduced and investigated to add to the understanding of the operating mechanism and characteristics of such systems. The intensities and vertical distributions of emission from several analytes and background species were observed and compared with the vertical distributions of Fe excitation and OH rotational temperatures, as well as to electrical characteristics. The effects of the discharge gap size, the pH and conductivity of the solution, the applied current, and the solution flow rate on these distributions were also studied. Detection limits for this system were found to be comparable to those of similar systems and mostly in range of tens of parts per billion.

In Chapter 5, the ion and electron populations of the SCGD were investigated. Electron number density, ionization temperature, and degrees of ionization are determined for the first time in any ELCAD-like system. Spectroscopic techniques were used to keep from perturbing the plasma, a range of conditions was explored, and two regions (the negative glow and the positive column) were observed. By using the Stark broadening of the hydrogen beta line, electron number densities near 8.5×10^{14} cm^{-3} for the negative glow and 2.5×10^{14} cm^{-3} for the positive column were found. From those results and

measurements of the relative strengths of Mg neutral and ionic lines, ionization temperatures of 5000 K for the negative glow and 4600 K for the positive column were calculated. In turn, these results were used to estimate the degrees of ionization and norm temperatures for a variety of elements. Analytical implications of the study are discussed.

In Chapter 6, use of a SCGD with complex samples is explored. The present state of knowledge in this regard is briefly reviewed and several previously undocumented effects are examined. Remedies to various interferences are proposed and evaluated. The implications of the results to the mechanistic understanding of ELCAD-like systems are discussed.

Chapters 7 and 8 describe a new version of this discharge. In Chapter 7, the modified design is introduced and its analytical performance using continuous sampling is evaluated. The modification from the original SCGD is primarily a reduction in discharge volume (nearly five-fold, to 2 mm^3) and a corresponding increase in power density. Using the new design, detection limits for a range of metals are greatly reduced, such that most now lie in the single and sub-part per billion range. Additionally, some of the matrix effects described in Chapter 7 are substantially lessened in the miniature SCGD.

Although continuous sampling is useful, transient analysis is required for certain applications, including chromatographic or similar separations, small-volume sampling, high-throughput sampling, and on-line preconcentration. The miniaturized SCGD seems particularly well suited to transient analysis by virtue of its low dead volume and high

sensitivity. Chapter 8 exploits two benefits of transient sample introduction: high throughput and small sample volume. Sampling 25 μL volumes at 1000 samples per hour, the discharge achieved detection limits ranging from 5 pg (Li) to 6 ng (Hg). Additionally, some matrix effects were lessened even beyond the level of the continuous-sampling SCGD.

In Chapter 9, another glow discharge for the elemental analysis of liquids is introduced. This small-scale (5 × 2 mm) plasma is maintained in atmospheric-pressure helium between a tubular cathode and a rod-shaped anode (both made of steel). The discharge extends between the two electrodes and an annular glow is visible within the cathode tube. An aerosol is introduced into the plasma through the cathode, and atomic emission is observed in the near-cathode region. In this study, we observe the effects of solvent addition on the plasma in terms of its electrical and spectroscopic characteristics and how they change with solution flow rate. Given that even a robust source such as the inductively coupled plasma is different under wet and dry conditions, it is not surprising that the discharge introduced here is affected by the presence of an aerosol. However, the discharge is stable even with significant solvent loading. In this preliminary investigation, flow injection has been used to establish detection limits for several metals between 7 ppb (0.7 ng absolute) for Cd and 111 ppb (11 ng absolute) for Cu.

Finally, Chapter 10 briefly describes future and ongoing research directions using glow discharge as an alternative source.

1.4 REFERENCES

[1] G. M. Hieftje, "Atomic-Absorption Spectrometry - Has It Gone or Where Is It Going", *J. Anal. At. Spectrom.*, 1989, **4**, 117.

[2] J. F. Tyson and E. Yourd In *Atomic Spectroscopy in Elemental Analysis*; M. Cullen, Ed.; CRC Press LLC: Boca Raton, FL, 2004.

[3] J. D. Batchelor, S. E. Thomas and B. T. Jones, "Determination of cadmium with a portable, battery-powered tungsten coil atomic absorption spectrometer", *Appl. Spectrosc.*, 1998, **52**, 1086.

[4] W. W. Harrison, C. Yang and E. Oxley, "Pulsed glow discharge", *Anal. Chem*, 2001, **73**, 480A.

[5] W. Grimm, "Eine neue glimmentladungslampe fur die optische emissionsspektralanalyse", *Spectrochim. Acta, Part B*, 1968, **23**, 443.

[6] R. K. Marcus, "Glow discharge atomic spectrometries: They're back ... and here to stay", *Spectroscopy*, 1992, **7**, 12.

[7] D. C. Duckworth and R. K. Marcus, "Radio-Frequency Powered Glow-Discharge Atomization Ionization Source for Solids Mass-Spectrometry", *Anal. Chem.*, 1989, **61**, 1879.

[8] C. J. Belle and J. D. Johnson, "In-Depth Compositional Profile Analysis of Alloys Using Optical Emission Glow-Discharge Spectrography", *Appl. Spectrosc.*, 1973, **27**, 118.

[9] C. L. Lewis, M. A. Moser, D. E. Dale, Jr., W. Hang, C. Hassell, F. L. King and V. Majidi, "Time-gated pulsed glow discharge: Real-time chemical speciation at the elemental, structural, and molecular level for gas chromatography time-of-flight mass spectrometry", *Anal. Chem.*, 2003, **75**, 1983.

[10] T. K. Starn, R. Pereiro and G. M. Hieftje, "Gas-sampling glow discharge for optical emission spectrometry. Part I: Design and operating characteristics", *Appl. Spectrosc.*, 1993, **47**, 1555.

[11] F. J. Andrade, W. C. Wetzel, M. R. Webb, G. Gamez, S. J. Ray and G. M. Hieftje, "A novel atmospheric pressure chemical ionization source. Part II: Desorption-ionization for the direct analysis of solid compounds." Submitted to *Anal. Chem.*, 2007

Chapter 2

An improved monochromatic imaging spectrometer.

2.1 INTRODUCTION

Spatial resolution in optical spectroscopic measurements can be valuable in the observation and characterization of heterogeneous samples and sources. For example, it has long been known that sources for atomic spectroscopy – including flames, inductively coupled plasmas, microwave plasmas, and glow discharges – exhibit such heterogeneity.[1-14]

A number of approaches have been used to obtain spatial resolution with optical probes. Point-by-point measurements can be made with relatively simple, sensitive, and inexpensive instrumentation. However, the time required to complete such a process is long when a large number of points must be investigated. For example, interrogating an array of 100 × 100 points with a one-s integration time would require 2.8 h if done in this fashion, not including the time taken to move from point to point. Long acquisition times prohibit the measurement of transient phenomena. Systems using interference filters in conjunction with two-dimensional imaging detectors are another approach to acquire data in two dimensions, and with greatly reduced acquisition times, but this requires different filters for each spectral line or band and is limited by the spectral bandpass in some

applications. Other techniques are available for spatial resolution, each with its own advantages and disadvantages.

The monochromatic imaging spectrometer (MIS) introduced by Olesik and Hieftje[15] uses a monochromator for spectral discrimination and a two-dimensional vidicon for detection, giving a monochromatic two-dimensional image. A later version of this instrument uses a CCD for detection. It has been used to examine inductively coupled plasmas (ICP)[8-9-11-14] and glow discharges.[10] It has been used both to study the fundamental properties and processes of plasmas[8-14] and to optimize the performance of plasmas.[9]

In the MIS described by Olesik and Hieftje,[15] displayed schematically in Figure 2-1, the image of the source is spatially scrambled at the entrance slit of the monochromator, and is reconstructed after passing through the exit slit. This is accomplished by placing the source at the focal length (f_{L1}) of a lens (L1) placed as close as practicable to the entrance slit (S1), making that slit serve as an aperture stop. Light from the source is therefore collimated before passing through the slit. This has the effect of performing a spatial Fourier transform on the image. This scrambled image is then reformed within the monochromator. In the simplest situation, the distance from M1 (the monochromator mirror usually used for collimation) to the grating is equal to the focal length of M1. In this case, an image of the source is formed on the grating. The image is re-collimated by M2 (the monochromator mirror usually used for focusing) before passing through the exit slit. Outside the monochromator, a second lens (L2) reforms the image of the source at its focal point, where the detector is placed. This refocusing process has the effect of

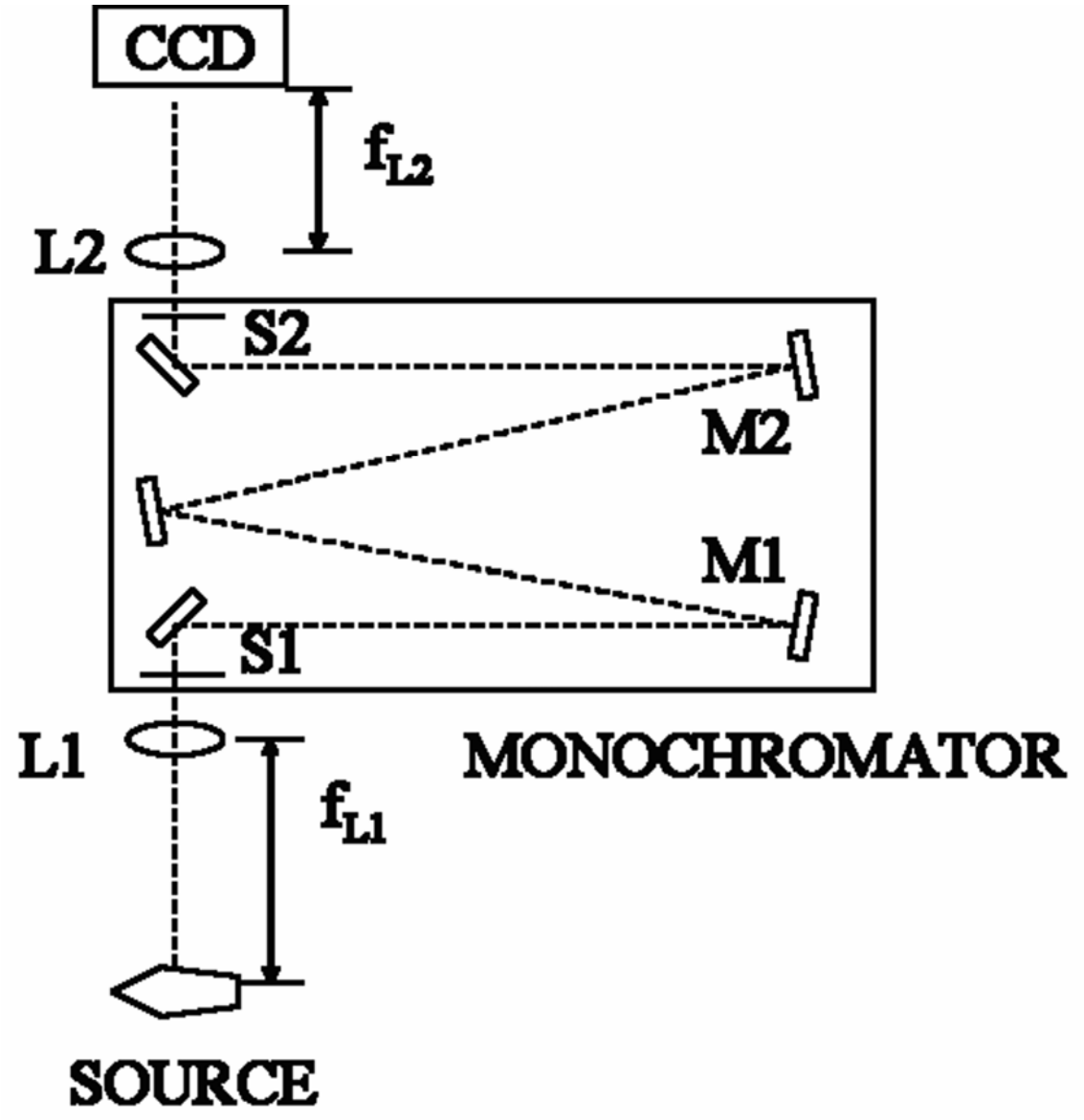

Figure 2-1. Monochromatic imaging spectrometer of Olesik and Hieftje:[15] L1, collimating lens; f_{L1}, focal length of lens L1; S1, entrance slit; M1, M2, concave mirrors; G, grating; S2, exit slit; L2, focusing lens; f_{L2}, focal length of lens L2.

performing an inverse spatial Fourier transform.

The spectral bandpass of this system is controlled by the widths of the entrance and exit slits, by the grating angle and groove spacing, and by the focal length of the monochromator. Because the image exists in Fourier space while passing through the entrance and exit slits of the monochromator, the image size is not restricted by the slit widths. Instead, narrowing the slits has an effect analogous to the degraded spectral resolution caused by shortening the distance the mirror travels in a Michelson interferometer. In the case of the MIS, it is the spatial resolution that is degraded, but only in the direction of the slit width (i.e. the horizontal direction in a typical arrangement). The spatial resolution is also determined by the optics outside the monochromator, the detector, and the fidelity of the entire optical system.

Olesik and Hieftje[15] discussed several effects that must be considered in the design of the MIS. Care must be taken to identify limiting apertures. For example, the intermediate image on the grating cannot be larger than the grating itself, and the effective width of the grating (width perpendicular to the optical path) will vary with grating angle. Also, the collimation may be imperfect. In the system used in the present study, the distance between M1 and the grating is approximately 34 cm, slightly shorter than the 35-cm focal length of mirror M1. As a result, the light exiting the monochromator is not truly collimated. When the light is not collimated at the slits of the monochromator, vignetting effects can occur. Vignetting by the slits can be minimized by placing the external lenses as close to the slits as is practicable. Also, a field-limiting effect can occur if the aperture of L1 is imaged near the intermediate or final source image. This effect is minimized by

placing L1 as close to the entrance slit as possible. Finally, aberrations due to the monochromator and external optics must also be considered. Most notably, the distances between the source and the collimating lens and the focusing lens and the detector must be adjusted for each significant change in wavelength to compensate for chromatic aberration (the wavelength dependence of f_{L1} and f_{L2}). Ideally, this is done by moving the source and detector rather than the lenses so that the aforementioned field-limiting effect can be avoided.

A drawback of the MIS that has not been fully considered is that the final reconstructed image width varies with wavelength. In fact, to our knowledge, the reason for this effect has not been described in the literature. It is this distortion that we will consider.

2.2 THEORETICAL

The distortion in question is a consequence of the fact that the angle of incidence on the grating is different from the angle of diffraction (shown in Figure 2-2). Analogously, a circular light projected onto a wall at a 45-degree angle would appear stretched out into an ellipse if it were viewed by someone at an angle perpendicular to the wall. Light forming a line of horizontal length l_i strikes the grating at an angle α, relative to the grating normal. It will cover a length l_g on the grating. The length l_g can be calculated from α and l_i by trigonometry:

$$l_g = l_i \cos \alpha \qquad (2\text{-}1)$$

The light then diffracts from the grating at an angle β, resulting in a line reduced to a length l_f. From trigonometry, it is found that

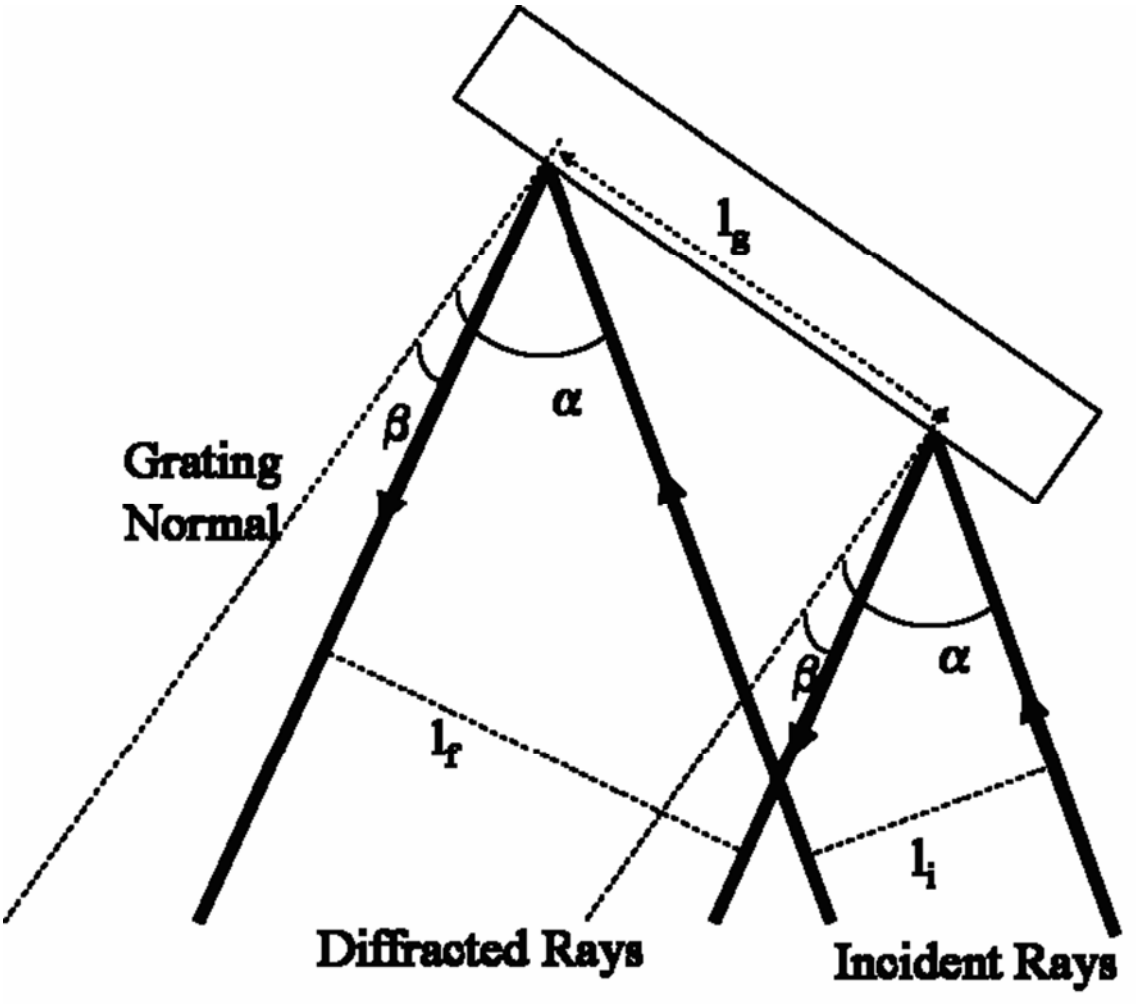

Figure 2-2. Two parallel rays diffracting from a grating: α, incident angle; l_i, initial separation of rays; l_g, separation of rays on the grating surface; β, angle of diffraction; l_f, final separation of rays.

$$l_f = l_g / \cos \beta \quad (2\text{-}2)$$

Combining these equations produces the result

$$l_f = l_i \cos \alpha / \cos \beta \quad (2\text{-}3)$$

This demonstrates that the horizontal dimension varies with the angles of incidence and diffraction.

There are at least three possible strategies for overcoming this distortion. Perhaps the most obvious is to measure the degree of distortion by imaging a source of known dimensions and then to correct for the measured degree of distortion. This option requires a calibration image at each wavelength, which requires a light source that is reasonably intense at all desired wavelengths or a set of light sources.

Another option is to use an instrumental approach. This approach uses a second monochromator (shown in Figure 2-3). If the subscript 1 is used to refer to the first monochromator and the subscript 2 is used to refer to the second, we have the two equations:

$$l_{f,1} = l_{i,1} \cos \alpha_1 / \cos \beta_1 \quad (2\text{-}4)$$

$$l_{f,2} = l_{i,2} \cos \alpha_2 / \cos \beta_2 \quad (2\text{-}5)$$

Because the light exiting the first monochromator is the same as the light entering the second monochromator, $l_{f,1} = l_{i,2}$. Using this equivalence to combine the equations, we find:

$$l_{f,2} = l_{i,1} (\cos \alpha_1 / \cos \beta_1) (\cos \alpha_2 / \cos \beta_2) \quad (2\text{-}6)$$

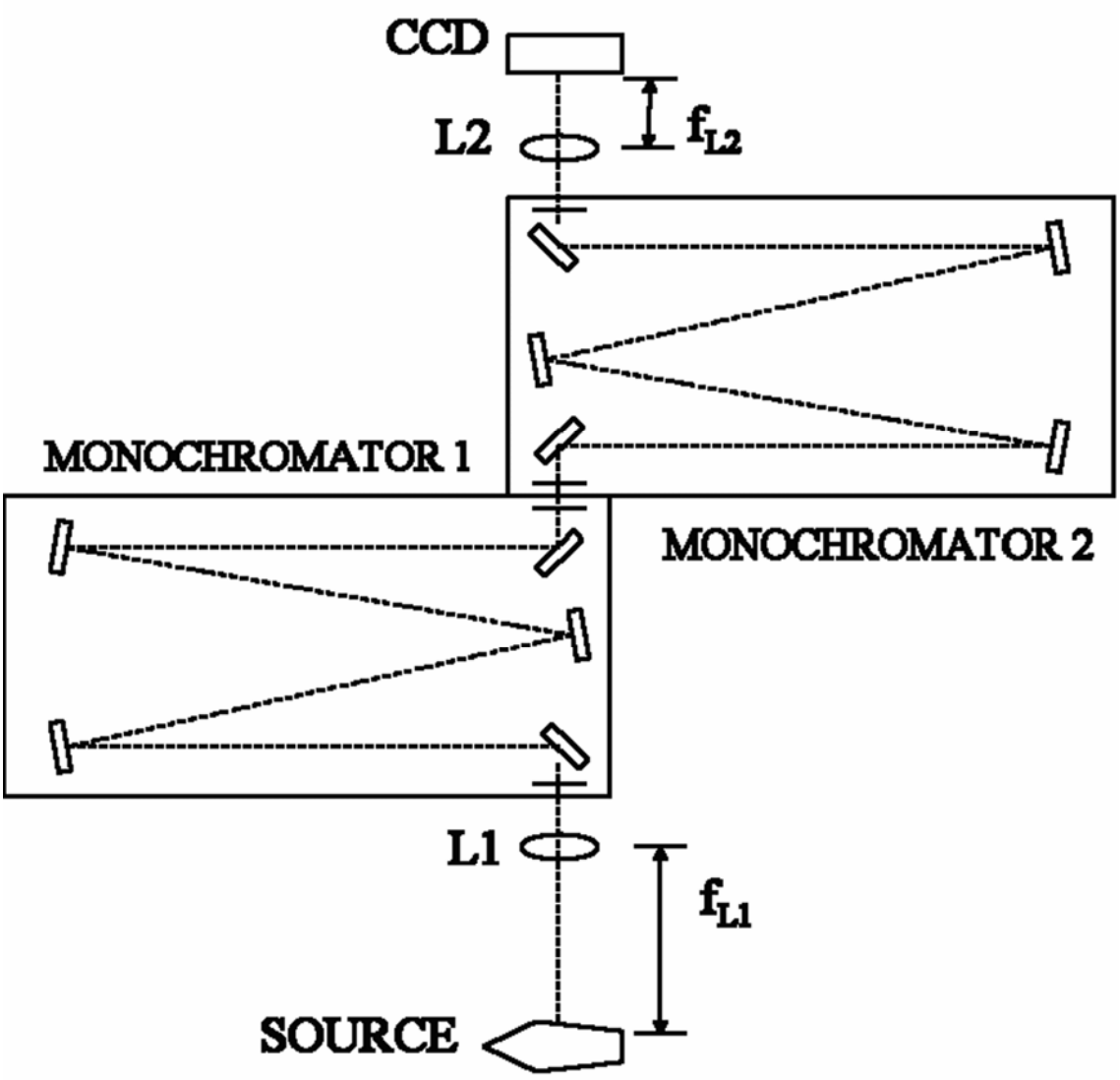

Figure 2-3. Corrected monochromatic imaging spectrometer: L1, collimating lens; f_{L1}, focal length of lens L1; L2, focusing lens; f_{L2}, focal length of lens L2.

In the case where $\alpha_1 = \beta_2$ and $\alpha_2 = \beta_1$, the equation reduces to:

$$l_{f,2} = l_{i,1} \tag{2-7}$$

The grating formula[16]

$$d (\sin \alpha + \sin \beta) = m\lambda \tag{2-8}$$

shows that doing this does not change the wavelength selected by the monochromator.

Alternatively, the distortion can be corrected mathematically, provided that certain wavelength-dependent values are known. Realizing that the angle between the light striking the grating and the light leaving the grating is fixed (it must equal the angle formed by the two mirrors and the grating and is equal to 2Φ by normal convention), it can be surmised that the difference between α and β must also be fixed. For this to be true, it is important that one of the angles be represented as negative and the other as positive when they are on opposite sides of the grating normal but that they both be given the same sign when on the same side of the normal. Using the grating formula (equation 2-8), equation 2-3, and certain parameters of the monochromator (for the monochromators used in this work, 2Φ was approximately 35.4º and the groove spacing (d) was 833.3 nm/groove), the distortion of the horizontal direction can be predicted.

The effectiveness of the latter two approaches will be evaluated. For the two-monochromator setup, the degree of distortion in the final image will be evaluated. For the mathematical correction, the distortion observed using a single monochromator will be compared to the predicted distortion.

2.3 EXPERIMENTAL

For spectral resolution, a McPherson (Model 270) 0.35-m Czerny-Turner monochromator was used with a 1200 grooves/mm grating. For spatial correction, a Heath (Model EU-700) 0.35-m Czerny-Turner monochromator was used with a 1200 grooves/mm grating. These two units are nominally the same, although purchased at different times. Light from the source was collimated by a 25-cm focal length, plano-convex, fused-silica lens. Light passing through the monochromator was re-imaged by a 15-cm focal length, plano-convex, fused-silica lens onto the detector. A Photometrics CH315/A CCD was used as the detector. The acquisition time was adjusted depending on the desired sensitivity. A 1951 USAF glass-slide resolution target (Edmund Optics), backlit by a tungsten lamp, was used to characterize the system. The target was positioned at a distance from L1 approximately equal to the focal length of L1. L2 was positioned at a distance from the CCD approximately equal to the focal length of L2. The positions of the target and L2 were both then adjusted for best spatial resolution. The slit widths of the first monochromator were set depending on the desired spectral resolution. The slit heights were 12 mm. The slits of the second monochromator were removed, resulting in a circular aperture 12 mm in diameter.

2.4 RESULTS AND DISCUSSION

As would be expected, care must be taken in positioning the second monochromator. In the system used here, the exit slit of the first monochromator could not be placed exactly at the entrance slit to the second monochromator because both slits were recessed.

Instead, the entrance slit to the second monochromator had to be placed approximately 5 centimeters further along the light path. The combination of slits from the monochromators resulted in a field stop. The field stop was widened when the slits of either monochromator were opened, so it was decided to remove the slits of the second monochromator altogether. This procedure effectively made the field stop larger than the field stop created by the grating. Further, when the two monochromators are not on the same horizontal plane, ghost images arise, placing an additional constraint on spatial resolution. Resolution is also adversely affected if the grating angles are not equal. Given the extremely large size of the slits in the second monochromator, the most significant light loss should be due to incomplete transmission by the second monochromator's optics and particularly the grating.

The magnification of the system is controlled by the collimating and imaging optics. For this system, the magnification was experimentally measured to be approximately 0.52. The spatial resolution of the instrument was derived from measurements obtained using the 1951 USAF target. The target test pattern consisted of groupings of three equal lines spaced a distance equal to their width. Resolution was judged based on the smallest-width lines that could be resolved with valley intensities of 50% or less peak intensity. The precision in this measurement is limited by the available sizes of line pairs. The detector-limited resolution is the case where the line width is the same as the pixel width (and a line pair width is equal to two pixels). At this magnification, given that the pixels are 24 μm wide, the detector-limited resolution is 10.9 line pairs/mm. For the single-monochromator system with 1-mm slit widths, 8.00 line pairs/mm were resolved

vertically and 3.17 line pairs/mm were resolved horizontally. For the single-monochromator system with 2-mm slit widths, 8.00 line pairs/mm were resolved vertically, and 4.00 line pairs/mm were resolved horizontally at the same wavelength. For the system using a second monochromator for correction, the resolution was degraded somewhat. With 1-mm slit widths, 8.00 line pairs/mm were resolved vertically but only 2.52 line pairs/mm were resolved horizontally. With 2-mm slit widths, 8.00 line pairs/mm were resolved vertically and 2.83 line pairs/mm were resolved horizontally. Although the reason for the loss of resolution is not entirely clear, it is likely from a cumulative effect of slight misalignments, the occurrence of which is likely to be increased with additional components. In particular, there is an inherent mismatch between the focusing and collimating mirrors' focal lengths and the distances between those mirrors and the gratings. Adding a second monochromator likely compounds any problems.

The distortion caused by the grating can be seen in Figure 2-4. The distortion caused by the grating angle was also determined from the target images. The distance between the centers of the first and third lines in the 1 line pair/mm grouping was measured in both the horizontal and vertical directions. The ratio of horizontal to vertical distance was then calculated. For the single-monochromator system, at a wavelength of 400 nm, the ratio was 1.17. At 500 nm, it was 1.23. At 600 nm, it was 1.29. At 700 nm, it was 1.36. The precision of these measurements was on the order of 0.02 (limited by the finite size of the pixels). The same procedure was performed to determine the effect of adding the second monochromator. For all wavelengths, the ratio was between 1.00 and 1.01,

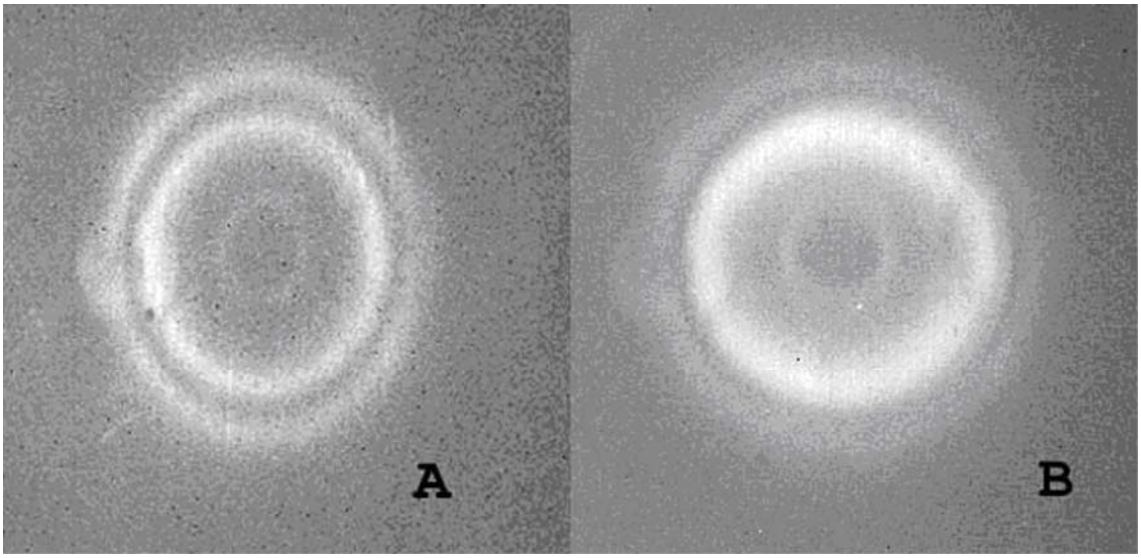

Figure 2-4. Images of a circular hollow cathode lamp acquired with (A) the single-monochromator MIS and (B) the double-monochromator MIS.

indicating that the distortion was corrected. For the single-monochromator system, the agreement between mathematically predicted and measured skew was excellent. The ratio l_f/l_i was predicted to be 1.18 at 400 nm, 1.24 at 500 nm, 1.30 at 600 nm, and 1.37 at 700 nm. The agreement is better than the precision to which the distortion could be measured. The hypothesized origin of the distortion is well supported by both sets of results.

The spectral resolution of the two-monochromator system was verified using the Ca 422.7 nm line from a hollow cathode lamp. The manufacturer's stated reciprocal dispersion is 2.0 nm per mm at the exit slit. With 1-mm slit widths, the full width at half maximum of the line was measured as 2.0 nm, in good agreement with the manufacturer's specifications.

2.5 CONCLUSIONS

The MIS can provide high-quality spectrally resolved two-dimensional images. However, it introduces a grating-angle-dependent distortion. This distortion results in a change in the width of an image with wavelength. A simple arrangement that adds a second monochromator corrects for this effect, although some spatial resolution is lost. The residual resolution is sufficient for many tasks. Presumably, a similar arrangement would compensate for any similar effect in the slitless spectrograph of the type used by Olesik and Hieftje.[19]

2.6 REFERENCES

[1] C. S. Rann and A. N. Hambly, "Distribution of atoms in an atomic absorption flame", *Anal. Chem.*, 1965, **37**, 879.

[2] T. E. Edmonds and G. Horlick, "Spatial profiles of emission from an inductively coupled plasma source using a self-scanning photodiode array", *Appl. Spectrosc.*, 1977, **31**, 536.

[3] M. W. Blades and G. Horlick, "The vertical spatial characteristics of analyte emission in the inductively coupled plasma", *Spectrochim. Acta, Part B*, 1981, **36B**, 861.

[4] M. W. Blades and G. Horlick, "Interference from easily ionizable element matrixes in inductively coupled plasma emission spectrometry: a spatial study", *Spectrochim. Acta, Part B*, 1981, **36B**, 881.

[5] S. R. Koirtyohann, J. S. Jones, C. P. Jester and D. A. Yates, "Use of spatial emission profiles and a nomenclature system as aids in interpreting matrix effects in the low-power argon inductively coupled plasma", *Spectrochim. Acta, Part B*, 1981, **36B**, 49.

[6] R. M. Belchamber and G. Horlick, "Noise-power spectra of optical and acoustic emission signals from an inductively coupled plasma", *Spectrochim. Acta, Part B*, 1982, **37**, 17.

[7] J. P. Walters and S. A. Goldstein, "Emission topography of a stable spark discharge train", *Spectrochim. Acta, Part B*, 1984, **39B**, 693.

[8] G. D. Rayson, A. F. Parisi and G. M. Hieftje, "Spatially resolved measurements as a vehicle for studying atomization mechanisms in an ICP", *Spectrochim. Acta, Part B*, 1989, **44B**, 999.

[9] N. N. Sesi, D. S. Hanselman, P. Galley, J. Horner, M. Huang and G. M. Hieftje, "An imaging-based instrument for fundamental plasma studies", *Spectrochim. Acta,*

Part B, 1997, **52B**, 83.

[10] M. J. Heintz, P. J. Galley and G. M. Hieftje, "Emission features of a conventional radio frequency glow discharge source and a magnetically enhanced source", *Spectrochim. Acta, Part B*, 1994, **49B**, 743.

[11] N. N. Sesi, A. MacKenzie, K. E. Shanks, P. Yang and G. M. Hieftje, "Fundamental studies of mixed-gas inductively coupled plasmas", *Spectrochim. Acta, Part B*, 1994, **49B**, 1259.

[12] N. N. Sesi and G. M. Hieftje, "Studies into the interelement matrix effect in inductively coupled plasma spectrometry", *Spectrochim. Acta, Part B*, 1996, **51B**, 1601.

[13] Y. Su, P. Yang, Z. Zhou, X. Wang, F. Li, B. Huang, J. Ren, M. Chen, H. Ma and G. Zhang, "Feasibility of applying microsecond-pulse glow discharge time of flight mass spectrometry in surface depth analysis", *Spectrochim. Acta, Part B*, 1998, **53B**, 1413.

[14] S. A. Lehn, K. A. Warner, M. Huang and G. M. Hieftje, "Effect of an inductively coupled plasma mass spectrometry sampler interface on electron temperature, electron number density, gas-kinetic temperature and analyte emission intensity upstream in the plasma", *Spectrochim. Acta, Part B*, 2002, **57B**, 1739.

[15] J. W. Olesik and G. M. Hieftje, "Optical imaging spectrometers", *Anal. Chem.*, 1985, **57**, 2049.

[16] J. D. Ingle and S. R. Crouch, *Spectrochemical Analysis*; Prentice Hall: Upper Saddle River, NJ, 1988.

Chapter 3

Surface elemental mapping using glow discharge—optical emission spectroscopy.

3.1 INTRODUCTION

The glow discharge (GD) is a versatile source, useful for elemental analysis of liquids[1-4] and solids, as well as molecular, structural, and elemental analysis of gases.[5-6] Even within applications to elemental analysis of solids, it shows great flexibility in that it can be used for bulk analysis or for depth profiling on scales ranging from several nanometers to hundreds of micrometers,[7-8] can be used over a broad concentration range,[8] and can be used as a source for optical emission, atomic absorption, atomic fluorescence, or mass spectrometry. Alternative powering schemes to direct current (dc) have contributed to the utility of the glow discharge. Radio frequency powering has a number of desirable features, most notably the ability to analyze non-conductive samples.[9] A pulsed powering scheme offers its own advantages, including enhanced signals, reduced sample heating, and more flexible control of sputtering rate.[7]

One area in which GD spectrometry is lacking, however, is lateral resolution. Spatial resolution within the plane of the sample surface is usually no better than the size of the sputtered area. For a Grimm or similar type of GD source, this sputtered area is typically a circle at least 4 mm in diameter, limiting resolution to this scale. To analyze more than

one spot with a typical glow discharge cell, the discharge must be terminated, the sample moved, and the discharge reignited and allowed to stabilize, increasing the potential for error and extending the analysis time. This problem is not unique to glow discharges. In laser ablation, spatial profiling is limited by shot-to-shot reproducibility,[10] but laser ablation does not require breaking vacuum to examine different positions. Moreover, laser ablation samples smaller areas.

Resolution on the scale of several millimeters to several centimeters is useful in assessing the homogeneity of Standard Reference Materials at the National Institute of Standards and Technology and the sputtering targets used in the microelectronics industry.[11] Inclusions (inhomogeneous impurities) in steel samples can affect the properties of steel.[12-15] It is the macro inclusions, which can reach hundreds of micrometers, that are the most harmful.[14-15] In fact, failure can be caused by just one large inclusion.[15] A rapid technique covering a large sample area is needed for determination and characterization of these impurities.[13]

In 1995, Winchester and Salit[11] demonstrated a novel GD cell with multiple independent discharges running simultaneously over different spots, which enabled simultaneous analysis with a multiplex (Hadamard transform) detection scheme. The lateral resolution was limited to 4.75 mm along rows and columns and 6.7 mm along diagonals, and there were gaps of several millimeters that were not sampled between the discharges, but these sizes are limits of the specific design of the prototype rather than the technique. In the same year, Hoffmann and Ehrlich[16] showed that the lateral distribution of GD emission above the plasma surface is influenced by the lateral distributions of elements within the

sample, but the resolution was too poor at that time to be of much analytical use. An implication of this study was that, when laterally heterogeneous samples are analyzed, different emission intensities might be observed (and therefore different concentrations calculated) depending on the orientation of a sample even if the same portion was sputtered. Winchester[17] verified this for a typical optical arrangement and demonstrated that the effect could be overcome with a different optical arrangement.

In the present work, a microsecond-pulsed glow discharge was used to greatly improve the resolution, and a 15-mm diameter area was sputtered at once. Ranges of gas flows, pulse frequencies, pulse potentials, pulse widths, and pressures were evaluated. Their effects on spatial resolution and relationships to atom transport were explored.

3.2 EXPERIMENTAL

A home-built Grimm-type glow discharge cell with a floating restrictor, shown in Figure 3-1, was used. The floating restrictor had a 15.0 mm inner diameter, which confined both the sputtering and viewing to an area of approximately that size (1.8 cm^2). The sample was tightened against the cathode by an aluminum plate, which was held against the cathode with aluminum bolts. The cell was cooled to 10 to 15 °C by a Neslab Coolflow CFT-33 Refrigerated Recirculator (Newington, NH). Argon of 99.998% purity was used (Air Products, Allentown, PA). The argon flow was regulated by an MKS Instruments type 1159A-010005V flow regulator (Burlington, MA). An Edwards E2M2 High Vacuum Pump (Crawley, Sussex, England) was used to maintain low pressure and remove sputtered material. A valve between the cell and the vacuum pump was

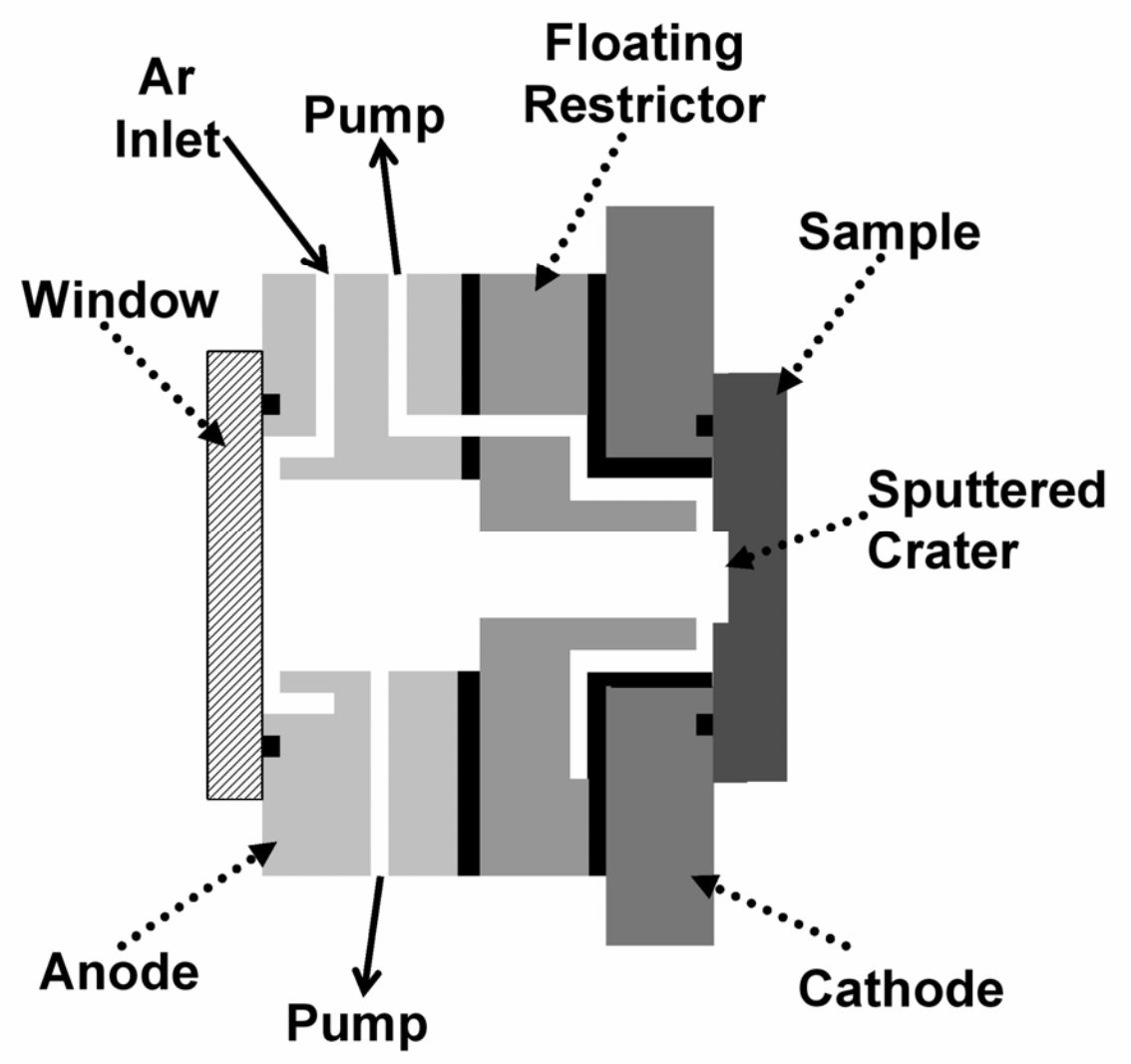

Figure 3-1. Cross section of the glow discharge cell (not to scale). Black areas are insulators, the window is fused silica, and the remainder of the cell body is brass. Inner diameter of the floating restrictor is 15.0 mm.

employed in combination with the flow regulator to adjust the pressure, which was monitored in the cell body with an MKS Instruments Baratron 122AA pressure gauge. For pulsed measurements, the discharge was powered by an Instrument Research Company model no. M3K-20-N Pulsed Power Supply (Columbia, MD). For dc measurements, a Hewlett Packard 6525 DC Power Supply was utilized.

The emission was monitored with a monochromatic imaging spectrometer of the kind described by Olesik and Hieftje.[18] The source was placed at the focal point of a 25-cm focal length plano-convex fused-silica lens. This lens collimated the light from the source and directed it into a Heath (Model EU-700) 0.35-m Czerny-Turner monochromator fitted with a 1200 lines/mm grating. After exiting the monochromator, the light was refocused onto a Photometrics CH350A CCD camera (Roper Scientific, Trenton, NJ) by means of a 15-cm focal length plano-convex fused-silica lens. The result is a monochromatic (1.5-nm bandpass) image with a magnification of 0.6. In the vertical direction, the image is good enough that a 56-µm valley between 56-µm lines on 1951 USAF glass-slide resolution target (Edmund Optics) backlit by a tungsten lamp are 30% as intense as the centers of the lines.

A nickel-chromium alloy sample (NIMONIC alloy 105 E3918 containing 75.2% Ni, 19.4% Cr, 5.4% other) with 0% to 0.01% Cu from Inco Europe Limited (Birmingham, England) was used as the bulk material. A 1.0-mm diameter copper plug in the form of a piece of copper wire inserted into the alloy was used as the inclusion.

3.3 RESULTS AND DISCUSSION

To allow the implications of each study to be better appreciated, our basic model is presented here; results will then be offered to support the model and to develop it. In a glow discharge, atoms are sputtered from the surface of the sample and then travel away from it by both diffusion and convective transport (with the gas flow). When those atoms reach certain regions, particularly the negative glow, they can be excited and emit light. The farther the atoms have been allowed to drift, the more smeared their distribution and the worse the spatial resolution will be. As a result, the spatial resolution will depend on the time between sputtering and emission as well as the speed at which the atoms move.

An image obtained with the imaging GD instrument is shown in Figure 3-2. The bright spot is above the copper pin and the dark area is over the nickel-chromium alloy. A dashed ring has been overlain to show the limits of the discharge cell. A distortion in the horizontal direction is seen when this type of imaging system is used.[19] To avoid this distortion, only vertical slices of the image were used in the subsequent evaluation. This is not a fundamental limitation of glow discharge imaging because other detection configurations could be used or the distortion could be corrected.

Emission from the same pin was imaged under a wide range of conditions (that is, a large number of combinations of the parameters discussed in the sections that follow), which produced a large data set. For each condition, 5 images of the Cu 327.4 nm emission and 5 images of the background (at 328.9 nm) were taken. To extract trends from the data, two numbers were necessary for each condition: a measure of the lateral width of the emission from the pin and a measure of the error in this width. To simplify the analysis,

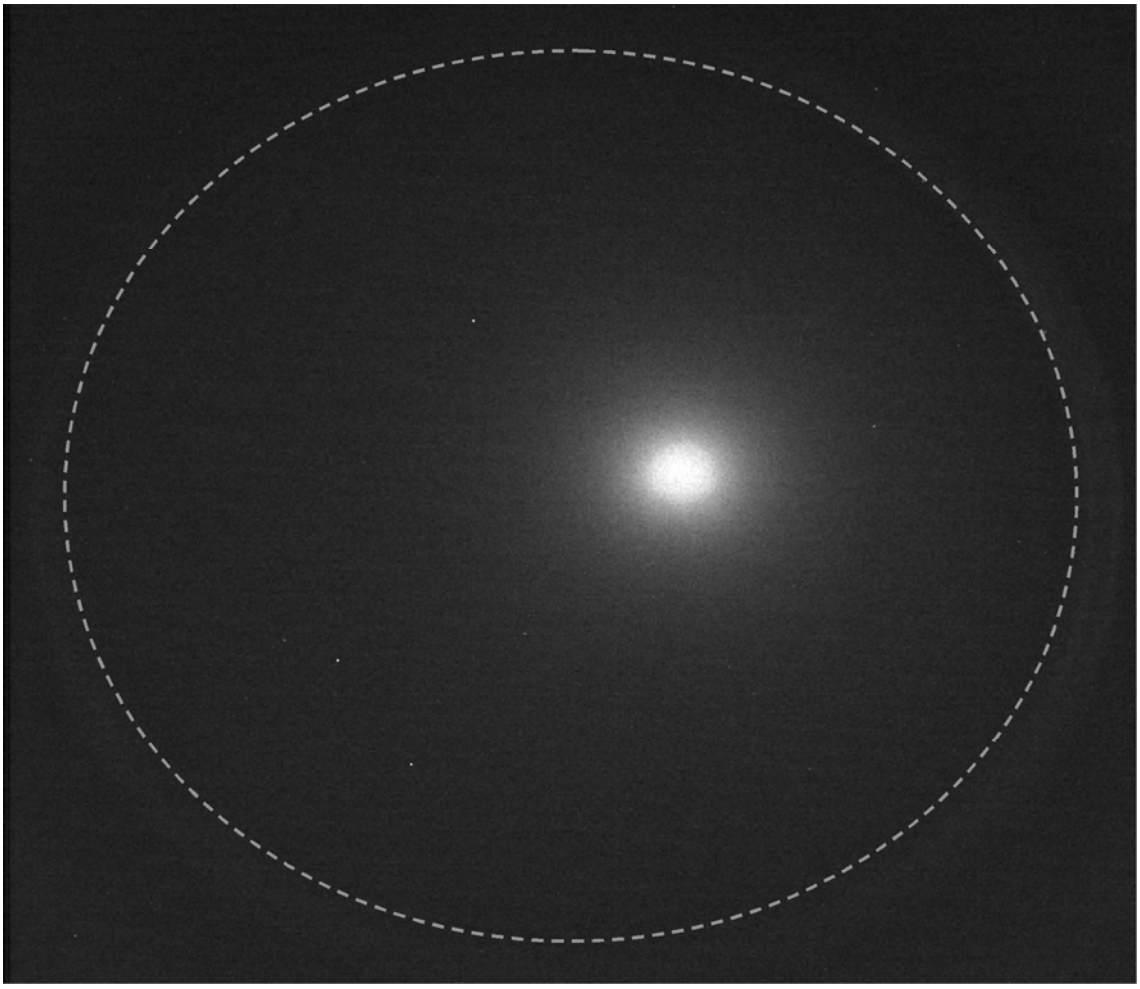

Figure 3-2. Background-corrected monochromatic image of the Cu I 327.4 nm line above a primarily Ni-Cr sample with a 1.0-mm diameter Cu insertion. The dashed ring shows the 15-mm diameter area sputtered by the discharge. Discharge Conditions: pulses of 1μs, 100 Hz, and 4.0 kV, and a pressure of 3.5 torr.

the 10 images were first reduced to a single vertical profile. A program written in house averaged the 5 images at 327.4 nm, averaged the 5 images at 328.9 nm, subtracted the latter from the former, and exported a one-dimensional slice along the y-axis of the resulting image. With Origin (OriginLab Corporation, Natick, MA), a Lorentzian function was fit to the observed profile (vertical slice) in order to determine its full width at half maximum (FWHM).

Although this process is an efficient way to arrive at widths for a large data set, it necessarily eliminates direct calculation of the error in these widths because only one width is returned for each condition. One might expect there to be a relationship between the intensity of a profile and the uncertainty in the fitting of that profile (that is, weaker signals will have lower signal-to-noise ratios than stronger signals, so there will be more uncertainty in the fit for weaker signals than for stronger signals).

For 14 conditions, which varied widely to ensure that the results would be applicable to the entire range of data, uncertainty in the width was calculated directly. That is, the 5 images (after background correction) were individually fit with Lorentzians, and the standard deviation among the 5 widths was calculated. Along with the width, the Lorentzian fit returns a peak area, which can be used as a measure of signal strength. These 14 sets were chosen to represent a range of emission intensities (and therefore a range of peak areas). The relative standard deviation (RSD) in FWHM was then plotted as a function of peak area (Figure 3-3) and a power curve was fit to the plot. The resulting curve had a power of -0.66. Although imperfect, errors estimated from this fit were judged to be adequate reflections of directly calculated errors for our purposes and

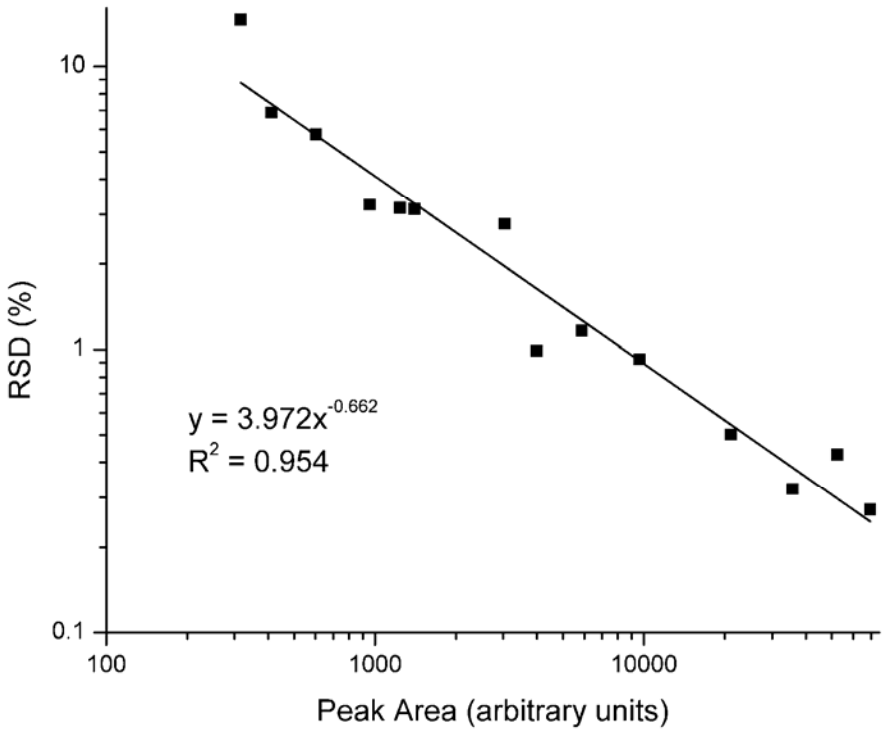

Figure 3-3. Relationship between uncertainty in peak FWHM (as percent RSD) and peak area. Glow discharge conditions were varied in order to encompass a wide range of peak areas.

are used throughout the remainder of the chapter wherever an estimated error in profile width is given.

3.3.1 Pulsed vs. dc operation of the GD

By using pulsed rather than dc powering, the resolution was improved significantly. At approximately 400 V dc (not pulsed) and 3 torr, the measured FWHM of the image from the 1-mm Cu inclusion was 2.3 mm. As will be shown later, the FWHM of the same pin when pulsed powering was used could be as narrow as 1.0 mm (the width of the pin itself). In a dc GD, energy is continuously being introduced into the system, so atoms that have traveled far from their original locations on the sample surface can still be excited and emit light. In a pulsed GD, the energy is available for a limited time, so the distance atoms can travel before emitting is correspondingly limited. Indeed, modeling predicts that the sputtered atom concentration is (axially, at least) relatively narrowly distributed and close to the cathode for the first few microseconds of a pulse[20] compared to the case of a dc GD.[21] Consequently, pulsed operation produces a narrower distribution and better resolution.

3.3.2 Convection

The glow discharge cell has a single argon inlet, the flow through which is regulated by a mass flow controller. The argon is directed towards the quartz window and then to the main cell body. The cell also has two outlets that connect outside the cell and lead to a vacuum pump. Flow through these outlets is restricted by a valve between the connection and the pump. One outlet resides in the main cell body while the second

surrounds the floating anode close to the sample. This arrangement creates forced convection (flow) from the main cell towards the sputtering crater then out to the perimeter of the sputtering crater. If this convection has a significant effect on the distribution of emission in a microsecond-pulsed glow discharge, it would be expected to spread the atoms and therefore their emission towards the perimeter of the sputtering crater. This spreading would result in broader lateral profiles at higher flow rates. In order to exclude pressure as a controlling variable, the outlet valve was adjusted to maintain a constant pressure of 2.75 Torr while the inlet mass flow controller was used to vary the Ar flow from 41 mL/min to 105 mL/min. Pulses of 2.75 kV and 4-μs duration, applied at a frequency of 100 Hz were used to sputter a nickel-chromium alloy with a 1.0 mm copper-pin insert. Five images of the Cu 327.4 nm emission and 5 measurements of the background (at 328.9 nm) were taken at each flow rate. As is shown in Figure 3-4, the FWHM of the Cu emission peak averaged 1.44 mm and varied by less (8 μm or 0.5% from the widest to the narrowest) than the smallest individual estimated standard deviation (10 μm). This variation was well below what was seen with other parameters, and no trend was observed. It can therefore be concluded that convection does not play a significant role under the conditions studied.

3.3.3 Pulse frequency

The pulse frequency or, more pertinently, the separation between pulses had a marked effect on the shape of the spatial emission profile. Figure 3-5 shows the distortion in peak shape that arises at short pulse separation times. To quantify this change, Fig. 3-6 shows the ratio of the width at 25% of the peak height to that at 75% of the peak height as

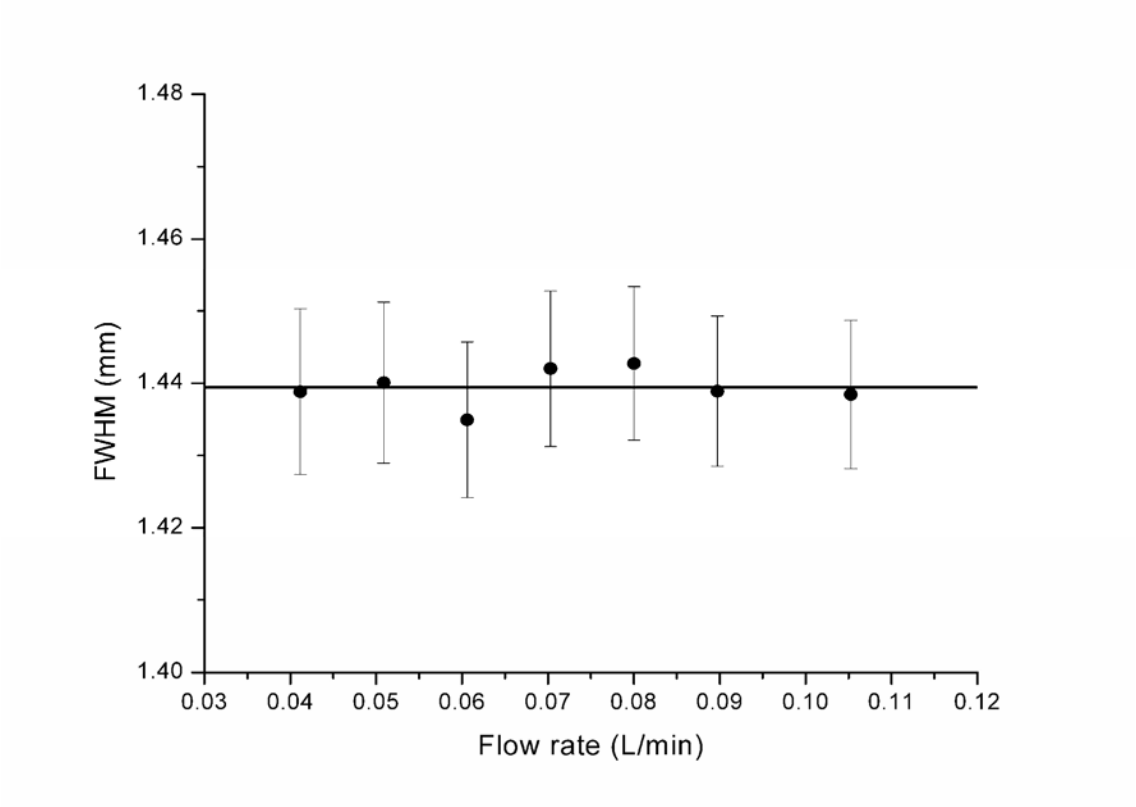

Figure 3-4. Effect of Ar flow on spatial resolution. 4.0 μs pulse, 2.75 kV, 2.75 torr, 100 Hz.

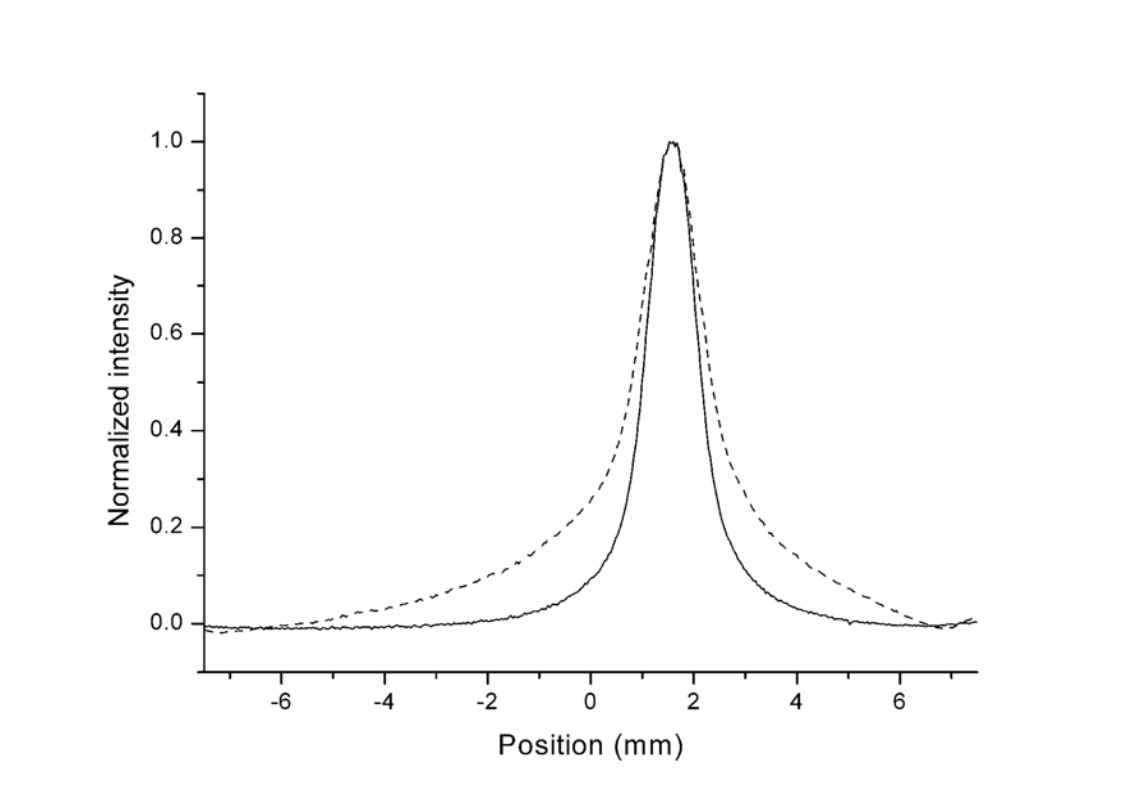

Figure 3-5. Effect of pulse separation on profile shape. Solid line shows 2.0 ms separation. Dashed line shows 0.3 ms separation. 1.0 μs pulse, 4.0 kV, 4.0 torr.

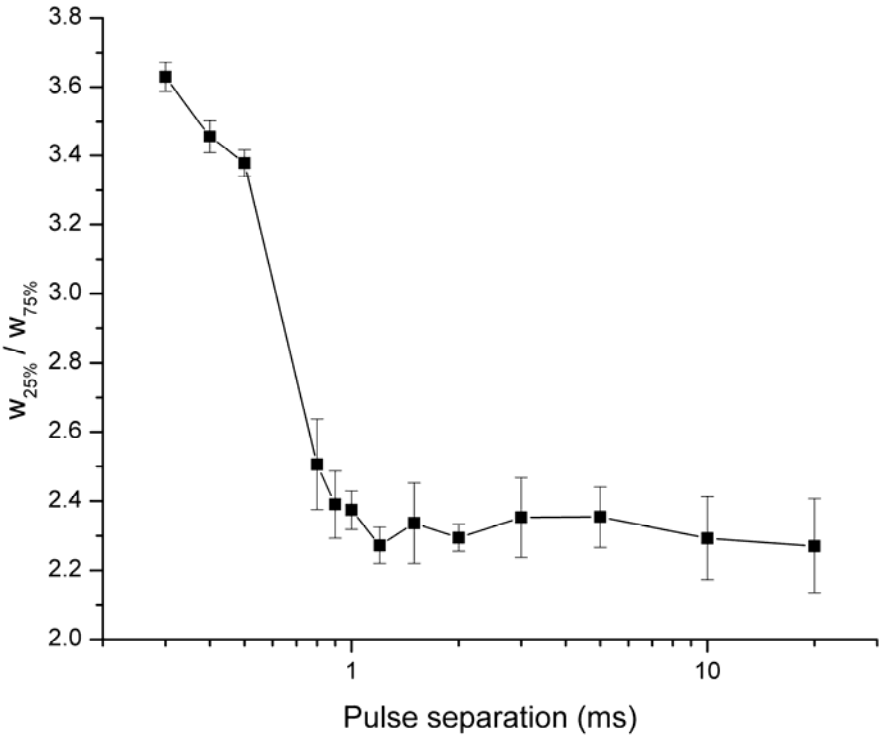

Figure 3-6. Effect of pulse separation on profile shape. 1.0 μs pulse, 4.0 kV, 4.0 torr.

a function of the temporal separation between pulses. There is a transition at pulse separation intervals around 800 μs from peaks with broad bases to peaks with narrower bases. This behavior can be explained as a sort of flushing time of the region of the cell where excitation occurs. At longer inter-pulse spacings, atoms have time to be almost entirely removed from the negative glow region (where most excitation and emission occurs) before the next pulse occurs. At shorter delays, there are two atom populations, one of which is from the prior sputtering pulse. This population has had time to diffuse somewhat, but not to drift out of the negative glow entirely. Differences in cell geometries and gas flows certainly affect the flushing time, but it is interesting that the time apparent in Figure 3-6 is on the same order as those found optimal by Pisonero et al.[22] (10-130 μs) in double-pulse experiments, where sputtering occurs on the first pulse and ionization is enhanced by a second pulse.

3.3.4 Potential

Figure 3-7 shows typical trends in FWHM when pulse potential was varied and pressure, pulse width, and frequency were held constant. Pulse potential does not appear to have an appreciable impact. If there is any trend, it is towards slightly improved resolution at higher potentials. Consequently, it is best to use high potentials to maximize signal.

3.3.5 Pressure

Figure 3-8 shows how FWHM varies with pressure while pulse width, frequency, and potential are held constant. The FWHM narrows significantly as pressure is raised from 1.25 to 2.5 torr, but declines only slightly between 2.5 and 3.0 torr. The trend fits well to

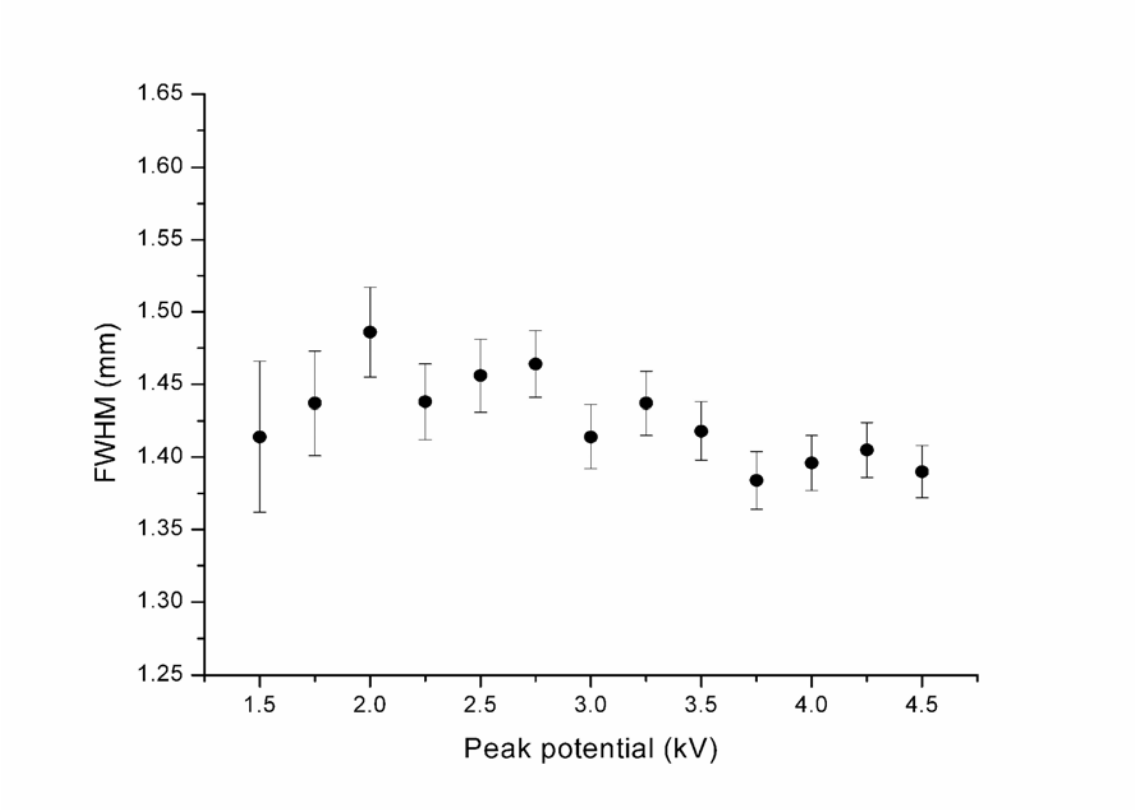

Figure 3-7. Effect of applied pulse potential on spatial resolution. 2.0 μs pulse, 2.5 torr, 100 Hz.

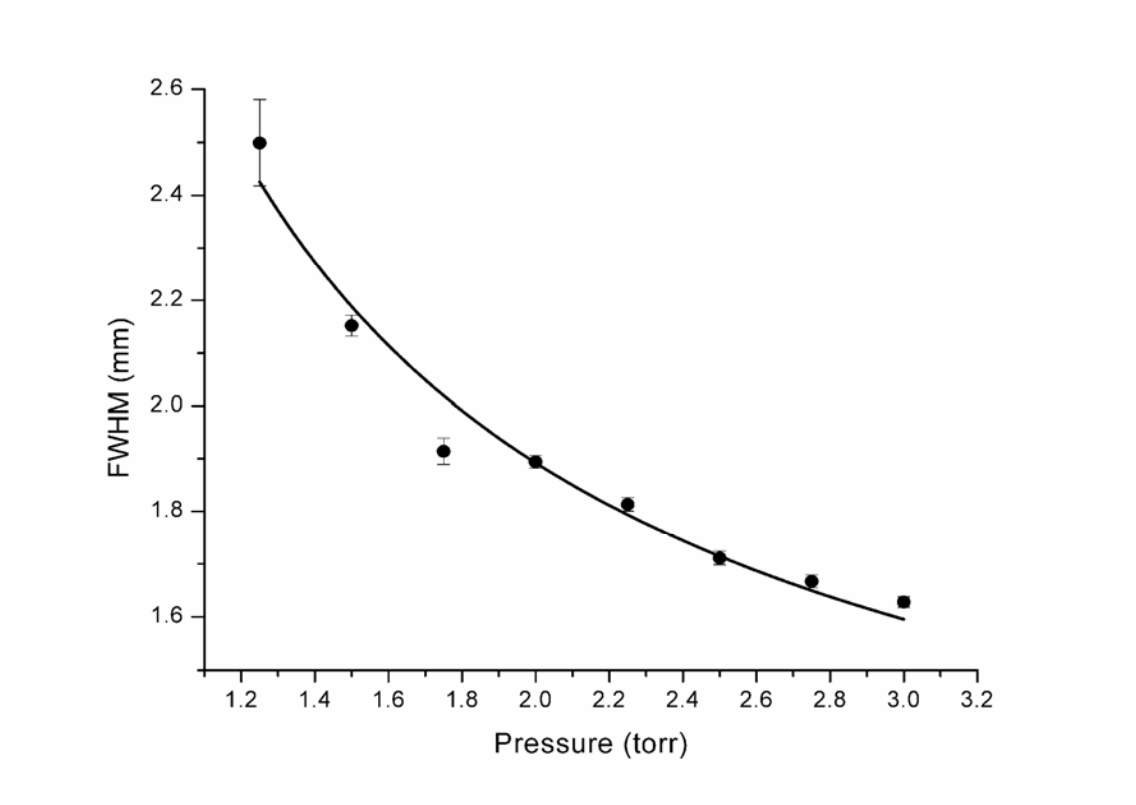

Figure 3-8. Effect of pressure on spatial resolution. Solid line is a 1/x fit to the data. 3.0-µs pulse, 3.0 kV, 100 Hz.

a 1/p dependence. This behavior likely has two related causes: diffusion and stopping distance. The exact contribution of diffusion to the relationship between pressure and profile width is complicated by the geometry of the cell and the relationship between intensities (summed perpendicular to the sample surface and over time) and actual concentrations. Further, the local gas density and temperature vary over the course of a discharge pulse.[23] Nonetheless, we can safely say that, because the diffusion coefficient is inversely proportional to pressure, the profile width should be greater at lower pressure, which is what is observed. Before moving by diffusion, however, the sputtered atoms travel a finite distance because of the momentum they receive during sputtering.[24] This distance is inversely proportional to number density in the ambient atmosphere, so it should be inversely proportional to pressure under otherwise fixed conditions. Again, the exact effect of this on profile width is difficult to establish, but it should be in the same direction as is observed. Whatever the relative contributions of the two causes, the results suggest that pressure should be kept above 2.5 Torr to optimize resolution, but that above this point pressure has a diminishing impact on resolution.

3.3.6 Pulse width

The FWHM was found to broaden with applied pulse width. As Figure 3-9 shows, the trend is well fit by a $t^{½}$ dependence. With shorter pulses, atoms do not have time to travel far before the pulse terminates, so their distribution during the time that they can be excited and emit is narrow. When longer pulses are employed, the sputtered atoms can travel farther during the time when energy is available for excitation, so their distribution during the time when they can emit is broader. Because average diffusion distance

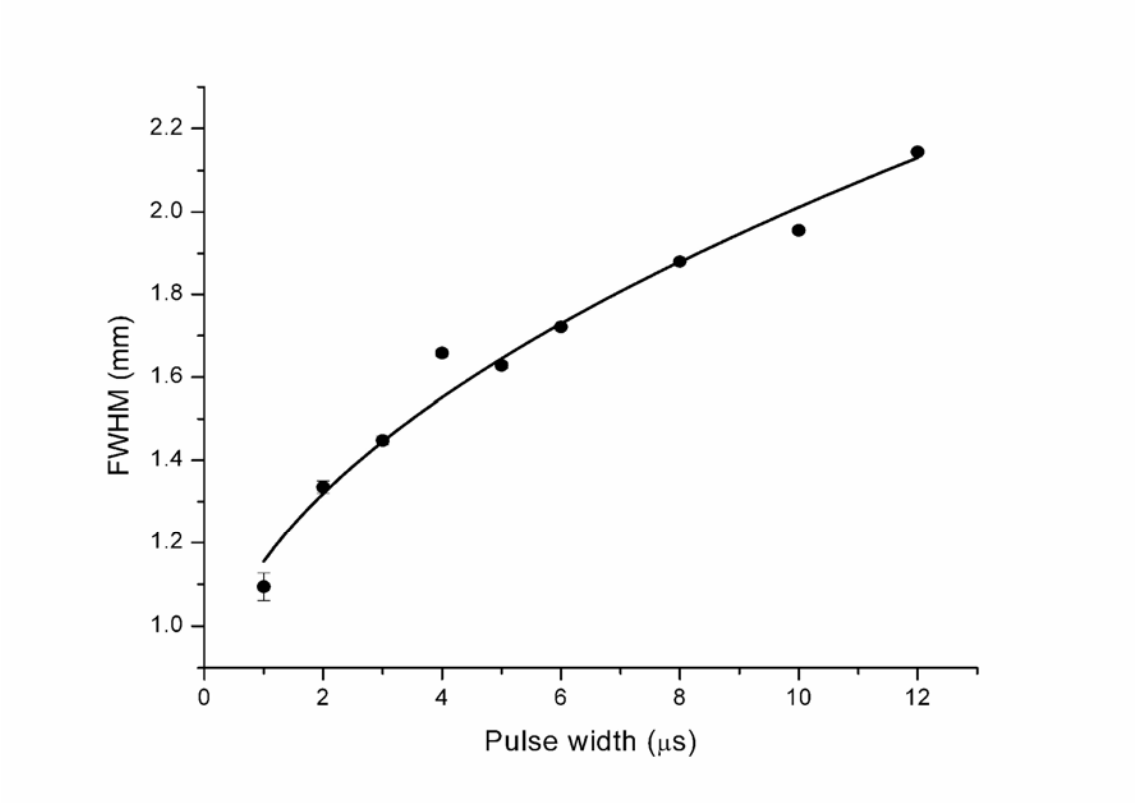

Figure 3-9. Effect of pulse width on spatial resolution. Solid line is a $x^{1/2}$ fit to the data. 2.0 kV 3.0 torr, 100 Hz.

follows a $t^{1/2}$ dependence, the FWHM would be expected to have a similar dependence if the emission occurred entirely at the end of the pulse. Although emission occurs throughout and even after the pulse, a $t^{1/2}$ dependence still fits the data well.

Short pulse widths mean that there is a correspondingly brief amount of time that energy is being put into the glow discharge, but emission can continue a short time after the pulse. Gated detection might further improve resolution by limiting observation of the emission to a selected period.

3.3.7 Evaluation of optimized conditions and potential for improvement

Pulses of 1 μs, 100 Hz, 4.0 kV, and a pressure of 3.5 torr, were chosen based on the results of the experiments above. The Cu pin itself was measured under magnification to be 1.02 ± 0.03 mm (FWHM) in diameter. This uncertainty results mainly from the fact that the pin is not perfectly circular. The emission peak over the pin was measured to be 1.00 ± 0.01 mm. Given the resolution of the optical system and the slight asymmetry of the pin, better results cannot be expected. Further refinements in the technique would first require a higher-resolution optical system and a smaller, more regularly shaped inclusion.

3.4 CONCLUSIONS

Glow discharge-optical emission spectrometry has been successfully used to image an inhomogeneity in elemental distribution. Using pulsed powering rather than dc greatly improved the resolution. Pulse width, pulse repetition rate, and pressure were found to have a significant impact on the resolution obtainable by the system. The effect of these

parameters was traced to atom transport. Under optimized conditions, the width of a 1 mm copper insertion corresponded to the FWHM of the emission above it to better than 100 μm accuracy. Limitations that are not inherent to the technique prevented resolution better than this level.

The obvious use of this technique is to add two dimensions to the analysis of conductive solids. With depth profiling, this capability would allow three-dimensional analysis of elemental distributions. Other uses may not be as obvious. One factor that limits attainable depth resolution in glow discharge spectrometry is the shape of the sputtering crater. Although the center of the crater might be flat, its edges can curve upwards or downwards.[8-9] When this is the case, worse depth resolution results because different depths are being sputtered at the edges than at the center. By using short pulses and observing only emission from the central portion of the discharge, the depth resolution might be improved. The technique could also be expanded to non-conductive samples by applying radio-frequency energy gated with μs-pulses. Research into this avenue is ongoing in our laboratory, with promising results.

Particularly if gated detection were used, this technique could be used to further examine analyte transport in a glow discharge. A small insertion would limit the initial position, a brief pulse would limit the initial time, gated detection would limit the final time, and spatially resolved detection (either of emission or another signal such as fluorescence) would establish the final position.

3.5 REFERENCES

[1] T. Cserfalvi, P. Mezei and P. Apai, "Emission studies on a glow discharge in atmospheric pressure air using water as a cathode", *J. Phys. D-Appl. Phys.*, 1993, **26**, 2184.

[2] W. C. Davis and R. K. Marcus, "An atmospheric pressure glow discharge optical emission source for the direct sampling of liquid media", *J. Anal. Atom. Spectrom.*, 2001, **16**, 931.

[3] M. A. Dempster and R. K. Marcus, "Analysis of amino acids and organometallic compounds by particle beam-hollow cathode glow discharge atomic emission spectrometry", *J. Anal. At. Spectrom.*, 2000, **15**, 43.

[4] M. R. Webb, F. J. Andrade, G. Gamez, R. McCrindle and G. M. Hieftje, "Spectroscopic and electrical studies of a solution-cathode glow discharge", *J. Anal. At. Spectrom.*, 2005, **20**, 1218.

[5] C. L. Lewis, M. A. Moser, D. E. Dale, Jr., W. Hang, C. Hassell, F. L. King and V. Majidi, "Time-gated pulsed glow discharge: Real-time chemical speciation at the elemental, structural, and molecular level for gas chromatography time-of-flight mass spectrometry", *Anal. Chem.*, 2003, **75**, 1983.

[6] T. K. Starn, R. Pereiro and G. M. Hieftje, "Gas-sampling glow discharge for optical emission spectrometry. Part I: Design and operating characteristics", *Appl. Spectrosc.*, 1993, **47**, 1555.

[7] C. Yang, K. Ingeneri, M. Mohill and W. W. Harrison, "Factors influencing signal profiles in microsecond pulsed glow discharge atomic emission spectrometry", *Anal. Chem.*, 1999, **71**, 5328.

[8] Y. Su, P. Yang, Z. Zhou, X. Wang, F. Li, B. Huang, J. Ren, M. Chen, H. Ma and G. Zhang, "Feasibility of applying microsecond-pulse glow discharge time of flight

mass spectrometry in surface depth analysis", *Spectrochim. Acta, Part B*, 1998, **53B**, 1413.

[9] M. Parker, M. L. Hartenstein and R. K. Marcus, "Influence of Discharge Parameters on the Resultant Sputtered Crater Shapes for a Radio Frequency Glow Discharge Atomic Emission Source", *Anal. Chem.*, 1996, **68**, 4213.

[10] W. W. Harrison, C. Yang and E. Oxley, "Pulsed glow discharge", *Anal. Chem.*, 2001, **73**, 480A.

[11] M. R. Winchester and M. L. Salit, "Design and initial characterization of a glow discharge atomic emission instrument for macro-scale elemental composition mapping of solid surfaces", *Spectrochim. Acta, Part B*, 1995, **50B**, 1045.

[12] L. M. Cabalin, M. P. Mateo and J. J. Laserna, "Large area mapping of non-metallic inclusions in stainless steel by an automated system based on laser ablation", *Spectrochim. Acta, Part B*, 2004, **59B**, 567.

[13] M. P. Mateo, L. M. Cabalin and J. J. Laserna, "Automated line-focused laser ablation for mapping of inclusions in stainless steel", *Appl. Spectrosc.*, 2003, **57**, 1461.

[14] J. Cheng, R. Eriksson and P. Jonsson, "Determination of macroinclusions during clean steel production", *Ironmaking Steelmaking*, 2003, **30**, 66.

[15] L. Zhang, B. G. Thomas, X. Wang and K. Cai, "Evaluation and control of steel cleanliness - review", *Steelmaking Conference Proceedings*, 2002, 85th, 431.

[16] V. Hoffmann and G. Ehrlich, "Investigations on the lateral distribution of the emission line intensities in the plasma of a Grimm-type glow discharge source", *Spectrochim. Acta Part B*, 1995, **50B**, 607.

[17] M. R. Winchester, "Optically induced analytical error in glow discharge optical emission spectrometry", *Appl. Spectrosc.*, 1996, **50**, 245.

[18] J. W. Olesik and G. M. Hieftje, "Optical imaging spectrometers", *Anal. Chem.*, 1985, **57**, 2049.

[19] M. R. Webb and G. M. Hieftje, "An improved monochromatic imaging spectrometer", *Appl. Spectrosc.*, 2006, **60**, 57.

[20] A. Bogaerts and R. Gijbels, "Modeling of a microsecond pulsed glow discharge: behavior of the argon excited levels and of the sputtered copper atoms and ions", *J. Anal. At. Spectrom.*, 2001, **16**, 239.

[21] A. Bogaerts and R. Gijbels, "Three-dimensional modeling of a direct current glow discharge in argon: is it better than one-dimensional modeling?" *Fresenius' J. Anal. Chem.*, 1997, **359**, 331.

[22] J. Pisonero, K. Turney, N. Bordel, A. Sanz-Medel and W. W. Harrison, "A double microsecond-pulsed glow discharge ion source", *J. Anal. At. Spectrom.*, 2003, **18**, 624.

[23] A. Bogaerts and R. Gijbels, "Hybrid Monte Carlo - fluid model for a microsecond pulsed glow discharge", *J. Anal. At. Spectrom.*, 2000, **15**, 895.

[24] R. S. Mason and M. Pichilingi, "Sputtering in a glow discharge ion source - pressure dependence: theory and experiment", *J. Phys. D-Appl. Phys.*, 1994, **27**, 2363.

Chapter 4

Spectroscopic and electrical studies of a solution-cathode glow discharge.

4.1 INTRODUCTION

Glow discharges have attracted increasing interest in recent years.[1] Both a cause and a result of this interest has been a broadening of samples that can be analyzed and an improvement in analytical performance. Gas-sampling discharges have permitted the analysis of flowing gases, and radio-frequency powering schemes have enabled the analysis of nonconductive solids and offered some advantages such as more rapid stabilization in the analysis of conductive solids.[1-2] Pulsed discharges have enhanced ionization and emission, improved signal-to-background discrimination through gated detection, improved depth resolution, and allowed molecular analysis of gases.[1-3-4]

Liquid samples present a greater challenge. Although cathodic sputtering introduces material from solid samples into the bulk of the discharge primarily as atoms, the relatively low gas temperatures are insufficient to desolvate liquid samples introduced into the bulk of the discharge. Additionally, water-related species lower the metastable population in the negative glow. For these reasons, most techniques have focused on drying a solution before introducing it into the glow discharge. Most commonly, this has been done by drying the sample onto a surface which is then used as the glow discharge

cathode. However, particle-beam devices and other nebulizers have also been used to desolvate flowing samples for analysis.[1-5-6] To preserve the glow discharge advantage of simplicity, a technique with comparable or superior performance but without the complexity of desolvation would be preferable.

The foundations for such a technique were laid down over a century ago, when Gubkin[7] introduced glow discharge electrolysis (GDE), a system in which a grounded electrolytic solution acts as the glow discharge cathode. In his studies and those that would follow over the next century, the focus was on the electrochemical reactions in the system, although Couch and Brenner[8] did observe emission from certain elements in the plasma. In recent years, GDE has also been used for surface modification.[9-10] The first use of GDE for analytical spectroscopy was in 1993 by Cserfalvi and co-workers,[11] who found that atomic emission was substantially enhanced at low pH. Their basic design consists of a glass capillary emerging upwards from a reservoir of electrolytic solution and a sample solution overflowing from the capillary into the reservoir. A glow discharge is sustained between the solution exiting the capillary and a metal anode a few millimeters above it. The pool of solution is grounded, and the electrical connection to the capillary exit is through the overflow, or a combination of the overflow and a salt bridge connecting the pool of solution to the solution within the capillary. In later papers, this design of GDE has been described as an electrolyte-cathode discharge (ELCAD).[12-26] Because of the necessity of the overflow connection in most designs, and because typical sample consumption is in the mL/min range, flow rates below 1.5 mL/min have not been reported and flow rates of about 8 mL/min are typical.

Variations on this idea have been introduced. A liquid-sampling atmospheric pressure glow discharge (LS-APGD) is designed similarly, but lacks the solution reservoir and instead uses a metal capillary in place of the glass one to electrically connect the solution.[27-29] It is not clear whether this difference fundamentally changes the discharge's mechanism. Moderate detection limits, all in the single parts per million range, have been reported for only a few elements so far, but LS-APGD solution flow rates can be significantly lower than ELCAD flow rates, and are typically less than 1 mL/min. A drop-spark discharge (DSD), which replaces the metal anode with a dripping electrolytic anode, is a pulsed source that operates similarly to the ELCAD.[26] Porous materials have also been used to create liquid-to-liquid discharges, but these discharges have not been used for analytical purposes and have exhibited quite different electrical characteristics.[30] Current fluctuations in a GDE system of a different design have also been used to detect both electrolytic and non-electrolytic compounds in a flowing sample.[31] A miniaturized ELCAD operating with sample flows below 5 µl/min has been described, but the source suffers from significant instabilities and analytical performance has not yet been reported.[32]

One attraction of a glow discharge source for solid sample analysis is its relatively low cost. ELCAD promises similar benefits. Notably, emission was enhanced in an air atmosphere compared to He or Ar atmospheres and detection limits were improved with an open system compared with a closed one.[18-20] Power requirements are low (typically under 75 W), a moderate resolution monochromator can be used due to a fairly uncomplicated spectrum, and the source itself is extremely inexpensive. Despite this low

cost and the relative newness of ELCAD, reported detection limits mostly fall in the tens of parts per billion, with a few in the single parts per billion range.[23-24]

However, the characterization of the source is far from complete and there are limitations in its current form. The robustness of ELCAD is not yet known and there is disagreement about its operating mechanism.[9-13-25-28-29-33] Although the sample flow rate has been reduced since the technique's introduction, the 3-4 mL/min optimum found in a recent study is still several times higher than the eluent flow from a typical liquid chromatograph.[24] Further research characterizing the source in terms of its strengths, limitations, and mechanisms is clearly needed.

4.2 EXPERIMENTAL

A representation of the source cell is shown in Figure 4-1. This cell is simpler than the design of most other ELCAD cells. The solution enters the cell through a 1-mL serological pipette that has been bent so the tip points upwards. Above this tip is a 1.6-mm diameter Ti anode to which a positive potential is applied through a 400-Ω ballast resistor. The solution overflows from the tip into an approximately 35 mL reservoir containing a grounded graphite electrode. This overflow creates an electrical connection between the solution at the pipette's tip and the graphite electrode. The position of the Ti anode is reproducibly controlled by means of a micrometer stage. To initiate the discharge, the anode is brought near (approximately 1 mm) the solution while a high potential (1-2 kV) is applied to it; however, a Tesla-coil spark can also be used. A rectangular black polyethylene divider supported by the pipette serves multiple purposes.

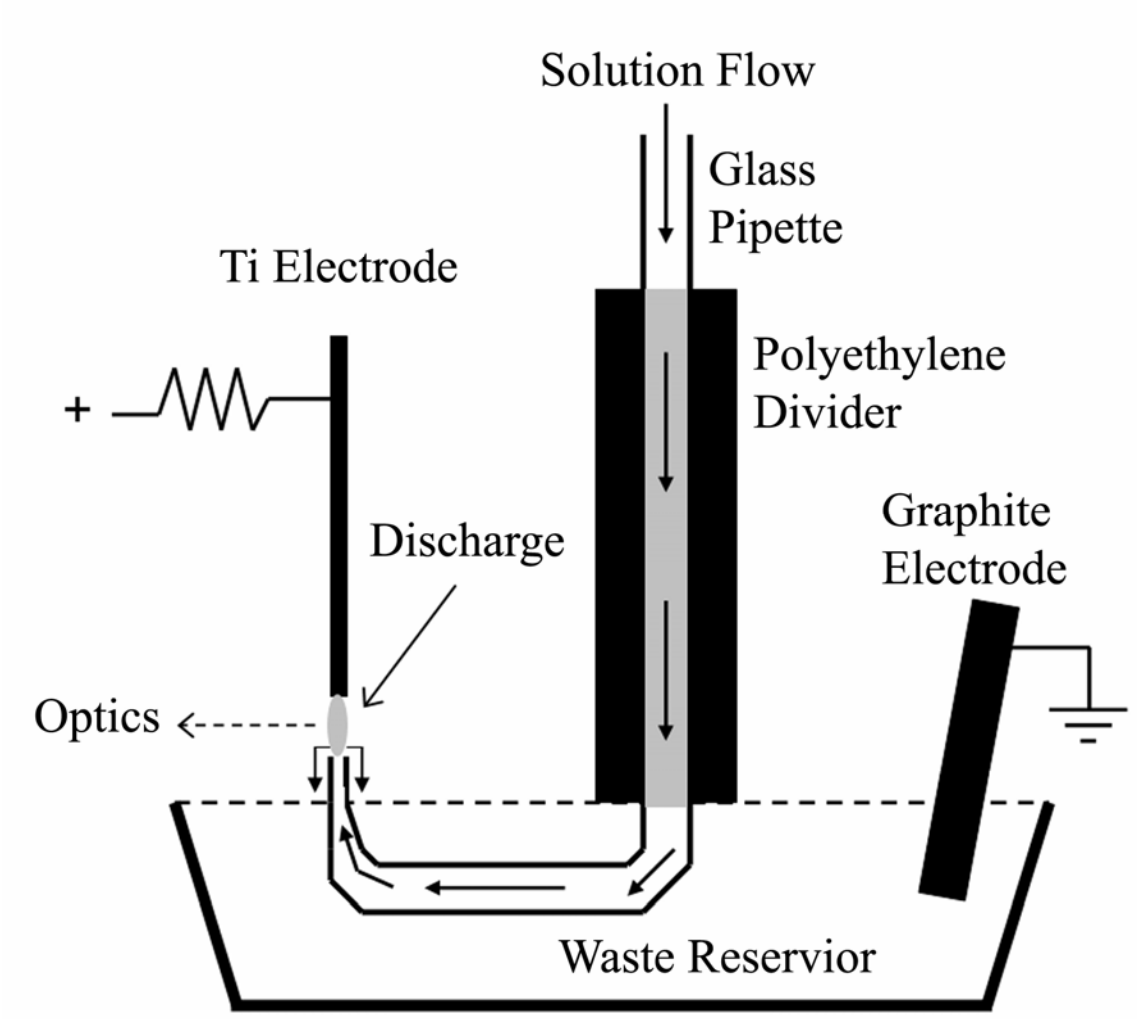

Figure 4-1. Diagrammatic representation of solution-cathode glow discharge.

It reduces the amount of hydrogen (produced at the graphite cathode) that reaches the discharge by impeding its path through the air, it blocks some background light from sources external to the discharge, and it wicks moisture over the sides of the reservoir so a constant solution level is maintained within the reservoir. The hydrogen is blocked intentionally because its presence has been known to lower emission in other glow discharges; the light is blocked to reduce background noise; and the reservoir level is held constant to prevent fluctuations in the voltage between the pipette tip and the graphite cathode.

The sample solution is supplied by a syringe pump (Harvard Apparatus PHD 2000 (Holliston, MA)) at a typical flow of 3.5 mL/min. The discharge is powered by a Kepco (Flushing, NY) BHK 2000-0.1MG high-voltage power supply operated in constant-current mode, typically at 80 mA. For a similarly designed cell, the effects of geometry and flow on the resistive drop between the pipette tip and the location of the graphite electrode were studied without a discharge present. A Cole-Palmer (Chicago, IL) Digital Conductivity Meter model 1481-60 with custom platinum electrodes was used for these measurements. The resistance of a material is directly proportional to its length and inversely proportional to its cross-sectional area. The resistance of the cell was found to be directly proportional to the height of the pipette tip above the solution in the reservoir (i.e. the length of the overflow connecting the solution at the tip to the bulk solution in the reservoir) and inversely proportional to the solution flow rate (as flow increases, the cross-sectional area of the overflow increases). To keep the resistance relatively low, the pipette tip was raised only 2 mm above the edge of the reservoir (approximately 3 mm

above the reservoir solution when the discharge is operating). The same conductivity meter attached to a Cole-Palmer (Chicago, IL) 1481-62 dip cell was used to measure solution conductivities.

The discharge was imaged 2.3:1 with a quartz lens onto the entrance slit of a 0.5-m Czerny-Turner spectrometer (Chromex 500IS/SM (Albuquerque, NM)). The spectrometer could be switched between operation as a monochromator with a PMT detector (Hamamatsu (Hamamatsu, Japan) R928 biased at -850 V) and operation as a spectrograph with a CCD detector (Roper Scientific, Trenton, NJ, model CH350A). Signals from the PMT were amplified by a Keithley (Cleveland, OH) 427 current amplifier. The output of this amplifier was recorded with a custom National Instruments (Austin, TX) LabVIEW program that also controlled the monochromator. Use of the CCD allowed wavelength resolution in the horizontal direction and spatial resolution in the vertical direction. This vertical position was calibrated by imaging the visible glow of the anode. Images were acquired with WinView/32 (Roper Scientific (Trenton, NJ)) and processed with Digital Optics (Auckland, New Zealand) V++ 4.0.

As approximations for the gas-kinetic and electron temperatures, OH rotational and Fe excitation temperatures, respectively, were determined. The OH rotational temperatures were calculated based on the rotational fine structure of the ($A^2\Sigma^+ \rightarrow X^2\Pi_i$) OH band at 306.4 nm by means of a Boltzmann plot.[34] Fe excitation temperatures were calculated similarly from atomic emission lines between 371 and 386 nm.[35]

4.3 RESULTS AND DISCUSSION

4.3.1 Spectral and electrical characterization

To verify that the simplified cell design does not adversely affect its performance, its electrical and spectroscopic characteristics were compared to those published for other designs.

The current-voltage behavior at discharge gaps from 1-4 mm is shown in Figure 4-2. In a normal glow discharge, the voltage stays nearly constant, and the discharge covers an increasing amount of the cathode as current is raised. In contrast, an abnormal glow discharge, the type ordinarily used in atomic spectroscopy, requires a greater voltage in order to produce a higher current, because of a restricted cathode area. In the present design, the cathode is completely covered over the entire range of currents used, so the discharge exhibits clearly abnormal behavior. The degree of abnormality varies among cells presented in the literature because early devices used a cathode large enough that it was not completely covered by the discharge. Also analogously to a metal-metal glow discharge, the required voltage to maintain a given current increases with the gap between the electrodes. In this system, this trend is linear (see Figure 2-2).

The continuous-flow limits of detection achieved with the present cell are shown in Table 4-1 alongside the best values reported in the literature, when available. These values were determined by using a PMT to collect emission from the lower (cathode-side) approximately 2.5 mm of the discharge. Emission from the region above this zone was blocked by affixing electrical tape to the spectrometer entrance slit. As has been

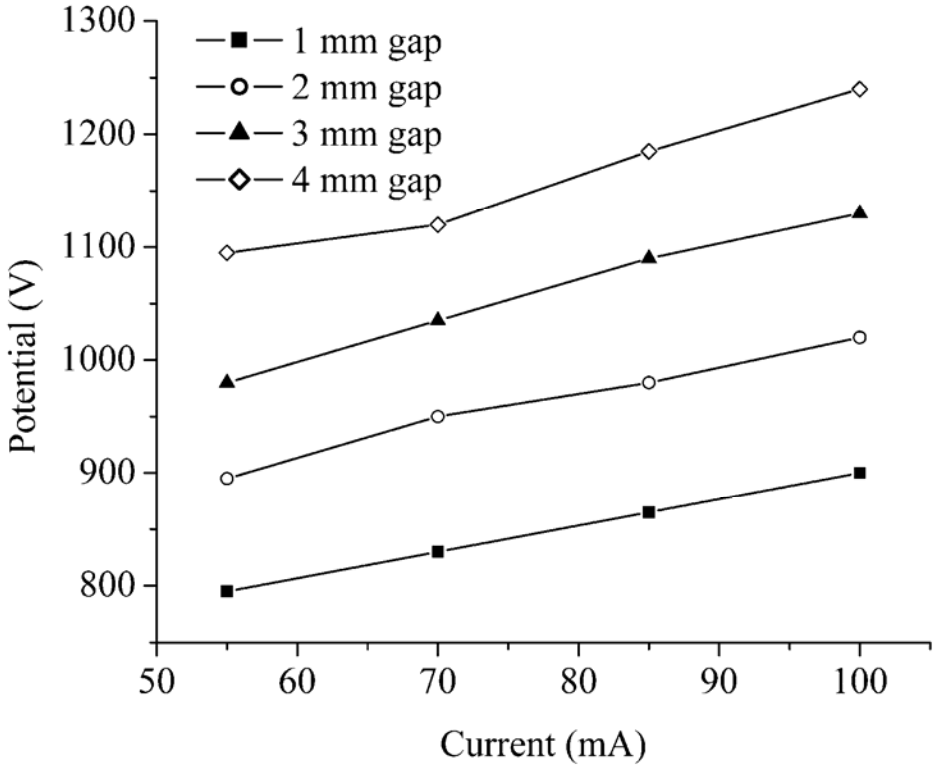

Figure 4-2. Effect of discharge current on applied potential for various discharge gaps.

Table 4-1. Limits of detection for the solution-cathode glow discharge. Solution pH = 1, electrolyte = HNO_3, solution flow rate = 3.5 mL/min, discharge current = 80 mA, discharge gap = 3 mm, sampling at 50 Hz for 10 seconds

		LOD (ppb)		
Analyte	Wavelength (nm)	Present work	Best reported	Flow-injection [d]
Cd	228.8	9	30 [a]	21
Cu	324.7	31	10 [a]	33*
Zn	213.9	42	300 [b]	24
Pb	368.3	82	10 [a]	42*
Ni	341.5	110	20 [c]*	51
Hg	253.7	349	80 [a]*	
K	766.5	13	1 [a]	
Mn	279.5	30	30 [c]*	
Mg	285.2	19	1200 [b]*	
Ca	422.7	23	600 [b]	
Na	589.0	0.8	1 [a]	
Cs	852.1	211		
Ag	338.3	5		
Sr	460.7	49		
Au	242.8	78		
Li	670.8	8		

[a] from Ref. [22].

[b] from Ref. [12], adjusted to 3σ definition.

[c] from Ref. [21].

[d] from Ref. [23], adjusted to 3σ definition.

* Previously used wavelength differs from present work.

previously found,[24] blocking the anode area is useful because of the blackbody radiation it emits. Additionally, as will be shown, blocking the area immediately below the anode reduces the N_2 background without substantially lowering most analyte emission. Detection limits were calculated based on the variance of the emission from a blank (50 Hz sampling for 10 seconds) compared to the emission from a solution containing between 100 and 1000 ppb (averaged sampling at 50 Hz over 10 seconds), depending on the sensitivity of the technique for that element. Similar to other studies,[20] we found that a 2-3 minute period was required for stabilisation after initiating the discharge, so we waited at least 8 minutes between starting the discharge and acquiring data. Also included for comparison are the limits of detection for flow-injection from a recent study.[24] Several literature values have been adjusted to the 3σ definition of detection limits for a fairer comparison. As Table 4-1 shows, the detection limits found with the present system are comparable to those found with earlier ones.

Likewise, the spectrum of this source (shown in Figures 4-3 and 4-4) resembles spectra found in the literature.[11-12-18-20-22] Unlike for many atomic spectroscopy sources, there is little background emission below 260 nm. Above this wavelength, there are several OH bands, with bandheads at 260.9, 281.1, and 306.4 nm. Next there is the N_2 second positive system, with bandheads visible from 337.1 to 405.9 nm. Additional bandheads are masked by OH emission at shorter wavelengths. A series of O II lines spreads from 391.2 to 470.1 nm. Beyond this, there are the Hβ (486.1 nm) line, the Hα (656.3 nm) line, and three O I lines (777.2, 777.4, & 777.5 nm), as well as Na I (589.0 & 589.6 nm) and K I (766.5 & 769.9 nm) lines from impurities in the blank solution.

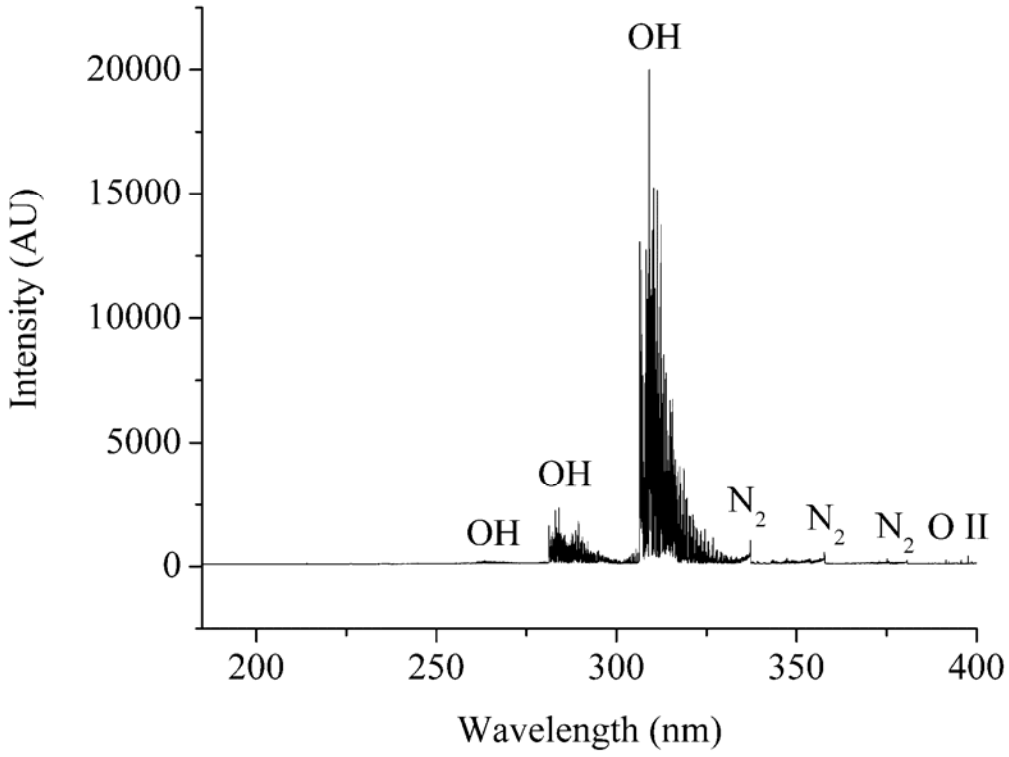

Figure 4-3. Background spectrum from 185 to 400 nm. Solution pH = 1, electrolyte = HNO_3, solution flow rate = 3.5 mL/min, discharge current = 80 mA, discharge gap = 3 mm.

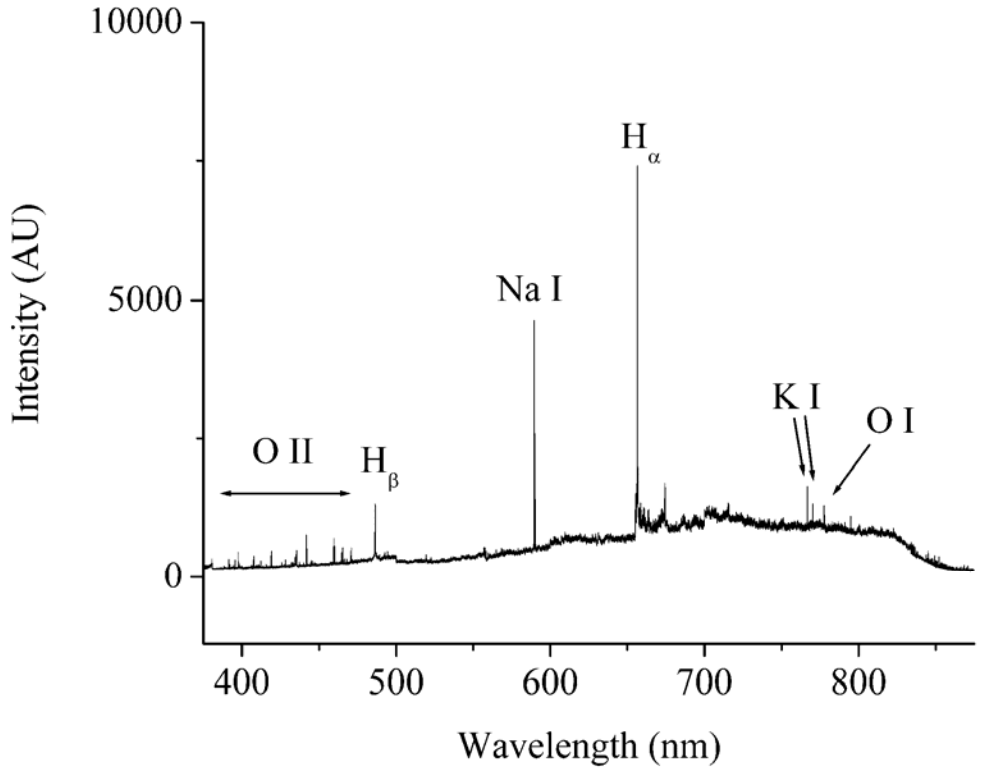

Figure 4-4. Background spectrum from 376 to 875 nm. Solution pH = 1, electrolyte = HNO_3, solution flow rate = 3.5 mL/min, discharge current = 80 mA, discharge gap = 3 mm. A long-pass filter was used from 500 to 655 nm to block second-order radiation at 250 to 327 nm.

In Figure 4-4, a long-pass filter was used from 500 to 655 nm to block second-order emission from OH.

4.3.2 Vertical distributions of emission and temperatures

In a typical analytical glow discharge, there are two regions of strong emission, separated from each other and from the electrodes by regions of weak or no emission. In order from the anode to the cathode, these regions are the anode dark space, the positive column, the Faraday dark space, the negative glow, and the cathode dark space. The positive column is less intense than the negative glow, but is often spatially much larger. Some parallels can be drawn between these zones and the regions observed in the present source, but there are also significant differences.

The vertical distributions of emission from several background species are shown in Figure 4-5. In these profiles, as well as in others, it can be noted that some emission appears to arise from above the anode (positions less than 0 mm) and below the cathode (positions greater than 3 mm). This pattern arises from three factors: the electrodes are cylindrical, so the plasma can, and does, extend around and in front of them; the cathode, being composed of water, is somewhat reflective; and the spatial resolution of the detection system is imperfect.

For the O I and O II traces, the current was 80 mA, the solution flow rate was 3.5 mL/min, the discharge gap was 3 mm, and the solution was acidified to pH 1.35 with nitric acid. For other species, the conditions were the same except that the current was 85 mA and the flow rate was 3 mL/min. The N_2 second-positive system bands are most

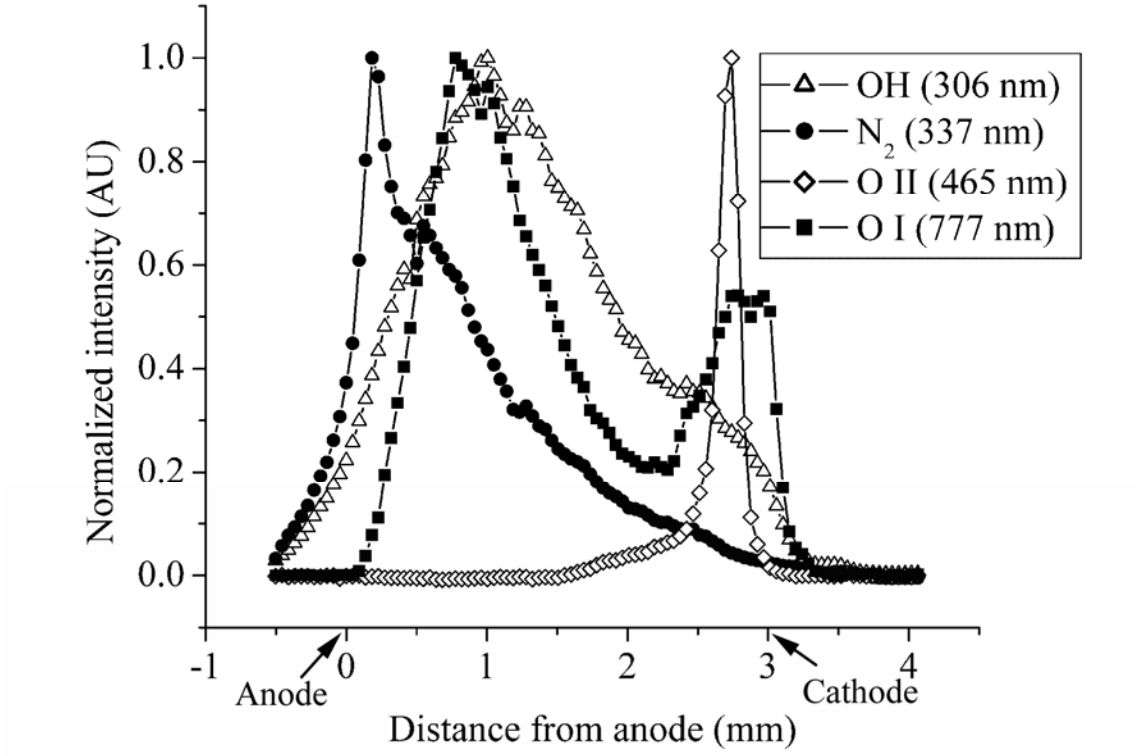

Figure 4-5. Vertical distributions of emission from background species. Anode located at 0 mm. Cathode located at 3 mm.

intense near the anode end of the positive column, and their intensity falls off smoothly in both directions. The OH emission intensity shows two regions, the negative glow and the positive column, but no observable Faraday dark space between them. The OH intensity in the positive column reaches nearly three times that of the negative glow. Neutral oxygen also shows two zones of emission, but with a distinct dip between them where the Faraday dark space would appear in a typical glow discharge. Here too, the positive column is more intense than the negative glow, by a factor of about two. Judged by the emission from analyte atoms, which will be shown later, the negative glow peak is near the cathodic edge of that region, and the emission actually extends slightly below the cathode. Singly-charged oxygen shows predominately one region of emission, also at the cathodic edge of the negative glow. There is weak O II emission in the rest of the negative glow and into the Faraday dark space, but no observable emission in the positive column.

Under the same conditions as were used for measurement of the non-oxygen background species, two temperatures were calculated. The Fe excitation temperature and the OH rotational temperature, the latter of which can be used as an approximation for the gas-kinetic temperature, are shown in Figure 4-6. The Fe excitation temperature is shown for only a portion of the gap. Near the anode, N_2 emission interferes with the Fe lines, and near the cathode, below the negative glow, Fe emission is too weak to permit an accurate calculation. It can be seen, however, that the Fe excitation temperature ranges from 2500 K to 5000 K over the observable region, and increases linearly from the anodic edge of the positive column through the negative glow. The OH rotational temperature

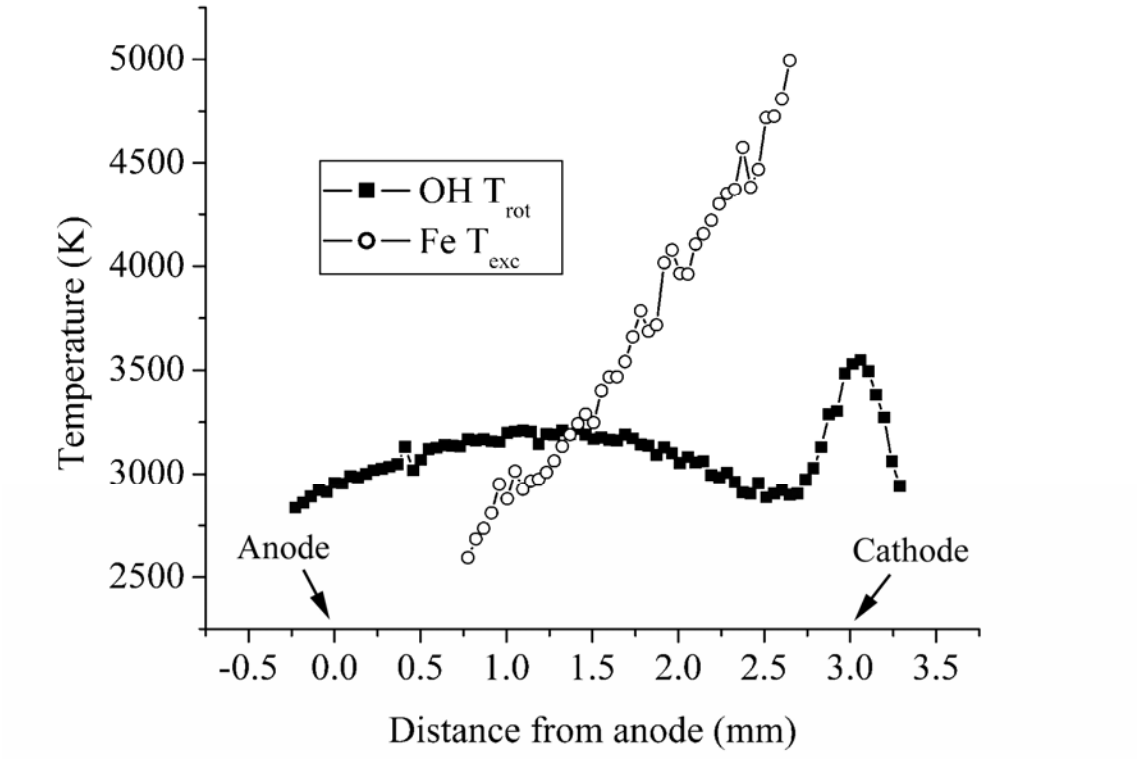

Figure 4-6. Typical OH rotational and Fe excitation temperatures. Anode located at 0 mm. Cathode located at 3 mm.

assumes a somewhat different shape. It peaks near the middle of the positive column, but is fairly constant at roughly 3000 K throughout most of the discharge. Below the negative glow, however, there is an increase in OH temperature to 3500 K that extends to the cathode before falling off. This high temperature near the cathode surface is consistent with that found in experiments and models in low pressure metal-metal glow discharges, which is attributed to this being the region where plasma species putting energy into the discharge gas have their highest energy.[36]

The vertical distributions of emission from analyte species vary by element and discharge conditions; examples are shown in Figures 4-7 through 4-9. For these measurements, the discharge current was 90 mA, the discharge gap was 3 mm, the solution flow rate was 3.5 mL/min, and the solutions were acidified to pH 1.35 with nitric acid. Some elements, such as Ba, Ca, Li, and Sr, exhibit a distinct dip in emission between the negative glow and the positive column, in the Faraday dark space. The relative intensities of these two regions vary by element, and the positive column intensity may even be greater than that of the negative glow. Other elements, such as K, Na, and Pb, have intense emission in the negative glow and weaker emission in the positive column, with no distinct dip in emission between these areas. Still others, such as Cu and Cd, have a positive column with intensity comparable to or greater than the intensity in the negative glow. Additionally, the positions of the peak negative glow emission and the minimum Faraday dark space emission, when that space is present, can vary by nearly 0.3 mm among elements.

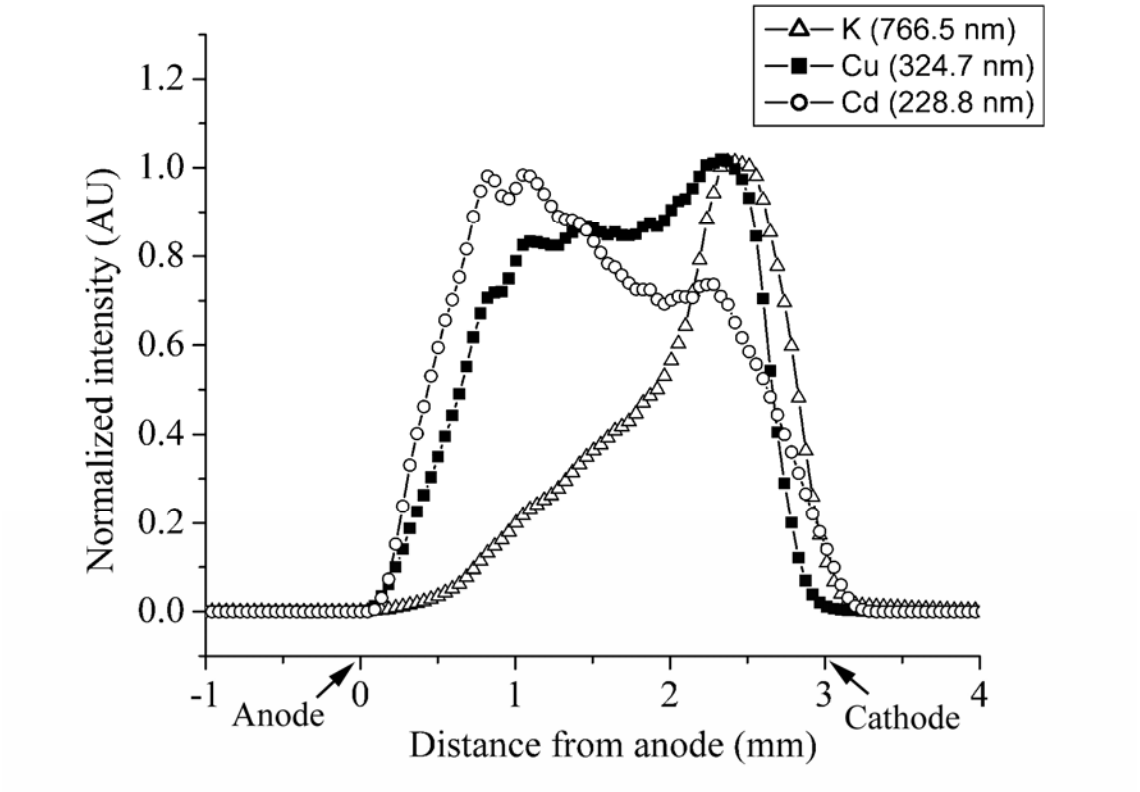

Figure 4-7. Vertical distributions of K, Cu, and Cd emission. Anode located at 0 mm. Cathode located at 3 mm.

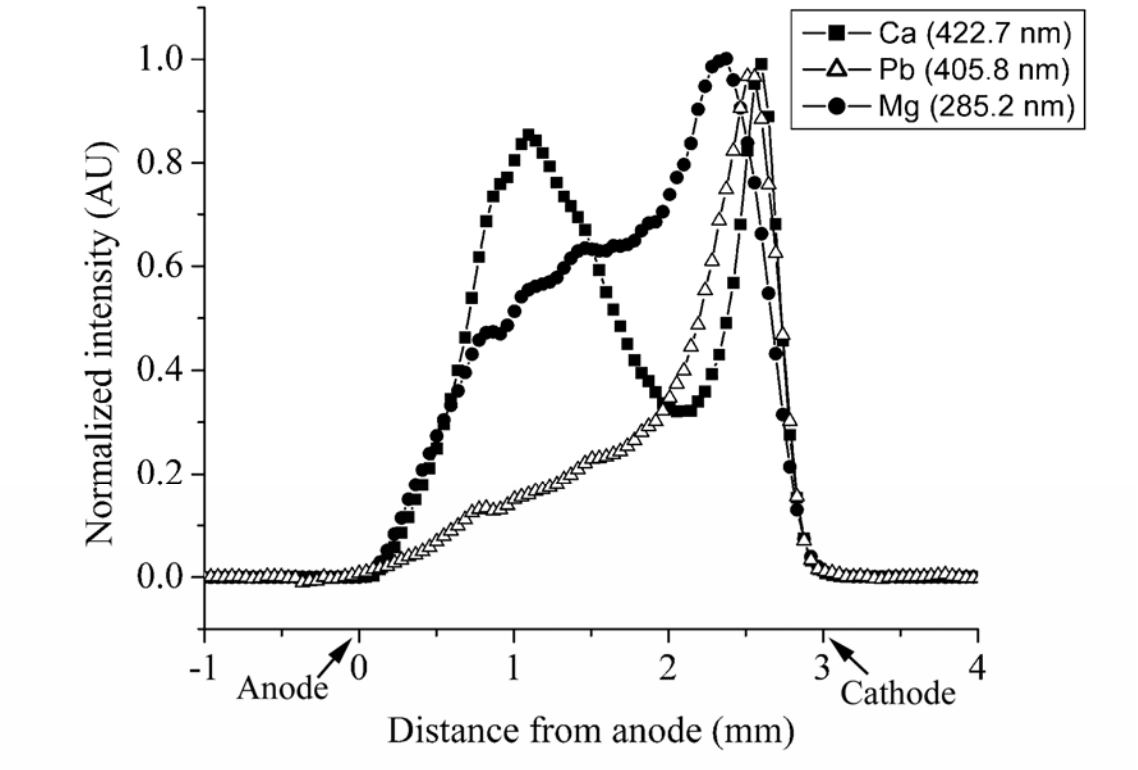

Figure 4-8. Vertical distributions of Ca, Pb, and Mg emission. Anode located at 0 mm. Cathode located at 3 mm.

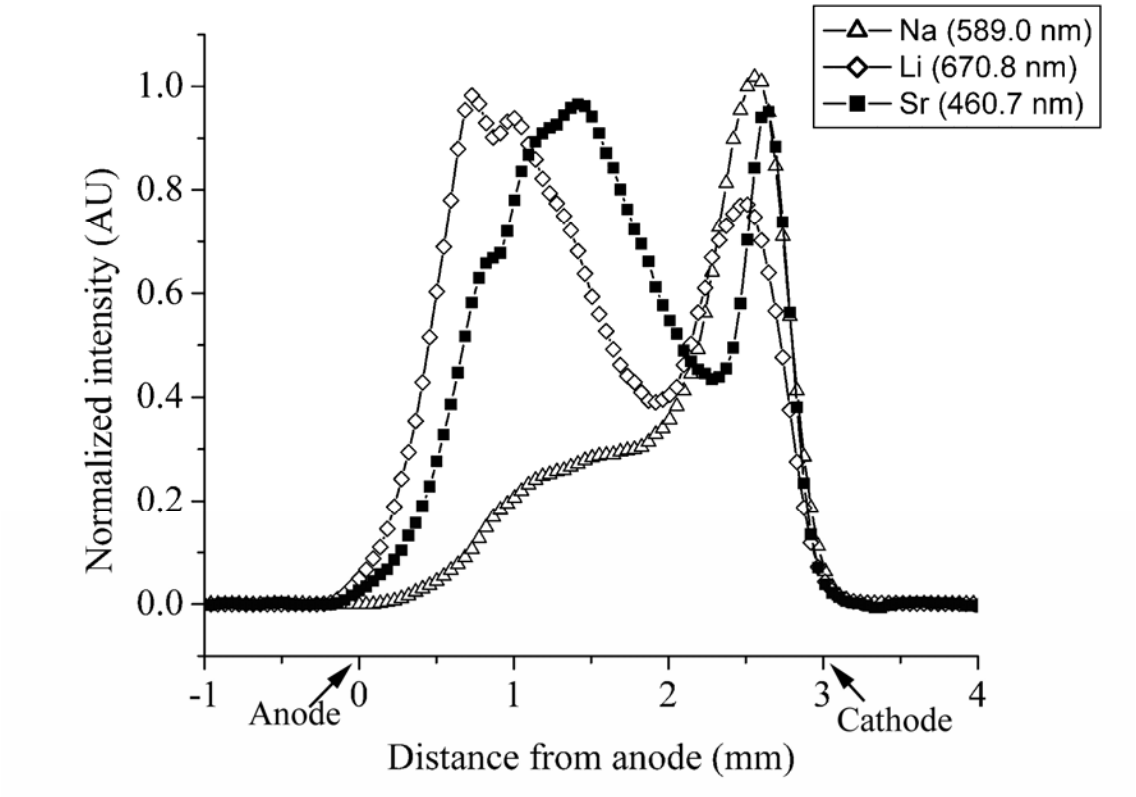

Figure 4-9. Vertical distributions of Na, Li, and Sr emission. Anode located at 0 mm. Cathode located at 3 mm.

It is important not to assign too much significance to these groupings, both because there are no sharp boundaries among them and because, as will be shown, changing conditions can move some elements from one group to another. The most important conclusions to draw are that the emission distributions vary by element and that the positive column is unexpectedly bright. We hypothesize that this behavior is related more to transport, desolvation, and atomization than to excitation. It seems likely that a significant portion of the analyte that does not exist as free atoms in the negative glow is atomized in or before the positive column.

4.3.3 Effect of source conditions on vertical distributions and electrical characteristics.

There have been several previous studies on the effects of pH on this type of source.[11-13-18-20-22-26] Overall, the emission was found to grow in intensity with decreasing pH. The apparent discharge voltage was found to rise sharply with pH at low pH, but to be nearly constant above pH 4.[11] The overall shape was roughly sigmoidal with an inflection point in the vicinity of pH 2.5. This shape has been attributed to a change in the cathode-fall potential with pH, and hypothesized to be the consequence of a two-mechanism system for electron emission, one dominant below pH 2.5 and the other dominant above pH 3.[11-13] It was noted, however, that the voltage drop across the solution (between the discharge and the graphite cathode) was not taken into account in these measurements. Accordingly, before addressing the effect of pH on vertical emission distributions, we should evaluate whether or not it is prudent to neglect this resistance.

A series of solutions adjusted to pH 0.8-1.9 with nitric acid was run through the cell

under the same operating conditions (3.6 mL/min, 3 mm discharge gap, 70 mA), and the potential required to maintain these conditions was measured. These solutions also contained 10 ppm Cu and Ca, as well as 1 ppm Na for the studies of vertical emission behavior that will be described later. The applied voltage was found to be inversely proportional to the solution conductivity and therefore directly proportional to the solution resistance, as shown in Figure 4-10. This pattern suggests that the effect of pH on potential is related to a change in the resistance of the solution rather than to a change in the cathode fall potential. To support this hypothesis, it would be desirable to track the trend with conductivity also at higher pH. However because of its geometry and flow rates, the present system requires a higher potential to maintain a given current than the systems used previously.[11] For this reason, solutions of pH greater than 2 cannot be analyzed. Instead, the conductivities of solutions in the pH range of 1 to 7.2 were measured, and the voltage that would be required to maintain the discharge was calculated, assuming that the trend found at low pH continued. Because the earlier study[11] used tap water acidified with sulfuric acid, the same was used here to better match that study. Figure 4-11 shows the predicted voltage as a function of pH. The potentials are higher due to the different geometry and flow rate, but the overall trend is the same. The graph can be fit by a sigmoidal function with an inflection point at pH 3.0, near the pH of ~2.5 observed in the earlier study. The difference in the initial composition of the tap water and the uncertainty in judging the inflection point visually from the earlier graph are likely responsible for part or all of this difference. The trend of the discharge voltage with pH appears to be attributable to the change in conductivity of the solution rather than to a change in the discharge potential.

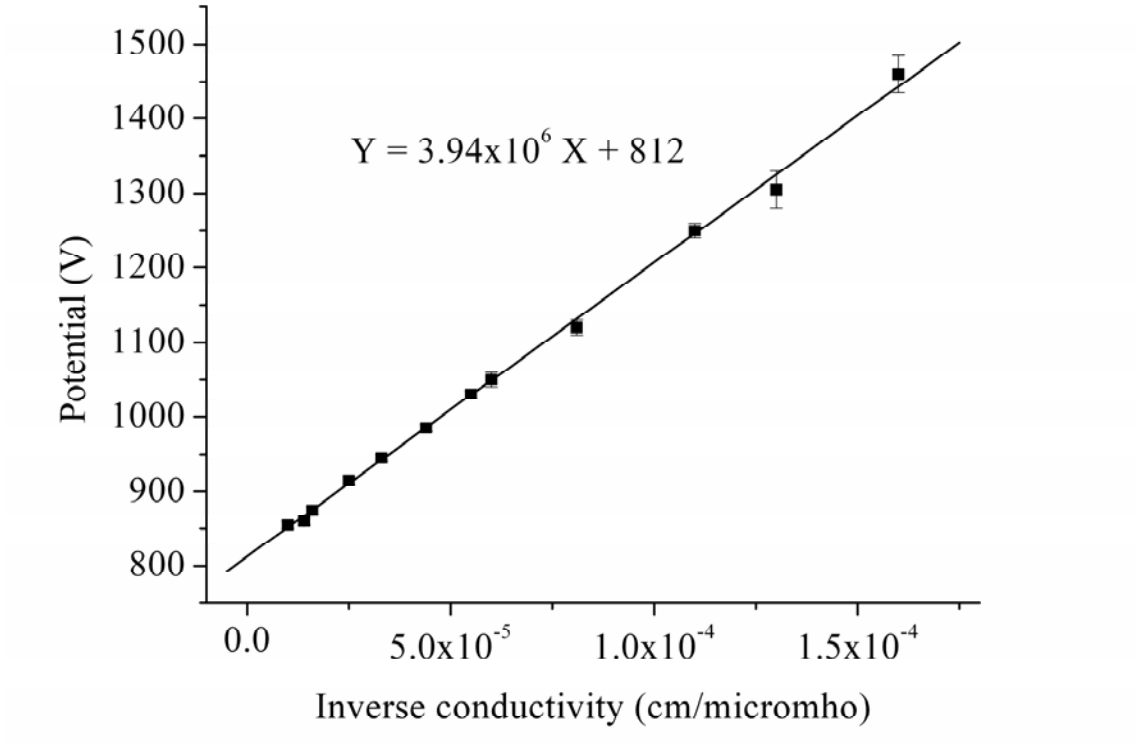

Figure 4-10. Effect of solution conductivity on applied potential. Electrolyte = HNO_3, solution flow rate = 3.6 mL/min, discharge current = 70 mA, discharge gap = 3 mm.

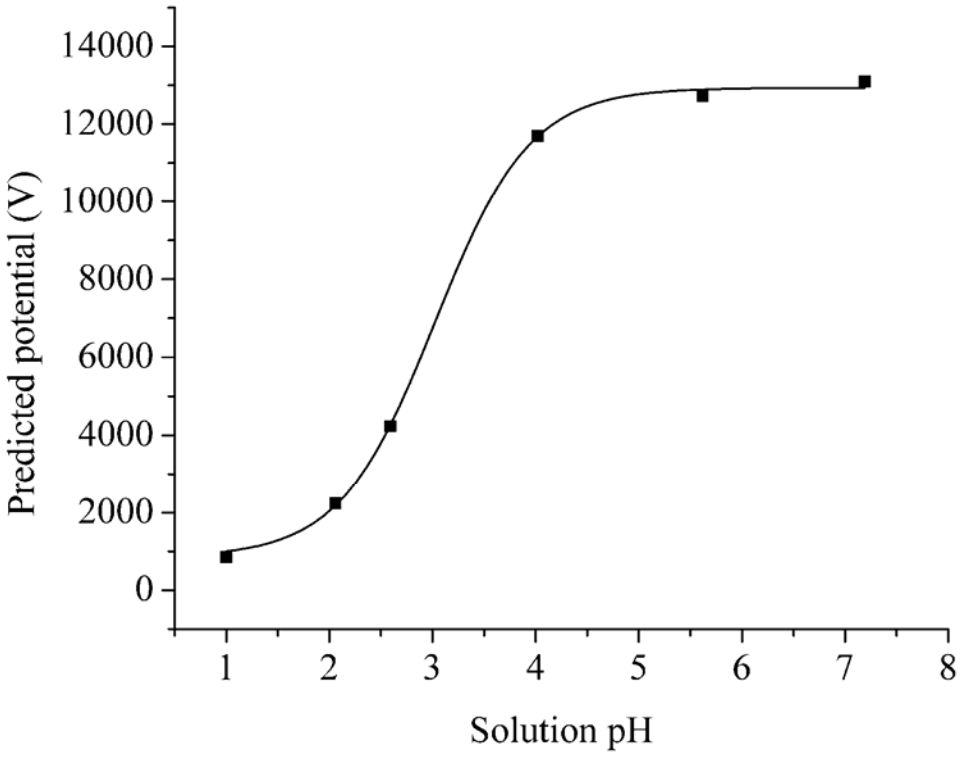

Figure 4-11. Predicted required potentials for a range of tap water samples acidified with sulfuric acid.

No significant differences were found in OH emission intensity, vertical emission distribution, or rotational temperature as pH was varied. Atomic emission, as has been previously reported,[11] goes up as pH is lowered. For Cu and Na, the vertical distribution of emission does not change with pH, but the intensities rise by factors of 5.4 and 6.4, respectively, as the pH drops from 1.9 to 0.8. For Ca emission, the vertical distribution does change, as shown in Figure 4-12. Only four conditions are shown for clarity. Over the pH range from 1.9 to 0.9, the overall emission rises by a factor of 8.0, the negative glow by 20.5, the Faraday dark space by 5.3, and the positive column by 4.2. The result is a transition, moving from pH 1.9 to 0.9, from a pattern of roughly equal positive column and negative glow emission intensities, to one with a distinct dip in between, to one in which the negative glow is nearly five times as intense as the positive column, with no dip in between. At present, the reason for this trend is not clear, but it seems likely that the chemistry of the solution, its conductivity, and/or changes in the negative glow combine to generate more free atoms in the negative glow at lower solution pH.

Further experiments were performed with solutions acidified to pH 1.35 with nitric acid and containing 10 ppm each of Fe, Mg, and Cu. For these experiments, the current was varied from 55 to 100 mA in 15 mA steps, the discharge gap from 1 to 4 mm in 1 mm increments, and the solution flow rate from 2 to 5 mL/min in 1 mL/min steps. Because sample consumption is more rapid at higher discharge currents, experiments with flow rates of 2 mL/min were performed only at currents of 55 and 70 mA. Due to spectral interference from N_2 bands, the Fe vertical emission distribution and temperature distributions were not assessed, but the emission distributions of OH, Cu, and Mg were

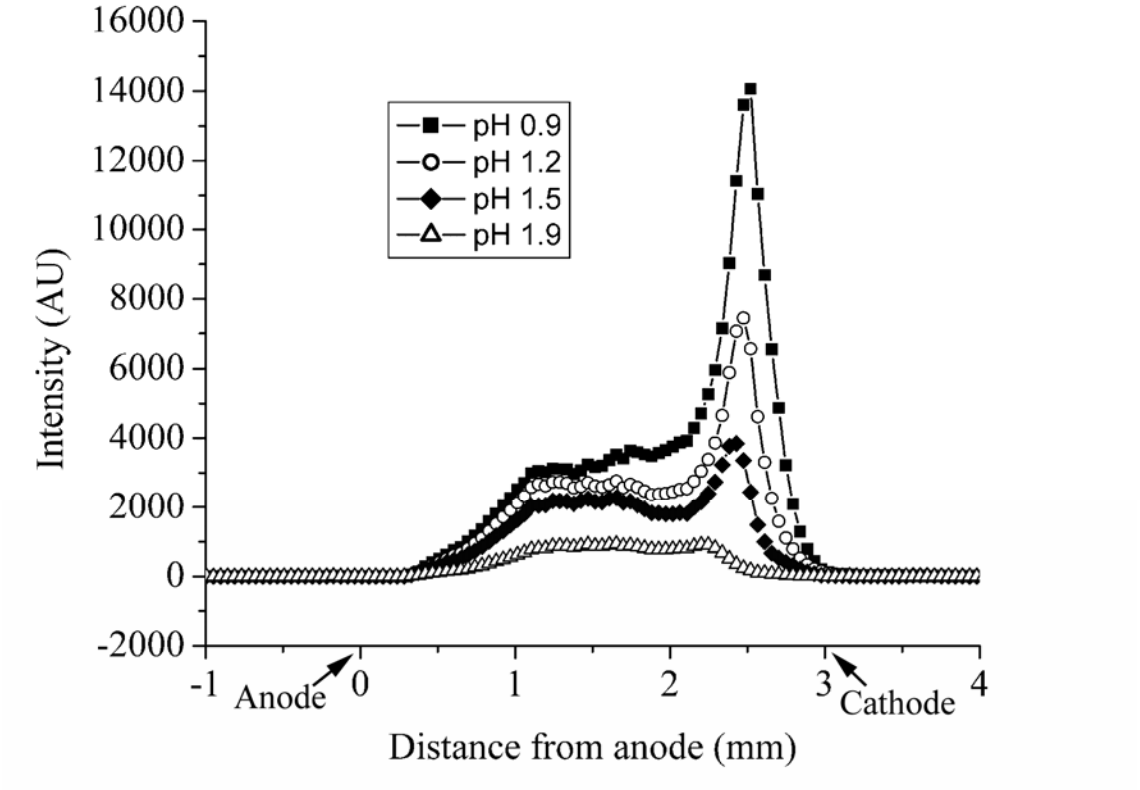

Figure 4-12. Vertical distributions of Ca (422.7 nm) emission at different pH. Anode located at 0 mm. Cathode located at 3 mm.

observed, as well as the distribution of the OH rotational temperature. The studied factors were found to be interdependent. For example, a trend found as current was varied (with all other factors held constant) appears slightly different when one or more of those other factors is changed. For this reason, trends are discussed in general terms and largely in a qualitative way, rather than attempting to give an exhaustive quantitative description of each of the many possible conditions observed. To highlight the trends, plots showing typical behavior due to a variable are shown.

It has been observed previously that atomic emission becomes stronger with increasing current.[11] Figure 4-13 shows that similar trends were found in the present work. Although emission from all regions rises with current, the positive column emission goes up more sharply than the negative glow emission, causing the ratio of the negative glow emission to the positive column emission to be smaller at higher currents. At 100 mA, the Cu positive column emission is comparable to or greater than its negative glow emission, and there is a distinct dip between the regions at this current at most flow rates and discharge gaps. The rates of these changes with current vary depending on the other conditions, but the positive column emission typically builds up by a factor of 3-4 as the current increases from 55 to 100 mA and the negative glow emission typically increases by a factor of 2-3 over this range. The positive column emission of Mg is not distinct at low current levels, so that region's rate of increase could not be ascertained, but the Mg negative glow typically rises by a factor of 3-4 over the same current range. The OH emission typically rises by a factor of less than 2 over this range whereas the OH rotational temperature does not change significantly.

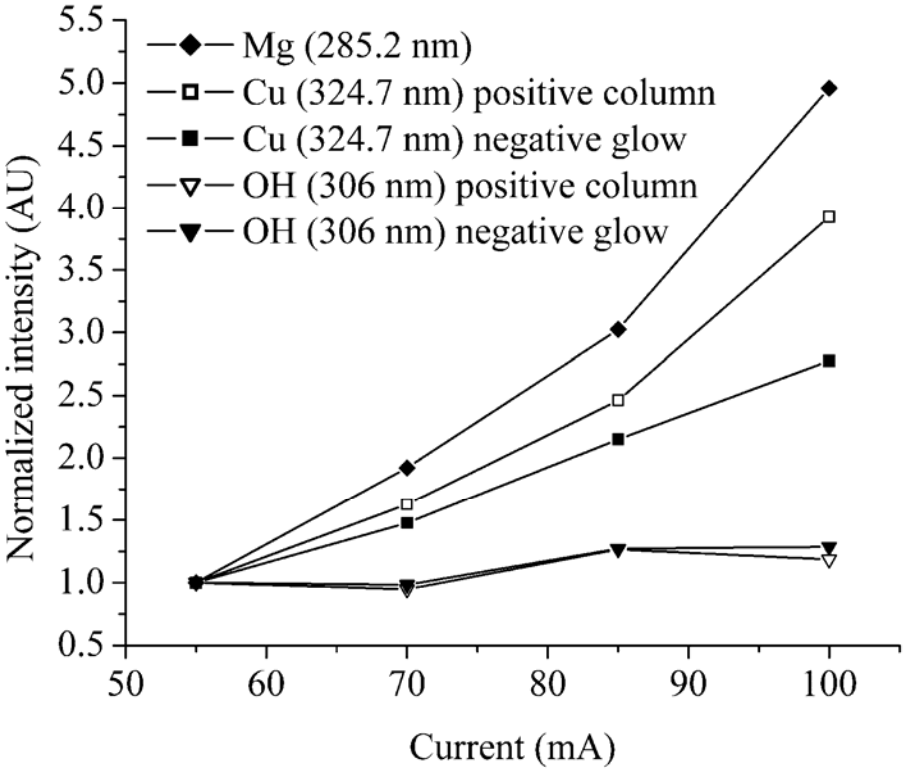

Figure 4-13. Typical effects of discharge current on emission. Electrolyte = HNO_3, solution flow rate = 4.0 mL/min, discharge gap = 3 mm.

The effects of the gap size are similar to those in a more traditional metal-metal glow discharge. Figure 4-14 shows typical trends. The analyte negative glow emission is essentially constant at gaps of 2 mm or greater, although it is sometimes more intense at 2-3 mm than at either extreme. The breadth of this region does not change perceptibly with gap sizes from 2-4 mm. The Cu positive column appears as a distinct zone at a gap of 2 mm. For most elements, the intensity in this region is sometimes greatest at a gap of 3 mm, but is typically nearly constant for gaps of 2-4 mm. Only the negative glow region is visible for OH at a gap of 1 mm. At larger gaps, the positive column appears and grows in height with gap size. This region's intensity generally rises with gap, but levels off or declines slightly at 4 mm under some conditions. The OH rotational temperature climbs with gap. As was noted previously, there are two peaks in OH rotational temperature, one below the negative glow and one near the middle of the discharge. The peak near the middle of the discharge typically elevates in temperature from around 2700 K at a gap of 1 mm to 3200 K at a gap of 4 mm. As the gap grows, the potential required to maintain a given current becomes larger. This temperature increase is due to the higher power dissipated across a larger gap. The peak below the negative glow, however, is roughly constant at 3600 K.

The solution flow rate has a significant impact on the emission, but the OH rotational temperature does not vary with flow rate. Figure 4-15 shows typical behavior. Overall, the OH emission strengthens with flow. The atomic emission generally increases with flow then levels off or declines above 3-4 mL/min. The negative glow shifts slightly closer to the anode as flow rises, as a consequence of the cathode surface moving

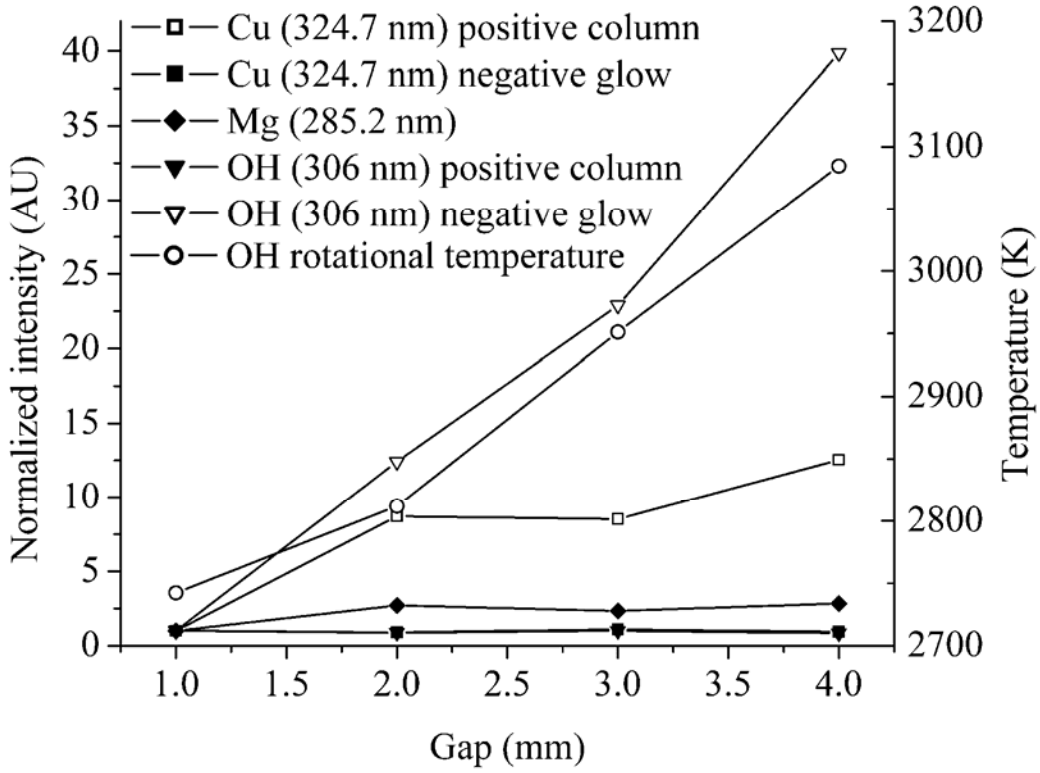

Figure 4-14. Typical effects of gap on emission and temperature. OH positive column and Cu positive column are coincident. Electrolyte = HNO_3, solution flow rate = 4.0 mL/min, current = 85 mA.

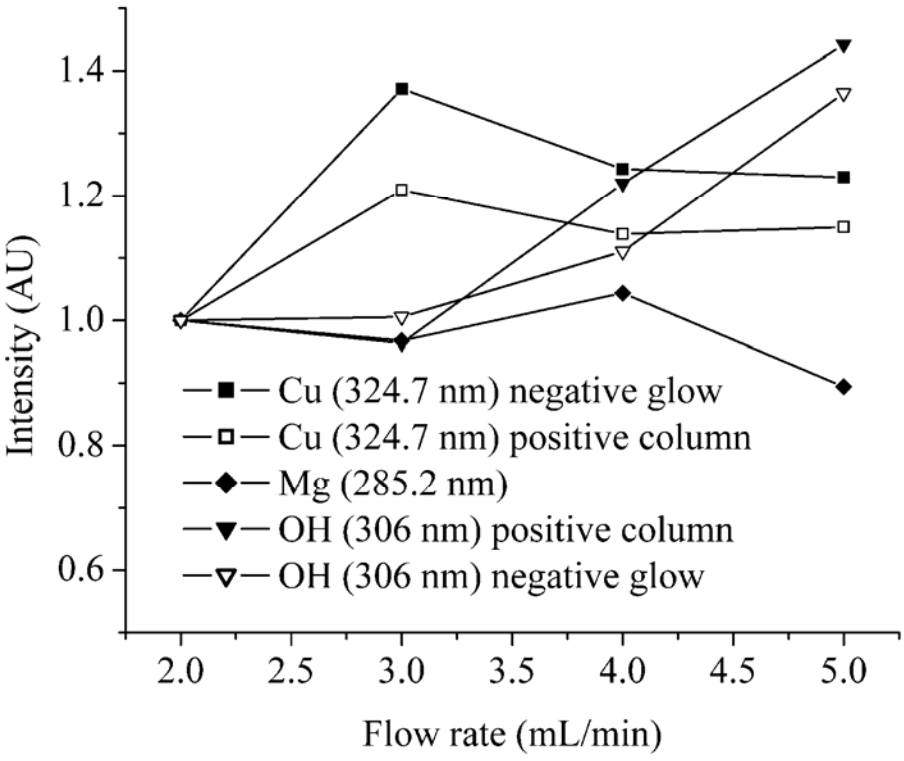

Figure 4-15. Typical effects of flow rate on emission. Electrolyte = HNO_3, discharge gap = 3 mm, current = 70 mA.

upwards. At a current of 70 mA and a gap of 4 mm, this shift is on the order of 0.08 mm between a flow rate of 2 mL/min and one of 5 mL/min. As the surface moves upwards, the exposed surface area becomes larger as well. It may be that this greater surface area raises the amount of both water and analyte that enters the discharge, explaining the increase in atomic emission from 2-4 mL/min and the greater OH emission with higher flow. The leveling off or reduction in atomic emission at higher flows may also be a consequence of additional water vaporization. This water or its products might solvate or otherwise bind atoms, or they may reduce the energy or number of electrons available for exciting the atoms.

4.4 CONCLUSIONS

A glow discharge using a solution as the cathode shows promise as a sensitive and inexpensive technique for elemental analysis of liquids. A better understanding of the effects of various parameters on the discharge can help with optimizing the discharge on a phenomenological basis and, if these effects can be understood on a more fundamental level, a mechanistic basis. The analyte and background profiles offer promise that better signal-to-noise ratios could be achieved for certain elements if emission were collected only from certain areas; however, the variations among the emission distributions of different elements limit the feasibility of this approach if ELCAD is to be used as a multi-elemental technique. Collecting emission from all but the zone 0.5 mm closest to the anode might (as was done here) offers a good compromise and is readily accomplished due to the small size of the discharge. Although the mechanisms within such a discharge are still unclear, the emission has now been shown to vary both in intensity and in

vertical distribution with pH, current, solution flow rate, discharge gap, and element. This emission has also been shown to have distinct regions. The relative intensities of these regions and their response to the various parameters studied suggests that a significant fraction of the emission for many elements not from atoms ejected by sputtering from the solution, as has been suggested,[15] but from metals desolvated and atomized some distance above the solution.

4.5 REFERENCES

[1] R. K. Marcus and J. A. C. Broekaert, *Glow Discharge Plasmas in Analytical Spectroscopy*, John Wiley & Sons: Chichester, England, 2003.

[2] T. K. Starn, R. Pereiro and G. M. Hieftje, "Gas-sampling glow discharge for optical emission spectrometry. Part I: Design and operating characteristics", *Appl. Spectrosc.*, 1993, **47**, 1555.

[3] C. L. Lewis, M. A. Moser, D. E. Dale, Jr., W. Hang, C. Hassell, F. L. King and V. Majidi, "Time-gated pulsed glow discharge: Real-time chemical speciation at the elemental, structural, and molecular level for gas chromatography time-of-flight mass spectrometry", *Anal. Chem.*, 2003, **75**, 1983.

[4] W. O. Walden, W. Hang, B. W. Smith, J. D. Winefordner and W. W. Harrison, "Microsecond-pulse glow discharge atomic emission", *Fresnius' J. Anal. Chem.*, 1996, **355**, 442.

[5] C. M. Strange and R. K. Marcus, "Aqueous sample introduction into a glow discharge device via a particle beam interface", *Spectrochim. Acta, Part B*, 1991, **46B**, 517.

[6] S. G. Schroeder and G. Horlick, "Evaluation of a hollow cathode atomic emission source designed for continuous solution sample introduction", *Spectrochim. Acta, Part B*, 1994, **49B**, 1759.

[7] J. Gubkin, "Elektrolytische Metallabscheidung an der freien Oberfläche einer Salzlösung", *Ann. Phys. Chem.*, 1887, **32**, 114.

[8] D. E. Couch and A. Brenner, "Glow discharge spectra of copper and indium above aqueous solutions", *J. Electrochem. Soc.*, 1959, **106**, 628.

[9] T. Suzuki, Y. Matsushima, Y. Mori, T. Yamazaki and T. Noma, *J. Mater. Sci.*, 2002, **37**, 595.

[10] A. M. Kutepov, A. G. Zakharov, A. I. Maksimov and V. A. Titov, "Physicochemical and Engineering Problems in Studies on Plasma-Solution Systems", *High Energy Chem.*, 2003, **37**, 317.

[11] T. Cserfalvi, P. Mezei and P. Apai, "Emission studies on a glow discharge in atmospheric pressure air using water as a cathode", *J. Phys. D-Appl. Phys.*, 1993, **26**, 2184.

[12] T. Cserfalvi and P. Mezei, "Direct solution analysis by glow discharge: electrolyte-cathode discharge spectrometry", *J. Anal. At. Spectrom.*, 1994, **9**, 345.

[13] T. Cserfalvi and P. Mezei, "Operating mechanism of the electrolyte cathode atmospheric glow discharge", *Fresnius' J. Anal. Chem.*, 1996, **355**, 813.

[14] T. Cserfalvi, "New analytical method for automatic measurement of metals in waste waters", *Magyar Kemikusok Lapja*, 1997, **52**, 502.

[15] P. Mezei, T. Cserfalvi and M. Janossy, "Pressure dependence of the atmospheric electrolyte cathode glow discharge spectrum", *J. Anal. At. Spectrom.*, 1997, **12**, 1203.

[16] P. Mezei, T. Cserfalvi and M. Janossy, "The gas temperature in the cathode surface-dark space boundary layer of an electrolyte cathode atmospheric glow discharge (ELCAD)", *J. Physics D: Appl. Phys.*, 1998, **31**, L41.

[17] P. Mezei, T. Cserfalvi, M. Janossy, K. Szocs and H. J. Kim, "Similarity laws for glow discharges with cathodes of metal and an electrolyte", *J. Phys. D-Appl. Phys.*, 1998, **31**, 2818.

[18] Y. S. Park, S. H. Ku, S. H. Hong, H. J. Kim and E. H. Piepmeier, "Fundamental studies of electrolyte-as-cathode glow discharge-atomic emission spectrometry for the determination of trace metals in flowing water", *Spectrochim. Acta, Part B*, 1998, **53B**, 1167.

[19] S.-H. Chang, H.-J. Kim, S.-T. Kim and Y.-M. Kim, "Fundamental studies on the development of on-line monitoring of trace mercury in drinking water", *Analytical Science & Technology*, 1999, **12**, 299.

[20] H. J. Kim, J. H. Lee, M. Y. Kim, T. Cserfalvi and P. Mezei, "Development of open-air type electrolyte-as-cathode glow discharge-atomic emission spectrometry for determination of trace metals in water", *Spectrochim. Acta, Part B*, 2000, **55B**, 823.

[21] P. Mezei, T. Cserfalvi, H. J. Kim and M. A. Mottaleb, "The influence of chlorine on the intensity of metal atomic lines emitted by an electrolyte cathode atmospheric glow discharge", *Analyst*, 2001, **126**, 712.

[22] M. A. Mottaleb, Y. A. Woo and H. J. Kim, "Evaluation of open-air type electrolyte-as-cathode glow discharge-atomic emission spectrometry for determination of trace heavy metals in liquid samples", *Microchem. J.*, 2001, **69**, 219.

[23] M. A. Mottaleb, J. S. Yang and H.-J. Kim, "Electrolyte-as-cathode glow discharge (ELCAD)/glow discharge electrolysis at the gas-solution interface", *Applied Spectroscopy Reviews*, 2002, **37**, 247.

[24] T. Cserfalvi and P. Mezei, "Subnanogram sensitive multimetal detector with atmospheric electrolyte cathode glow discharge", *J. Anal. At. Spectrom.*, 2003, **18**, 596.

[25] A. I. Maksimov, V. A. Titov and A. V. Khlyustova, "Electrolyte-as-Cathode Glow Discharge Emission and the Processes of Solution-togplasma Transport of Neutral and Charged Species", *High Energy Chemistry*, 2004, **38**, 196.

[26] V. V. Yagov and M. L. Gentsina, "Effect of Supporting Electrolyte Composition on the Intensity of Metal Lines in Electrolyte-Cathode Discharge Spectra", *J. Anal. Chem.*, 2004, **59**, 64.

[27] W. C. Davis and R. K. Marcus, "An atmospheric pressure glow discharge optical emission source for the direct sampling of liquid media", *J. Anal. Atom. Spectrom.*, 2001, **16**, 931.

[28] R. K. Marcus and W. C. Davis, "An Atmospheric Pressure Glow Discharge Optical Emission Source for the Direct Sampling of Liquid Media", *Anal. Chem.*, 2001, **73**, 2903.

[29] W. C. Davis and R. K. Marcus, "Role of powering geometries and sheath gas composition on operation characteristics and the optical emission in the liquid sampling-atmospheric pressure glow discharge", *Spectrochim. Acta, Part B*, 2002, **57B**, 1473.

[30] K. K. Tazmeev and B. K. Tazmeev, "Porous elements in plasma generators with a liquid electrolytic cathode." *Journal of Engineering Physics and Thermophysics*, 2003, **76**, 868.

[31] C. J. Herring and E. H. Piepmeier, "Liquid-Interfaced Oscillating Glow Discharge Detector for A Flowing Liquid System", *Anal. Chem.*, 1995, **67**, 878.

[32] G. Jenkins and A. Manz, "A miniaturized glow discharge applied for optical emission detection in aqueous analytes", *J. Micromech. Microeng.*, 2002, **12**, N19–N22.

[33] Y. Matsushima, A. Tezuka, K. Sumida, K. Maeda, T. Noma, T. Yamazak and T. Suzuki, "An approach to estimate the sputtering yield of water in glow-discharge electrolysis", *J. Mater. Sci. Letters*, 2003, **22**, 1259.

[34] U. Engel, C. Prokisch, E. Voges, G. M. Hieftje and J. A. C. Broekaert, "Spatially resolved measurements and plasma tomography with respect to the rotational temperatures for a microwave plasma torch", *J. Anal. At. Spectrom.*, 1998, **13**, 955.

[35] Y.-i. Sung and H. B. Lim, "Plasma temperature measurement of a low-pressure inductively coupled plasma using spectroscopic methods", *J. Anal. At. Spectrom.*, 2003, **18**, 897.

[36] A. Bogaerts, R. Gijbels, G. Gamez and G. M. Hieftje, "Fundamental studies on a planar-cathode direct current glow discharge. Part II: numerical modeling and comparison with laser scattering experiments", *Spectrochim. Acta, Part B*, 2004, **59B**, 449.

Chapter 5

Spectroscopic characterization of ion and electron populations in a solution-cathode glow discharge.

5.1 INTRODUCTION

The first use of a glow discharge incorporating a solution as the cathode for analytical atomic spectroscopy was in 1993 by Cserfalvi et al.,[1] who later named this source an electrolyte-cathode discharge (ELCAD).[2] Sporadic atomic emission from a similar source had been observed in 1959 by Couch and Brenner,[3] and the basic technique, known as glow-discharge electrolysis, had been used in electrochemistry since its invention in 1887 by Gubkin.[4] In an ELCAD, a solution with a pH lower than 2.5 is introduced upwards at a flow of 3.5-10 mL/min through a tube whose outlet is 1.5-5 mm beneath a solid anode, and potentials on the order of 1 kV and currents greater than 30 mA are applied.[1-2]

Initial detection limits were generally in the range of hundreds of parts per billion to single parts per million.[2] Since that time, a number of studies, which have been summarized in a review,[5] involving both practical considerations and fundamental characterizations have expanded knowledge of the system and contributed to an improvement of analytical performance. Initial experiments showed that lower pH and higher current produced stronger emission[1]. Later experiments by Yagov and Gentsina[6]

revealed that emission decreases at higher electrolyte (acid or otherwise) concentrations than were initially employed. Mezei et al.[7] showed that emission rises with pressure until around 2 bar, at which point it falls. Park et al.[8] showed that emission intensity is somewhat, but not strongly, dependent on discharge-gas identity and that air yields more intense emission than He or Ar. Kim et al.[9-10] showed that opening the discharge cell to atmosphere improves analytical performance by enhancing stability. As a result of the knowledge accumulated through these studies, typical detection limits have dropped by around two orders of magnitude so they are generally in the single to tens of parts per billion for steady-state measurements[9-11] and comparable for those elements that have been studied in flow-injection analysis.[12]

In spite of the previously mentioned studies and others, there is much left to be learned about this type of discharge. The knowledge gained from fundamental studies has the potential to further improve analytical performance as earlier studies have. Among the parameters that are not yet known are the relative and absolute sizes of the electron and ion populations. The electron number density, in particular, has been proposed as an important variable in the mechanism by Cserfalvi et al.[7-13-14]

The work presented here characterizes the electron number density, the ionization temperature, and element-specific ion-to-atom ratios. These characteristics are monitored as a function of location within the discharge and as functions of various changes made to the discharge. The consequences of the observed characteristics are discussed in relation to analytical performance.

5.2 EXPERIMENTAL

The ELCAD cell has been described previously[11] and is shown in Figure 5-1. The solution enters the cell through a 0.3-mL portion of a 1-mL serological pipette that has been bent so the tip points upwards 3 mm below a 1.6-mm diameter Ti anode. A Kepco (Flushing, NY) BHK 2000-0.1MG high-voltage power supply operated in constant-current mode is connected to this anode through a 400-Ω ballast resistor. The solution overflows from the tip into an approximately 35-mL reservoir containing a grounded graphite electrode. This overflow creates an electrical connection between the solution at the pipette's tip and the graphite electrode. The discharge can be initiated by bringing the anode within approximately 1 mm of the solution or by using a metal syringe needle to make contact between the anode and the solution and then withdrawing the needle from the solution while maintaining contact with the anode to transfer the discharge to the Ti anode.

A black rectangular polyethylene divider supported by the pipette serves multiple purposes. It reduces the amount of hydrogen (produced at the graphite cathode) that reaches the discharge, it blocks some light from sources external to the discharge by impeding its path through the air, and it wicks moisture over the sides of the reservoir so a constant solution level is maintained within the reservoir. The hydrogen is blocked intentionally because its presence has been known to lower emission in other glow discharges; the light is blocked to reduce background noise; and the reservoir level is held constant to prevent fluctuations in the ohmic drop across the solution between the pipette tip and the graphite cathode.

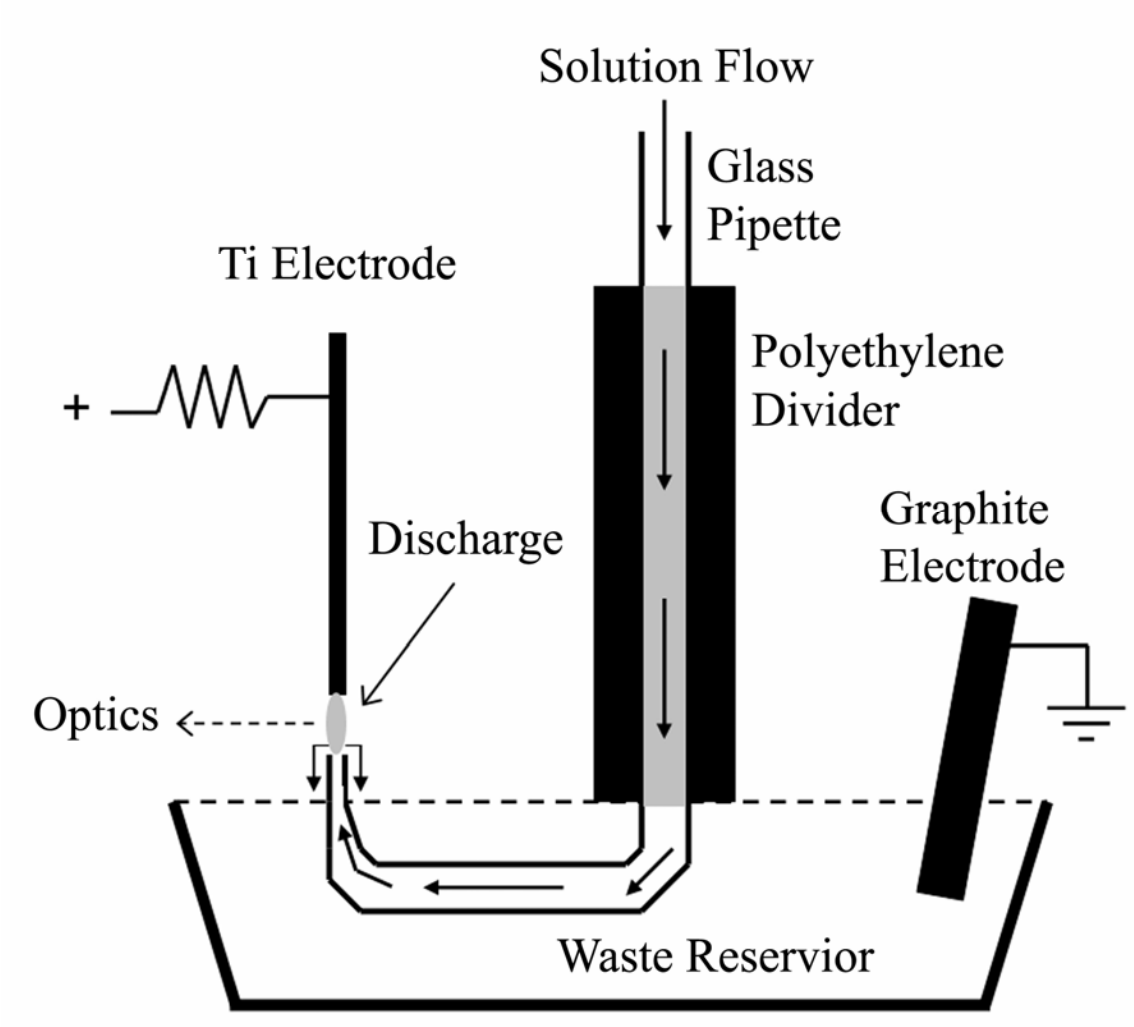

Figure 5-1. Diagrammatic representation of solution-cathode glow discharge.

Aside from what has been described to this point, two different sets of equipment are used in this work.

For the H_β measurements, solution is supplied by a syringe pump (Harvard Apparatus PHD 2000 (Holliston, MA)) at 3.5 mL/min. A Model HR1000 Jobin-Yvon (Longjumeau, France) monochromator was used in an arrangement which has been described previously.[15] In brief, a collimating lens, dove prism, and focusing lens were used in series to rotate the image of the plasma 90º and project it onto the 20-μm-wide entrance slit of the monochromator at a magnification of 0.4. A CCD camera (Roper Scientific, Trenton, NJ, model CH350A) at the focal plane of the monochromator detected the lateral distribution of emission in one dimension and its spectral distribution in the other. A National Instruments (Austin, TX) LabVIEW program written by Starn et al.[16] is used to calculate electron number densities based on Stark broadening of the H_β line.

In other measurements, solution is supplied by using a Global FIA MilliGAT (Fox Island, WA) flow-injection system. Before reaching the pump, the sample solution passes through a 6-port 2-way switch, connected as shown in Figure 5-2. This allows the sample to be changed without interrupting the solution flow so the discharge does not need to be extinguished between samples. The syringes are necessary to purge the intake lines of any air bubbles introduced as the tubing is moved between samples. The discharge is imaged 2.3:1 with a quartz lens onto the entrance slit of a Chromex (Albuquerque, NM) 500IS/SM 0.5-m Czerny-Turner spectrometer. Spatial resolution is accomplished by blocking portions of the imaged plasma with electrical tape affixed to

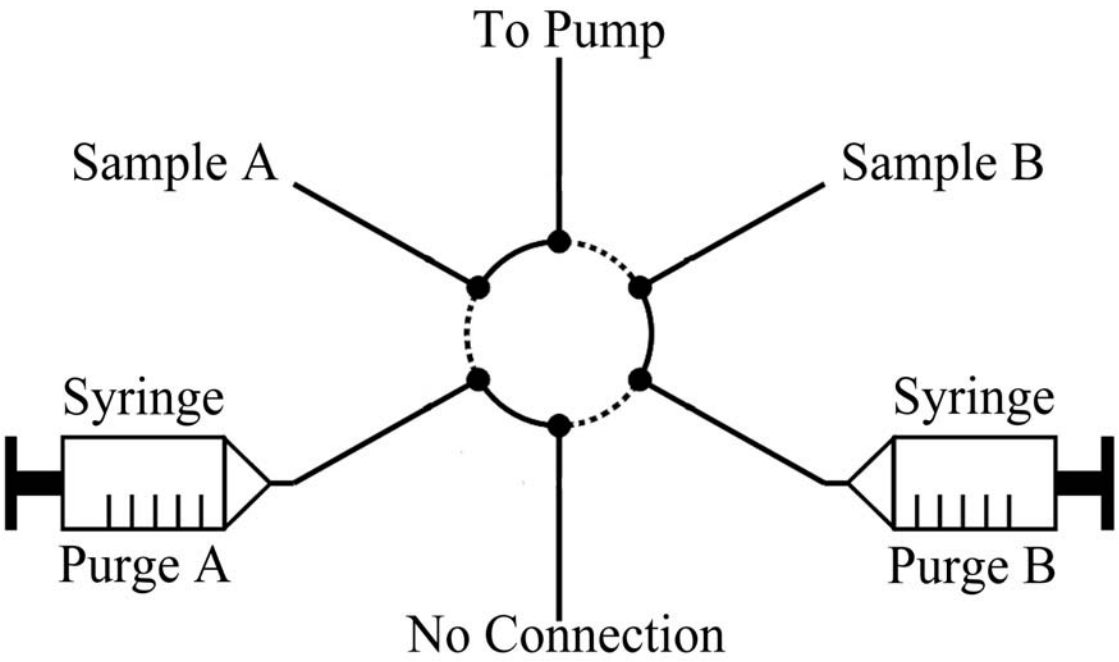

Figure 5-2. 2-way 6-port valve with sample A directed to the discharge.

the spectrometer entrance slit. Detection is accomplished with a Hamamatsu (Hamamatsu, Japan) R928 PMT biased at -850 V amplified by a Keithley (Cleveland, OH) 427 current amplifier. The output of this amplifier is recorded with a custom LabVIEW program that also controls the monochromator.

5.3 RESULTS AND DISCUSSION

5.3.1 Electron number density

Several methods were considered for the determination of electron number densities; Stark broadening of the H_β line was chosen because it provides reasonable accuracy and precision with a relatively simple experimental setup and does not perturb the plasma or require an assumption of thermodynamic equilibrium.[17] For Stark broadening to be a viable method, other sources of broadening need to be either insignificant or taken into account. The H_β peak width (full width at half maximum) from a typical ELCAD was measured to be 182 pm. Based on interpolation from tables[18] that take plasma temperature into account, this half-width corresponds to an electron number density of approximately 8.7×10^{14} cm^{-3}. Natural broadening is on the order of hundredths of picometers,[19-21] and a 0.05 pm broadening would produce only a 0.04% error in this estimate, so this contribution can be neglected. Pressure broadening in an analytical flame, which is comparable to the ELCAD in terms of gas temperature and pressure, is from one to a few picometers.[19-21] Even in an ICP, which has a higher temperature than either the ELCAD or a flame, pressure broadening is only a few picometers.[22] From the cited tables, a 5 pm contribution from pressure broadening would produce a 4% error,

which was judged to be acceptable and, ultimately, was several times smaller than the experimental uncertainty. Lower electron number densities in the positive column make this error relatively larger than in the negative glow, but it is still smaller than the experimental error. Other broadening was accounted for as discussed below.

The H_β line profiles were measured at two locations: in the negative glow (approximately 0.2 mm above the cathode) and in the positive column (approximately 1.2 mm above the cathode). A LabVIEW program[16] was used to calculate electron number densities after transformation of the data (which contained lateral information on one axis and spectral information on the other) by QuickBasic into a series of monochromatic images. Thomsen and Helbig[23] found that omitting the central portion of the H_β line profile yields better agreement between experimental and theoretical profiles because the assumption of static ions leads to predictions of a larger central dip than is experimentally observed. With this in mind, the central portion of the H_β line (the portion with intensity greater than approximately 70% of the maximum) was omitted from the fitting. To account for the contribution of Doppler broadening, the gas-kinetic temperature, which can be reasonably approximated by the OH rotational temperature, is required. Based on previous results,[11] a gas temperature of 3000 K was used. Another influence on the observed profile that must be accounted for is instrumental broadening. The measured profile of the 422.7 nm line of a Ca hollow cathode lamp was used for this purpose because it is narrow compared to the instrumental broadening and relatively close in wavelength to the H_β line.[16]

To calculate accurate electron number densities, lateral emission profiles are ordinarily

transformed into radial profiles. If radial symmetry can be assumed, this procedure can be performed by means of an Abel inversion. Unfortunately, this process tends to amplify noise and therefore reduce precision, particularly near the center of the discharge. In some cases, particularly in measurements of the positive column, noise in the background emission was too great for Abel inversion to be feasible. To assess the impact of not using radially resolved profiles, Abel inversion was performed on one lateral profile by using the Nestor-Olsen algorithm.[24] As Figure 5-3 shows, the results obtained using lateral and radial profiles for the negative glow region of a 60 mA discharge agree to well within the error of the measurement (calculation of the error is described below). Also shown in the figure is the lateral profile for the positive column under the same conditions. All three profiles show that the electron number density is very flat until the edges of the discharge, where it drops slightly before the emission becomes too weak for accurate measurement. It is no doubt this flatness that renders the Abel inversion unimportant.

To better analyze trends, average n_e were calculated for each region. For this purpose, the apparently constant n_e in the (horizontally) central region was assumed to be constant in fact. The mean and standard deviation of n_e were then calculated based on this assumption. The precision of the measurement was limited by both noise and the resolution of the results provided by the LabVIEW program. Twice the larger of the standard deviation or the program's resolution is given as the error for the remainder of this text. Based on these definitions, the laterally resolved n_e ($8.5\pm1.9\times10^{14}$ cm^{-3}), and

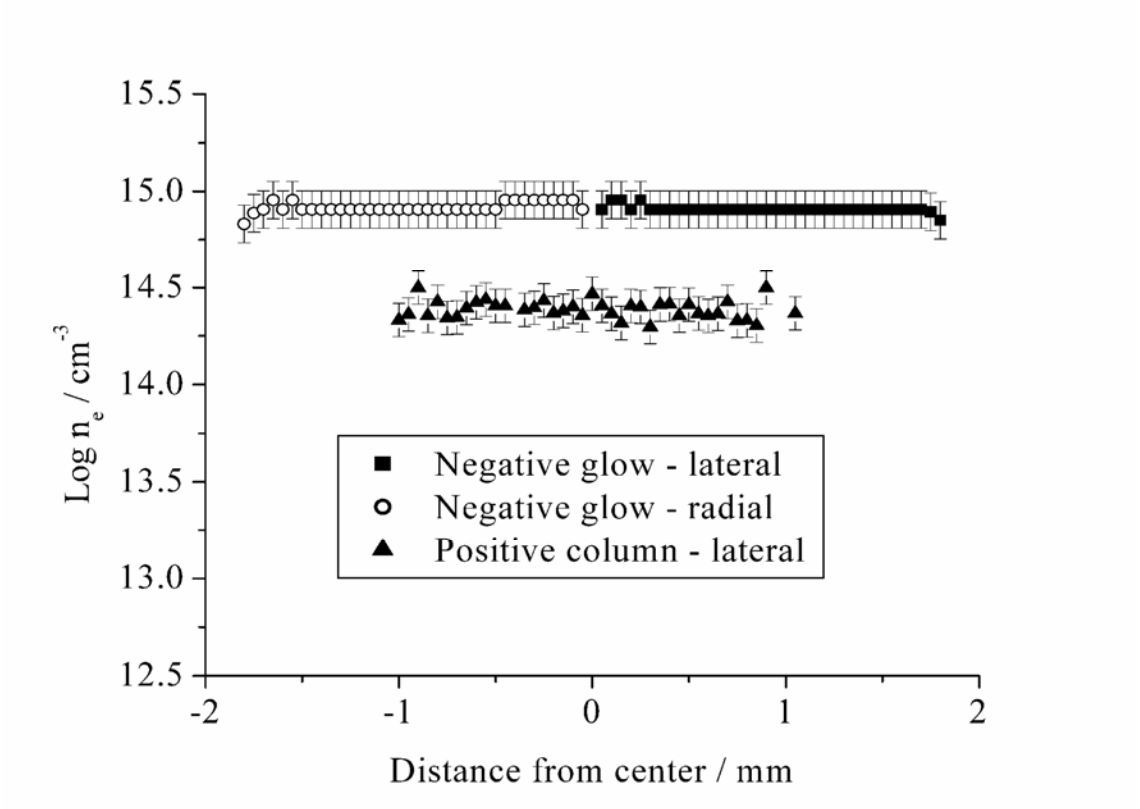

Figure 5-3. Electron number densities in different regions of the ELCAD, estimated by means of lateral and radially resolved data. Negative glow and positive column are approximately 0.2 and 1.2 mm above the cathode, respectively. For clarity, only half the lateral and radial profiles are shown for the negative glow. Discharge current — 60 mA; solution pH — 1.0 (in HNO_3).

radially resolved n_e ($8.3\pm1.9\times10^{14}$ cm^{-3}) are not significantly different. The positive column n_e ($2.5\pm0.5\times10^{14}$ cm^{-3}) is significantly lower than that of the negative glow. These values approach those typically found for an inductively coupled plasma (~10^{15} cm^{-3}),[17] and are quite a bit higher than those commonly found for a low-pressure glow discharge (~10^{11} cm^{-3}).[25]

Three variables were chosen for evaluation in this study. Solution pH was chosen because the dependence of emission on pH was proposed by Cserfalvi et al.[7-13-14] to involve a higher electron number density at low pH. Discharge current was chosen because it affects the electron number density in low-pressure metal-cathode glow discharges.[25] Electrolyte identity was chosen because it has been shown to affect emission.[6-26] The effects of pH and current on n_e are shown in Figures 5-4 and 5-5, respectively. No trend is apparent in either case. Electrolyte identity also did not have a statistically significant impact on n_e. At 60 mA and pH 1.0, HCl, HNO_3, and H_2SO_4 produced electron number densities of $2.4\pm0.4\times10^{14}$ cm^{-3}, $2.5\pm0.5\times10^{14}$ cm^{-3}, and $2.5\pm0.3\times10^{14}$ cm^{-3}, respectively. In the negative glow under the same conditions, HCl, HNO_3, and H_2SO_4 produced electron number densities of $8.1\pm1.8\times10^{14}$ cm^{-3}, $8.5\pm1.9\times10^{14}$ cm^{-3}, and $8.7\pm2.0\times10^{14}$ cm^{-3}, respectively.

5.3.2 Ionization temperature

By combining the Saha and Boltzmann equations,[17-22-27] the ionization temperature can be calculated if the electron number density and the ratio of intensities of an atom and an ion line of the same element (as well as various constants associated with this element and these lines) are known.

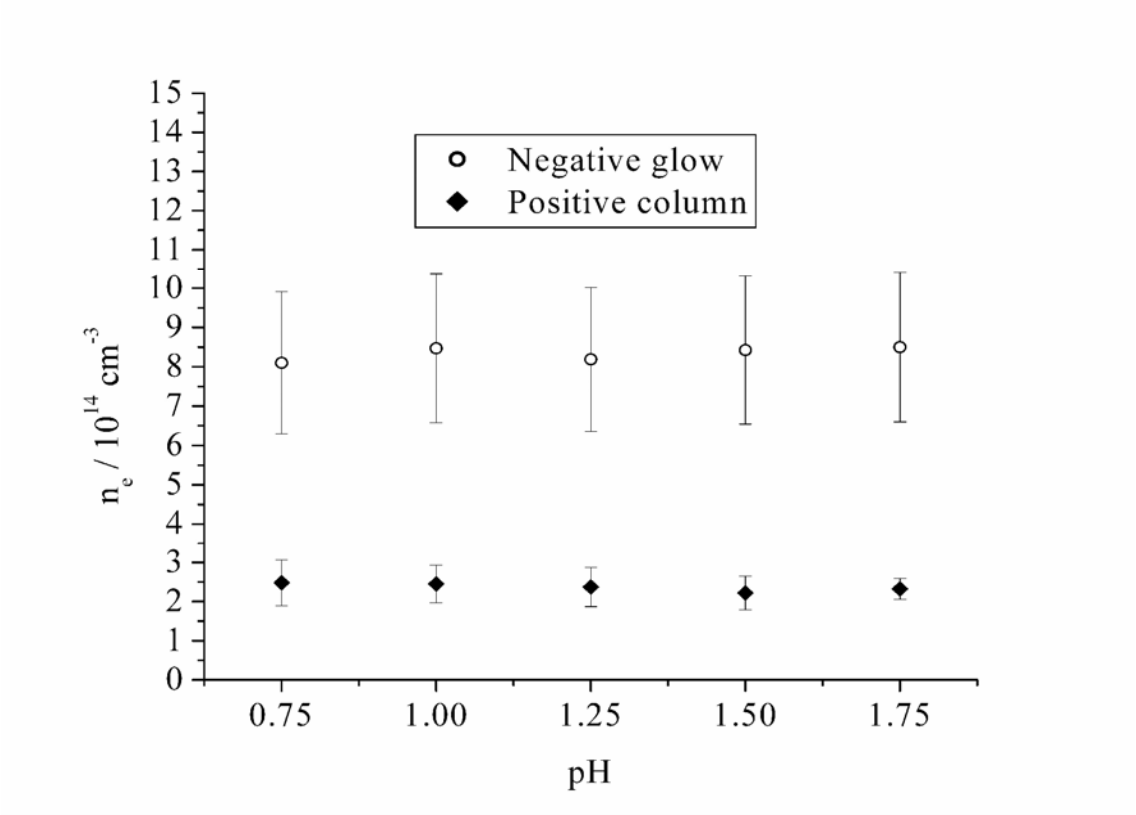

Figure 5-4. Electron number densities as a function of pH. Discharge current was 60 mA and HNO_3 was used to provide the desired pH.

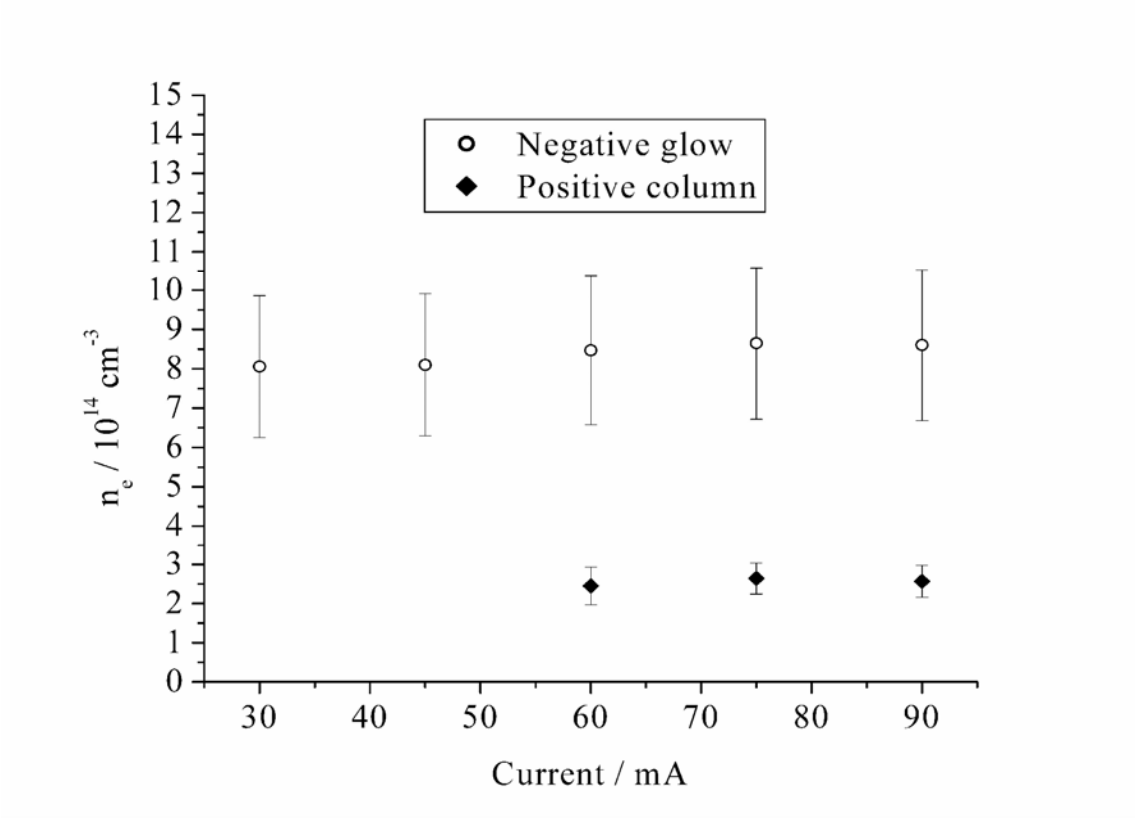

Figure 5-5. Electron number densities as a function of current. Solution pH was adjusted to 1.0 using HNO_3.

$$\frac{n_e(I_{kl}^{+}A_{pq}\lambda_{kl}^{+})}{I_{pq}A_{kl}^{+}\lambda_{pq}} = \left(\frac{2g_k}{g_p}\right)\left(\frac{2\pi m_e kT}{h^2}\right)^{3/2} \exp\left(-\frac{E_i + E_k - E_p}{kT}\right) \quad (5\text{-}1)$$

Here the + superscript indicates the ion; subscripts indicate energy levels (subscripted k, l, p, and q are the ion upper level, ion lower level, atom upper level, and atom lower level, respectively); n_e is the electron number density, as determined previously; I is the observed emission intensity; A is the transition probability for spontaneous emission; λ is the wavelength of the emission line; g is the statistical weight of the level; m_e is the electron mass; k is the Boltzman constant; h is the Planck constant; E_k and E_p are the excitation energies of the repective levels; E_i is the ionization potential; and T is the temperature to be calculated as the ionization temperature.

Although the various temperatures are not in thermodynamic equilibrium, it is often necessary to assume they are for the purpose of calculations. The ionization temperature and excitation temperature are assumed to be equal in this case. Important considerations are that the lines be near in wavelength to reduce any wavelength bias of the detection apparatus and that the excited states involved be close in energy to minimize the impact of the excitation temperature. The lines used in this study, Mg II 279.6 nm and Mg I 285.2 nm, can be used for this purpose because they are separated by only 5.6 nm and the involved excited states are separated by only 0.09 eV. Mg II 280.2 nm, a more commonly used line, was not employed for this study because it is only approximately half as intense as the Mg II 279.6 nm line.

At 75 mA and pH 1.0 HNO_3, the Mg I 285.2 nm : Mg II 279.6 nm intensity ratio was 38.0 ± 1.6 in the negative glow and 58.6 ± 9.8 in the positive column. Based on these

values and the previously calculated electron number densities, T_{ion} was calculated to be 5038 ± 60 K in the negative glow and 4623 ± 34 K in the positive column under these conditions. No trend greater than the calculated uncertainty was seen with current or pH.

5.3.3 Analytical consequences

Based on the electron number density and the calculated ionization temperatures, the fractions of an element present as ions and atoms can be calculated from the Saha equation. For this computation, it is necessary to know the partition functions of the atoms and ions at the ionization temperature, which are obtainable from the polynomial approximations given by Irwin.[28] The element-specific degrees of ionization were calculated for the ELCAD negative glow (T_{ion} = 5000 K, $n_e = 8.5\times10^{14}$ cm^{-3}), ELCAD positive column (T_{ion} = 4600 K, $n_e = 2.5\times10^{14}$ cm^{-3}), and, for comparison, an argon ICP (T_{ion} = 7500 K, $n_e = 1\times10^{15}$ cm^{-3}). These last values are well within the range of values found in the literature,[29] and are the same as those used by Ohata and Furuta for a similar purpose.[30] The results are plotted versus ionization energy in Figure 5-6.

From Figure 5-6, the majority of elements exist mostly as neutrals. Among the minority of elements that exist mostly as ions are the alkali metals, which produce only weak ionic emission because of their closed shell structure as ions. Based on this observation, atomic lines should be more analytically useful for most elements than ionic lines, and line selection should be better aided by references for weakly ionizing sources such as flames and low-pressure glow discharges than by references to strongly ionizing sources such as the ICP. Indeed, all of the best ELCAD detection limits so far have been reported

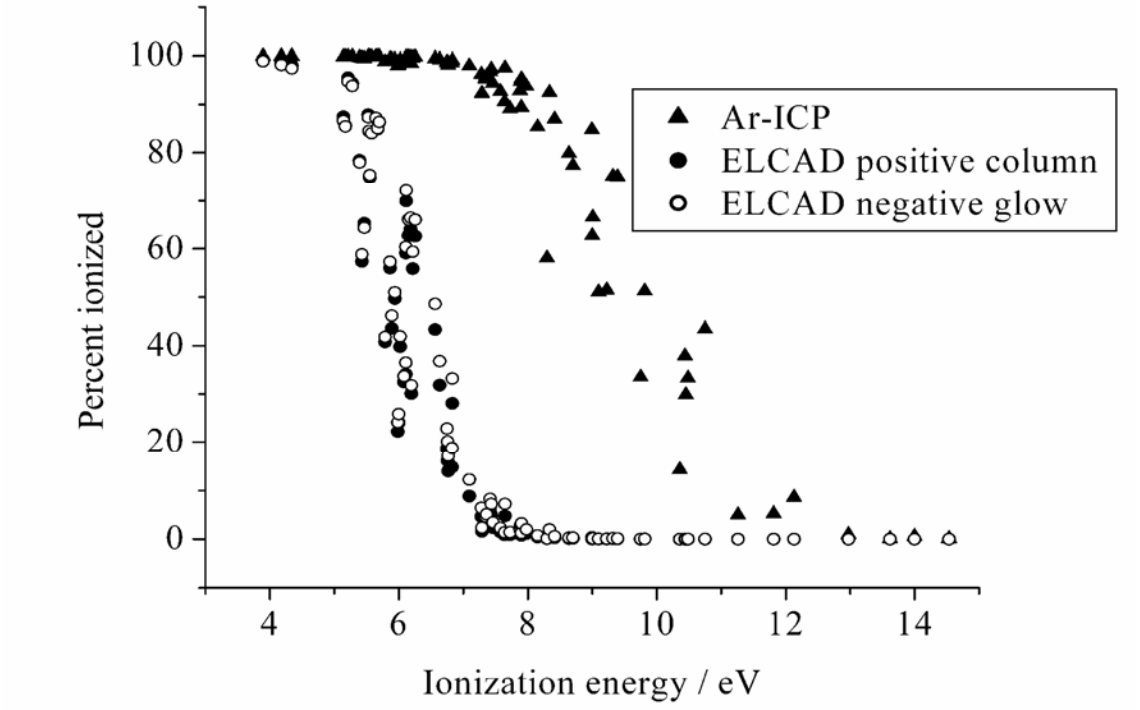

Figure 5-6. Comparison of the degrees of ionization in the ELCAD and a typical Argon ICP. ELCAD negative glow conditions were T_{ion} = 5000 K and $n_e = 8.5\times10^{14}$ cm^{-3}. ELCAD positive column conditions were T_{ion} = 4600 K and $n_e = 2.5\times10^{14}$ cm^{-3}. ICP conditions were T_{ion} = 7500 K, $n_e = 1\times10^{15}$ cm^{-3}.

for atomic lines. Additionally, because ion lines are mostly absent, chances of spectral interference are reduced.

These predicted degrees of ionization are valid only as long as the electron density and temperature are unaffected by the presence of the analyte or concomitant elements. In flames, this assumption is not valid because the electron number density is highly dependent on the identities and concentrations of elements in the sample. For example, Luecke[31] experimentally found that, in an air-acetylene flame at roughly 2200 K, magnesium was 46.2% ionized at a concentration of 25 ppb but only 1.5% ionized at a concentration of 400 ppb. As a result, the sensitivity (background-corrected signal divided by concentration) varies by almost a factor of two over this range, making quantitation difficult. Further, because other elements from the sample will affect the electron number density in the flame, the degree of ionization (and therefore the emission and absorption) of a given element will depend on the concentrations of other elements. To combat this interference, an ionization buffer, commonly a cesium salt, is often used. This buffer raises the electron concentration to a level where changes caused by the presence of other elements become insignificant. In an ICP, in contrast, the background electron concentration is high enough that the introduction of 1000 ppm of an easily ionized element should raise the electron concentration by only about 0.1%,[17] so this type of interference is insignificant.

Because, as Figure 5-6 shows, the ELCAD produces a lower degree of ionization than the ICP, fewer electrons will be added to the discharge for the same number of atoms intruduced into it. At the same time, the background electron concentration in the

ELCAD is nearly as high as in the ICP. The combination of these two factors implies that the sort of ionization interference seen in flames should not occur in the ELCAD. Correspondingly, we have seen no evidence of ionization interference in ELCAD calibration plots. To better evaluate whether or not there is an ionization interference, sensitivity is plotted as a function of concentration in Figure 5-7. An ionization interference, which is not present, would produce an increase in sensitivity at higher concentrations.

With optimization of emission as a goal, it is worthwhile to consider how a change in ELCAD temperature would affect emission. The fraction of an element present as neutrals can be calculated from the Saha equation and the fraction of those neutrals in a given excited state can be calculated by means of the Boltzmann equation. The product of those two fractions is proportional to the emission intensity at a given temperature and electron number density. This product was calculated for all elements for which detection limits by ELCAD have been reported in the literature. The emission lines used were those for which the lowest detection limit has been reported. Partition functions were calculated as described above. Degeneracies and excited-level energies were obtained from reference volumes.[32-35] Although not strictly valid, equilibrium was assumed between the ionization and excitation temperatures, and the electron number density was assumed to be 8.5×10^{14} cm^{-3} regardless of temperature.

This calculation was performed for temperatures of 1000 – 9000 K in increments of 500 K. At first, emission rises with temperature as the fraction of atoms in the excited state grows. Simultaneously, the total number of neutral atoms declines due to ionization. At

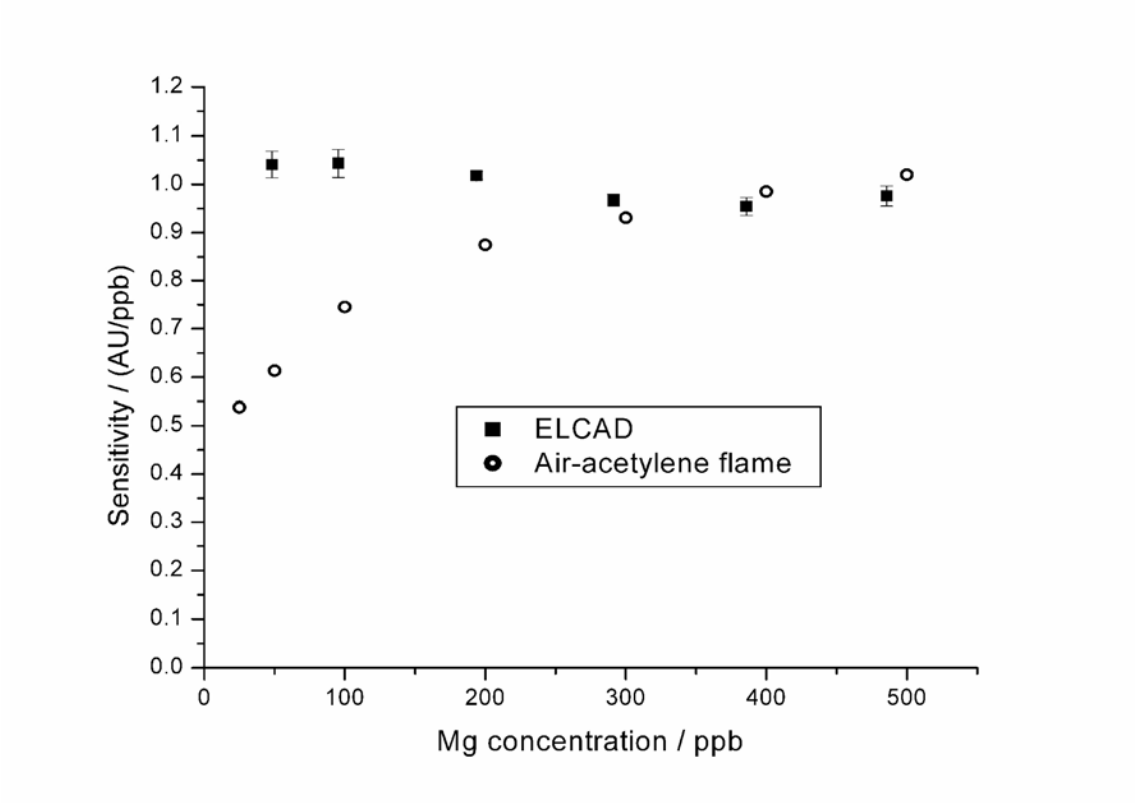

Figure 5-7. Evaluation of the effect of concentration on sensitivity. ELCAD data are based on five ten-second integrations when the discharge was operated at 75 mA and solutions were adjusted to pH 1.0 with HNO_3. Flame data are from Luecke.[31] Constant sensitivity for the ELCAD source suggests an absence of the classical ionization interference.

a high enough temperature, the effect of ionization is greater than the effect of excitation, so emission drops. The point of maximum emission is known as the norm temperature.[17] This temperature was calculated by fitting the rising edge of the curve to a Gaussian and the falling edge to a Lorentzian. The peaks of the two curves agreed to within 1% in all cases and the average of these peaks is reported as the norm temperature in Table 5-1, alongside the relative emission at several temperatures.

Clearly, no single temperature is optimal for all elements. The temperature determined for the ELCAD negative glow (5000 K) gives a fair compromise between elements that are easy to ionize and those that are difficult to excite. If the temperature can be adjusted, a higher rather than lower temperature might be desirable because easily ionized elements such as alkali and alkaline metals are present in relatively high concentrations in many applications. However, no method for significantly increasing the excitation temperature of an ELCAD has yet been reported.

5.4 CONCLUSIONS

The electron number density, ionization temperature, and degrees of ionization in the ELCAD are presented for the first time. The variance of these values was surprisingly low. In particular, the insensitivity of electron number density to current differs from the behavior found in low pressure glow discharges, and its stability with pH contrasts with predictions that changes in electron number density play a role in the ELCAD's pH-sensitive behavior.[7-13-14] The relatively high electron number density suggests that calibration curves obtained using the source should not be subject to nonlinearities from

Table 5-1. Norm temperatures and predicted temperature-dependent relative emission intensities of various analytes at wavelengths for which detection limits have been previously reported in the ELCAD.

Element	Wavelength (nm)	Norm Temperature (K)	Intensity relative to maximum				
			3000 K	4000 K	5000 K	6000 K	7000 K
Cs	852.1	3260	88%	38%	10%	4%	2%
K	766.5	3610	55%	72%	16%	6%	3%
Na	589.0	4240	13%	93%	50%	16%	7%
Sr	460.7	4340	6%	84%	54%	16%	7%
Li	670.8	4390	15%	87%	46%	13%	6%
Ca	422.7	4620	2%	58%	79%	24%	9%
Al	396.2	5380	1%	18%	88%	76%	32%
Cr	357.9	5400	0%	16%	86%	69%	25%
Pb	368.4	5780	0%	5%	56%	95%	46%
Mg	285.2	5800	0%	3%	51%	96%	45%
Mn	279.5	5810	0%	3%	50%	95%	44%
Fe	248.4	6100	0%	1%	30%	99%	63%
Ag	338.3	6120	0%	3%	38%	99%	61%
Ni	341.5	6250	0%	3%	32%	96%	66%
Cu	324.7	6270	0%	3%	33%	95%	68%
Cd	228.8	6760	0%	0%	7%	61%	99%
Zn	213.9	7050	0%	0%	4%	41%	100%
Au	242.8	7330	0%	0%	4%	35%	93%
Hg	253.6	7530	0%	0%	2%	25%	85%

concentration-dependent degrees of ionization as those from flames are, which agrees with the authors' experience. Calculations based on the degree of ionization and the excitation in the source show that the ELCAD provides a good compromise between ideal conditions for detection of easily and less easily ionized elements, but that somewhat higher temperatures would give an even better compromise.

5.5 REFERENCES

[1] T. Cserfalvi, P. Mezei and P. Apai, "Emission studies on a glow discharge in atmospheric pressure air using water as a cathode", *J. Phys. D-Appl. Phys.*, 1993, **26**, 2184.

[2] T. Cserfalvi and P. Mezei, "Direct solution analysis by glow discharge: electrolyte-cathode discharge spectrometry", *J. Anal. At. Spectrom.*, 1994, **9**, 345.

[3] D. E. Couch and A. Brenner, "Glow discharge spectra of copper and indium above aqueous solutions", *J. Electrochem. Soc*, 1959, **106**, 628.

[4] J. Gubkin, "Elektrolytische Metallabscheidung an der freien Oberfläche einer Salzlösung", *Ann. Phys. Chem.*, 1887, **32**, 114.

[5] M. A. Mottaleb, J. S. Yang and H.-J. Kim, "Electrolyte-as-cathode glow discharge (ELCAD)/glow discharge electrolysis at the gas-solution interface", *Applied Spectroscopy Reviews*, 2002, **37**, 247.

[6] V. V. Yagov and M. L. Gentsina, "Effect of Supporting Electrolyte Composition on the Intensity of Metal Lines in Electrolyte-Cathode Discharge Spectra", *J. Anal. Chem.*, 2004, **59**, 64.

[7] P. Mezei, T. Cserfalvi and M. Janossy, "Pressure dependence of the atmospheric electrolyte cathode glow discharge spectrum", *J. Anal. At. Spectrom.*, 1997, **12**, 1203.

[8] Y. S. Park, S. H. Ku, S. H. Hong, H. J. Kim and E. H. Piepmeier, "Fundamental studies of electrolyte-as-cathode glow discharge-atomic emission spectrometry for the determination of trace metals in flowing water", *Spectrochim. Acta, Part B*, 1998, **53B**, 1167.

[9] H. J. Kim, J. H. Lee, M. Y. Kim, T. Cserfalvi and P. Mezei, "Development of open-air type electrolyte-as-cathode glow discharge-atomic emission spectrometry for

determination of trace metals in water", *Spectrochim. Acta, Part B*, 2000, **55B**, 823.

[10] M. A. Mottaleb, Y. A. Woo and H. J. Kim, "Evaluation of open-air type electrolyte-as-cathode glow discharge-atomic emission spectrometry for determination of trace heavy metals in liquid samples", *Microchem. J.*, 2001, **69**, 219.

[11] M. R. Webb, F. J. Andrade, G. Gamez, R. McCrindle and G. M. Hieftje, "Spectroscopic and electrical studies of a solution-cathode glow discharge", *J. Anal. At. Spectrom.*, 2005, **20**, 1218.

[12] T. Cserfalvi and P. Mezei, "Subnanogram sensitive multimetal detector with atmospheric electrolyte cathode glow discharge", *J. Anal. At. Spectrom.*, 2003, **18**, 596.

[13] T. Cserfalvi and P. Mezei, "Operating mechanism of the electrolyte cathode atmospheric glow discharge", *Fresnius' J. Anal. Chem.*, 1996, **355**, 813.

[14] P. Mezei, T. Cserfalvi, M. Janossy, K. Szocs and H. J. Kim, "Similarity laws for glow discharges with cathodes of metal and an electrolyte", *J. Phys. D-Appl. Phys.*, 1998, **31**, 2818.

[15] N. N. Sesi, D. S. Hanselman, P. Galley, J. Horner, M. Huang and G. M. Hieftje, "An imaging-based instrument for fundamental plasma studies", *Spectrochim. Acta, Part B*, 1997, **52B**, 83.

[16] T. K. Starn, N. N. Sesi, J. A. Horner and G. M. Hieftje, "A LabVIEW program for determining electron number density from Stark broadening measurements of the hydrogen-beta line", *Spectrochim. Acta, Part B*, 1995, **50B**, 1147.

[17] T. Hasegawa, M. Umemoto, H. Haraguchi, C. Hsiech and A. Montaser, "Fundamental properties of inductively coupled plasmas." in *Inductively Coupled Plasmas in Analytical Atomic Spectrometry*, A. Montaser and D. W. Golightly, VCH Publishers, Inc.:New York, 1992.

[18] R. A. Hill, "Tables of electron densities as a function of the halfwidth of Stark-broadened hydrogen lines." *Quant. Spectrosc. Radiat. Transfer*, 1964, **4**, 857.

[19] G. F. Kirkbright and M. Sargent, *Atomic Absorption and Fluorescence Spectroscopy*; Academic Press Inc. Ltd.: London, 1974.

[20] B. Welz and M. Sperling, *Atomic Absorption Spectrometry*; Wiley-VCH: Weinhein, 1999.

[21] W. G. Schrenk, *Analytical Atomic Spectroscopy*; Plenum Press: New York, 1975.

[22] J. M. Mermet, "Fundamental principles of inductively coupled plasmas" in *Inductively Coupled Plasma Spectrometry and its Applications*, S. J. Hill, Sheffield Academic Press:Sheffield, 1999

[23] C. Thomsen and V. Helbig, "Determination of the electron density from the Stark broadening of Balmer Beta-comparison between experiment and theory", *Spectrochim. Acta, Part B*, 1991, **46B**, 1215.

[24] O. H. Nestor and H. N. Olsen, "Numerical Methods for Reducing Line and Surface Probe Data", *SIAM Review*, 1960, **2**, 200.

[25] D. Fang and R. K. Marcus, "Use of a cylindrical Langmuir probe for the characterization of charged particle populations in a planar, diode glow discharge device", *Spectrochim. Acta, Part B*, 1990, **45B**, 1053.

[26] P. Mezei, T. Cserfalvi, H. J. Kim and M. A. Mottaleb, "The influence of chlorine on the intensity of metal atomic lines emitted by an electrolyte cathode atmospheric glow discharge", *Analyst*, 2001, **126**, 712.

[27] C. A. Bye and A. Scheeline, "Saha-Boltzmann statistics for determination of electron temperature and density in spark discharges using an echelle/CCD system", *Appl. Spectrosc.*, 1993, **47**, 2022.

[28] A. W. Irwin, "Polynomial partition function approximations of 344 atomic and molecular species", *Astrophysical Journal, Supplement Series*, 1981, **45**, 621.

[29] A. Montaser and D. W. Golightly, *Inductively Coupled Plasmas in Analytical Atomic Spectrometry*, VCH Publishers, Inc.: New York, 1992.

[30] M. Ohata and N. Furuta, "Spatial characterization of emission intensities and temperatures of a high power nitrogen microwave-induced plasma", *J. Anal. At. Spectrom.*, 1997, **12**, 341.

[31] W. Luecke, "The ionization behavior of the alkaline earth metals in the air-acetylene and nitrous oxide-acetylene flames", *Spectrochim. Acta, Part B*, 1992, **47B**, 741.

[32] C. E. Moore, *Atomic Energy Levels, Volume 1*, 1949, **Volume 1**,

[33] C. E. Moore, *Atomic Energy Levels, Volume 2*, 1949, **Volume 2**,

[34] C. E. Moore, *Atomic Energy Levels, Volume 3*, 1949, **Volume 3**,

[35] D. R. Lide, *CRC Handbook of Chemistry and Physics*, CRC Press, 1995

Chapter 6

Use of a solution-cathode glow discharge for the analysis of complex mixtures.

6.1 INTRODUCTION

The inductively coupled plasma (ICP), particularly when coupled with mass spectrometric (MS) detection, is rightly recognized as a powerful tool for elemental analysis, but that power comes with significant costs. Gas (>15 L min^{-1} Ar) and power (>1 kW) consumption are high and, along with the need for vacuum equipment, effectively tie an ICP-MS to the laboratory. With these considerations in mind, it is easy to appreciate the continued use of other techniques (e.g. electrothermal vaporization atomic absorption and flame atomic absorption and emission) and the interest in development of new sources, particularly miniaturized ones.

The electrolyte-cathode discharge (ELCAD) is an alternative source for elemental analysis of liquid solutions first introduced by Cserfalvi and coworkers in 1993.[1] It has a small footprint, low power consumption (<75 W), and operates in atmospheric-pressure air. In essence, it is a glow discharge using an electrolytic solution as the cathode and a metal rod as the anode. The electrolytic solution serves as the sample in the ELCAD, just as the solid cathode often does in a conventional low-pressure glow discharge.

Despite its simplicity, the ELCAD performs quite well. Detection limits for a range of metals are generally in the 10s of ppb[2-3] and short-term precision is typically around 1% for ppm concentrations (this work). One aspect that is in need of further study is how well complex solutions can be analyzed. For our purposes, complex solutions are samples that differ from standards in more ways than the concentration of the analyte being determined. Acidified tap water (often with additional metals added) has been used as the sample solution several times,[1-3-9] but the concentrations measured by ELCAD have not been compared to those measure by other techniques. Similarly, acidified diluted milk (3 mL in 1 L) has been analyzed using ELCAD,[7] but without comparison to known values.

Experience with flames and other plasmas suggests we should expect interferences of some sort. Such interferences should be studied to establish both the limitations of the technique and ways to overcome those limitations when possible. Further, effects of concomitant species have sometimes provided insight into operational mechanisms of other techniques.[10-11]

Before reporting the results of this study, it is worthwhile to review what is already known about analyzing complex samples with ELCAD.

6.1.1 Spectral interferences

Spectral interferences can be placed broadly into two categories: background emission and concomitant species emission. The former can impair performance, especially by constraining detection limits, but is not particular to complex samples. Rather, it is the

latter that is relevant in the present context. Some sources, such as the ICP and the low-pressure glow discharge, are line-rich, which increases the potential for spectral overlap. In the ELCAD, very little ionic emission is observed.[12-13] The electron number density (8.5×10^{14} cm^{-3}) and the ionization temperature (5000 K) have been used to predict the degree of ionization for various elements in the plasma and found it to be quite low for most elements (less than 10% for the majority of the 88 elements considered).[12] Low ionic emission is expected to make spectral overlap somewhat less common.

Recently, two studies[2-8] have shown that the spatial distribution of analyte emission varies by element. It is possible that this feature could be exploited to reduce spectral interference, although the gains are unlikely to be worth the additional complexity.

6.1.2 Ionization interference

Ideally, the ratio of atoms to ions of an analyte should be unaffected by either the concentration of the analyte or the concentrations of other sample concomitants. If this is true, a calibration plot based on either the atom concentration or the ion population in the source (for example, on measuring atomic or ionic emission) will be useful for calculating concentrations of the element in the solution. In reality, this ratio is proportional to the electron number density (assuming that other plasma characteristics are unchanged).[14] In a flame, the electron number density is affected significantly by electrons produced by the ionization of even low concentrations of metals because the background electron number density is comparatively low. This results in gas-phase atom and ion populations (and therefore atom and ion emission and absorption) that are nonlinear with solution concentrations and are altered by the presence of other elements.

In an ICP, the background electron number density is high enough (typically measured as around 10^{15} cm^{-3})[14] that changes caused by elements in the sample solution are insignificant. As was previously mentioned, the electron number density in the ELCAD has been measured to be 8.5×10^{14} cm^{-3}, nearly as high as the ICP. Given that, ionization interference would not be expected in an ELCAD. Supporting this, the same paper showed no evidence of this interference in an ELCAD under conditions where it would have been pronounced in a flame.[12]

6.1.3 Electrolyte effects

Early ELCAD experiments showed that pH has a strong effect on analyte emission.[1] To produce analyte emission from the ELCAD, a pH below about 2.5 is required, with a more acidic pH producing stronger emission. Over a pH range of 0.8 to 1.9, which roughly covers the practical range of the technique, emission decreases linearly 5 to 8-fold for the elements studied in a recent paper.[2] Given that pH is a logarithmic scale, this translates to changes in acid concentration having relatively smaller effects on emission when the starting concentration is high than when it is low. For example, a 2 mM acid addition to a solution originally having a pH of 2 would shift the pH by 4%, but the same amount of acid added to a solution originally having a pH of 1 would only shift the pH by 0.9%. Since emission is linearly related to pH, the relative change in emission will be less for the pH 1 solution than the pH 2 solution. For this reason, and because of the increased emission, we recommend using a relatively low pH and typically use a pH of 1.

It has been show that the supporting electrolyte identity has a significant effect on

emission as well, and that electrolytes other than acids can be used. Mezei et al.[15] found that using acids as the supporting electrolyte results in greater emission than using salts and that there is variation according to the acid anion. Specifically, they determined the sequence of analyte emission to be $H_2SO_4 < HNO_3 < HCl$ and suggested use of HCl. We suggest HNO_3 instead for reasons of chemical compatibility. Yagov and Gentsina[16] had similar results for a source akin to the ELCAD, the drop-spark discharge (DSD). A DSD differs from an ELCAD in that the anode is also an electrolytic solution rather than a solid metal.

6.2 EXPERIMENTAL

The equipment used in this study has been diagrammed and described in detail previously,[2-12] so only a brief description will be given here. The sample solution enters the cell through a portion of a 1-mL serological pipette that has been bent so the tip points upwards a few millimeters below a 1.6-mm diameter Ti anode. Except where noted, the gap was 3 mm. A Kepco (Flushing, NY) BHK 2000-0.1MG or BHK 1000-0.2MG high-voltage power supply operated in constant-current mode is connected to this anode through a 400-Ω ballast resistor. Unless otherwise noted, an 80 mA current was used. The sample solution overflows from the tip into an approximately 35-mL reservoir containing a grounded graphite electrode. This overflow creates an electrical connection between the solution at the pipette's tip and the graphite electrode. Unless otherwise noted, the solution was acidified with nitric acid to pH 1. The discharge is initiated by bringing the anode close to the solution.

A black rectangular polyethylene divider supported by the pipette reduces the amount of hydrogen (produced at the graphite cathode) that reaches the discharge, blocks some light from sources external to the discharge, and wicks moisture over the sides of the reservoir so a constant solution level is maintained within the reservoir. The hydrogen is blocked because its presence is known to affect emission in other glow discharges;[11] the light is obstructed to reduce background noise; and the reservoir level is held constant to prevent fluctuations in the ohmic drop across the solution between the pipette tip and the graphite cathode.

Solution is supplied using a Global FIA MilliGAT (Fox Island, WA) flow-injection system. A 6-port 2-way switch allows the sample to be changed without interrupting the solution flow. The discharge is imaged at a magnification of 2.3:1 with a quartz lens onto the entrance slit of a Chromex (Albuquerque, NM) 500IS/SM 0.5-m Czerny-Turner spectrometer. Observation is limited to approximately the bottom two thirds of the discharge by using electrical tape affixed to the monochromator entrance slit. Detection is accomplished with a Hamamatsu (Hamamatsu, Japan) R928 PMT biased at -850 V, which feeds a Keithley (Cleveland, OH) 427 current amplifier. The output of this amplifier is recorded with a custom LabVIEW (National Instruments Corporation, Austin, Texas) program. Except where otherwise noted, emission intensities and standard deviations are based on ten consecutive measurements of the same sample, where each measurement is the averaged intensity from a 10-second period acquired at 1 kHz .

6.3 RESULTS AND DISCUSSION

6.3.1 Dynamic range

To minimize sample handling and thereby reduce the likelihood of contamination and the time needed to analyze a sample, it is preferable not to dilute the solution. A broad dynamic range makes dilution less likely to be necessary. The benefits of a large dynamic range are even greater for complex samples, as elements may be present at widely disparate concentrations and samples made through different degrees of dilution might otherwise be necessary. This is a particular problem in flame AAS, which typically has a linear range of only about two orders of magnitude.[17-19]

To evaluate the dynamic range of ELCAD, calibration curves (shown as log-log plots in Figure 6-1) were constructed for 5 elements (Ca, Cd, Cu, Na, and Pb). For each element two linear fits were calculated. The first was based on all of the data that were within the linear range (these fits are shown in Figure 6-1). The second was based on the last point contained in that curve and the first point not contained in that curve (i.e., the first point for which nonlinearity was apparent). The concentration at which extrapolated (i.e., calculated from the first curve) and interpolated (i.e., calculated from the second curve) emission calculated from these two curves differed by 5% was used to define the upper bound of the linear range. This, it should be noted, is a conservative estimate, as a curved line (the true shape) connecting the last two points will diverge rather slowly from the linear fit. Table 6-1 shows the limits of detection, approximate concentrations at which calibration curves become nonlinear (presumably due to self-absorption), and linear dynamic ranges based on these extremes.

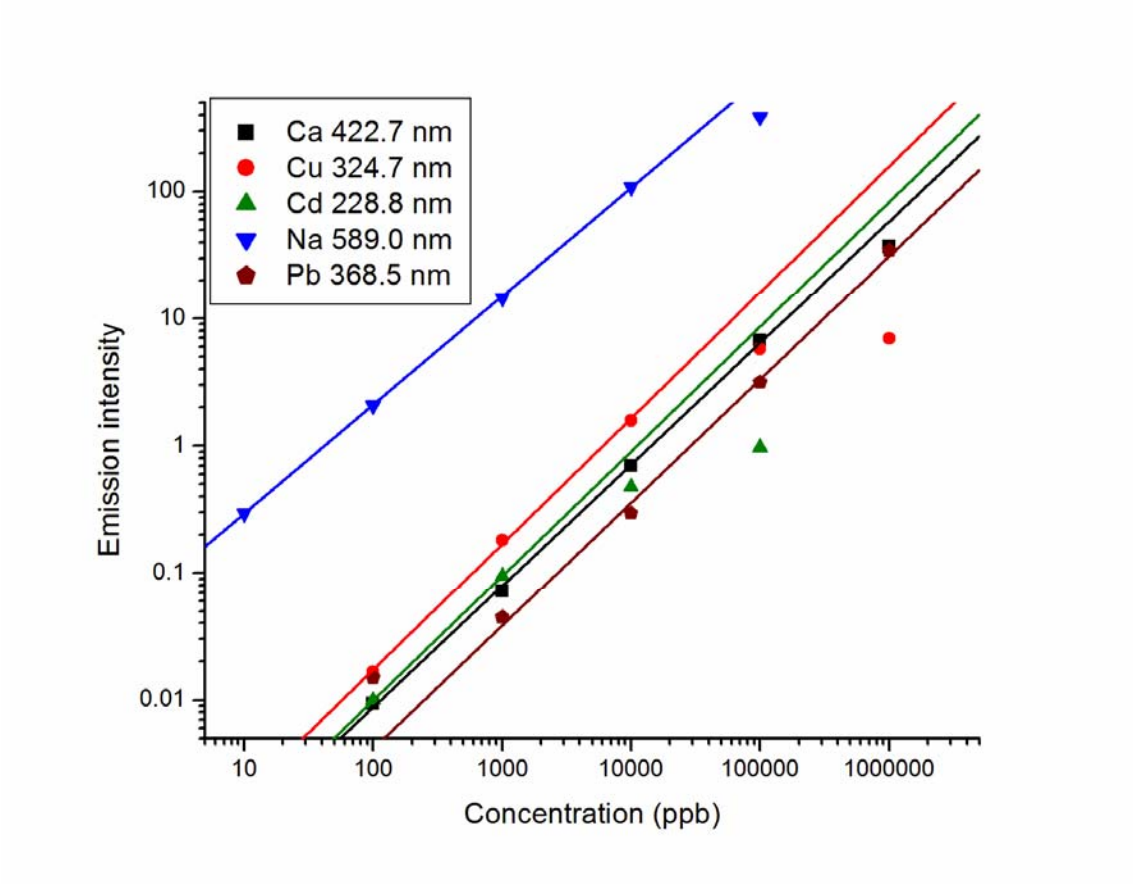

Figure 6-1. Calibration plots for several elements. Lines are fits to the linear portions of the data.

Table 6-1. Working range details for several elements.

Element	Wavelength (nm)	Slope of log-log plot	Detection limit (ppb)	Upper bound (ppm)	Working range (orders)
Ca	422.7	0.956	20	110	3.7
Cu	324.7	0.990	30	11	2.6
Cd	228.8	0.980	10	1.1	2.0
Na	589.0	0.855	0.8	11	4.1
Pb	368.5	0.970	80	> 1,000	≥ 4.1

Calibration plots for four of the elements have log-log plots with slopes very close to one, which would be expected from a perfectly linear relationship. The exception is sodium, the behavior of which might be explained as the result of an improper assumption that the only significant source of sodium is that which is intentionally added. In fact, our blanks have ppb-level sodium impurities. Adjusting the "known" concentrations upwards would result in a slope closer to one, but this adjustment was not made because the contaminant level in these particular samples is not known with sufficient certainty.

The linearity range varies from 2.0 (Cd) to at least 4.1 (Pb) orders of magnitude, which is an improvement on atomic absorption but is not as broad as ICP emission or ICP mass spectrometry. This relatively large linear range arises from the optical thinness of the source. An optically thin source has efficient emission (reflected in a high excitation temperature) from comparatively low atom concentrations and a short pathlength (narrow physical thickness). The ELCAD has both of these characteristic (>5000 K Fe excitation temperature and 2 mm diameter). As in other emission-based techniques, the range can likely be expanded by using weaker lines at higher concentrations. It should be noted, however, that the sparse nature of ELCAD spectra, which was an advantage in the context of section 6.1.1, is a disadvantage from this viewpoint.

6.3.2 Effect of phosphate on calcium

In some ways (e.g., gas temperature), the ELCAD is more comparable to a chemical flame than to an ICP. Accordingly, interferences that are present in flame-based techniques are likely in the ELCAD. Chemical interferences, such as the binding of calcium by phosphate, are a notable example. To test for the presence of this interaction,

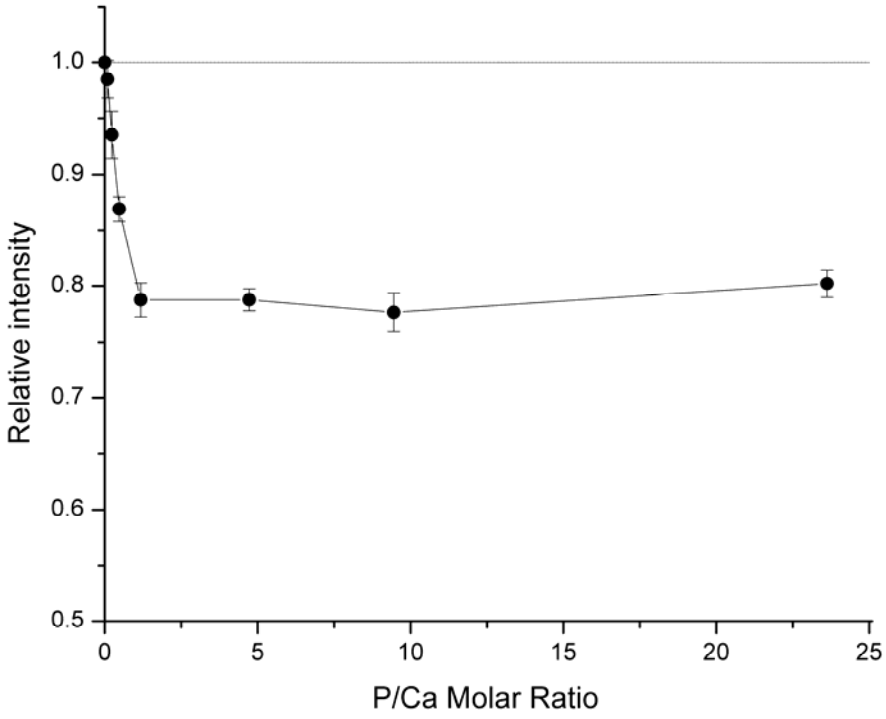

Figure 6-2. Response of calcium 422.7 nm emission to increasing amounts of phosphate (added as H_3PO_4). Upper line shows emission level with no phosphate present.

a series of solutions with 2 ppm Ca and increasing amounts of phosphate was analyzed. The result is graphed in Figure 6-2. The interference appears to take the same form as in a chemical flame, although it is less severe than in an air-acetylene flame under common conditions (cf. Smets[20]). As phosphate concentration (added as H_3PO_4) is increased, calcium emission first drops, then levels off at about 79% relative to emission from the matrix-free sample. This leveling off takes place near a P/Ca molar ratio of 1, as in a flame.[20] The lesser magnitude of the effect here likely results in part from the higher gas temperature of ELCAD compared to air-acetylene flames.[2-20]

Higher temperatures reduce the phosphate interference in flames by improving vaporization. Adjusting the ELCAD discharge current was tested as a remedy here on the hypothesis that it might also improve vaporization. Two series of experiments were performed. One involved varying the current from 30 to 80 mA (30, 40, 55, 67, and 80 mA) while the blank-corrected emission from a solution of 2.5 ppm Ca and 27 ppm PO_4^{3-} (from H_3PO_4) was compared to that from a solution of 2.5 ppm Ca with no phosphate. The second used 20 ppm PO_4^{3-} (from Na_2HPO_4) and 2 ppm Ca with currents of 60, 80, and 100 mA. No trend or significant variation was seen within either data set. This is perhaps not surprising, since the rotational temperature (which is a good reflection of gas temperature) is not affected significantly by current in the ELCAD.[2]

In chemical flames the gas temperature can be varied by using different oxidant/fuel combinations. In ELCAD, changing the gap has been shown to affect the rotational temperature.[2] Consequently, the effect of gap width on this interference was determined at a discharge current of 70 mA. Blank-subtracted emission from a solution of 27 ppm

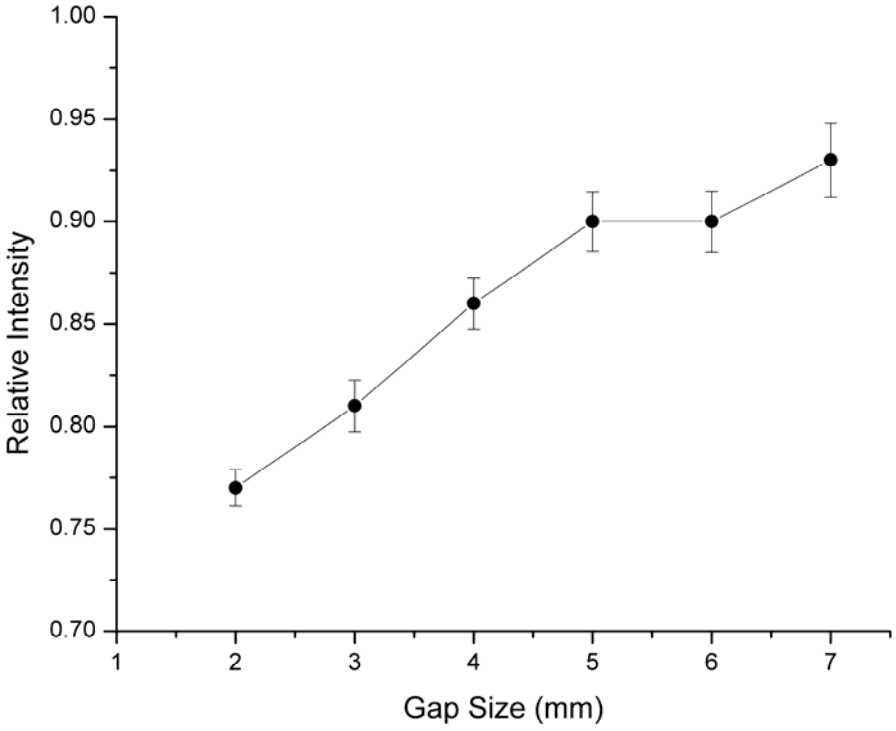

Figure 6-3. Improvement in accuracy of calcium analysis in a 2.5 ppm Ca, 27 ppm PO_4^{3-} (added as H_3PO_4) solution with increasing gap size. Emission intensity at 422.7 nm is given relative to emission from at 2.5 ppm Ca solution with no PO_4^{3-}.

PO_4^{3-} (from H_3PO_4) and 2.5 ppm Ca was compared to that from a solution of 2.5 ppm Ca. The results are shown in Figure 6-3. There is a reduction in the matrix effect as the gap is widened. Adjusting the gap could therefore potentially be used to diagnose the presence of a phosphate interference. For example, if the concentration calculated at a gap of 3 mm does not match the concentration calculated at a gap of 5 mm, the presence of an interferent can be assumed. Simply increasing the gap, however, does not seem a tenable solution to removing this interference. Even at a gap of 7 mm, which is more than twice what is typically used, a 7% suppression remains, and the rate of improvement appears to be declining. A more detailed study might reveal a reliably predictive relationship between the true concentration and the calculated concentrations at multiple gaps. Diagnostics, particularly one such as this that does not require adulterating the sample, are valuable in that they can be used to decide whether or not more time-consuming interference-reduction methods are necessary.

One such method is the addition of lanthanum. In flames, lanthanum is used to preferentially bind phosphate, thereby freeing calcium. To test this remedy, solutions of calcium; calcium and phosphate; calcium and lanthanum; and calcium, phosphate, and lanthanum were prepared. When present, the concentrations were 2.5 ppm Ca, 27 ppm PO_4^{3-}, and 1000 ppm La. Lanthanum was added as $La(NO_3)_3 \cdot 6H_2O$, and phosphate was added as H_3PO_4. Two blanks, one with 1000 ppm La and one with none, were also prepared. Reported values are the intensity of the sample minus the intensity of the relevant blank. The discharge gap for these experiments was 3.5 mm, and the current was 75 mA. In line with previous results, the solution with both calcium and phosphate

produced 85% of the emission intensity of the solution with calcium alone. The solution of calcium and lanthanum produced slightly less emission, 83% of the calcium-only solution. The solution of calcium, lanthanum, and phosphate produced 99% as much emission as the calcium and lanthanum solution (82% as much as the calcium-only solution). The difference between the two lanthanum-containing solutions is within experimental error (1.4% difference compared to 1.8% (phosphate-containing) and 1.8% (phosphate-free) relative standard deviation), although it is possible that there is some small residual phosphate interference. It appears from these results that lanthanum, when present at high concentrations, also produces a matrix effect on calcium, so calibration curves must contain the same amount. At 1000 ppm, in addition to suppressing calcium emission by 17%, La reduced the background emission by 13% and the total voltage drop (including ballast resistor, discharge, and solution) by 3%. Although it was not examined in detail, this interference appears to be at least similar to the one discussed in section 6.3.4.

The pattern of the effect with respect to phosphate concentration, the impact of temperature on the interference, and the alleviation of the suppression when lanthanum is added all point to similar origins in ELCAD and flames. It is likely, then, that the more general oxyanion interference with alkaline earth elements exists and can be remedied by conventional (for a flame) means.

6.3.3 Charge bias

To reach the negative glow, species from the solution must migrate towards a more positive potential. Since the elements analyzed by ELCAD are generally positively

charged in solution, it is quite likely that the electric field impedes their migration. This is of concern primarily for two reasons. Most directly, a charge bias might exist where forms of the same element with different charges in solution would migrate into the plasma with different efficiencies, causing a biased emission signal and incorrect calculation of concentration. Further, the presence or absence of such a bias could inform the operational model. The charge difference need not be directly from the oxidation state of the element. In fact, because the solution pH is regulated and is held relatively low, oxidation state is probably a lesser concern than the difference in charge between "bare" atomic cations and metals covalently bound to other atoms. It is this difference that we chose to evaluate by comparing solutions of permanganate and dichromate to solutions with their respective metals as cations.

Three chromium standard curves were constructed, one each based on $Cr(NO_3)_3$, K_2CrO_7, and $(NH_4)_2CrO_7$. The relative standard deviations of the slopes, in the same order, were 0.4%, 0.5%, and 0.9%. The slopes of the two Cr(VI)-based calibrations differed by 3% , which may have been due to a combination of enhancement by NH_4 and suppression by K (see section 6.3.4). The slope of the Cr(III)-based curve was 13% lower than the average of the other curves.

To study the same effect with Mn, a 4 ppm solution of $KMnO_4$ was divided in two. Sodium bisulfite was added to one solution (enough to make the solution clear) to reduce the manganese to Mn(II) from Mn(VII). The Mn(VII) emission (which had a 0.9% RSD) was 16% more intense than the Mn(II) emission (which had a 0.5% RSD). While a Na matrix effect (see section 6.3.4) might account for a few percent of this change, it does

not account for most of it.

In both cases, the polyatomic anion containing a high oxidation state metal resulted in more emission per metal atom in solution than did the lower oxidation state atomic cation. The most apparent conclusion is that the species retain their charges, which hinder migration for positive ions but aid it for negative ions. Alternatively, or complementarily, cations may need to be neutralized prior to migration (for example, by oxide formation as argued by Cserfalvi and Mezei[21]), while anions can migrate with their charges intact.

The metals in the polyatomic anions obviously must be converted to free atoms before they can produce atomic emission. The observed emission trends imply that the increase in transport efficiency more than compensates for any loss in atomization efficiency, and/or atoms originating as atomic cations in solution are also bound (again, possibly as oxides) and must go through a similar atomization process.

6.3.4 Cation effects

The impact of only a few cations on emission of analytes and the discharge in general were studied in detail, but other cations appear to exhibit similar behavior (see section 6.3.2 for evidence of analyte-emission suppression by high concentrations of lanthanum). Figures 6-4 and 6-5 show the impacts of equimolar concentrations of several cations (introduced as chloride salts) on analyte emission and background emission, respectively. Emission was measured as the average of five 10-second measurements that have been corrected by subtraction of either the blank emission at the same wavelength with the

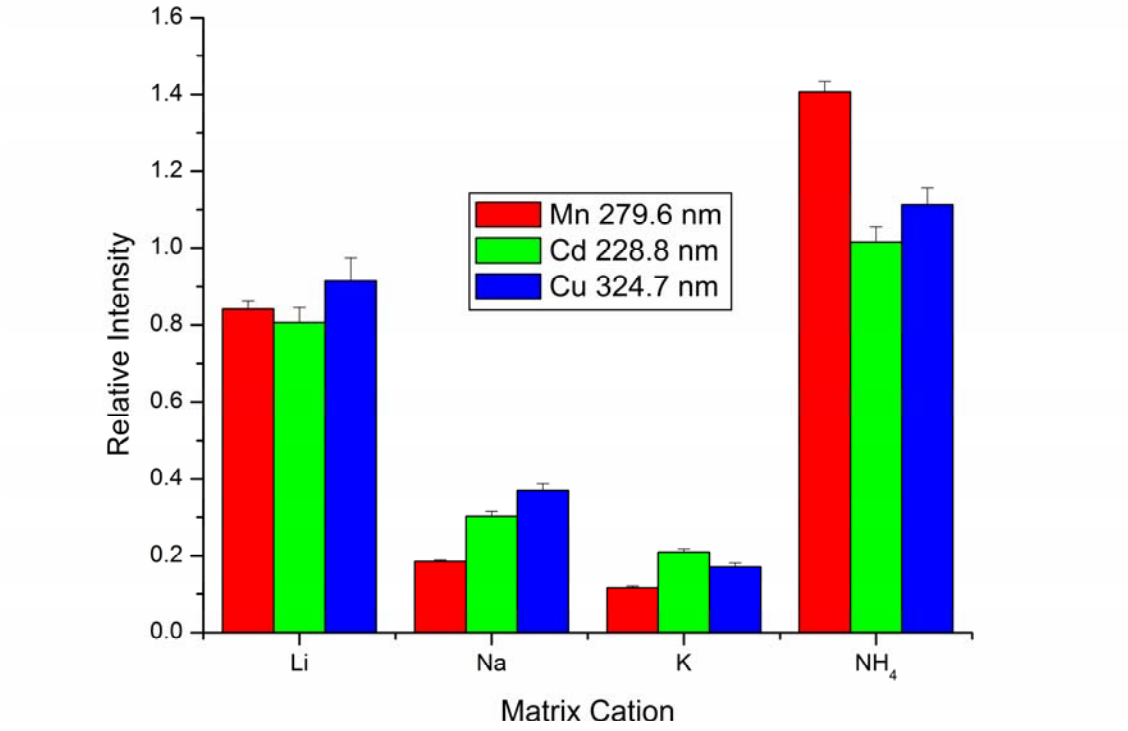

Figure 6-4. Effect of equimolar (25 mM) concentrations of several chloride salts on analyte emission. Intensities have been corrected for blank emission. A relative intensity of 1 denotes absence of a matrix effect.

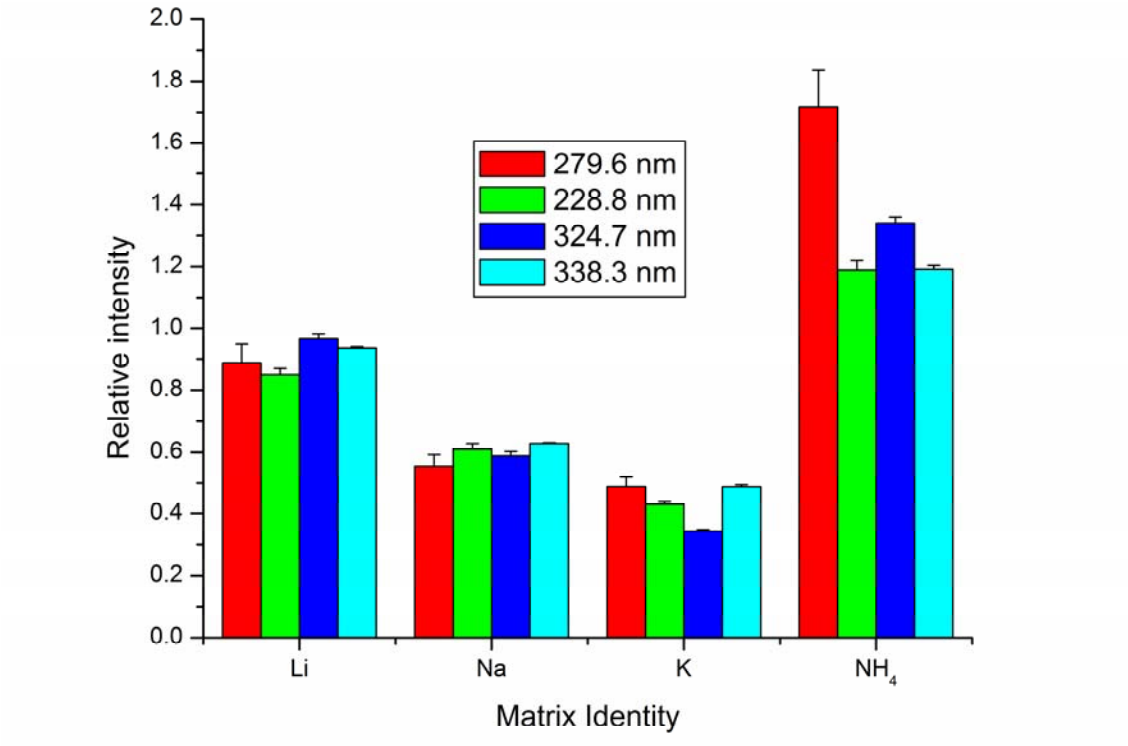

Figure 6-5. Effect of equimolar (25 mM) concentrations of several chloride salts on background emission at several wavelengths. Intensities have been corrected for dark current. A relative intensity of 1 denotes absence of a matrix effect.

same matrix (Figure 6-4) or the dark signal (Figure 6-5). This emission signal was then divided by an emission signal measured in the same way except without matrix in the solution. The plotted relative intensities are the results of this calculation. The error bars represent the error computed by propagating through the calculations the various standard deviations from the measurements. Notably, the continuum emission is suppressed or enhanced by approximately the same factor for a given matrix at every monitored wavelength. The suppression or enhancement of analyte emission by a given matrix is also similar for the metals observed. This clustering suggests methods for ameliorating the interference. Internal standards could certainly be used to lessen the inaccuracies, but there is enough scatter between elements that significant error would remain.

Other correction approaches might be found in the flexibility of the ELCAD system. Boosting the current, for example, intensifies emission. Two cadmium sample-blank pairs, one with 25 mM sodium and one without, were prepared. Emission from the matrix-free blank at the cadmium wavelength (228.8 nm) was recorded. Emission from the matrix-containing (but cadmium-free) solution was then monitored. The discharge current was adjusted until the background emission from the matrix-containing solution matched that of the matrix-free blank. This adjustment required a current of 110 mA, 38% higher than the original 80 mA. The emission from the solution containing both cadmium and sodium was next measured with the current at 110 mA and compared to the emission from the solution containing cadmium but not sodium with the current at 80 mA. With suitably reproducible wavelength accuracy or multiple detectors, this procedure could be simplified to omit the blanks. Without adjusting the current, the

suppression was 70%. By adjusting the current, this error was reduced to 38%, which is still unacceptably large.

Related approaches might be more fruitful. For example, an internal standard could be combined with adjusting the current, with the idea that the emission from the standard would be restored at the same point as that of the analyte. As will be shown shortly, the power deposited across the discharge also drops in the presence of a matrix. Restoring this power by increasing the current to the appropriate level might also recover the analyte emission. Unfortunately, both of these approaches require the application of higher voltages than were available in this study.

Another fix would be to dilute the sample. Obviously, this requires that the suppression is less at lower matrix concentrations, and dilution comes at a cost to sensitivity. This was one reason for the next series of experiments, in which the effects of increasing sodium concentrations were measured. Another reason was to gain insight into the reason for the effect. To that end, parameters beyond just emission were monitored. Figure 6 summarizes the results for a sodium matrix.

As Figure 6-6 shows, six variables were monitored: Ca 422.7 nm emission, background emission at 422.7 nm, power deposited in the discharge, resistance across the solution, OH rotational temperature, and Fe excitation temperature. Several sets of solutions were used and not all measurements were made simultaneously. Sodium was introduced from a nitrate standard.

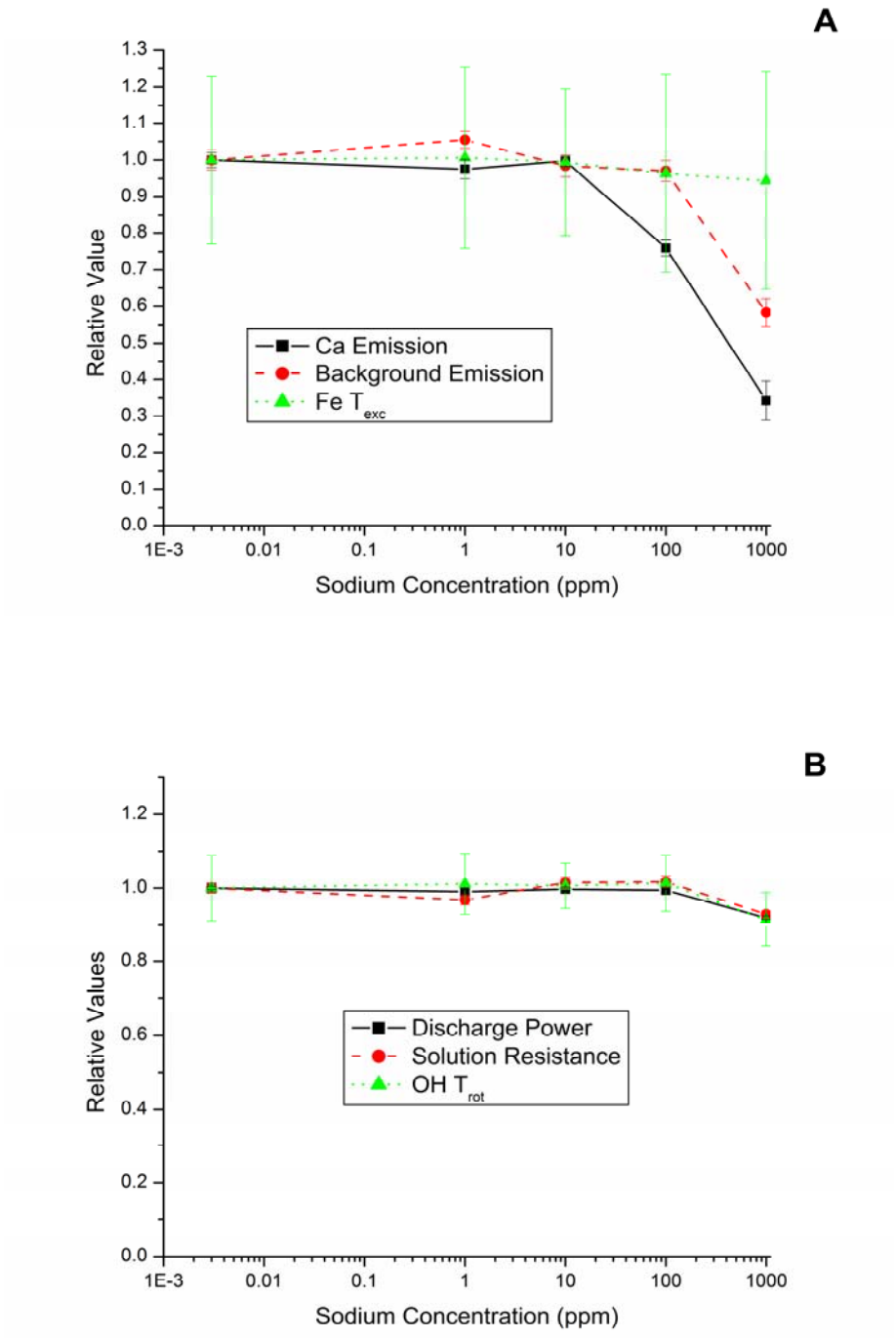

Figure 6-6. Effect of matrix (Na) concentration on various discharge parameters. Calcium and background emission were measured at 422.7 nm. OH rotational and Fe excitation temperatures were calculated from Boltzmann plots such as in Figure 6-7. Error bars represent one standard deviation.

Iron was present (at approximately 10 ppm) only when its excitation temperature was being measured. This excitation temperature and the OH rotational temperature were both calculated from Boltzmann plots of a collection of lines.[22-23] For OH, the lines were 308.33, 308.52, 308.73, 309.53, 309.86, 311.02, and 311.48 nm. For Fe, they were 371.99, 373.49, 373.71, 381.58, 382.04, 382.59, 383.42, and 385.99 nm. In both cases, the averages of peak areas from five spectra acquired by scanning the monochromator wavelength were used in the calculations.

Voltage probes were present only when solution resistance and discharge power were measured. These electrical characteristics were measured simultaneously with each other but separately from other factors. One probe was attached to the anode of the discharge. A second was attached to a wire that was inserted through the ELCAD capillary so that its bare tip was located just below the solution surface. The distance from the surface was well under 1 mm, but a more exact measurement is difficult because the solution level is lower when the discharge is on than when it is off. The voltage difference between the two probes was multiplied by the current to calculate the discharge power. The voltage between the solution probe and ground was divided by the current to compute the solution resistance. Admittedly, both measurements will be somewhat off because of the small distance between the solution-probe tip and the solution surface. However, this error does not seem to be substantial and should be consistent among measurements.

Ten 10-second measurements were averaged for each Ca emission data point. Matrix-matched blanks (also taken from ten 10-second measurements) were used for background

correction. These same blank-corrected measurements were used to monitor background emission. In this latter case, a 300-second dark measurement (with the plasma extinguished) was subtracted before the results were plotted.

As Figure 6-6 shows, all six factors are constant, or nearly so, through 100 ppm Na, except for Ca emission and the Fe excitation temperature. At 1000 ppm, however, all of the measured values drop. Ca emission declines the most substantially, down to 66% lower than in a matrix-free situation. Background emission falls by a lesser 32%. Other factors go down by a lower, but fairly uniform, approximately 10%.

The observed matrix effect is likely to arise from a mixture of sources, so several that are consistent with the evidence will be discussed below.

Solution resistance can be expected to correlate with energy lost to the solution as heat. In the cell design used here, the pipette that delivers the sample solution passes through the waste reservoir, which allows the solution to be heated before reaching the discharge. The small cross-sectional area of the overflow connecting the discharge to the waste reservoir is responsible for the bulk of the solution resistance[2] and is therefore an area of high resistive heating. It has been shown that heating the solution results in higher ELCAD emission.[24] A possible explanation is that heating lowers the surface tension and improves transport into the discharge and/or results in smaller droplets that can be more readily desolvated. High matrix concentrations lower the solution resistance and the solution heating, which should decrease transport and/or desolvation efficiency.

Introducing large amounts of a metal, particularly one as easily ionizable as sodium, is

likely to raise electron and ion populations in the plasma. To check this hypothesis, the half-width of the 486.1 nm hydrogen-beta line was measured for two conditions: a blank solution and a solution containing 500 ppm sodium (which is close in concentration to the 25 mM solution used earlier). With the monochromator slits narrowed to 10 μm (giving 15 pm resolution), emission was collected at 30 pm intervals over a 643 pm window symmetrically encompassing the H_{β} peak. The points were collected in two passes as a check against drift (none was apparent). For the blank solution, a 30-second average of data collected at 1 kHz was used for each point. This time was increased to 50 seconds for the matrix-containing solution in anticipation of weaker signals. In fact, once the baseline was subtracted, the signals were comparable in magnitude. The peaks have Voigt profiles but are dominated by Lorentzian character. Origin (OriginLab Corporation, Northampton, MA) was used to fit the two peaks to Lorentzian curves. The full widths at half maximum (FWHM) computed by the program were 148 and 184 pm for the matrix-free and matrix-containing solutions, respectively. Calculating exact electron number densities from these widths is not possible because there are several factors that are not controlled. Notably, other sources of broadening have not been compensated, and the measurement is not restricted to a single spatial location. Vertically, both the negative glow and a portion of the positive column (which have significantly different electron number densities[12]) are included, and no attempt at radial resolution was made. With those caveats in mind, it seems worthwhile to obtain a crude estimate of the difference in electron number densities. Interpolating from tables,[25] we calculate number densities of 6.5×10^{14} cm^{-3} in the absence of matrix and 8.9×10^{14} cm^{-3} with 500 ppm sodium. This increase is substantial, but its precise magnitude should be

treated with some skepticism for the above-mentioned reasons.

Whether or not it is by 37%, it is clear that there is some elevation in electron number density caused by Na. This change would be expected to reduce the plasma resistance, and therefore the power deposited in it. Indeed, with 1000 ppm sodium, an 8.8% drop in discharge power is observed relative to the power with lower Na concentrations. With less power deposited, the OH rotational temperature also drops by 8% (from 2980 to 2730 K).

The behavior of the Fe excitation temperature (Figure 6-6a) stands out from other factors. This temperature appears to drop only slightly, rather than showing an abrupt change. The rather large errors associated with spectroscopic temperature measurements, however, caution against too much weight being given to the small changes observed. Even the change between the temperature above the matrix-free solution (5930 K) and the 1000 ppm Na solution (5600 K) might not be real. Assuming it is, this 6% change in excitation temperature is not enough to account for the drop in calcium emission, but looking more deeply into the measurements is revealing. Figure 6-7 shows the Boltzmann plots used to calculate the excitation temperature. The slopes of such plots and excitation temperature are inversely proportional. The degree of scatter, and its potential effect on the slopes, support caution in giving too much credence to the small changes in temperature that were calculated. The highest sodium concentration curve stands out, however, not because of its slope, but because of its offset.

The y-intercept of each plot in Figure 6-7 is proportional to:

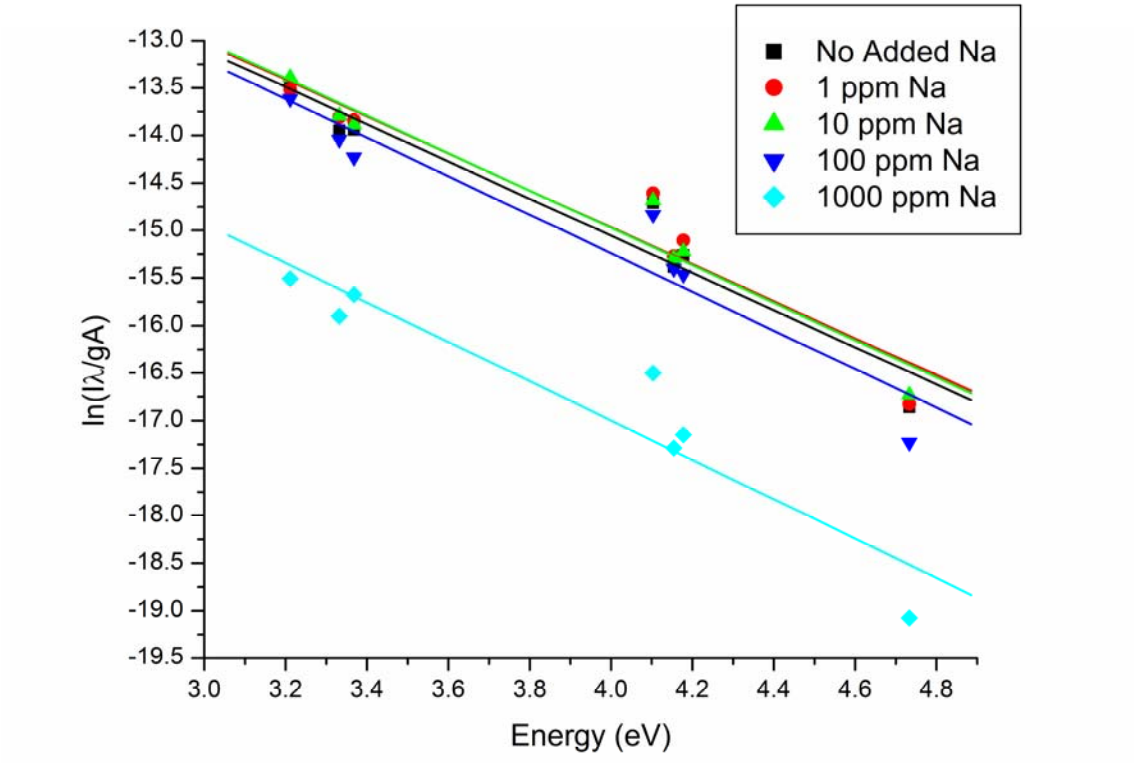

Figure 6-7. Boltzmann plots used to determine iron excitation temperatures at different concentrations of sodium.

$$\ln\left[\frac{nlhc}{4\pi Z(T)}\right] \tag{6-1}$$

where l is the path length of the source, h is Planck's constant, and c is the velocity of light. Only n (the atom number density) and $Z(T)$ (the partition function) are not constant. Given the excitation temperature, the partition function can be calculated from polynomial equations given by Irwin.[26] Solving for the relative number densities shows that the atom population drops substantially (by 77%) in the plasma above the solution with the highest matrix concentration (1000 ppm) relative to the Na-free solution. For the other samples, atom populations vary by ±6.5% relative to their average, with no directionality to the trend. Given that the relative standard deviations calculated from the least-squared fits vary between 11 and 15%, only the difference between the 1000 ppm solution and the others is significant. More detail is provided in Table 6-2.

Also shown in Table 6-2 are the results of a further analysis. We can back-calculate the relative intensities of the lines used in the original calculation from the equation:

$$\frac{I}{I_0} = \left(\frac{n}{n_0}\right)\left(\frac{Z(T_0)}{Z(T)}\right)\exp\left(\frac{E_p}{kT_0} - \frac{E_p}{kT}\right) \tag{6-2}$$

where E_p is the excitation energy of the level from which the emission occurs and I is the intensity of that emission. Terms subscripted with zero refer to the condition with no added matrix, and terms without subscripts refer to the condition with matrix (n, I, and T) or are not a function of matrix (E_p and k). More importantly, we can use the same equation to determine the relative contributions of concentration and excitation to the observed variation. The term in the left-most brackets is the relative atom population.

Table 6-2. Evaluation of excitation and concentration (transport) components of observed Fe emission in Na matrix. See text for basis of computations.

Sodium concentration (ppm)	Average emission	Excitation component	Concentration component
0	1.00	1.00	1.00
1	1.09	1.04	1.05
10	1.09	0.96	1.14
100	0.84	0.77	1.09
1000	0.15	0.67	0.22

The remainder of the right side of the equation is the relative emission efficiency, which is temperature-based. The product of the two terms, as the equation shows, is the relative emission intensity (I/I_0). To simplify the comparison, the relative values for all seven emission lines for a given solution were averaged. These averages are reported in Table 6-2. The contribution from concentration is relatively steady through 100 ppm, but drops dramatically (down to 22% of the original) at 1000 ppm. Clearly, the high concentration of Na has reduced the Fe population in the discharge. The excitation component drops more gradually and less severely (to 67% of the original at 1000 ppm). Again, the degree of temperature change is very uncertain.

Combined, the above results suggest that the observed matrix effect can be divided into excitation and transport. The components have already been sketched, but they will be restated based on the combined evidence.

A likely mechanism for the excitation effect starts with the introduction of an easily ionized element into the plasma. Through an increase in ion and electron populations, the discharge becomes more conductive. With less resistance, the amount of energy deposited in the plasma is reduced. Lower power leads to a cooler and generally less energetic plasma.

"Transport" is used rather broadly here to refer to the combined processes involved in converting an atom in solution to a free atom in the discharge. Evidence suggests that, just as in other plasmas, this process could be further divided into droplet formation, desolvation, vaporization, and atomization. The latter three steps are tied into the same mechanism as the excitation effects. A cooler plasma will be less efficient at desolvation,

vaporization, and atomization.

The magnitude of the transport effect (a 78% reduction at a Na concentration of 1000 ppm) makes us believe that there is more to it than just a change in the plasma energy. It seems likely that aerosol droplet formation is also affected. The mechanism of droplet formation in the ELCAD has not yet been clearly established, but solution viscosity should influence the ease of droplet formation and the droplet size. High salt concentrations reduce solution heating by increasing conductance. Cooler solutions are more viscous, and would be expected to produce larger droplets that are more difficult to desolvate.

There may be further transport effects. An important clue to the ELCAD's mechanism is that desolvation, vaporization, and atomization proceed to a significant degree in a very small space. Emission for many elements peaks well within a millimeter from the solution surface, in the negative glow.[2-8] The velocity of analyte species leaving the solution and the size of the droplets containing those analytes are both unknown, so the residence time cannot be calculated. It seems unlikely, however, that the observed level of desolvation could take place in this short space by a purely thermal mechanism. Between the solution and the negative glow is the cathode fall, where there is a large potential drop in a small space. Cserfalvi and Mezei estimate the field in this region to be on the order of 10^7 V/m.[21] Passing initially neutral droplets through high fields has been used to decrease the mean droplet size.[27-28] As we have shown, this matrix effect lowers the field strength, which would be expected to hamper this mode of desolvation. Of course, droplets from the ELCAD cathode might not be initially neutral. The situation

might be similar to electrospray, where droplets are initially charged, helping to liberate them from the solution.

Thoroughly explicating this possibility would be beyond the scope of the present work, but some exploration of the implications is appropriate. Solution surface roughness caused by boiling could result in high local fields, possibly as high as would be needed for charged-droplet ejection. If so, the temperatures at this interface could influence the surface roughness and therefore droplet formation. The surface-tension effect explained earlier is also consistent with this mechanism. Field strength would affect both droplet formation and desolvation. Ion concentration in the solution would also impact the efficiency of droplet formation, and competitive effects might reduce analyte concentration in droplets when a high cation concentration is present. In fact, an electrospray-like mechanism might explain at least part of the strong dependence of emission on electrolyte identity and concentration (see section 6.1.3).

6.4 CONCLUSIONS

A variety of potential complications to the use of ELCAD for the analysis of complex solution have been considered. A number of interferences have been shown to be either minimal or easily remedied, but others remain significant. The worst matrix effect arises from high concentrations of cations. This problem can be easily diagnosed by the reduction in background emission and the presence of strong emission from the interferents. This diagnostic aid is simple to implement in an emission-based system such as the present one, where wavelength can readily be scanned or in one where

multiple wavelengths can be monitored simultaneously. The response of the ELCAD to these interferents provides clues to a possible mechanism, in which droplet formation and desolvation are both enhanced by the strong electric field of the cathode fall and in which the discharge temperature is altered. Overall, previous literature in which interferences in flames are examined serves as a useful preliminary guide to gauging similar effects in the ELCAD.

6.5 REFERENCES

[1] T. Cserfalvi, P. Mezei and P. Apai, "Emission studies on a glow discharge in atmospheric pressure air using water as a cathode", *J. Phys. D-Appl. Phys.*, 1993, **26**, 2184.

[2] M. R. Webb, F. J. Andrade, G. Gamez, R. McCrindle and G. M. Hieftje, "Spectroscopic and electrical studies of a solution-cathode glow discharge", *J. Anal. At. Spectrom.*, 2005, **20**, 1218.

[3] T. Cserfalvi and P. Mezei, "Subnanogram sensitive multimetal detector with atmospheric electrolyte cathode glow discharge", *J. Anal. At. Spectrom.*, 2003, **18**, 596.

[4] T. Cserfalvi and P. Mezei, "Direct solution analysis by glow discharge: electrolyte-cathode discharge spectrometry", *J. Anal. At. Spectrom.*, 1994, **9**, 345.

[5] T. Cserfalvi and P. Mezei, "Operating mechanism of the electrolyte cathode atmospheric glow discharge", *Fresnius' J. Anal. Chem.*, 1996, **355**, 813.

[6] P. Mezei, T. Cserfalvi and M. Janossy, "Pressure dependence of the atmospheric electrolyte cathode glow discharge spectrum", *J. Anal. At. Spectrom.*, 1997, **12**, 1203.

[7] M. A. Mottaleb, Y. A. Woo and H. J. Kim, "Evaluation of open-air type electrolyte-as-cathode glow discharge-atomic emission spectrometry for determination of trace heavy metals in liquid samples", *Microchem. J.*, 2001, **69**, 219.

[8] P. Mezei, T. Cserfalvi and L. Csillag, "The spatial distribution of the temperatures and the emitted spectrum in the electrolyte cathode atmospheric glow discharge", *J. Phys. D-Appl. Phys.*, 2005, **38**, 2804.

[9] P. Mezei, T. Cserfalvi, M. Janossy, K. Szocs and H. J. Kim, "Similarity laws for glow discharges with cathodes of metal and an electrolyte", *J. Phys. D-Appl. Phys.*, 1998, **31**, 2818.

[10] G. C. Y. Chan and G. M. Hieftje, "Using matrix effects as a probe for the study of the charge-transfer mechanism in inductively coupled plasma-atomic emission spectrometry", *Spectrochim. Acta Part B*, 2004, **59**, 163.

[11] V. D. Hodoroaba, V. Hoffmann, E. B. M. Steers and K. Wetzig, "Emission spectra of copper and argon in an argon glow discharge containing small quantities of hydrogen", *J. Anal. At. Spectrom.*, 2000, **15**, 951.

[12] M. R. Webb, G. C. Y. Chan, F. J. Andrade, G. Gamez and G. M. Hieftje, "Spectroscopic characterization of ion and electron populations in a solution-cathode glow discharge", *J. Anal. At. Spectrom.*, 2006, **21**, 525.

[13] Y. S. Park, S. H. Ku, S. H. Hong, H. J. Kim and E. H. Piepmeier, "Fundamental studies of electrolyte-as-cathode glow discharge-atomic emission spectrometry for the determination of trace metals in flowing water", *Spectrochim. Acta, Part B*, 1998, **53B**, 1167.

[14] J. M. Mermet, "Fundamental principles of inductively coupled plasmas" in *Inductively Coupled Plasma Spectrometry and its Applications*, S. J. Hill, Sheffield Academic Press: Sheffield, 1999

[15] P. Mezei, T. Cserfalvi, H. J. Kim and M. A. Mottaleb, "The influence of chlorine on the intensity of metal atomic lines emitted by an electrolyte cathode atmospheric glow discharge", *Analyst*, 2001, **126**, 712.

[16] V. V. Yagov and M. L. Gentsina, "Effect of Supporting Electrolyte Composition on the Intensity of Metal Lines in Electrolyte-Cathode Discharge Spectra", *J. Anal. Chem.*, 2004, **59**, 64.

[17] E. Beinrohr, P. Csemi and J. F. Tyson, "Continuous-Flow Dilution for Flame Atomic-Absorption Spectrometry Using a Variable Volume Dilution Chamber and Peak Area Measurement", *J. Anal. At. Spectrom.*, 1991, **6**, 307.

[18] M. A. Taher, "Atomic absorption spectrometric determination of trace zinc in alloys and biological samples after preconcentration with [1-(2-pyridylazo)-2-naphthol] on microcrystalline naphthalene", *Analyst*, 2000, **125**, 1865.

[19] M. Sperling, Z. L. Fang and B. Welz, "Expansion of Dynamic Working Range and Correction for Interferences in Flame Atomic-Absorption Spectrometry Using Flow-Injection Gradient Ratio Calibration with a Single Standard", *Anal. Chem.*, 1991, **63**, 151.

[20] B. Smets, "Vaporization Interference of Sulfate and Phosphate Anions on the Calcium Flame Atomic-Absorption Signal", *Analyst*, 1980, **105**, 482.

[21] T. Cserfalvi and P. Mezei, "Investigations on the element dependency of sputtering process in the electrolyte cathode atmospheric discharge", *J. Anal. At. Spectrom.*, 2005, **20**, 939.

[22] Y.-i. Sung and H. B. Lim, "Plasma temperature measurement of a low-pressure inductively coupled plasma using spectroscopic methods", *J. Anal. At. Spectrom.*, 2003, **18**, 897.

[23] U. Engel, C. Prokisch, E. Voges, G. M. Hieftje and J. A. C. Broekaert, "Spatially resolved measurements and plasma tomography with respect to the rotational temperatures for a microwave plasma torch", *J. Anal. At. Spectrom.*, 1998, **13**, 955.

[24] V. A. Titov, V. V. Rybkin, A. I. Maximov and H. S. Choi, "Characteristics of atmospheric pressure air glow discharge with aqueous electrolyte cathode", *Plasma Chemistry and Plasma Processing*, 2005, **25**, 503.

[25] R. A. Hill, "Tables of electron densities as a function of the halfwidth of Stark-broadened hydrogen lines." *Quant. Spectrosc. Radiat. Transfer*, 1964, **4**, 857.

[26] A. W. Irwin, "Polynomial partition function approximations of 344 atomic and molecular species", *Astrophysical Journal, Supplement Series*, 1981, **45**, 621.

[27] D. B. Hager and N. J. Dovichi, "Behavior of Microscopic Liquid Droplets near a Strong Electrostatic-Field - Droplet Electrospray", *Anal. Chem.*, 1994, **66**, 1593.

[28] R. N. Savage and G. M. Hieftje, "Enhancement of Pneumatic Nebulization Efficiency through Application of an Electric-Field", *Rev. Sci. Instrum.*, 1978, **49**, 1418.

Chapter 7

Compact glow discharge for the elemental analysis of aqueous samples.

7.1 INTRODUCTION

Glow discharge (GD) plasmas have been used in spectroscopy for about 100 years,[1, 2] with the introduction of the Grimm glow discharge lamp[3] about 40 years ago marking a significant turning point in their utility as atom sources for spectrochemical analysis. In its most established forms (two-electrode, low-pressure (about 1-10 Torr), direct-current discharges with the sample serving as the cathode), the GD is suited for elemental analysis of solid conductors, but it has been shown to have much greater versatility when modified in powering or geometry. For example, radio-frequency powering allows the sampling of nonconductive solids, and pulsed powering with an inlet for gaseous samples permits rapid elemental, structural, and molecular analysis of gases.[4, 5]

Solution analysis with glow discharges has presented a significant challenge, in part because typical glow discharges lack the temperature required to evaporate the solvent and atomize any remaining particles. Solution analysis with a typical glow discharge requires that the sample be dried and deposited on[6] or mixed with[7] a solid, or made into an aerosol and then subjected to extensive drying (e.g., through a particle-beam interface).[8] However, it has been known since 1887 that it is possible to ignite a glow

discharge between a metal electrode and a sufficiently conductive aqueous solution.[9] The use of such an arrangement came to be called glow discharge electrolysis (GDE).[10] It was not until 1959 that atomic emission was observed from such a plasma,[11] and only in 1993 was quantitative analysis performed with a modified design.[12] The modified design was later called an electrolyte cathode discharge (ELCAD)[13] and has evolved since that time in response to several studies. Kim et al. designed an open-air ELCAD,[14] which outperformed earlier, enclosed designs. While earlier designs had been operated at various pressures and with various gases, this newer source operates in atmospheric-pressure air. In 2003, Mezei et al. introduced a version of this design[15] which they now refer to as an abnormal ELCAD.[16] Flow injection analysis with this source is promising, but continuous sampling performance has not yet been reported.

Various ELCAD-like, GDE-based discharges have been explored, including the liquid sampling-atmospheric pressure glow discharge,[17] the drop-spark discharge,[18] the electrolyte jet cathode glow discharge,[19] and the liquid electrode spectral emission chip.[20] In 2005, Webb et al. described a simplified design[21, 22] (referred to herein as a solution-cathode glow discharge or SCGD for convenience in distinguishing it from other arrangements) that exhibits similar detection limits to and better short-term stability than the open-air ELCAD.[14, 23] The SCGD offers certain advantages, which are possessed to varying degrees also by other GDE-based systems, over other solution-analysis techniques. This type of discharge does not require any compressed gases, unlike most flames (which require fuels and sometimes oxidants) and most other plasmas (which often require a noble gas). The power used with an SCGD is typically around 70 W,

which is much less than that commonly used by plasmas suitable for solution analysis. For example, the inductively coupled plasma (ICP) generally operates at 1-1.5 kW. Both of these traits make the somewhat SCGD less expensive to operate than many techniques, but that is not the primary advantage they impart. High gas and power requirements make sources such as the ICP impractical as field instruments. In contrast, the SCGD appears to have great potential in this regard, in part for the same reasons and in part because of its compact size. This new source also has a simple design and uses direct-current powering, which reduce construction costs. Finally, detection is accomplished through emission, which makes the source naturally multielemental. In contrast, flames more commonly make use of atomic absorption, which ordinarily require switching primary light sources between elements.

Several studies of the SCGD[21, 22] led to the supposition that at least some of the solution is transported into the discharge as droplets, possibly charged and emanating from the rough solution surface in a manner reminiscent of electrospraying. Further, the potential gradient near the sample surface is conjectured to enhance desolvation in a manner similar to that observed when droplets are passed through the high fields near a corona discharge.[24] These considerations lead to the possibility of enhancing atomic concentrations in the discharge by increasing the field gradients near the sample, which might be accomplished by reducing the cathode diameter. Even if the suppositions are wrong, reducing the discharge width might enhance emission merely by concentrating similar amounts of power and of sample atoms in a smaller area.

In this paper, we present a new version of the SCGD with a cathode surface area

approximately one-fifth that of the previous version. Optimization of several parameters is performed and analytical figures of merit are determined.

7.2 EXPERIMENTAL

The SCGD used here is similar to that described previously.[21, 25] A photograph of the new system can be seen in Figure 7-1. A sample solution is delivered through a glass tube that has been bent into a J-shape. In this case, the tube is a 10 μL disposable micro-pipet (Fisher Scientific Company, Pittsburgh, PA) with a 1.1-mm outer diameter and a 0.38-mm inner diameter. A portion of the solution that is not vaporized by the discharge overflows into a glass waste reservoir and this overflow serves as an electrical connection between the discharge and the solution reservoir. A graphite electrode in the reservoir grounds the solution. Due to the wide electrical path within the waste reservoir, its composition appears to have an insignificant impact compared to the composition of the narrow solution overflow. Several mm above the exit of this capillary (the exact distance was varied as described later) is a tungsten electrode. The tungsten was tapered to a rounded point; the discharge anchors to a 0.7-mm diameter spot on this point (the other end of the discharge is attached to the capillary tip and fills the 1.1-mm outer diameter of the capillary). A 1-kΩ resistor between the tungsten anode and the positive output of a high-voltage power supply (Kepco BHK 2000-0.1MG, Flushing, NY) is used to stabilize the discharge current. The discharge current and voltage varied from one experiment to another, as is described later. The rim of the waste reservoir is 2 mm below the capillary tip, but the reservoir solution level near the capillary when the discharge is in operation is approximately 2 mm lower than this rim. Excess solution overflows from the reservoir,

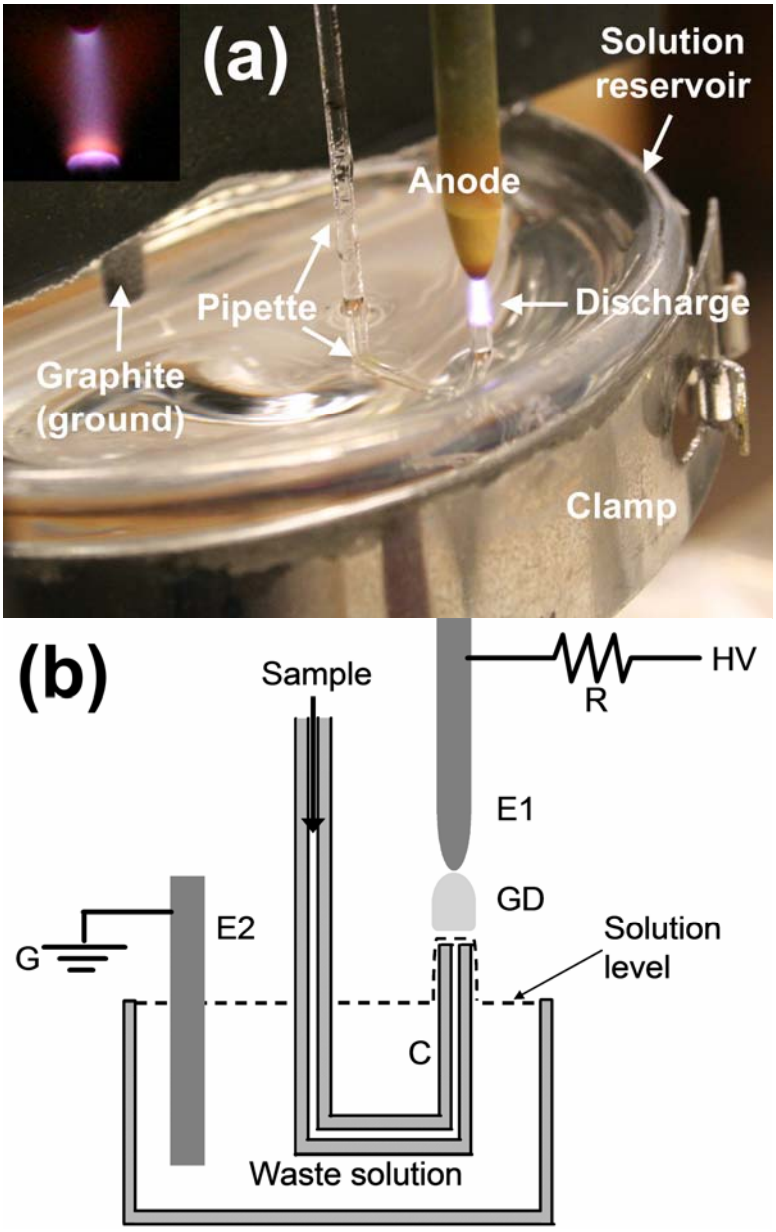

Figure 7-1. Photographs (a) and diagram (b) of the SCGD. (a) The main photo shows the discharge in the context of the cell, while the inset (upper left) shows only the discharge itself. The orange-yellow region above the solution is 589.0 and 589.6 nm emission from sodium, present at 500 ppb in the sample solution. (b) The diagram shows the main parts of the discharge cell: (HV) high voltage power supply, (E1) tungsten anode, (GD) glow discharge, (C) capillary, (E2) graphite electrode, and (G) ground. The plastic separator is omitted to avoid clutter.

and a piece of plastic placed across the container prevents the solution level from increasing above the rim.

Sample solution was fed to the discharge by a Gilson (Middleton, WI) peristaltic pump. This sort of pump has several advantages over others that have been used with the previous SCGD design. In particular, peristaltic pumps do not limit the deliverable solution volume, are inexpensive, are not easily clogged, and have readily and inexpensively replaceable tubing if corrosion occurs. Unfortunately, peristaltic pumps do not provide as smooth of a flow as some other pumps do. To reduce fluctuations, a home-built pulse damper was included between the pump and the SCGD. The damper consisted of a knotted (specifically, a chain sinnet, also known as a daisy chain) length of peristaltic pump tubing (two 1.52-mm inner diameter Tygon® tubes joined to make an approximately 90 cm length before knotting). This system is a simple and inexpensive way to reduce fluctuations. Prior to the peristaltic pump, a two-way six-port valve was used in a previously described arrangement[25] to allow samples to be switched without interrupting the solution flow. Although this pumping system increases the dead volume of the overall system, a sample could, in theory, be inserted between the pulse damper and the discharge, giving a low dead volume.

The discharge was imaged at a magnification of 2.3:1 by a quartz lens onto the 10-µm entrance slit of a 0.5-m Czerny-Turner monochromator (Chromex 500IS/SM, Albuquerque, NM). A Hamamatsu R928 photomultiplier tube (PMT) (Hamamatsu, Japan) biased at -850 V was used as the detector. Current from the PMT was amplified by a Keithley 427 current amplifier (Cleveland, OH) and recorded by a custom National

Instruments (Austin, TX) LabVIEW program.

7.3 RESULTS AND DISCUSSION

The discharge was characterized electrically at a number of solution flow rates, as shown in Figure 7-2. The gap, or height of the discharge, was 2.9 mm. The results displayed in Figure 7-2 were obtained by adjusting the potential and allowing the current to vary, but testing this and the reverse approach (adjusting current and allowing potential to vary) at 2.46 mL/min did not reveal any differences between the two. The plot is given with voltage on the y-axis to comply with the convention of the glow discharge literature. The voltage measurements are corrected for the drop across the 1-kΩ resistor, but not for the one across the solution. This latter drop is flow-rate dependent; because the cross-section of the overflow solution is greater at higher flow rates, the resistance and voltage are lower as well. In glow discharges, voltage increases with current density, rather than current, and current-voltage relationships can be used to classify the discharge as either normal or abnormal. In normal glow discharges, the current density and the voltage remain nearly constant as the current and amount of the cathode covered by the discharge increase. Once the cathode is completely covered, the discharge enters the abnormal regime, and current cannot be raised without increasing the current density and the voltage. From the data shown in Figure 7-2, it is clear that the source used here is an abnormal glow discharge, which is typical of analytical glow discharges but not universal among GDE-based methods.

A flow rate around 2.4 mL/min avoids instabilities found at lower flow rates but keeps

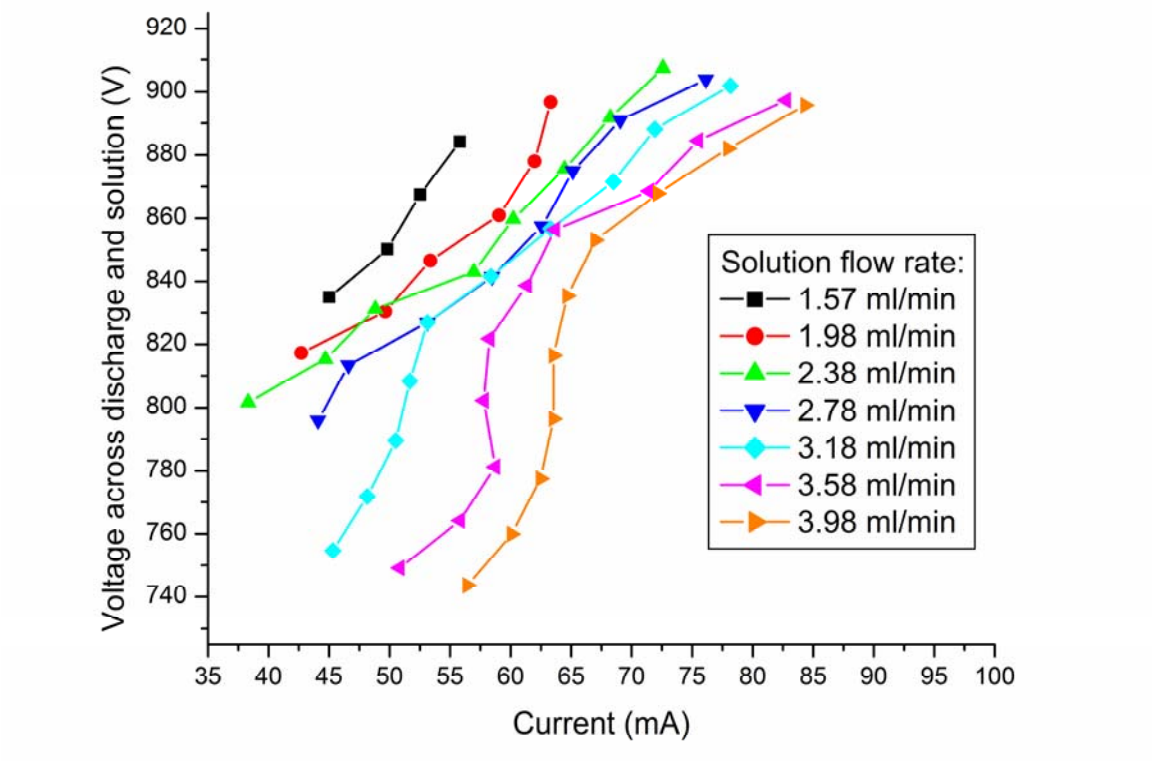

Figure 7-2. The dependence of discharge potential on discharge current at several solution flow rates.

the current-voltage relationship monotonic over a broad range of both variables. However, these results did not provide much insight into what values those variables should have. To make this decision, optimization was performed by using a 2.38 mL/min flow rate, as described below. Ultimately, a slightly higher flow rate (2.46 mL/min) was used in evaluating the optimized performance. This latter value, it should be noted, is a 30% reduction from the 3.5 mL/min flow rates typically used in the larger version of this source and required for reasonable performance with the abnormal ELCAD.[15]

A 500 ppb magnesium solution (aqueous, adjusted to pH 1.0 with HNO_3) was used as a test sample in further optimizing the discharge performance. Two figures of merit were monitored to judge this performance: relative standard deviation (RSD) and detection limit (DL). The RSD was calculated from ten measurements, each being the ten-second average of blank-corrected emission signals acquired at 1 kHz. The DL was calculated as the concentration yielding an emission signal three times the standard deviation of the blank signal, assuming that the relationship between signal and concentration was linear through at least 500 ppb. The standard deviation of the background signal was calculated based on ten measurements of emission from a blank solution (i.e., an aqueous solution adjusted to pH 1.0 with HNO_3) obtained in the same fashion as the signal measurements.

The first parameter evaluated in this way was the discharge potential; the results are shown in Figure 7-3. For this test, the gap was again held constant at 2.9 mm. A nominal minimum RSD was found near 920 V (with a corresponding current of about 71 mA), but the variation across the studied range is practically and statistically insignificant, so RSD is not a valuable parameter in optimizing voltage. At first, an

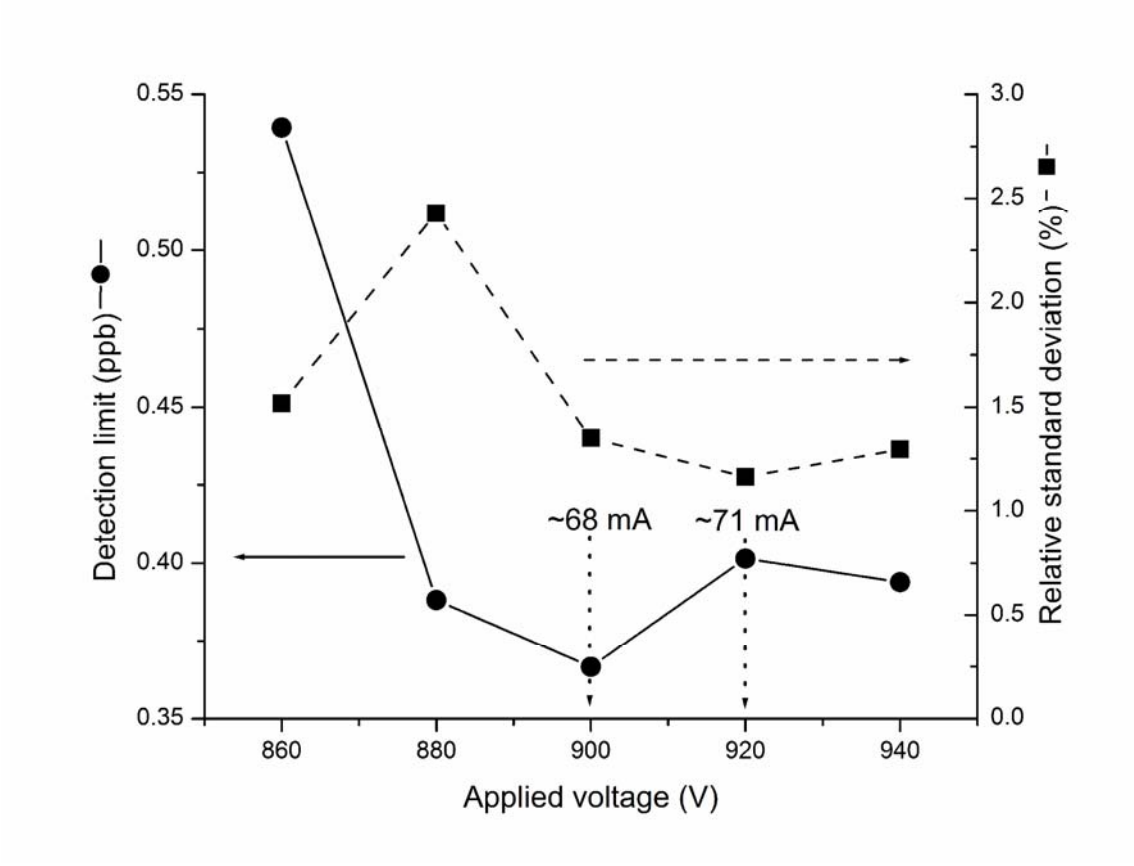

Figure 7-3. Optimization of discharge potential. Squares correspond to the right axis and show the dependence of the relative standard deviation of magnesium 285.2 emission from a 500-ppb sample (ten 10-second integrations, background corrected) on discharge potential. Circles correspond to the left axis and show the dependence of the magnesium detection limit (using the same line and sampling) on discharge potential.

apparently linear increase in analyte emission with voltage results in a lower DL at 880 V than at 860 V. However, the absolute fluctuations in blank signal emission (i.e., the fluctuations on a constant scale not made relative to the emission magnitude) also go up with voltage. The latter increase is slower than the former at first, but the rates of change are similar between 880 and 940 V, so the DLs are fairly constant over that range. The observed minimum detection limit is found at 900 V (about 68 mA), but the significance of the difference between this minimum and adjacent points is practically and statistically insignificant, so any nearby voltages can be used without losing meaningful performance. A current of 70 mA, which falls between the observed minima of the two figures of merit, was chosen for further work, primarily to keep the power low while remaining well above the point where the DL degrades.

The next tested parameter was the discharge gap (separation between the solution surface and the tungsten anode). The trends in this case were much clearer and more significant than those involving the discharge voltage (see Figure 7-4). The RSD has a minimum at a gap near four mm. At smaller gaps, the emission intensity drops, while the absolute fluctuations are not much weaker. Emission increases with gap size because the positive column extends without largely changing the brightness of a given volume. Although the emission is stronger at larger gaps, the absolute fluctuations also become greater. This might be an effect of increased susceptibility to air currents. The DL shows a similar trend with gap, although the minimum is shifted to smaller gaps (to around 2.5 mm) and it is not clear that the increase at even smaller gaps is statistically significant. The minima of both parameters are relatively flat with gap, and these minima overlap.

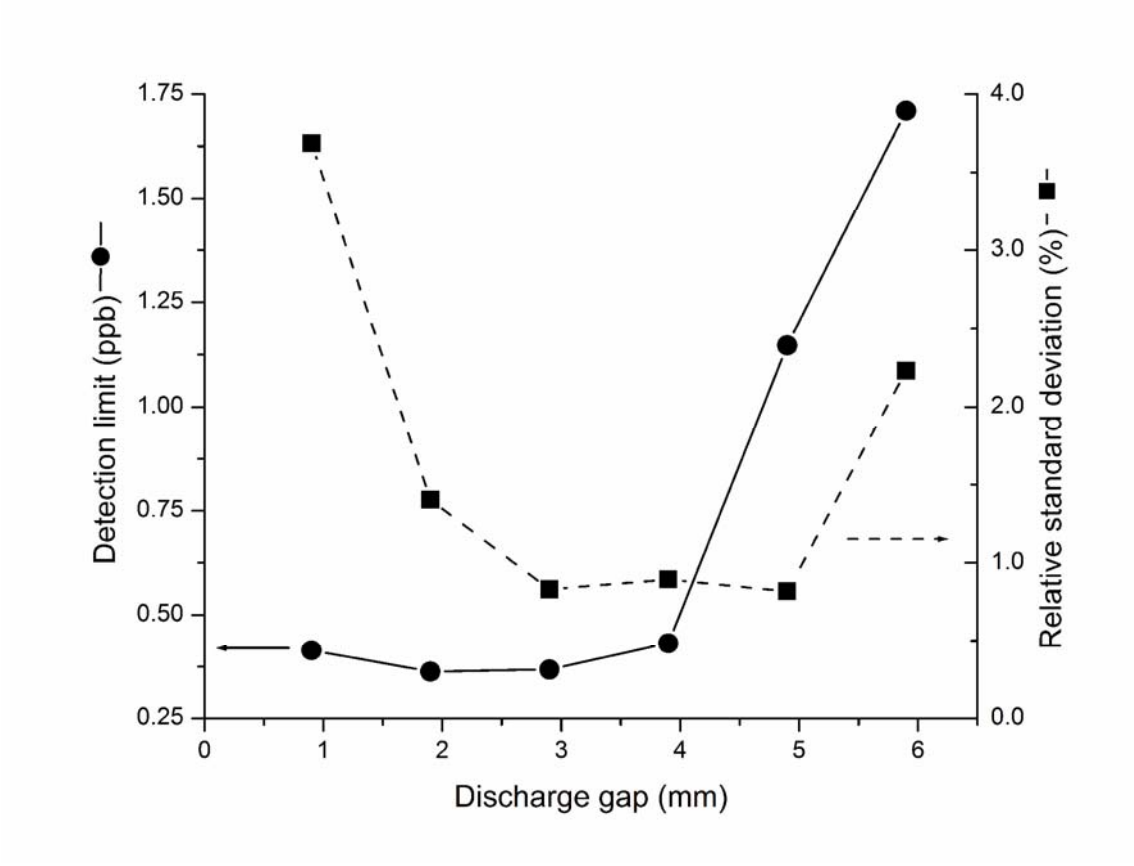

Figure 7-4. Optimization of discharge gap. Squares correspond to the right axis and show the dependence of the relative standard deviation of magnesium 285.2 emission from a 500-ppb sample (ten 10-second integrations, background corrected) on discharge gap. Circles correspond to the left axis and show the dependence of the magnesium detection limit (using the same line and sampling) on discharge gap. In both cases, discharge potential was adjusted to maintain a 70 mA current.

Accordingly, a compromise gap of 3.2 mm can be used without sacrificing significant performance in either RSD or DL.

Although it is not the optimum, the performance at a gap of 0.9 mm is noteworthy. Microplasmas have been defined as plasmas having at least one dimension less than one millimeter.[26] By this definition, a SCGD operated at a gap of 0.9 mm is a microplasma, particularly because it also has a sub-millimeter (0.7 mm) diameter at its top. Analysis of liquid samples by microplasmas has been difficult, with detection limits of a single ppm level or worse being typical.[26, 27] To our knowledge, the 0.4 ppb detection limit for magnesium reported here is below published values for solution samples for any element using any microplasma.

It would be possible to adjust discharge conditions independently for each element in a sample, but such optimization would slow down analysis in a sequential system (such as is used here) and would preclude simultaneous determination in a spectrometric system with multiple detectors or detector elements. Because one strength of this source, being emission-based, is the possibility of rapid sequential or even simultaneous detection, we have chosen to use a single set of conditions for all studied elements. Given that discharge conditions have disparate effects on different analyte and background emission features in a similar source,[21] this single set of conditions is unlikely to be optimal for all analytes. Depending on the priorities of the analyst, alternative conditions might produce a more favorable compromise. The conditions chosen for evaluation of the analytical performance of this source here were a gap of 3.2 mm, a solution flow rate of 2.5 mL/min, and a potential of 1.0 kV (yielding a current of 70 mA). Solutions of 500

ppb in the element of interest and blank solutions were used to determine both the DL and the RSD. As earlier, ten 10-second integrations were used for each sample and for a blank solution of otherwise matching composition (aqueous, adjusted to pH 1.0 with HNO_3). An Edmund Optics (Barrington, NJ) GG 475 long-pass filter (greater than 88% transmission above 500 nm, less than 0.1% transmission below 460 nm) was used to block second-order emission when sodium and lithium performance was tested. The results are shown in Table 7-1. The RSDs found for the SCGD are mostly between 1-2%, comparable to the 1% value commonly quoted for ICP-AES.[28] Detection limits were calculated as the concentration that would produce emission equal to three times the standard deviation of the blank emission. Included for comparison are detection limits for the larger SCGD and values described as "general detection limits" for radial-viewed ICP emission spectrometry.[29] As Table 7-1 shows, the geometry and conditions used here result in an order of magnitude or more improvement in detection limits for most elements over the values found with the larger SCGD. These improved detection limits are on par with the ICP-AES values for most elements, and better than them for the rest. This comparison should not be misconstrued as a claim that the detection limits for this new source are universally equal to or better than those of ICP-AES, since instrumental changes (e.g., using axial viewing) can improve ICP-AES detection limits. However, SCGD detection limits might similarly be improved; for example, a spectrometer with higher resolution and/or greater light throughput (that is, a spectrometer more similar to those typically used with an ICP) would likely enhance performance somewhat. Additionally, it is not clear whether the ICP detection limits were determined using only one set of conditions (as was done here for the SCGD) or by what method the ICP

Table 7-1. Comparison of the analytical performance of the miniature SCGD, the earlier, larger SCGD and ICP-AES.

Element	Wavelength (nm)	Present work RSD (%)	Present work DL (ppb)	Earlier SCGD DL (ppb)[a]	ICP-AES DL (ppb)[b]
Hg	253.7	1.9	22	350	20
Pb	405.7	1.7	6	82	7
Cu	324.7	2.9	4	31	2
Cd	228.8	1.4	2	9	1
Ag	338.3	1.9	0.3	5	1
Mg	285.2	0.9	0.2	19	0.3
Na	589.0	1.2	0.1[c]	0.8[c]	2
Li	670.8	1.5	0.06	8	1

*Wavelengths and relative standard deviations (RSD) refer only to the present study. All wavelengths are for neutral atomic lines. Values for present study are calculated based on 500-ppb samples. [a] Values are from Webb et al.[21] [b] Values are from Hill et al.[29] [c] Approximation of detection limit based on noise in a solution containing Na at a concentration above the detection limit.

detection limits were calculated. The comparison, then should be viewed as only approximate.

Sodium detection limits are currently restricted by contamination in the blank. Assuming that the background at 588.0 nm is equal to the background of a true blank at the 589.0 nm sodium emission line, the background concentration of sodium is calculated to be 2 ppb by standard addition (using solutions for which the added sodium is 1.2 and 12 ppb). Because this contamination level is more than an order of magnitude over the calculated detection limit, it is likely that the impurities have a significantly detrimental effect on the detection limit of sodium. The calculated detection limit can best be viewed as an estimate of the detection limit that could be achieved with a sodium-free blank, and is likely to be biased high since the noise in the background emission adjacent to the sodium line is less than the noise in the sodium line itself.

Despite this blank problem, sodium stands out as representative of a group with very good detection limits when referenced to both the same elements in ICP-AES and to other elements in SCGD emission spectrometry. The other members of this group studied here are lithium and silver. What all three share is that atomic (rather than ionic) emission lines are used in ICP-AES for the lowest detection limits. In an ICP, most elements are extensively ionized, so ionic emission lines are generally more sensitive. Sodium, lithium, and silver are all mostly ionized in an ICP, but lack strong ionic emission lines in the accessible UV or visible regions, forcing analysts to use spectral lines from the smaller atomic population. In contrast, most metals are found primarily as atoms in the SCGD,[25] so atomic lines are used for analysis. Although the DLs of the two

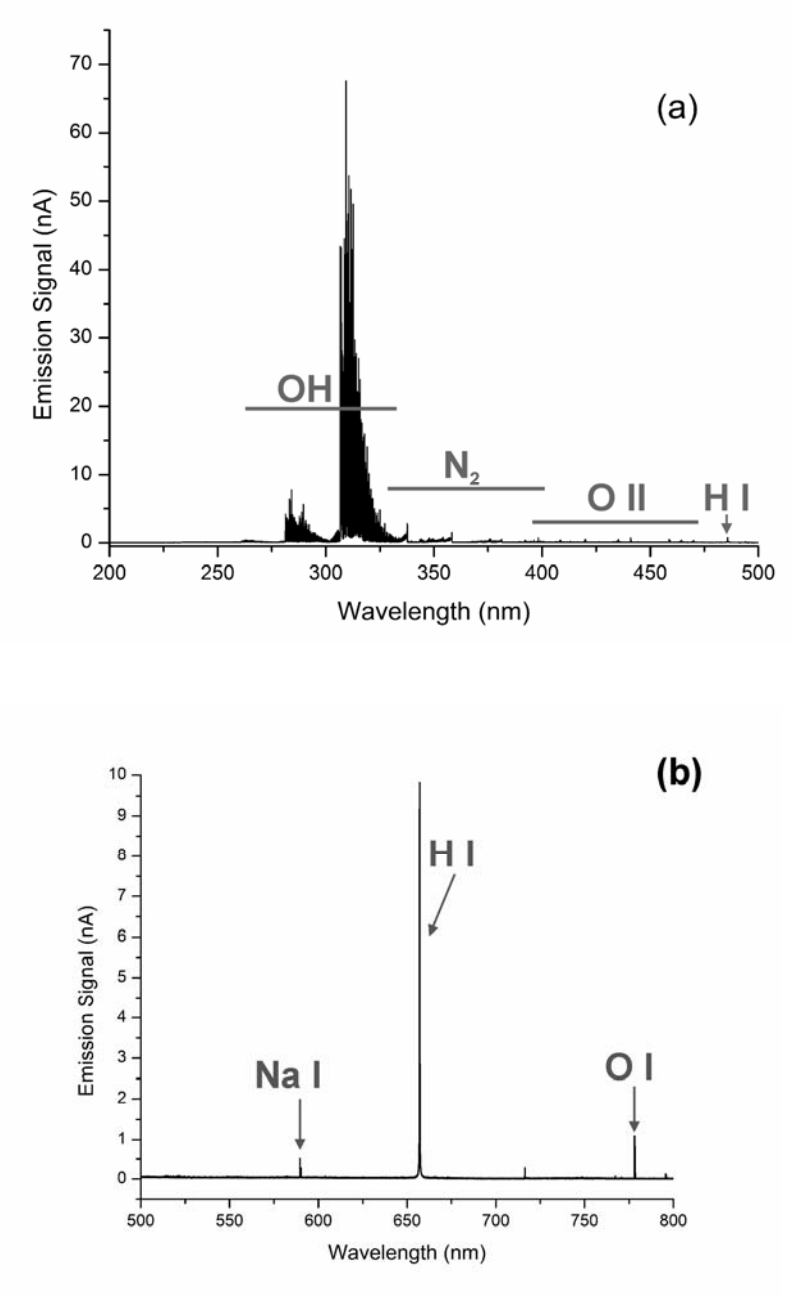

Figure 7-5. Background (aqueous blank adjusted to pH 1.0 with HNO_3) spectrum of the SCGD: (a) between 200 and 500 nm and (b) between 500 and 800 nm. A long pass filter was used in Figure 7-5b to block second-order light. Prominent features include emission from hydroxyl radical (OH), diatomic nitrogen (N_2), singly ionized atomic oxygen (O II), neutral atomic hydrogen (H I), neutral atomic sodium (Na I), and neutral atomic oxygen (O I).

systems are comparable for elements in their majority form, ICP performance is poorer than that of SCGD when the elements of interest (*e.g.*, Li and Na) lack easily accessible strong ionic lines. Sodium and lithium detection limits are further enhanced because their respective emission wavelengths (589.0 and 670.8 nm) lie in the visible, where there is very little background from the SCGD. Other alkali metals are expected to have low detection limits by the same reasoning.

The background emission spectrum of the new, smaller SCGD, shown in Figure 7-5, is very similar to that of the larger SCGD, which has been described in detail.[21] The previously mentioned long-pass filter was used for Figure 7-5b to block second-order emission. The most intense emission is from OH radical; atomic hydrogen, atomic and ionic oxygen, and molecular nitrogen are also observed, as is emission from sodium and potassium impurities. Notably, despite the fact that the plasma is in contact with a tungsten electrode, no tungsten lines are observed. Although the molecular bands can interfere with certain analyte emission lines (e.g. the 405.9 nm N_2 band with the 405.7 nm Pb line), the background is generally weak and uncomplicated. Similarly, spectra from elements in the sample are generally simple and dominated by neutral atomic lines. For example, the 280.3 nm magnesium ionic line to 285.2 nm magnesium atomic line ratio is only 0.02 (measured with a 2 ppm Mg solution). Such a low ratio suggests that significant interference from ion lines is rare in this source.

Calibration curves were constructed for several elements (Cd, Pb, Na, and Li). Linearity was tested by taking the logarithms of the concentrations and signals and then applying a linear fit to those values. For a perfectly linear calibration, the slope of such a curve

should be one. The y-intercept provides a measure of relative sensitivity, with larger intercepts indicating greater sensitivity. Lead, lithium, and cadmium all show good linearity. Lead and lithium calibrations are linear even up to 80 ppm (the highest concentration tested). Lead exhibited a linear range of at least four orders of magnitude (slope = 0.96, y-intercept = -3.7, R^2 = 0.997) and lithium at least six orders of magnitude (slope = 1.02, y-intercept = -1.8, R^2 = 0.998). Cadmium has a shorter linear range, approximately three orders of magnitude (slope = 1.00, y-intercept = -3.2, R^2 = 1.000), with the intensity rolling off between 1.2 and 12 ppm. Sodium calibration, in contrast, is not linear (slope = 0.85, y-intercept = -0.75, R^2 = 0.998). However, as indicated by the R^2 value, the trend is smooth over the nearly six order of magnitude range (also through 80 ppm) that was tested, allowing the use of a non-linear calibration curve.

Additionally, these calibration curves were used to check the previously determined detection limits. For Cd, the calculated detection limit was 2 ppb, whether determined based on 12 ppb, 500 ppb, 1.2 ppm samples, or the slope of a fit to all these points and a blank. For Li, the calculated detection limit was between 0.03 and 0.07 ppb based on 1.2 ppb, 12 ppb, 120 ppb, 1.2 ppm, 12 ppm, and 80 ppm samples and was 0.06 ppb based on the slope of a line containing all of these points and a blank. For Pb, the calculated detection limit was between 4 and 17 ppb based on 12 ppb, 120 ppb, 1.2 ppm, 12 ppm, and 80 ppm solutions, and was 14 ppb based the slope of a plot including all of these and a blank. The lowest concentrations produced the lowest detection limits (*e.g.*, 12 ppb produced a 4 ppb detection limit), as would be expected based on the above-mentioned slope of close to, but slightly less than, one. As was mentioned, Na response was clearly

nonlinear. Thus, it is not surprising that calculated detection limits for this element varied with the concentration used. The calculated detection limit ranged from 0.1 to 0.4 based on concentrations of 1.2 ppb, 12 ppb, 120 ppb, 1.2 ppm, and 12 ppm, and was 0.4 ppb based on the slope of a line including all those points and a blank. As with Pb, the lowest detection limits for Na were calculated using the lowest-concentration samples, as would be expected from a log-log slope less than one.

Matrix effects (i.e., the changes in apparent concentration caused by variations in sample constituents other than the analyte itself) are a concern that must be addressed with any analytical method. Based on previous results with the larger SCGD,[22] two potential interferences were selected for evaluation: the effects of easily ionized elements on emission from other elements and the effect of phosphate on calcium atomization. In the former case, 25 mM sodium was chosen as the interferent on cadmium, copper, and manganese (2 ppm each in single-analyte solutions). The emission for matrix-free and matrix-containing samples was compared, and the percent suppression was calculated. Conditions were the same as were used for the determination of detection limits and for the construction of calibration curves. Emission intensities were corrected based on background emission at nearby wavelengths. The new source performed better (exhibited less suppression) than the larger SCGD (35% vs. 65% suppression for copper, 44% vs. 70% for cadmium, and 57% vs. 81% for manganese). A complicating factor in this comparison is the mode of electrical operation; the previous results were obtained under constant current conditions, but voltage was held constant here. The parameter not held constant varies with matrix composition (voltage decreases or current increases), so

the two modes of operation result in different plasma conditions. Manganese suppression by sodium was measured under both constant-current and constant-voltage conditions. The suppression was found to be significantly more with a constant current of 73 mA than with a constant voltage of 1.0 kV, which produced a current of approximately 73 mA with no matrix present (72% for constant current vs. 57% for constant voltage). As suggested in an earlier paper on the larger SCGD,[22] the matrix effect appears to work in part by lowering the power deposited into the plasma. Interestingly, this does not appear to be the whole story, since constant-voltage operating gives a higher power in the presence of matrix, but lower analyte emission in that condition. It appears that constant-voltage operation has a strong positive effect, but the new source displays a lesser matrix effect than the larger SCGD in constant-current operation as well.

The vaporization interference of phosphate on calcium is temperature-dependent; it is less significant at higher temperatures than at lower ones. It is possible that the higher power density of the miniaturized SCGD might increase the temperature or improve vaporization in some other way. The OH rotational temperature (T_{OH}) of the new source was determined and compared to that of the larger SCGD using the 308.33, 308.52, 308.73, 309.24, 309.53, 309.86, 310.60, 311.02, and 311.48 nm OH lines and a Boltzmann plot. At a flow rate of 3.5 mL/min and a current of 80 mA, T_{OH} of the larger SCGD was 2960±240 K. At a flow rate of 2.5 mL/min and a current of 71 mA, T_{OH} of the miniaturized SCGD was 3090±150 K. If a difference exists, the method is not precise enough to demonstrate it. In the larger SCGD, a 4.7:1 molar ratio of P:Ca (P added as H_3PO_4, 2 ppm Ca added as an aqueous standard) resulted in a calcium emission

suppression of 21% compared to a solution with the same calcium concentration but no phosphate. Analyzing solutions of the same composition with the new source, only a 14% suppression was observed. It was found that the interference is less when larger gaps are used for the SCGD, so a portion of this improvement might be due to the slightly different gaps used with the new source (3.2 mm) and the older design (3 mm). The remainder of the effect is likely attributable to the higher power density of the new source. Further characterization is necessary, but it appears that the new source exhibits interferences that are similar in nature to, but of lesser magnitude than, those of the earlier design. That said, these effects still remain substantial compared to the ICP, and further work towards understanding and reducing them would be worthwhile.

7.4 CONCLUSIONS

The glow discharge described here shows potential in several areas. Its performance, size, and cost make it attractive as a field instrument. If sample can be injected after the pulse dampers, small solution dead volumes suggest potential as a detector for various types of transient analyses. Such analyses could provide the combination of high throughput, speciation through coupling with separation, small sampling volumes, and preconcentration.

7.5 REFERENCES

[1] R. K. Marcus and J. A. C. Broekaert,"Introduction" in *Glow Discharge Plasmas in Analytical Spectroscopy*, R. K. Marcus and J. A. C. Broekaert, John Wiley & Sons Ltd.:West Sussex, 2003.

[2] V. Hoffmann, M. Kasik, P. K. Robinson and C. Venzago, "Glow discharge mass spectrometry", *Anal. Bioanal. Chem.*, 2005, **381**, 173.

[3] W. Grimm, "Eine neue glimmentladungslampe fur die optische emissionsspektralanalyse", *Spectrochim. Acta Part B*, 1968, **23**, 443.

[4] C. L. Lewis, M. A. Moser, D. E. Dale, Jr., W. Hang, C. Hassell, F. L. King and V. Majidi, "Time-gated pulsed glow discharge: Real-time chemical speciation at the elemental, structural, and molecular level for gas chromatography time-of-flight mass spectrometry", *Anal. Chem.*, 2003, **75**, 1983.

[5] T. K. Starn, R. Pereiro and G. M. Hieftje, "Gas-sampling glow discharge for optical emission spectrometry. Part I: Design and operating characteristics", *Appl. Spectrosc.*, 1993, **47**, 1555.

[6] J. M. Brackett and T. J. Vickers, "Characterization of a Continuous Sample Delivery Glow-Discharge", *Spectrochim. Acta Part B*, 1984, **39**, 837.

[7] C. M. Barshick, D. C. Duckworth and D. H. Smith, "Analysis of Solution Residues by Glow-Discharge Mass-Spectrometry", *J. Amer. Soc. Mass Spectrom.*, 1993, **4**, 47.

[8] T. M. Brewer, J. Castro and R. K. Marcus, "Particle beam sample introduction into glow discharge plasmas for speciation analysis", *Spectrochim. Acta Part B*, 2006, **61**, 134.

[9] J. Gubkin, "Elektrolytische Metallabscheidung an der freien Oberfläche einer Salzlösung.", *Ann. Phys. Chem.*, 1887, **32**, 114.

[10] A. Hickling and M. D. Ingram, "Glow-discharge electrolysis", *J. Electroanal. Chem.*, 1964, **8**, 65.

[11] D. E. Couch and A. Brenner, "Glow discharge spectra of copper and indium above aqueous solutions", *J. Electrochem. Soc.*, 1959, **106**, 628.

[12] T. Cserfalvi, P. Mezei and P. Apai, "Emission studies on a glow discharge in atmospheric pressure air using water as a cathode", *J. Phys. D-Appl. Phys.*, 1993, **26**, 2184.

[13] T. Cserfalvi and P. Mezei, "Direct solution analysis by glow discharge: electrolyte-cathode discharge spectrometry", *J. Anal. At. Spectrom.*, 1994, **9**, 345.

[14] H. J. Kim, J. H. Lee, M. Y. Kim, T. Cserfalvi and P. Mezei, "Development of open-air type electrolyte-as-cathode glow discharge-atomic emission spectrometry for determination of trace metals in water", *Spectrochim. Acta, Part B*, 2000, **55B**, 823.

[15] T. Cserfalvi and P. Mezei, "Subnanogram sensitive multimetal detector with atmospheric electrolyte cathode glow discharge", *J. Anal. At. Spectrom.*, 2003, **18**, 596.

[16] P. Mezei and T. Cserfalvi, "The investigation of an abnormal electrolyte cathode atmospheric glow discharge (ELCAD)", *J. Phys. D-Appl. Phys.*, 2006, **39**, 2534.

[17] W. C. Davis and R. K. Marcus, "An atmospheric pressure glow discharge optical emission source for the direct sampling of liquid media", *J. Anal. At. Spectrom.*, 2001, **16**, 931.

[18] V. V. Yagov and M. L. Gentsina, "Effect of Supporting Electrolyte Composition on the Intensity of Metal Lines in Electrolyte-Cathode Discharge Spectra", *J. Anal. Chem.*, 2004, **59**, 64.

[19] V. V. Yagov, M. L. Getsina and B. K. Zuev, "Use of electrolyte jet cathode glow discharges as sources of emission spectra for atomic emission detectors in flow-injection analysis", *J. Anal. Chem.*, 2004, **59**, 1037.

[20] C. G. Wilson and Y. B. Gianchandani, "Spectral detection of metal contaminants in water using an on-chip microglow discharge", *IEEE Transactions on Electron Devices*, 2002, **49**, 2317.

[21] M. R. Webb, F. J. Andrade, G. Gamez, R. McCrindle and G. M. Hieftje, "Spectroscopic and electrical studies of a solution-cathode glow discharge", *J. Anal. At. Spectrom.*, 2005, **20**, 1218.

[22] M. R. Webb, F. J. Andrade and G. M. Hieftje, "Use of the Electrolyte Cathode Glow Discharge (ELCAD) for the Analysis of Complex Mixtures", *J. Anal. At. Spec.*, 2006, **In Press**, DOI:10.1039/b616989a.

[23] M. A. Mottaleb, Y. A. Woo and H. J. Kim, "Evaluation of open-air type electrolyte-as-cathode glow discharge-atomic emission spectrometry for determination of trace heavy metals in liquid samples", *Microchem. J.*, 2001, **69**, 219.

[24] D. B. Hager and N. J. Dovichi, "Behavior of Microscopic Liquid Droplets near a Strong Electrostatic-Field - Droplet Electrospray", *Anal. Chem.*, 1994, **66**, 1593.

[25] M. R. Webb, G. C. Y. Chan, F. J. Andrade, G. Gamez and G. M. Hieftje, "Spectroscopic characterization of ion and electron populations in a solution-cathode glow discharge", *J. Anal. At. Spectrom.*, 2006, **21**, 525.

[26] V. Karanassios, "Microplasma for chemical analysis: analytical tools or research toys?" *Spectrochim. Acta Part B*, 2004, **59**, 909.

[27] J. Franzke and M. Miclea, "Sample analysis with miniaturized plasmas", *Appl. Spectrosc.*, 2006, **60**, 80A.

[28] J. A. C. Broekaert, *Analytical Atomic Spectrometry with Flames & Plasmas*; Wiley-VCH Verelag GmbH: Weinheam, 2005.

[29] S. J. Hill, A. Fisher and M. Foulkes,"Basic Concepts and Instrumentation for Plasma Spectrometry" in *Inductively Coupled Plasma Spectrometry and its Applications*, S. J. Hill, Blackwell Publishing Ltd.:Oxford, 2007.

Chapter 8

High-throughput elemental analysis of small aqueous samples using a compact glow discharge.

8.1 INTRODUCTION

Miniature plasmas are emerging tools for spectrochemical analysis. While a variety of successful designs have been reported for gas analysis, few miniature plasmas have proven successful for solution analysis because most lack the gas temperatures and residence times required to remove the sample solvent. The most successful miniature plasmas for liquid analysis have been based on glow discharge electrolysis (GDE),[1] a type of glow discharge in which the sample solution serves as one of the electrodes. Atomic emission from elements initially in the sample solution can be observed in the plasma, as first noted by Couch and Brenner.[2] Cservalvi et al.[3] were the first to make use of this emission for analytical purposes, in an arrangement they later called an electrolyte-cathode discharge (ELCAD).[4] Various GDE-based, ELCAD-like discharges have been described since that time, including the liquid sampling-atmospheric pressure glow discharge (LS-APGD),[5] the drop-spark discharge,[6] the liquid electrode spectral emission chip,[7] and the electrolyte jet cathode discharge.[8] One particularly simple design, referred to as a solution-cathode glow discharge (SCGD),[9] has recently been improved greatly by reducing its size.[10] This new version exhibits detection limits and

precision levels comparable to those of many inductively coupled plasma–atomic emission spectrometers (ICP-AES) for a range of elements.

In the initial characterization of the miniature SCGD, continuous sampling was employed. Such sampling is certainly commonplace and worthwhile, but there are strong reasons why transient sampling might be used. Transient sampling allows more samples to be analyzed in a shorter time. It also generally results in consumption of smaller sample volumes, a benefit when a limited amount of sample is available. Alternatively, a relatively large sample volume can be subjected to preconcentration, resulting in a small volume with a higher concentration of the analyte.[11-15] Often in combination with preconcentration, matrix removal can be performed.[11-13-15] Transients also offer a convenient way to extend the working range of a technique, since low concentrations can be quantitated based on emission near the peak intensity, while high concentrations can be quantitated at a point in the transient where the sample has been diluted.[16] Similarly, the diluted part of the transient can be used to avoid some matrix effects, since the matrix will also be diluted at this point.[16-17] Often, the chemical form is of interest rather than just the elemental concentration; speciation, the determination of this chemical form, is often performed by means of an on-line separation technique that produces a transient sample.[18-20]

The miniaturized version of the SCGD seems particularly well suited to transient analysis. Detection is accomplished through emission, which, with a proper detection scheme, enables the simultaneous determination of multiple elements. Because transients are, by definition, present for only a short time, simultaneous determination is a great

advantage. The narrow capillary (0.38-mm inner diameter) used in the miniature SCGD to deliver the sample solution reduces dead volume and therefore should limit dispersion, producing more intense and narrower peaks. Furthermore, direct sampling removes the need for a spray chamber and the associated washout time.[21] Low and simple (direct current) power requirements, operation in ambient air, and a small footprint all combine to make integration with a separation instrument (e.g., an HPLC tower) feasible.

The SCGD is not the first GDE-based source to be used with transient sampling. The LS-APGD has been used solely for transient sampling since its introduction. Detection limits reported for that source are in the single ppm and single to tens of nanograms range, injection-to-injection relative standard deviations are less than 15%, and peak widths are 10-25 seconds, depending on the powering geometry and solution flow rate (which ranged from 0.3 to 0.7 mL/min).[22] It has been reported that a smaller version of the LS-APGD with lower flow rates produces similar detection limits,[23] but precision and peak widths have not yet been published. A version of the ELCAD has also been adapted for transient analysis.[24] After adjustment to the 3σ definition, detection limits for that source were 20-50 ppb (0.8-2 ng) for several metals. Peak width and precision were not reported, but the peak width can be estimated to be four seconds (1.5 seconds at half maximum) based on published figures. The flow rate could not be reduced below 3.4 mL/min without degrading detection limits by several orders of magnitude. Neither the ELCAD nor the LS-APGD has been evaluated for high-throughput analysis.

The present study will concentrate on simulating high-throughput analysis of small samples by the miniature SCGD. Such analyses place many of the same requirements on

the spectroscopic source as do the other kinds of transient analysis, so positive results here are promising for other applications. Sampling 25-µL volumes at 1000 samples per hour, the discharge achieved detection limits ranging from 5 pg (Li) to 6 ng (Hg). Precision was generally in the range of 1-2% for samples with concentrations more than an order of magnitude above the detection limit. Sodium matrix effect was decreased compared to continuous operation.

8.2 EXPERIMENTAL

The SCGD cell has been described previously,[10] so only a brief account will be given here. A block diagram of the final system is shown in Figure 8-1, but the configuration varied somewhat from one experiment to another. The solution is pumped through a J-shaped (1.1-mm outer diameter, 0.38-mm inner diameter) glass capillary such that it exits flowing upward. Directly (3.2 mm) above the solution emerging from this capillary is a 3.1-mm diameter tungsten rod with a rounded point. The plasma is ignited between a 0.7-mm diameter area on the tungsten rod (the anode) and the solution surface (the cathode). A portion of the solution overflows into a waste reservoir roughly 35 mL in volume. This overflow solution provides an electrical connection to a graphite rod located in the reservoir. The graphite rod is grounded, while a positive high potential is applied to the tungsten rod. A 1.0-kΩ resistor between the 1.0-kV output of the power supply (Kepco BHK 2000-0.1MG, Flushing, NY) and the tungsten rod acts as a ballast against fluctuations in discharge current. The 1.0 kV output used here resulted in a discharge current of approximately 70 mA .

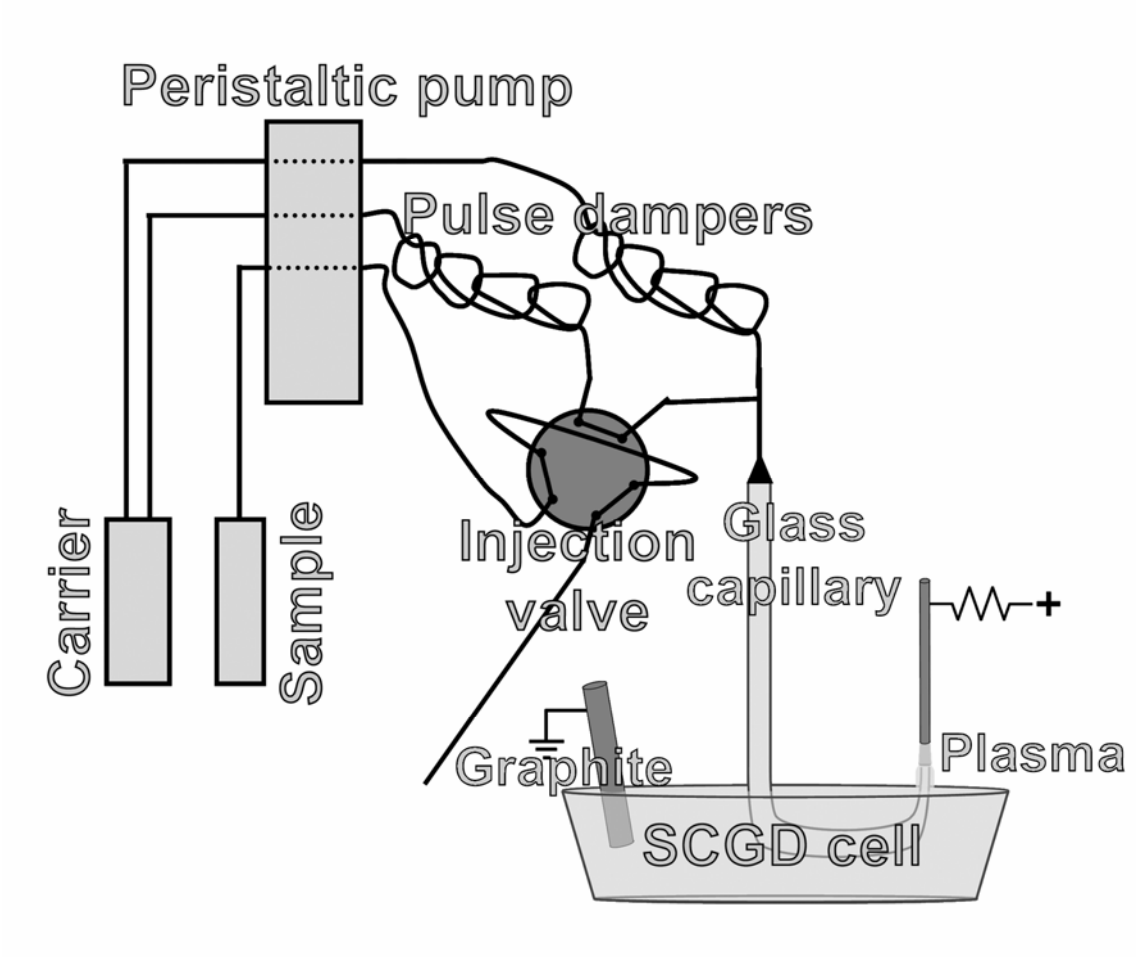

Figure 8-1. Schematic of the final experimental setup used in this study.

Detection was accomplished by imaging the discharge at a magnification of 2.3:1 by a quartz lens onto the 10-μm entrance slit of a 0.5-m Czerny-Turner monochromator (Chromex 500IS/SM, Albuquerque, NM). A Hamamatsu R928 photomultiplier tube (PMT) (Hamamatsu, Japan) biased at -850 V was used as the detector. Current from the PMT was amplified by a Keithley 427 current amplifier (Cleveland, OH) and recorded with a National Instruments (Austin, TX) USB-6009 data acquisition unit and a custom LabVIEW program. An Edmund Optics (Barrington, NJ) GG 475 long-pass filter (greater than 88% transmission above 500 nm, less than 0.1% transmission below 460 nm) was used to block second-order emission when sodium and lithium performance was tested.

Solution transport varied with experiment. In all cases, a single Gilson (Middleton, WI) peristaltic pump was used to deliver all solutions (this pump can simultaneously control up to four separate channels of solution). Two or three channels were used. The carrier channel provided 2.5 mL/min of an aqueous solution (pH 1.0; adjusted with HNO_3) to a 6-port 2-way injection valve. One of two valves was used in a given experiment. The valves were designated manual (Upchurch V-451) and automatic (Rheodyne 7010). When the automatic valve was used, switching was accomplished by means of a Rheodyne 5710 pneumatic actuator, which was driven by a square wave produced by a Beckman 9010 function generator. The injection channel was used to fill a sample loop (25 or 50 μL, depending on the experiment) attached to the valve. In some experiments, there was a supplemental flow of a solution having the same composition as that in the carrier channel at 0.4 mL/min added with a T-connector between the valve and the

discharge. In such cases, the total flow rate (sum of carrier and supplemental flow rates) was 2.9 ml/min. For the carrier and supplemental channels, home-built pulse dampers, which have been described previously,[10] were inserted between the pump and the discharge. A pulse damper was not included in the injection channel.

8.3 RESULTS AND DISCUSSION

Several strategies were evaluated for the integration of flow injection with the miniature SCGD. The first was a simple coupling with the manual injection valve placed inline between the peristaltic pump and the discharge, with the SCGD operated in constant-voltage mode. In this case, a 50-µL injection loop was filled with a 500 ppb solution of lithium. A drawback of this approach is that the flow was briefly interrupted when the valve switched between the *load* and *inject* positions. Because the discharge current flows through the sample solution fountain, halting the solution flow also interrupts the current and extinguishes the discharge. During the time that the solution flow is interrupted, pressure builds up behind the valve, so a small spike in flow rate occurs when the interruption ends. This spike momentarily shortens the gap between the solution and the tungsten anode, reigniting the discharge. Although the discharge is operating by the time sample solution reaches it, it has not yet stabilized, so injection-to-injection variations are significant. Figure 8-2, showing emission from 5 consecutive 50-µL injections of a 500 ppb Li solution, illustrates the degree of these variations, which have a relative standard deviation of 9.5% by peak area. Although this level of precision is adequate for some applications, this first method was rejected for further study. Still, the narrowness of the peaks (1.2 seconds wide at half maximum) and their high

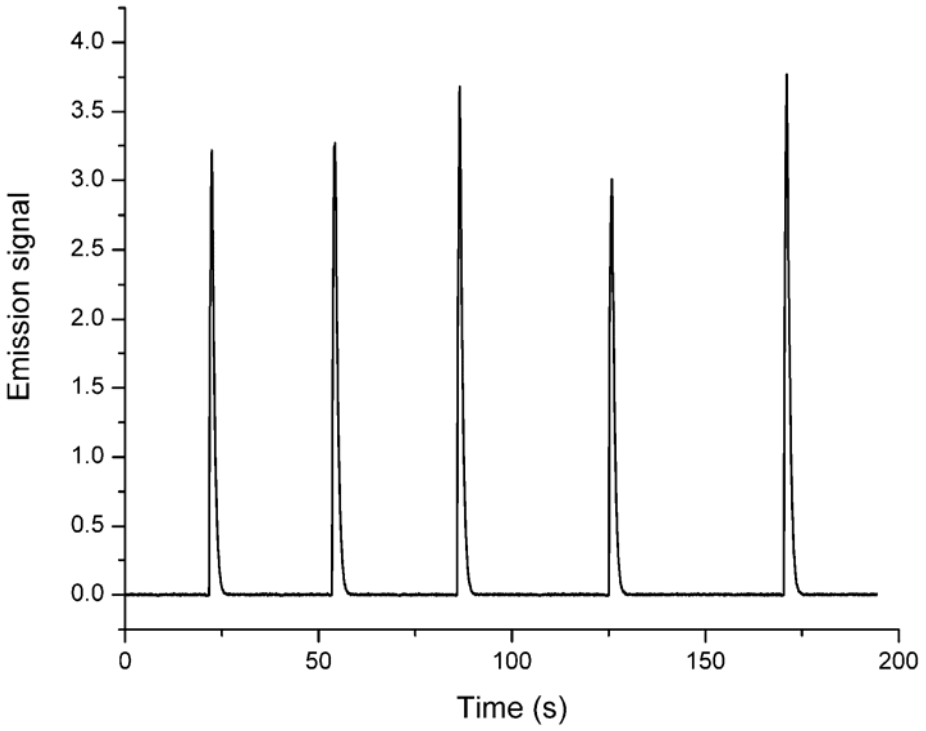

Figure 8-2. Manual 50 µL injections of 500 ppb lithium without supplemental flow.

amplitudes encouraged exploration of other strategies.

In a second approach, the automatic injection valve with a 25-µL sample loop was used with the SCGD operated in constant-current mode. With the faster valve switching and the power supply automatically adjusting its output voltage to maintain the discharge, the plasma was not extinguished during the valve transition. However, it was forced into an arc-like state, which resulted in a similarly variable signal and also caused damage to the capillary. This damage was evidenced by the discharge occasionally changing to the arc-like state during continuous-flow operation when a capillary had previously been used in this second injection strategy. Because such damage is clearly unacceptable, this second strategy was also rejected.

The third method made use of a supplemental flow, added between the valve and the discharge. The setup used in this strategy is shown in Figure 8-1. The automatic valve was once again employed with a 25-µL injection loop, and the SCGD was operated in constant-voltage mode. With this design, the discharge did not extinguish or become arc-like during valve changeover. As can be seen in Figure 8-3, the resulting transients (500 ppb lithium) are much more reproducible than with the previous strategies. Although the discharge fluctuated slightly during switching, it appears to have stabilized before the solution reached it 0.4 seconds later. In fact, if the valve is switched during the time when an injection is passing through the plasma, the fluctuation appears as a depression in emission only about 30-ms long. With this method, ten 25-µL injections of 500 ppb lithium with only 3.6-second spacing between them resulted in a relative standard deviation of 0.8% by area. Because this precision is better than the 1.5%

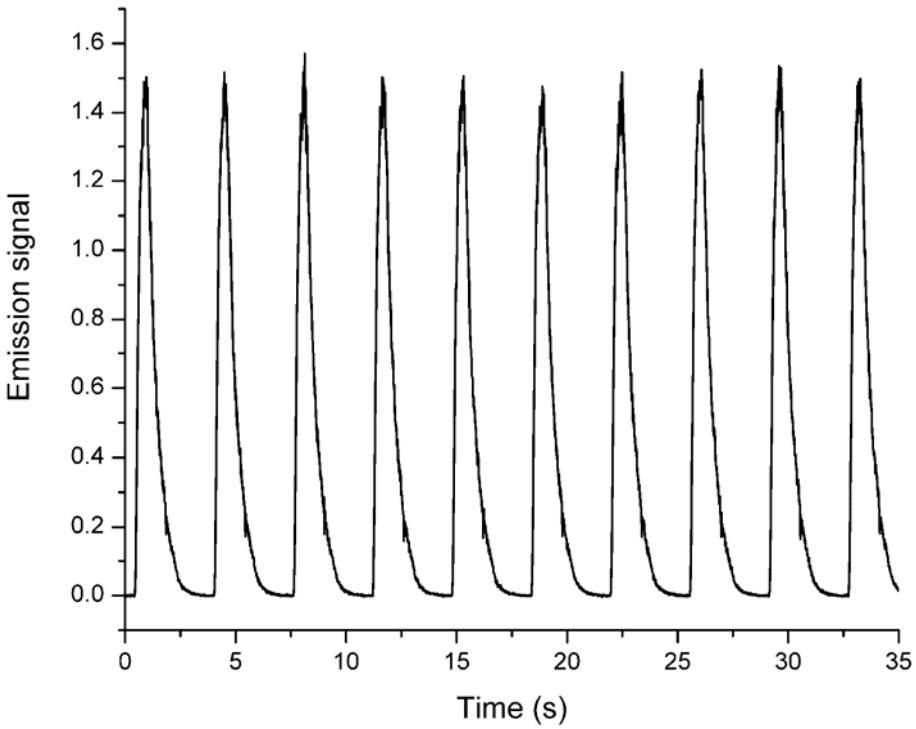

Figure 8-3. Automated 25 μL injections of 500 ppb lithium with supplemental flow. Note that the time axis is shorter than in Figure 8-2.

relative standard deviation found during continuous introduction of a 500 ppb lithium solution with the same discharge system, any switching-related plasma fluctuations were judged to be insignificant.

The dispersion of the arrangement in Figure 8-1 was evaluated by comparing the peak signal from a 25-μL, 500-ppb lithium injection to the signal observed when the same solution was introduced continuously through the carrier pump channel. The peak intensity (averaged over 10 injections) was 80% of the continuous value (averaged over 1.5 minutes), giving a dispersion of 1.2. Associated with this low dispersion is a narrow peak; the full width at half maximum is only 0.7 seconds. This narrowness permits rapid sampling. The 3.6-second spacing between samples used here equates to a 0.28 Hz sampling rate, or 1000 samples per hour. Of course, the current design actually injects aliquots of the same sample repeatedly, but a more sophisticated injection system should allow samples to be switched between injections.

Analytical performance was tested under these simulated high-throughput conditions. The sample solutions in all cases were 500 ppb of the element being studied. Ten injections of the sample and ten injections of the blank were used. The emission was integrated for a 0.55-second portion of the peak. This integration window was chosen because it was found to result in the lowest detection limits when a 500 ppb lead solution was used as a test sample, but there was little variation across a wide selection of windows. The same window was then used for the rest of the studied elements. The relative standard deviations (RSDs) were calculated as the variation in emission of ten 500 ppb samples after correction by the average emission of ten blank solutions (aqueous

solutions adjusted to pH 1.0 with HNO_3). From these same samples, the detection limits were calculated as the concentration that yielded emission equal to three times the standard deviation of the blank emission. The results of these measurements are shown in Table 8-1. Included for comparison are the same figures of merit for continuous sampling obtained with the same source, reported previously.[10] The transient detection limits found in the present study are between 3 and 12 times worse than those for continuous sampling of the same elements. This difference is the consequence of a shorter integration time (the ten-second integration time employed in continuous sampling was 18 times longer than the integration time used for the transient), slight dilution (both from dispersion and from the supplemental flow) that occurs in transient sampling, and some variability from multiple injections. Nevertheless, the transient detection limits are comparable to or as much as an order of magnitude better than those obtained with the earlier, larger version of the SCGD with continuous sampling. Notably, the detection limits in absolute (mass) terms are extremely low, ranging from 5 pg (lithium) to 6 ng (mercury), with the majority lying in the sub-ng range.

The RSDs found with this transient-sampling mode from 500 ppb (13 ng) solutions are mainly between 1-2%, similar to those for the same source with continuous sampling. The exceptions are for those elements with relatively poorer detection limits. It is not surprising that a fairly high RSD (18%) was found for a 500 ppb mercury solution because this concentration is very near the 270 ppb detection limit for Hg. When a 10 ppm mercury solution was used, the RSD dropped to 2.2%.

Calibration curves were prepared for Pb, Cd, Li, and Na. The curves were log-log plots,

Table 8-1. Analytical performance of the SCGD.

Element	Wavelength (nm)	Transient RSD (%)	Transient DL (ng)	Transient DL (ppb)	Continuous RSD (%)[a]	Continuous DL (ppb)[a]
Hg	253.7	18	6	274	1.9	22
Pb	405.7	10	1.5	61	1.7	6
Cu	324.7	4.1	0.6	24	2.9	4
Cd	228.8	2.1	0.4	15	1.4	2
Ag	338.3	1.2	0.06	2	1.9	0.3
Mg	285.2	1.0	0.03	1	0.9	0.2
Na	589.0	1.4	0.009	0.4	1.2	0.1
Li	670.8	0.8	0.005	0.2	1.5	0.06

Transient detection limits (DL) and relative standard deviations (RSD) are based on ten 25-µL injections of 500 ppb solutions and ten 25-µL injections of matching blanks. [a]Continuous DL and RSD values are from a previous study[10] and are based on ten 10-second integrations using 500 ppb solutions and ten 10-second integrations using matching blanks.

so linearity could be assessed (a slope of one on such a plot indicates perfect linearity). The y-intercept gives an indication of the relative sensitivity for different elements (with larger intercepts indicating higher sensitivity). Lead (slope = 1.02, y-intercept = -2.3, R^2 = 1.000) and lithium (slope = 0.99, y-intercept = 0.21, R^2 = 1.000) showed excellent linearity over the entire range studied here (the most concentrated solution was 80 ppm). Cadmium (slope = 0.92, y-intercept = -1.5, R^2 = 1.000) and sodium (slope = 0.91, y-intercept = 0.88, R^2 = 0.999) showed fair linearity over a shorter range; for both elements, 12 ppm solutions fell within the linear range, but 80 ppm solutions clearly did not.

Additionally, these calibration curves were used to check the previously determined detection limits. For Li, the calculated detection limit was between 0.08 and 0.1 ppb (2 and 3 pg) based on 1.2 ppb, 12 ppb, 120 ppb, 1.2 ppm, 12 ppm, and 80 ppm samples and was 0.1 ppb (3 pg) based on the slope of a line containing all of these points and a blank. For Pb, the calculated detection limit was between 60 and 70 ppb (1 and 2 ng) based on 120 ppb, 1.2 ppm, 12 ppm, and 80 ppm solutions, and was 60 ppb (1 ng) based the slope of a plot including all of these and a blank. For Cd, the calculated detection limit was between 15 and 21 ppb (0.4 and 0.5 ng), based on 120 ppb, 1.2 ppm, and 12 ppm samples, and was 21 ppb (0.5 ng) based on the slope of a fit to all these points and a blank. As would be expected given Cd's log-log slope less than one, the lowest concentration sample produced the lowest calculated detection limit for this element. For Na, the calculated detection limit ranged from 0.1 to 0.6 ppb (3 to 15 pg) based on concentrations of 1.2 ppb, 12 ppb, 120 ppb, 1.2 ppm, and 12 ppm, and was 0.6 ppb (15 pg) based on the slope of a line including all those points and a blank. Since Na also had

a log-log slope of less than one, it is not surprising that the lowest concentration sample resulted in the lowest calculated detection limit.

By using the tail of the transient flow-injection peak, the upper concentration limit can be raised. For example, in the case of cadmium, a 0.55-second integration beginning 3.05 seconds after the injection produces a calibration curve that remains very linear (slope = 0.97, R^2 = 1.000), with the 80 ppm standard included. Understandably, because this dynamic-range extension is accomplished through dilution, the detection limit is also degraded. Based on the 12 ppm standard, the detection limit for this strategy is 520 ppb. Of course, since the difference is in processing rather than acquisition, multiple calibration curves can be created for a given flow-injection transient based on the same data, to cover a range of sample concentrations without increasing the number of injections required.

Similarly, such dilution can be used to reduce some matrix effects. Two matrix effects have previously been studied with the miniature SCGD operated in continuous-sampling mode: the interference of phosphate on calcium and the interference of sodium on several elements.[10] In the case of phosphate, flow injection would not be expected to reduce the effect because it is related to solute-particle vaporization. Such interferences are dependent on the ratio of the interferent to the analyte rather than the absolute concentration of the interferent. To test this assumption, 2 solutions of 2 ppm Ca were prepared. One solution also contained 7.2 ppm P (added as H_3PO_4), for a P:Ca molar ratio of 4.7:1. In continuous-sampling experiments, calcium emission was 14% lower for the phosphate-containing solution than for the phosphate-free solution. Using flow

injection, the depression was a nearly identical 13%.

The sodium matrix effect would be expected to be less severe in a flow injection arrangement because it is dependent on the interferent concentration. To test this supposition, separate solutions of 2 ppm Cu, Cd, or Mn were prepared along with solutions with the same analytes and 25 mM Na. The emission was monitored at the appropriate wavelengths (324.7 nm for Cu, 228.8 nm for Cd, and 279.6 nm for Mn) and background was corrected using nearby wavelengths. The results are reported as the percent reduction in emission for the sodium-containing solutions versus that for the solutions without added sodium. These results were compared to previously reported results for continuous sampling with the same source and samples.[10] As expected, the transient sample introduction performed better (exhibited less suppression) than continuous flow (23% vs. 35% for Cu, 24% vs. 44% for Cd, and 45% vs. 57% for Mn).

In addition to reducing the matrix effect, transient sampling also allows such effects to be identified because the transient shape is different for a sodium-containing sample than for one without sodium. Figure 8-4 shows a series of transients for 2 ppm Mn with and without 25 mM Na. The sodium-containing solution produces transients that are wider relative to their height than those from solutions without added sodium. This is because the sodium interference is greater near the transient peak, where sodium concentrations are greater. It might be expected that accuracy would be improved by using only the tail of the flow injection transient because dilution of the matrix is greatest there.

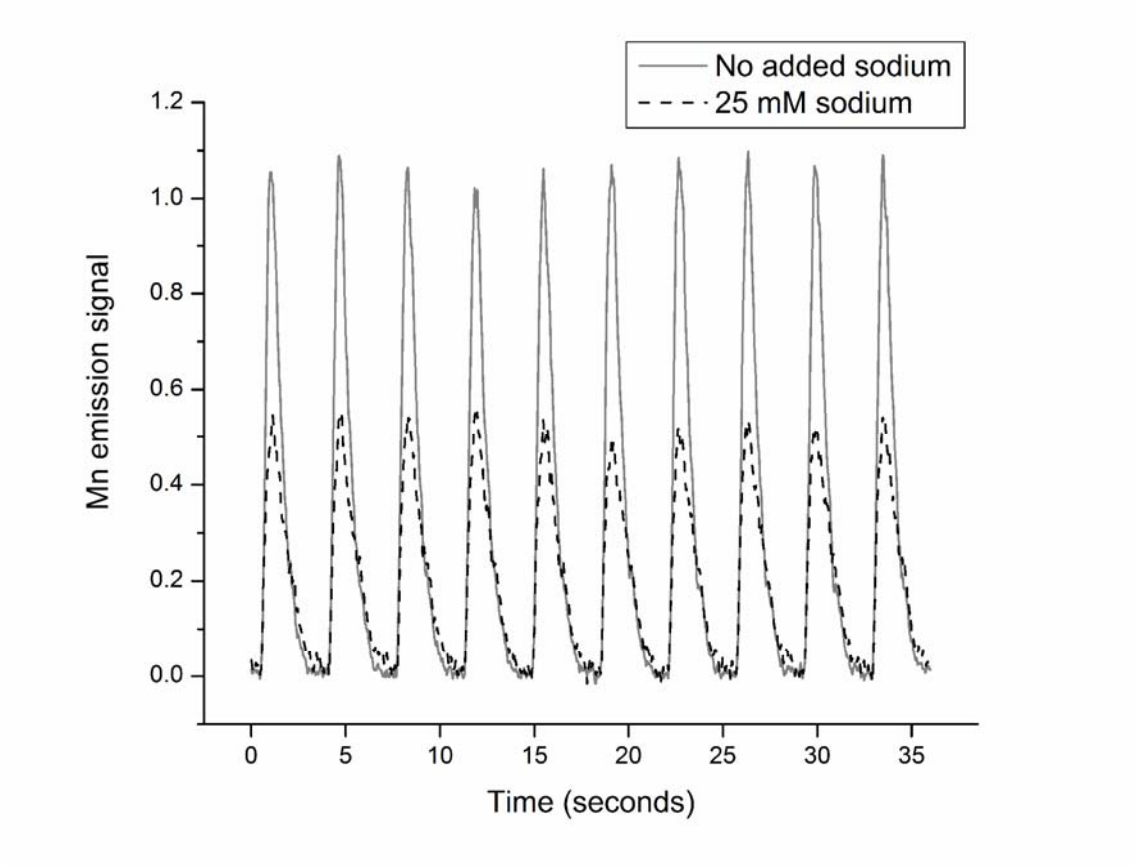

Figure 8-4. Emission at 279.6 nm from 25-µL injections of a 2 ppm Mn solution with (solid gray line) and without (dashed black line) 25 mM Na. Note that the shapes of the transients are altered in the presence of Na.

Unfortunately, the emission is actually slightly enhanced in this region, leading to inaccuracies in the opposite direction (that is, leading to measured concentrations higher than the actual concentration). It not entirely clear why this enhancement occurs, but the trend holds for all three analytes (Cu, Cd, and Mn) that have been studied. One possibility is that there is some lag time involved in returning the plasma and other source components to normal conditions. The composition of the solution that makes the electrical connection might affect the powering for longer than the sodium affects other processes in the plasma. The applied voltage is fixed and is divided among the ballast resistor, the plasma, and the solution according to the resistance of each. The resistance of the thin layer of solution overflowing from the capillary tip is the most significant part of the overall solution resistance. If this resistance drops, a greater voltage will be applied to the plasma, increasing analyte emission. A lag between the plasma conditions and the overflow resistance might cause the observed trend (enhanced emission at the tail of a matrix-containing transient). Other time lags in the plasma or the power supply might also play a role.

Although using the tail of the peak alone will not produce an accurate measurement of the analyte concentration, including it should improve the accuracy. A two-second integration window, which encompasses most of the transient, was tested using the same data as above. For all elements, there was a substantial lessening in suppression compared to the 0.55-second integration window used earlier (16% vs. 23% Cu, 16% vs. 24% for Cd, and 28% vs. 45% for Mn). A concern might be that changing the integration window would affect the precision or detection limit, but the differences were not

significant, as Table 8-2 shows. This finding suggests that longer integration times should be used when matrix effects of this sort might be present.

8.4 CONCLUSIONS

The results found in this initial study are quite promising, and further work is likely to yield additional improvement. For example, better valving (e.g., a make-before-break valve) might obviate the need for a supplemental flow. However, the supplemental flow might prove to be an advantage in future studies involving other types of transient analysis. Separation and preconcentration techniques could require solution compositions that are not ideal for use with SCGD, or which vary with time. The supplemental flow could be used to adjust the solution composition after separation or preconcentration. Additionally, adjustments in supplemental flow volume, composition, or interface design might improve performance. The dead volume between the valve and the discharge might be reduced through a different geometry (a shorter and/or narrower channel), thereby elevating instantaneous signal and narrowing transients. Alternatively or concurrently, a somewhat larger sample volume might be used. If the strategies are combined, signal might be increased while throughput is maintained. The results shown here also suggest that coupling of the SCGD to separation and online preconcentration methods is feasible and should be pursued.

Table 8-2. Comparison of analytical performance of the miniature SCGD with two different length integration windows.

Element	Wavelength (nm)	0.55-second integration RSD (%)	0.55-second integration DL (ppb)	2-second integration RSD (%)	2-second integration DL (ppb)
Cd	228.8	1.7	16	1.4	12
Cu	324.7	0.8	25	0.7	32
Mn	279.6	2.0	11	1.5	11

Detection limits (DL) and relative standard deviations (RSD) are based on ten 25-µL injections of 2 ppm solutions and ten 25-µL injections of matching blanks.

8.5 REFERENCES

[1] J. Gubkin, "Elektrolytische Metallabscheidung an der freien Oberfläche einer Salzlösung.", *Ann. Phys. Chem.*, 1887, **32**, 114.

[2] D. E. Couch and A. Brenner, "Glow discharge spectra of copper and indium above aqueous solutions", *J. Electrochem. Soc*, 1959, **106**, 628.

[3] T. Cserfalvi, P. Mezei and P. Apai, "Emission studies on a glow discharge in atmospheric pressure air using water as a cathode", *J. Phys. D-Appl. Phys.*, 1993, **26**, 2184.

[4] T. Cserfalvi and P. Mezei, "Direct solution analysis by glow discharge: electrolyte-cathode discharge spectrometry", *J. Anal. At. Spectrom.*, 1994, **9**, 345.

[5] W. C. Davis and R. K. Marcus, "An atmospheric pressure glow discharge optical emission source for the direct sampling of liquid media", *J. Anal. At. Spectrom.*, 2001, **16**, 931.

[6] V. V. Yagov and M. L. Gentsina, "Effect of Supporting Electrolyte Composition on the Intensity of Metal Lines in Electrolyte-Cathode Discharge Spectra", *J. of Anal. Chem.*, 2004, **59**, 64.

[7] C. G. Wilson and Y. B. Gianchandani, "Spectral detection of metal contaminants in water using an on-chip microglow discharge", *IEEE Transactions on Electron Devices*, 2002, **49**, 2317.

[8] V. V. Yagov, M. L. Getsina and B. K. Zuev, "Use of electrolyte jet cathode glow discharges as sources of emission spectra for atomic emission detectors in flow-injection analysis", *J. Anal. Chem.*, 2004, **59**, 1037.

[9] M. R. Webb, F. J. Andrade, G. Gamez, R. McCrindle and G. M. Hieftje, "Spectroscopic and electrical studies of a solution-cathode glow discharge", *J. Anal. At. Spectrom.*, 2005, **20**, 1218.

[10] M. R. Webb, F. J. Andrade and G. M. Hieftje, "A Compact Glow Discharge for the Elemental Analysis of Aqueous Samples", *Anal. Chem.*, 2007, **Submitted**,

[11] X. P. Yan, Y. Li and Y. Jiang, "A flow injection on-line displacement/sorption preconcentration and separation technique coupled with flame atomic absorption spectrometry for the determination of trace copper in complicated matrices", *J. Anal. At. Spectrom.*, 2002, **17**, 610.

[12] J. Munoz, J. R. Baena, M. Gallego and M. Valcarcel, "Development of a method for the determination of inorganic cadmium and cadmium metallothioneins in fish liver by continuous preconcentration on fullerene and flame atomic absorption spectrometry", *J. Anal. At. Spectrom.*, 2002, **17**, 716.

[13] G. Abbasse, B. Ouddane and J. C. Fischer, "Determination of total and labile fraction of metals in seawater using solid phase extraction and inductively coupled plasma atomic emission spectrometry (ICP-AES)", *J. Anal. At. Spectrom.*, 2002, **17**, 1354.

[14] T. Shamspur, M. H. Mashhadizadeh and I. Sheikhshoaie, "Flame atomic absorption spectrometric determination of silver ion after preconcentration on octadecyl silica membrane disk modified with bis[5-((4-nitrophenyl)azosalicylaldehyde)] as a new Schiff base ligand", *J. Anal. At. Spectrom.*, 2003, **18**, 1407.

[15] T. Sawatsuk, J. Shiowatana and A. Siripinyanond, "Matrix removal and analyte preconcentration before inductively coupled plasma spectrometric detection: use of a laboratory-made hollow fibre flow filtration unit", *J. Anal. At. Spectrom.*, 2006, **21**, 1331.

[16] M. Sperling, Z. L. Fang and B. Welz, "Expansion of Dynamic Working Range and Correction for Interferences in Flame Atomic-Absorption Spectrometry Using Flow-Injection Gradient Ratio Calibration with a Single Standard", *Anal. Chem.*, 1991, **63**, 151.

[17] D. M. McClenathan, S. J. Ray and G. M. Hieftje, "Novel flow injection strategies for study and control of matrix interferences by inductively coupled plasma time-of-flight mass spectrometry", *J. Anal. At. Spectrom.*, 2001, **16**, 987.

[18] J. Morton, V. A. Carolan and P. H. E. Gardiner, "The speciation of inorganic and methylmercury in human hair by high-performance liquid chromatography coupled with inductively coupled plasma mass spectrometry", *J. Anal. At. Spectrom.*, 2002, **17**, 377.

[19] K. Polec-Pawlak, D. Schaumloffel, J. Szpunar, A. Prange and R. Lobinski, "Analysis for metal complexes with metallothionein in rat liver by capillary zone electrophoresis using ICP double-focussing sector-field isotope dilution MS and electrospray MS detection", *J. Anal. At. Spectrom.*, 2002, **17**, 908.

[20] P. Bratter, I. N. Blasco, V. E. N. de Bratter and A. Raab, "Speciation as an analytical aid in trace element research in infant nutrition", *Analyst*, 1998, **123**, 821.

[21] M. Wu and G. M. Hieftje, "A New Spray Chamber for Inductively Coupled Plasma Spectrometry", *Appl. Spectrosc.*, 1992, **46**, 1912.

[22] W. C. Davis and R. K. Marcus, "Role of powering geometries and sheath gas composition on operation characteristics and the optical emission in the liquid sampling-atmospheric pressure glow discharge", *Spectrochim. Acta, Part B*, 2002, **57B**, 1473.

[23] J. L. Venzie and R. K. Marcus, "Micro-scale analytical plasmas for liquid chromatography detection", *Anal. Bioanal. Chem.*, 2005, **381**, 96.

[24] T. Cserfalvi and P. Mezei, "Subnanogram sensitive multimetal detector with atmospheric electrolyte cathode glow discharge", *J. Anal. At. Spectrom.*, 2003, **18**, 596.

Chapter 9

The annular glow discharge: a small-scale plasma for solution analysis.

9.1 INTRODUCTION

Inductively coupled plasmas (ICPs) are well known for their usefulness in analyzing solution samples, but they are the exception rather than the rule for plasmas. Microwave plasmas and low-pressure glow discharges, for example, lack the thermal energy or aerosol residence time necessary for efficient desolvation.[1-2] Even when plasmas have regions with high thermal energy, properties of the plasma can prevent aerosols from effectively penetrating into these regions. An apt example is the ICP itself. At lower frequencies (e.g. 5 MHz), a spheroidal plasma forms, and gas expansion near this region pushes much of the aerosol towards the cooler outer region of the plasma.[1-2] At the frequencies now typically used (27 and 40 MHz) and with a high gas velocity through the centre of the ICP, an annular plasma forms more easily, and much of the aerosol is channelled to the center, which is cooler than the annular region but still quite hot.[1-3]

A recent trend in analytical chemistry has been towards miniaturization, and researchers involved with plasma spectrochemistry have followed this trend with an array of miniaturized plasmas, mostly designed for atomic or molecular detection of gas chromatography effluents.[4-6] Motivations for the development of such plasmas are

mostly related to cost, potential for portability, and integration with chromatographic and other separation instrumentation. Typical properties of these plasmas that address those motivations are small footprint, low gas and power consumption, low construction costs, and the lack of a need for vacuum equipment. Attention is sometimes focused on plasmas with at least one dimension below an arbitrary 1-mm cut-off (which are commonly classified as microplasmas even when they have other dimensions of several millimeters or even a few centimeters), but the advantageous traits of miniaturized plasmas should not be expected to obey this sharp distinction.

Reviewers of the field seem encouraged by recent progress with gaseous samples, but tend to be considerably less optimistic when solution sample introduction is used,[4-6] at least in the absence of nearly complete separation of the analyte from the liquid solvent. This requirement is typically ill-suited for continuous analysis and ordinarily involves the use of transient sample introduction (e.g. electrothermal vaporization[6]) or requires different conditions for different analytes (e.g. hydride generation[7]). Perhaps because of a combination of shorter residence times and lower gas temperatures, miniaturized plasmas tend to have even more difficulty with solution samples than their larger cousins. In fact, they often become unstable or are extinguished when an aerosol is added. By the standards of solution analysis with miniaturized plasmas, a significant accomplishment is the miniaturized ICP (described by its inventors as an atmospheric-pressure microplasma jet).[6-8] This device achieves a detection limit of 5 ppm for sodium with electrospray sample introduction but does not tolerate the higher solvent loads of even a micronebulizer.

It should be noted that successful solution analysis by miniaturized plasmas has been accomplished by means of variations on glow discharge electrolysis (GDE), an electrochemical technique discovered by Gubkin in 1887.[9] In GDE, a glow discharge is maintained with at least one electrode consisting of an electrolytic solution. Notable applications of this technique to atomic emission spectrometry include the electrolyte-cathode discharge (ELCAD)[10-12] and the liquid-sampling atmospheric-pressure glow discharge (LS-APGD).[13-14] In both of these techniques, the cathode is typically the solution sample. In all GDE-based techniques, the emission is highly dependent on the electrolyte concentration, which leads to two constraints that can be disadvantages: solutions must have high electrolyte concentrations for good sensitivity and these concentrations must be highly consistent between standards and samples if acceptable quantification is desired.[11-13]

In the present work, we introduce a miniaturized plasma that is stable even with a significant solvent load. This plasma belongs to a general class of atmospheric-pressure helium discharges.[15] One such discharge reported in the literature is capable of elemental analysis of aerosols, but this discharge uses an order of magnitude higher power and achieves detection limits significantly worse than the source presented here.[16] In our experience, tolerance to solvent loading is not a general property of these discharges. It is likely that the particular geometry of the source presented here is the factor that allows it to perform so well, just as the ICP geometry contributes to its success. In this new source, a sample aerosol is directed through a tubular cathode, within which there is an annular negative glow. For this reason, we describe this as an annular glow discharge.

This source differs from a classical hollow cathode glow discharge, in which the negative glow is spheroidal.

9.2 EXPERIMENTAL

The experimental setup for the new source is diagrammed in Figure 9-1. Sample solutions were supplied by a PHD-2000 syringe pump (Harvard Apparatus, Holliston, MA) and the flow of ultra-high-purity helium (Airgas, Inc., Radnor, PA) was regulated by a Tylan model FC-280 mass flow controller. Helium flow was maintained at 1.5 L/min. Sample solutions were prepared from DI water. Both were fed through a Meinhard (Golden, CO) TR-50-A1 concentric nebulizer. Large droplets were removed from the resulting aerosol by a Wu-Hieftje vertical rotary spray chamber (LECO, St. Joseph, MI), which was drained by a Perkin-Elmer (Norwalk, CT) Minipuls 2 peristaltic pump. After the spray chamber, the aerosol passes through a 45-mm long, 5-mm diameter glass tube. The glass tube is connected through a male-male Swagelok® connector to a brass chamber, which is wrapped in glass wool for thermal insulation. The chamber is 11 mm in diameter and 8 cm long. The cathode, a 2-mm inner-diameter steel tube, screws into the other end of the brass chamber. The anode is a 7.4-mm diameter steel rod with a rounded tip. The anode and cathode are separated by 5 mm, at a slight angle so the discharge contacts the anode approximately 0.5 mm off the axis of the cathode. This arrangement was adopted to simplify axial viewing.

The discharge was powered by a Kepco (Flushing, NY) 1000 BHK-0.2MG high voltage power supply. A positive potential was supplied to the anode and the cathode was

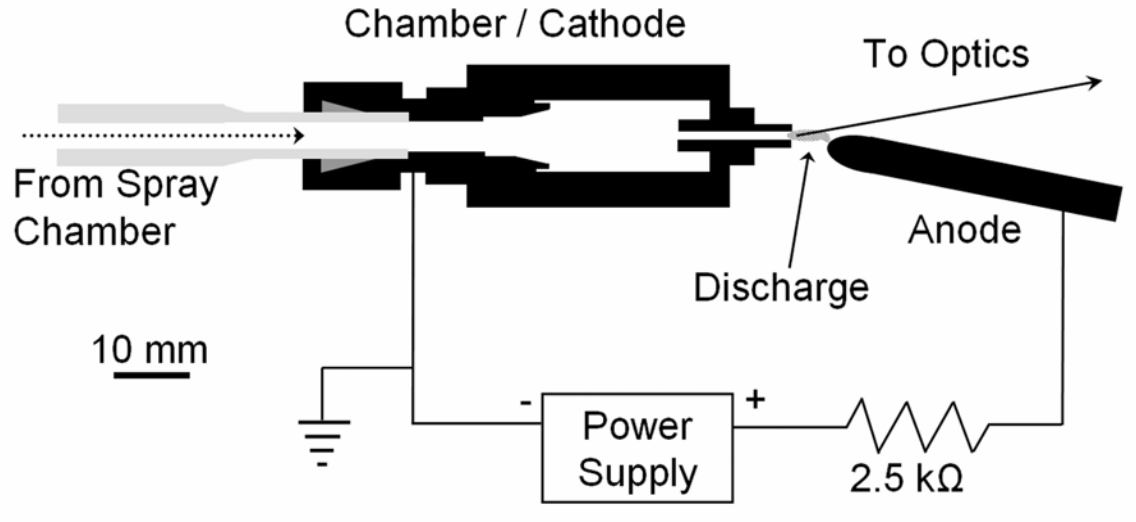

Figure 9-1. Diagram of annular glow discharge. Upper portion is approximately to scale. Black areas are metals (brass or steel).

grounded. Two 1.25-kΩ resistors were placed in series with the anode and the power supply to stabilize the discharge. Typical power usage was 75 W, with 40 W dropped across the plasma. For dc voltage measurements, a Fluke (Everett, WA) model 175 digital multimeter was used in combination with a Fluke 80K-40 high-voltage probe. For the measurement of noise power spectra, a Tektronix (Richardson, TX) TDS 2024 digital oscilloscope was used in combination with a AK-510 high-voltage probe (R. S. R. Electronics, Inc., Avenel, NJ); a fast Fourier transform was performed by the oscilloscope using its flat-top algorithm. For current measurements, a 2.1-Ω resistor was placed in series with the discharge, between the cathode and ground, and the potential drop across it was converted to current through it by means of Ohm's law. This voltage measurement was made using a Tektronix DM252 multimeter.

An Ocean Optics (Dunedin, FL) USB2000 spectrometer with a fibre optic attachment was used to determine what region of the plasma produced analyte emission; the arrangement used in this study was based on the observation that emission is strongest in the near-cathode region. The emission was measured nearly on-axis to the cathode, but at an approximately 9° angle so the anode did not block the light from reaching the spectrometer. A 7-cm focal length fused-silica lens focused light onto the monochromator entrance slit with a magnification of approximately 0.36. The monochromator was a McPherson (Chelmsford, MA) EU-70 unit with 50-µm slits, providing 0.1-nm resolution. The current from a Hamamatsu (Hamamatsu, Japan) R928 photomultiplier tube was converted to voltage by a Keithley (Cleveland, OH) 427 Current Amplifier. The voltage was recorded with LabVIEW (National Instruments,

Austin, TX). Fast Fourier transforms were performed by a LabVIEW program that normalized the emission before the power spectra were calculated, using a flat-top algorithm.

9.3 RESULTS AND DISCUSSION

9.3.1 Visual observations

In the following description, the cathode axis is defined as the central axis of the cathode tube (i.e., the axis parallel to the cathode's inner and outer walls). A bright annular glow, believed to be the negative glow, is observable inside the cathode. Its outer diameter is such that no space is visible between it and the inner wall of the cathode (2-mm diameter), although there is presumably a dark space in the single to tens of micrometers in thickness.[17] The glow itself appears to be a few hundred micrometers thick, leaving a dark central channel between 1 and 1.5 mm in diameter. A glow, possibly the positive column, also extends between the cathode and the anode. Near the cathode, this second glow is mostly diffuse and dim, except for one thin brighter region starting near the cathode wall and extending at a slight angle to the cathode axis so that it intersects this axis about 3 mm from the cathode. Between the cathode and this intersection point, the bright region becomes more diffuse and, by the intersection point, the dim diffuse and bright thin regions have merged into a single bright diffuse region. This region extends along the cathode axis until the anode, at which point it bends sharply to intersect the anode, which lies half a millimeter off the cathode axis in the arrangement studied here. This diffuse region is about 2 mm in diameter at the anode. On the anode surface, there

is another bright glow. This region is very thin perpendicular to the anode surface, but takes the form of an ellipse in the plane parallel to the anode surface. Note that the anode surface contacted by the discharge is not perpendicular to the cathode axis but is nearly parallel to it and also that this surface is curved rather than flat. The ellipse is elongated (about 3 mm) in the direction nearly parallel to the cathode axis compared to the direction nearly perpendicular to it (about 2 mm). Between the diffuse region and the anode glow, there appears to be a dark region, but its small size (perhaps less than 100 μm) makes it difficult to observe. A photo of the discharge is shown in Figure 9-2.

Although the thin bright region often remains stably anchored to one spot on the cathode for periods of several hours of continuous operation, it can also become unstable, hopping between two points with periods of hundreds of milliseconds to minutes. This instability is obviously detrimental to analytical measurements because movement of the bright zone into and out of the region imaged onto a spectrometer entrance aperture will change the emission intensity measured by that spectrometer. It is not clear at present why the region anchors to a particular spot or what causes it to hop, but it is clearly something that would be desirable to control. Work to overcome this instability is currently underway. All of the measurements presented here were performed while the bright region was stably anchored to a single spot.

When an aerosol is introduced through the tubular cathode, the thin bright region becomes more diffuse and less distinct from the dimmer diffuse region. Aside from this change, the description of the dry discharge holds.

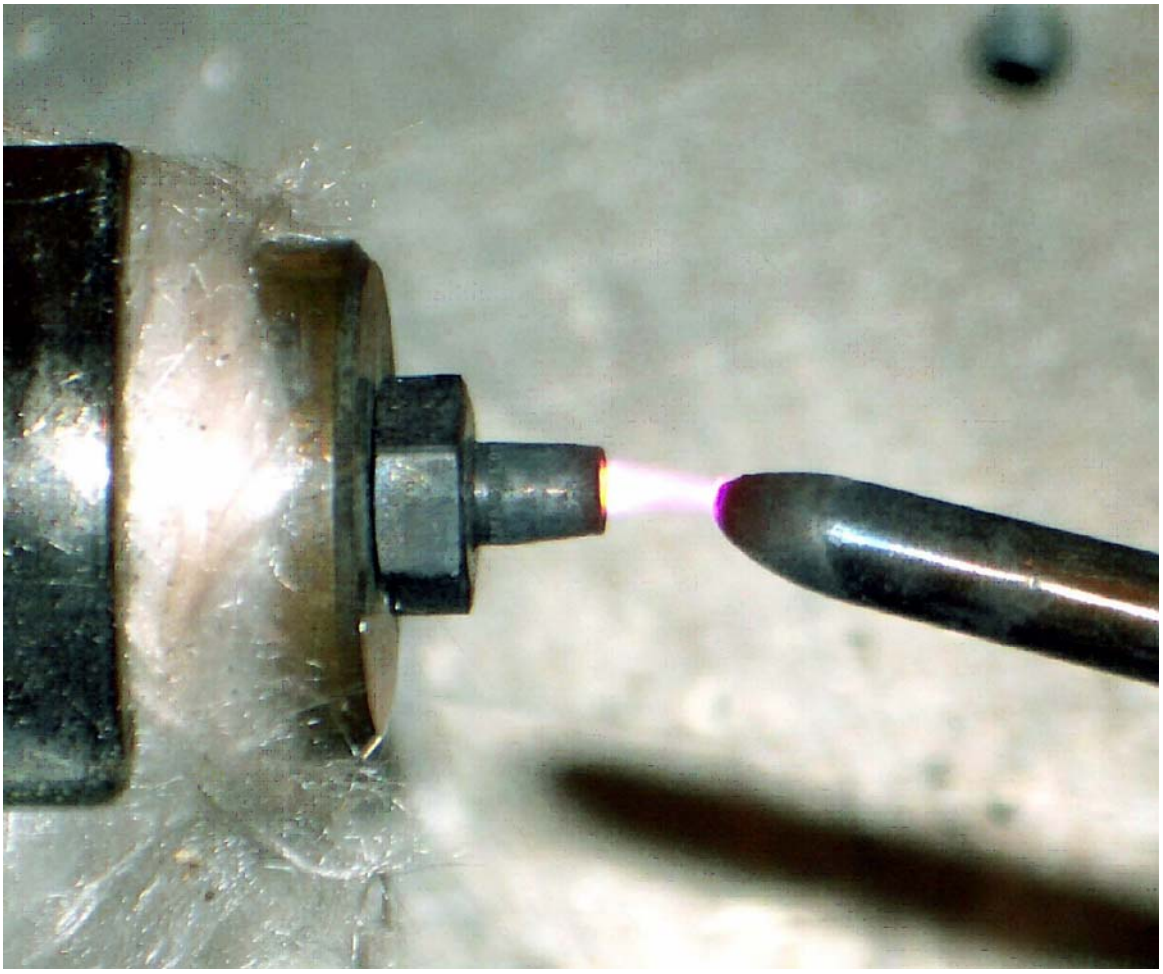

Figure 9-2. Photograph of the annular glow discharge.

These discharge regions certainly merit further study, but this coverage would be outside the scope of the present work. However, they appear to be highly analogous to the regions of another atmospheric pressure helium discharge, which was studied by Andrade et al.[15] It also should be noted that, based on observations with the Ocean Optics spectrometer and on imaging the source onto the slit of a monochromator from different angles, the majority of analyte (metals introduced in the aerosol) emission is from near or within the cathode tube.

9.3.2 Electrical characterization

The electrical characteristics of the plasma under a range of solvent loads can be seen in Figure 9-3. Let us first consider the dry plasma. The slope of this plot, the dynamic resistance, is negative. It should be noted that there is a voltage drop across the ballast resistors that is not included in this measurement and is large enough to make the total resistance positive; this feature serves to stabilize the plasma. Negative resistance is ordinarily seen as an indication of an arc rather than a glow discharge, but the magnitudes of the current and voltage here are atypical for an arc. Also, under certain conditions, similar plasmas have shown a positive resistance or a resistance that changes from negative to positive with increasing current.[15] It seems likely then, that there are two or more processes occurring with opposing resistances. Positive dynamic resistance is a familiar property of an abnormal glow discharge and is described elsewhere,[17-19] so it merits little description here. In an abnormal glow discharge (a discharge in which the available cathode surface is covered by the discharge as is typical in analytical spectroscopy), increases in the current density require greater potentials, imparting a

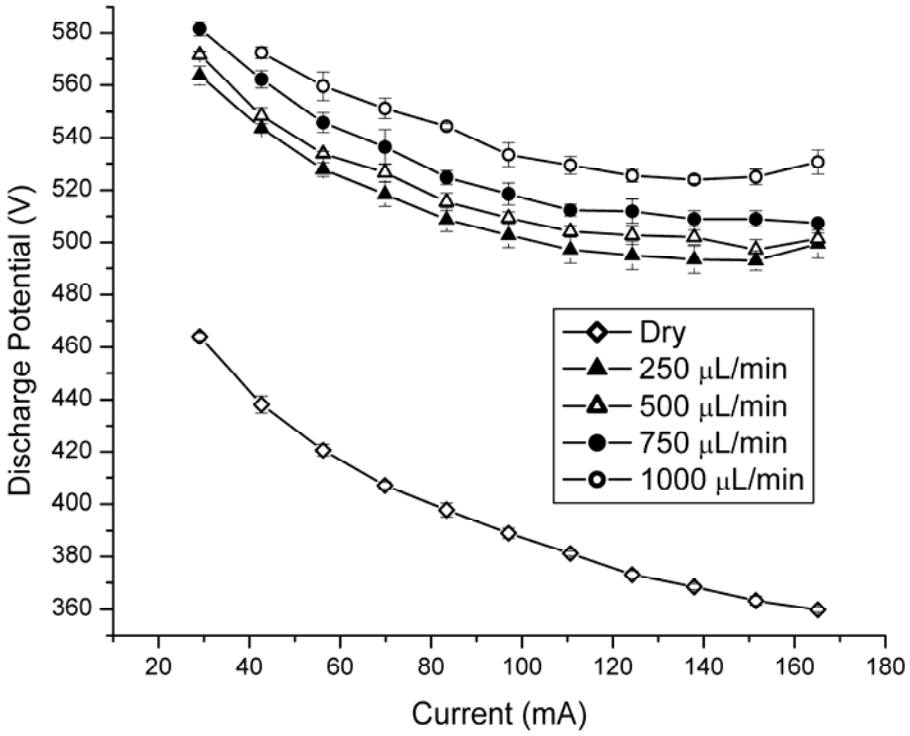

Figure 9-3. Electrical characteristics of the annular glow discharge under different solution (DI water) flow rates. Error bars represent twice the standard deviation of 5 measurements.

positive dynamic resistance.[17-19] In a normal glow discharge, where the available cathode is not completely covered, zero dynamic resistance is found because higher currents increase the cathode-surface coverage rather than the current density. The negative resistance here might be explained in part by Joule heating,[17] which grows as current density rises; in turn, the consequently higher temperature lowers the density of the gas and therefore reduces the potential required to maintain a glow discharge.[17-18] Whether or not this heating plays a role in the observed behavior, this negative dynamic resistance is common among atmospheric pressure glow discharges with large positive columns.[15-20]

When the influence of solution flow rate on the discharge (for example, Figure 9-4) is interpreted, it is important to realize that the solvent transport efficiency climbs rapidly as flow rate decreases, such that it is only a few percent at a typical flow rate of 1 mL/min but can be as high as 80% at very low flow rates (10 μL/min).[21] Of course, these values will vary with the nebulizer-spray chamber combination, the gas flow, and the nebulizer-gas identity.[22-24] The result is that the mass of solvent leaving the spray chamber and entering the discharge (the aerosol) does not scale linearly with solution flow rate and varies relatively little across the flow range used here.

To test the relationship between solution and aerosol flow rates, a U-shaped tube filled with Drierite (Xenia, OH) 8 mesh anhydrous calcium sulfate was attached to the output of the spray chamber to trap the aerosol. The mass change was measured and divided by the time to establish the aerosol flow rate. The results are plotted as aerosol flow rate vs. solution flow rate in Figure 9-4 (squares connected by dashed lines; right axis). Between solution flow rates of 240 and 1800 μL/min (a 650% increase), the aerosol flow rate only

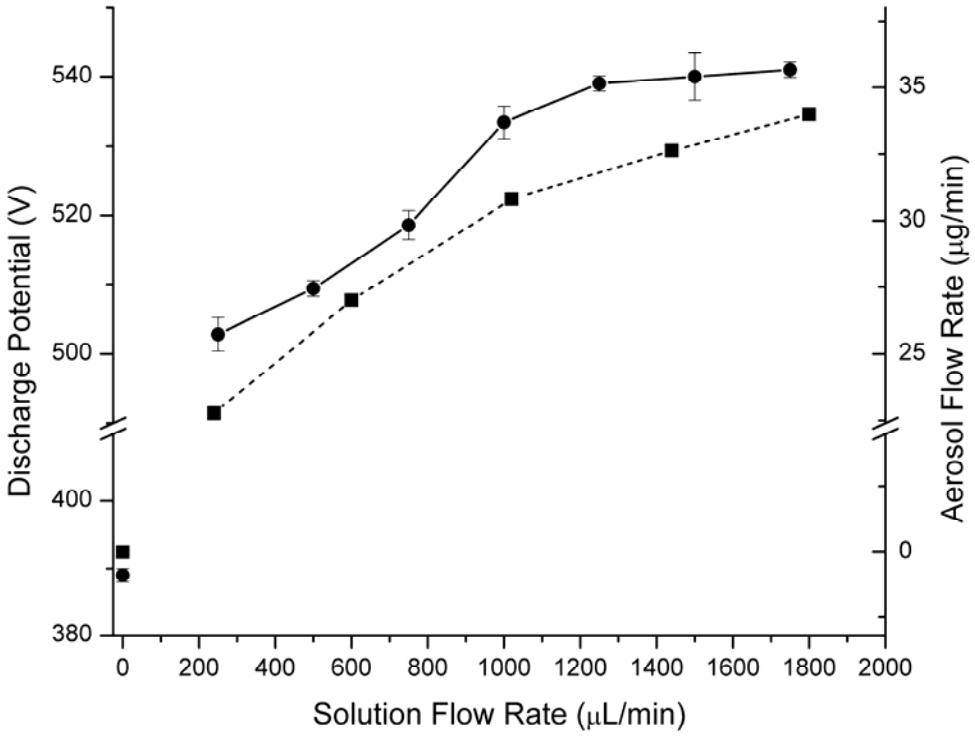

Figure 9-4. Effect of solution (DI water) flow rate on discharge potential (circles with solid lines) and aerosol flow rate (squares with dashed lines). Error bars on discharge potential measurements represent twice the standard deviation of 5 measurements. A current of 100 mA was maintained for potential measurements and the discharge was disconnected for aerosol measurements. Note that the y-axes are not continuous.

changes from 22.8 to 34.0 μg/min (a 49% increase).

There are two notable effects of the aerosol on the electrical characteristics of the annular discharge. The first is that the potential, and therefore the power, required to maintain a given current is greater as the sample-solution flow rate is raised. This behavior is best shown in Figure 9-4. The second, shown in Figure 9-3, is that the dynamic resistance becomes somewhat less negative, then slightly positive, at high currents under higher solution flow-rate conditions. Molecular gases such as water provide a larger number of pathways for energy loss (e.g. electronic, vibrational, and rotational excitation) than do atomic gases, so, in the presence of molecular gases, electrons are more likely to lose their energy before causing ionization, making the breakdown potential higher.[17-25] This higher breakdown voltage elevates the positive resistance. The presence of droplets in the aerosol presumably provides another pathway for energy loss (evaporation), adding to the effect. Changes in the plasma temperature might play some role as well, although the direction of the temperature change and the magnitude of temperature's influence have not yet been established. Possibilities include evaporative cooling, higher power deposition via rotational and vibrational paths which, in turn, lead to heating, and cooling by spreading thermal energy through the more diffuse plasma that exists when water is present.

9.3.3 Spectral features

Figures 9-5 and 9-6 show emission spectra of the annular discharge under dry and wet conditions, respectively. The vertical scales in the two figures are equal and the emission goes off-scale (over 100 arbitrary units) at 309 and 337 nm in Figure 9-5. Observable

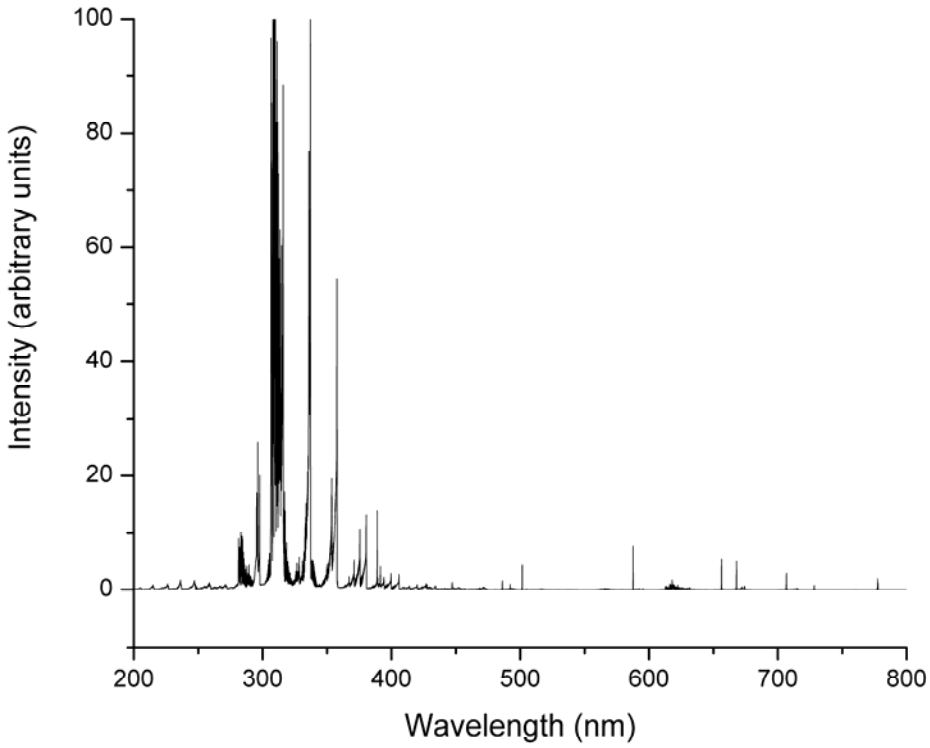

Figure 9-5. Annular glow discharge spectrum with no aerosol or vapour added. Note that emission goes off scale at 309 and 337 nm. A current of 100 mA was maintained.

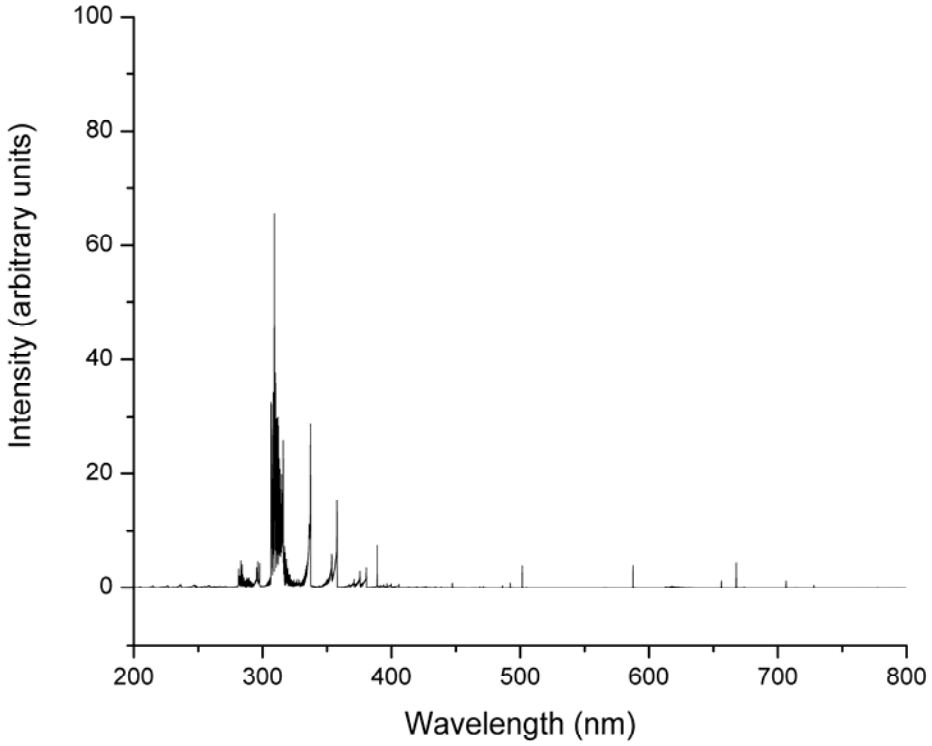

Figure 9-6. Annular glow discharge spectrum with aerosol and vapor resulting from a 500 μL/min flow of DI water. A current of 100 mA was maintained.

molecular species are NO (γ system with double-headed, blue-degraded bands below 300 nm), OH (red-degraded bands with bandheads at 281 and 306 nm), and N_2 (blue-degraded bands prominent from 300 to 450 nm). Observable atomic species are helium atom (388.9, 438.8, 447.2, 471.3, 492.2, 501.6, 504.8, 587.6, 667.8, 706.5, and 728.1 nm), singly charged helium ion (468.6 nm), oxygen (777.2, 777.4, and 777.5 nm), hydrogen (486.1 and 656.3 nm), and iron (248.3, 248.8, 249.1, 250.1, 251.1, 252.3, 252.7 nm). Most of these features (NO, OH, N_2, O, and H) can be ascribed to atmospheric gases that are not excluded from the plasma. The helium is obviously the plasma support gas. The iron emission, although weak, is evidence of some erosion of the cathode or anode surface, but emission from other elements in the steel is not seen. It should be noted that although an oxide layer forms on both electrodes, erosion of the surfaces has not been great enough to affect the plasma noticeably.

The measured intensity of all observed background emission features (continuum, molecular, and atomic) declines when aerosol is added. Some of the energy is drained from the plasma in ways that do not lead to emission, such as the evaporation of droplets, but some of this effect is likely due to the discharge becoming more diffuse, leading to a smaller fraction of the total emission being collected through the monochromator entrance slit.

The analyte emission, however, goes up with solution flow rate, as is shown for cadmium in Figure 9-7. The trend of this increase is typical for nebulizer-based sample introduction and is the result of a combination of higher analyte input and declining

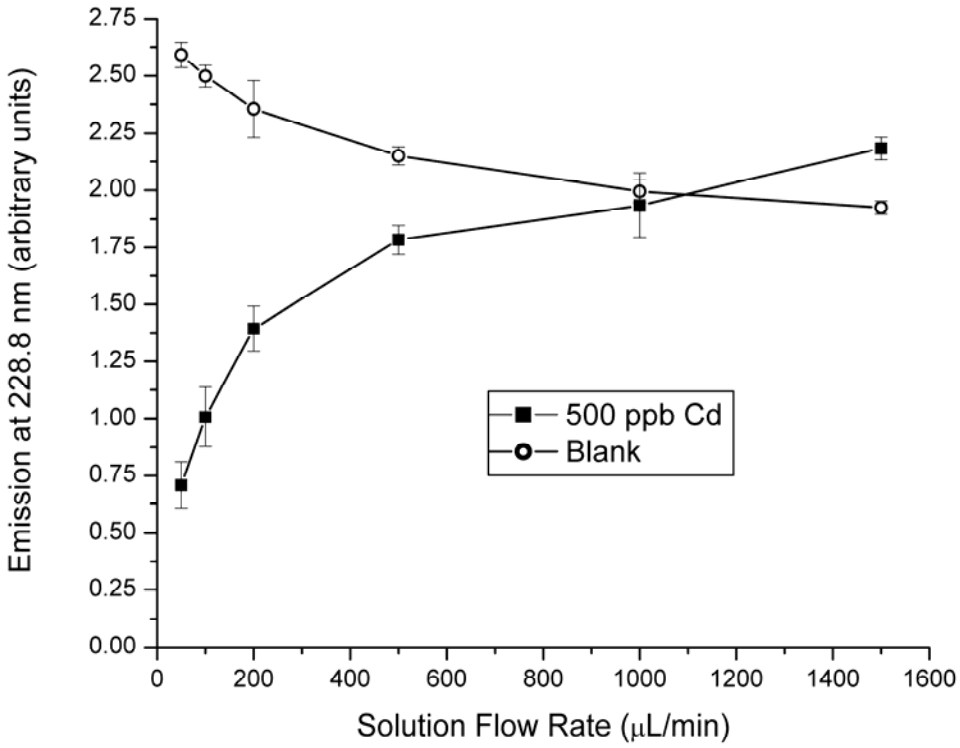

Figure 9-7. Emission of cadmium signal (background-subtracted) and background as a function of solution flow rate. Each point is the average of five 30-second integrations and error bars represent twice the standard deviation of those readings. A current of 100 mA was maintained.

nebulizer efficiency.[21-23] The efficiency of aerosol production drops sharply as flow rate increases, so the amount of analyte reaching the plasma climbs only gradually as solution flow is raised. Although it is likely that there is some depression of the analyte emission at higher solvent loads, this effect is masked by the influence of nebulizer efficiency.

9.3.4 Noise power spectra

Noise power spectra were collected, under both wet and dry conditions, for the electrical potential (discharge voltage) and for emission of background species. The averages of 15 measurements were plotted for electrical measurements in Figure 9-8 and the averages of 24 measurements were plotted for the 309.2 nm OH emission, 587.6 nm He emission, and 228.8 nm Cd emission in Figures 9-9, 9-10, and 9-11, respectively. A 107.5 Hz peak in some spectra appears to be environmental noise unrelated to the discharge (it is present even when the discharge is turned off) and its intensity fluctuates. Otherwise, there are no discrete frequencies in the spectra. Rather, the spectra are composed of white and flicker (1/f) noise. Although not shown in the figures, frequencies up to 500 Hz have been measured, with no additional features observed aside from harmonics of 107.5 Hz.

Noise spectra measured from some other plasmas often contain sharp features at discrete frequencies.[26-27] However, these features usually arise from the peristaltic pump used for sample introduction or from vortex instabilities surrounding the plasma; a syringe pump was employed here, so the discrete peaks would not be expected.[26] Further, flicker noise in the ICP arises mainly from the sample introduction system.[26-28-29] Given that fact, it is not surprising that the flicker noise in the voltage observed here becomes larger when an aerosol is introduced into the discharge. More surprisingly, the flicker noise in emission

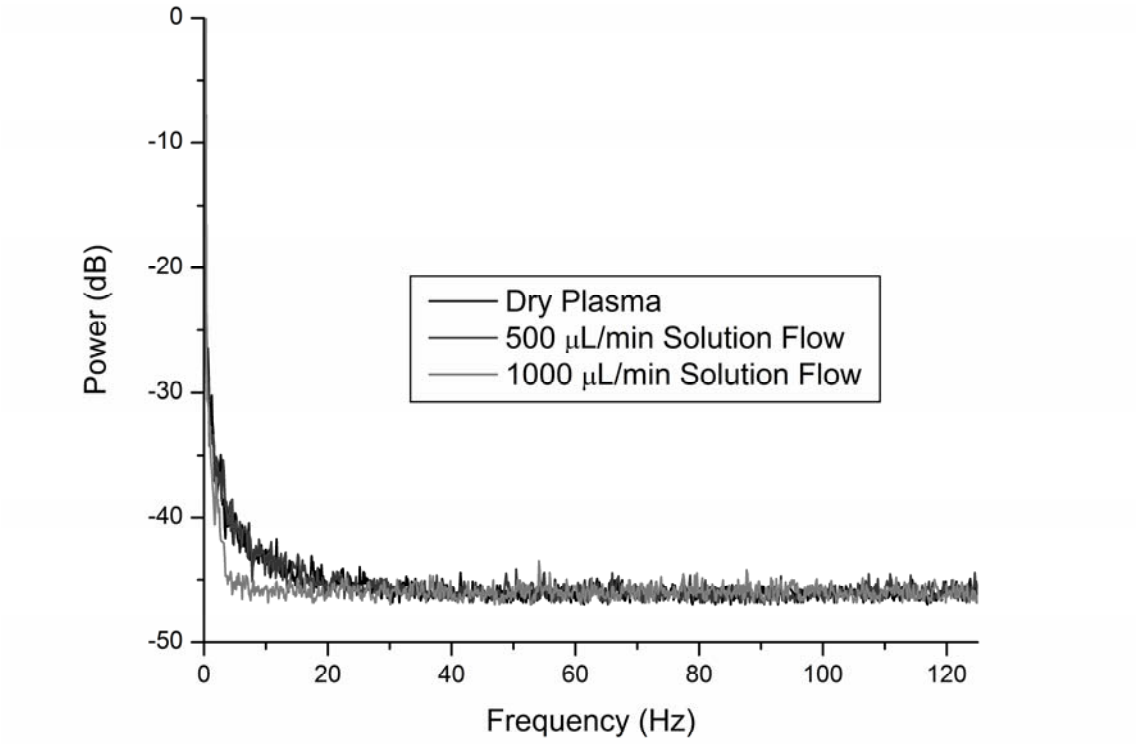

Figure 9-8. Noise power spectra of voltage fluctuations under different solvent (DI water) loads. A current of 100 mA was maintained. Voltage varied with flow rate as in Figure 9-4.

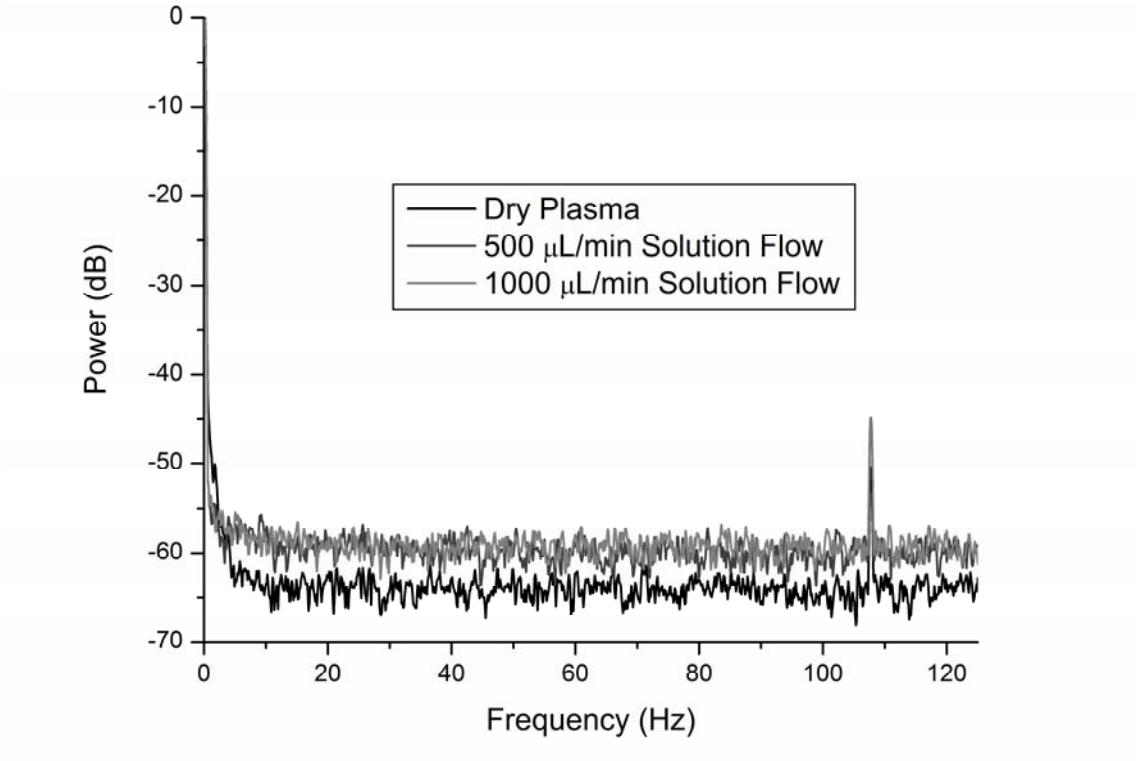

Figure 9-9. Noise power spectra of 309.2 nm OH emission fluctuations under different solvent loads. A current of 100 mA was maintained.

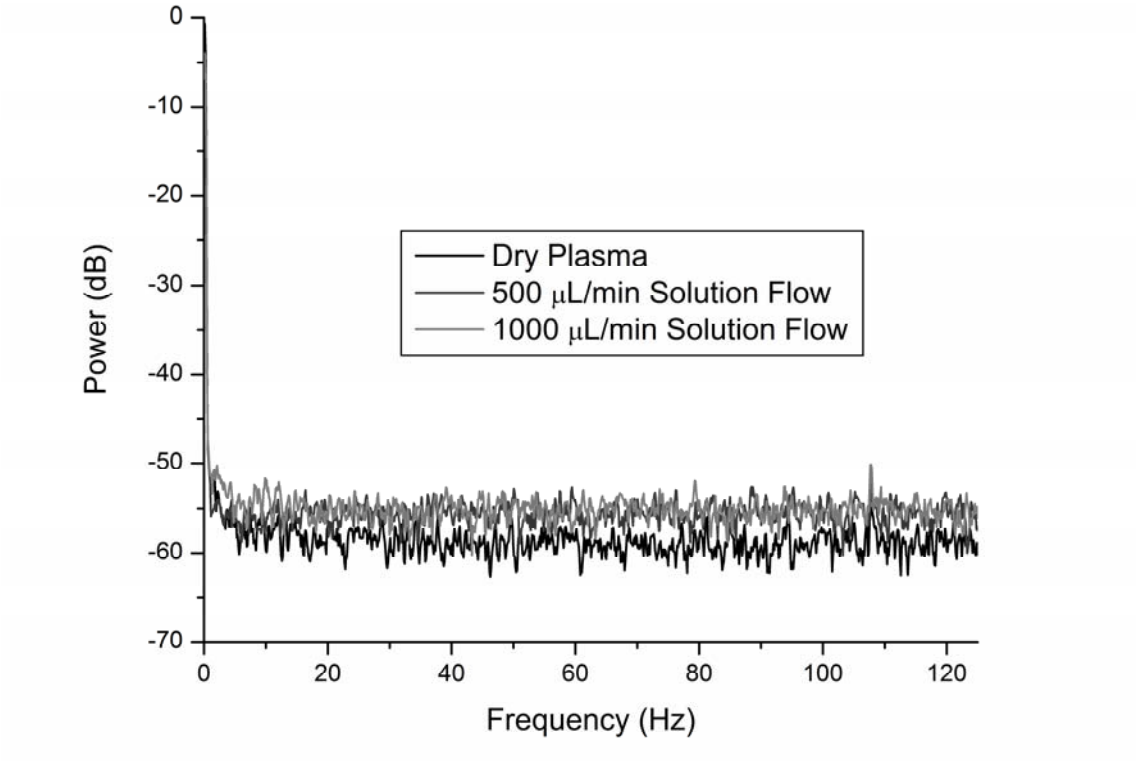

Figure 9-10. Noise power spectra of 587.6 nm He emission fluctuations under different solvent loads. A current of 100 mA was maintained.

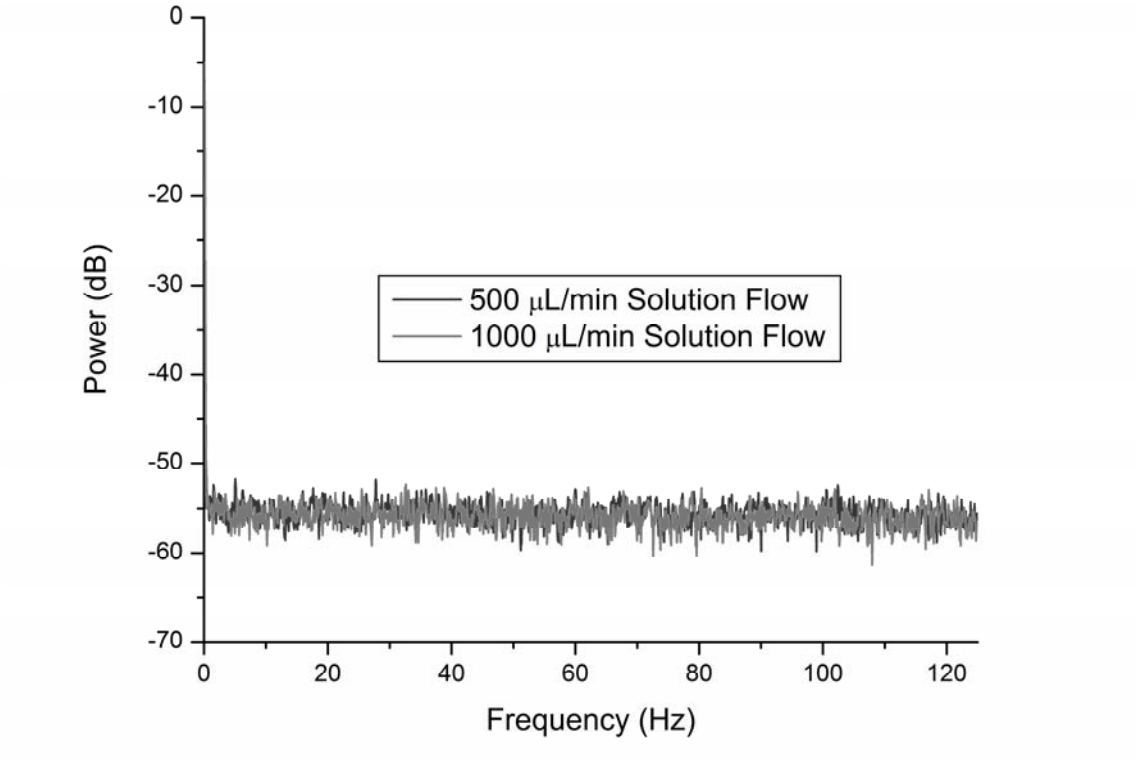

Figure 9-11. Noise power spectra of 228.8 nm Cd emission fluctuations under different solvent loads. A current of 100 mA was maintained.

is not greatly elevated by the addition of aerosol. The white noise, however, does go up slightly in the background emission (OH and He) when solution is added. This increase is no doubt a result of the higher solvent load, which raises OH emission intensity, and the presence of droplets, which produce random fluctuations in most emission features. Probably because the mass of solution making it to the plasma is changed only slightly with the doubling of solution flow rate, there is no observed difference between the noise power spectra for any parameter measured for flows of 500 and 1000 μL/min.

9.3.5 Analytical performance

Our preliminary work has concentrated on broad characterization of the plasma and on the influence of an aerosol, but the ultimate goal is to use this discharge for elemental analysis. Consequently, a preliminary evaluation of analytical performance has been made even though the system has not been fully optimized. Because it is intended that this system will be coupled eventually to a separation technique, flow injection was used to test the feasibility of transient analysis. It should be recognized that dilution of the sample, limited integration time, and uncertainty in the synchronization with a manual injection are expected to worsen the analytical performance somewhat compared with continuous injection.

Figure 9-12 shows transients for several 100-μL injections of a 500 ppb cadmium solution at carrier flow rates from 125 to 2000 μL/min. Higher flows were not used because the upper end of this range already exceeds the specifications of the nebulizer manufacturer. The full widths at half maximum are approximately twice what the total duration of the transient would be if there were no broadening, and tailing can be seen. It

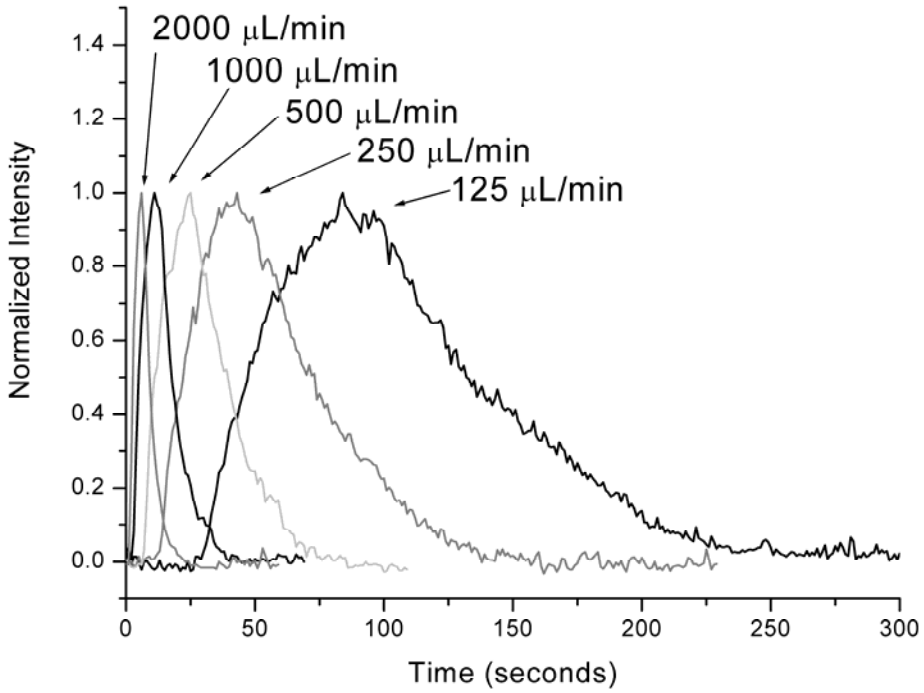

Figure 9-12. Cadmium 228.8 nm signal from 100-μL injections of 500 ppb Cd at different carrier-solution flow rates. A current of 100 mA was maintained.

would certainly be desirable to lessen this broadening, but it would not be prohibitive for many separations. Some broadening can be attributed to spreading between the injection loop and the nebulizer tip, some to the washout time of the spray chamber, and some to the region between the spray chamber and the plasma (because of both the dead volume and the shape). If the last region plays a significant role, reducing its volume in future generations of this discharge should result in narrower transients.

With the carrier solution supplied at 500 μL/min, 10 injections of 100 μL and 10 injections of a blank were performed for 400-ppb solutions of several metals. A 25-second window encompassing the peak of transient was integrated, and analytical figures of merit, shown in Table 9-1, were calculated. Detection limits are calculated as the concentration required for a signal three times the standard deviation of the background. Additionally, using triplicate 100 μL injections of 0, 32, 160, 800, and 4000 ppb cadmium, a standard curve with an R^2 of 0.9998 was obtained, showing good linearity for this element over at least 3 orders of magnitude.

It is interesting to compare these detection limits to those of other techniques, particularly the ICP. We can quite readily compare the performance of the instrument used here to complete instruments, but this is not what we are truly interested in. Rather, we would like to compare the two sources (the ICP and AGD), which requires correcting for other differences. Specifically, the resolution of the spectrometer can greatly affect performance.

Table 9-1. Analytical performance based on 100 µL injections of 400 ppb at a carrier-solution flow rate of 500 µL/min.

Element	Wavelength (nm)	Detection limit (ppb)	Detection limit (ng)	RSD (%)
Cd	228.8	7	0.7	2
Mn	279.5	60	6	10
Mg	285.2	12	1	7
Cu	324.7	111	11	4

Boumans and Vrakking[30-31] have examined the dependence of detection limit on spectral resolution. For convenience, an abbreviated treatment is provided here. (Mermet et al. have undertaken a similar study, with similar conclusions.)[32]

Two equivalent forms of the detection limit equation are shown below with an intervening step to better demonstrate their equivalence:

$$c_L = kc_0 \frac{\sigma_B}{x_0} = kc_0 \frac{\sigma_B / x_B}{x_0 / x_B} = kc_0 \frac{RSD_B}{SBR} \qquad (9\text{-}1)$$

Where c_L is the concentration detection limit, k is a constant (we have chosen 3), c_0 is the concentration in the sample, σ_B is the standard deviation of the blank emission, x_0 is the signal (the emission from the sample less the emission from the blank), x_B is the blank emission, RSD_B is the relative standard deviation of the blank, and SBR is the ratio of signal to background emission.

When flicker noise dominates, RSD_B is independent of spectrometer slit width. Under these conditions, the relationship between spectral bandpass and c_L is governed by the relationship between spectral bandpass and SBR. Boumans and Vrakking arrived at relationships between the SBR and the effective line width ($\Delta\lambda_{eff}$). Which relationship hold depends on the relative magnitudes of the physical line width ($\Delta\lambda_{phys}$) and the instrumental bandpass ($\Delta\lambda_{instr}$), which combine to form the effective bandpass:

$$\Delta\lambda_{eff}^2 = \Delta\lambda_{phys}^2 + \Delta\lambda_{instr}^2 \qquad (9\text{-}2)$$

In situations where the physical line width is greater than twice the instrumental bandpass, the signal increases proportionally to bandwidth and the background increases

proportionally to the square of the bandwidth, making the SBR inversely proportional to the effective line width.[30-31] The value of this relationship is that it enables us to predict the SBR, and therefore detection limit, that would be expected with the same source but a different spectrometer. By doing this, we can compare source performance independent of spectrometer bandwidth. The relationship is as follows, with numbered subscripts referring to different spectrometers.

$$c_{L,2}/c_{L,1} = SBR_1/SBR_2 = \Delta\lambda_{eff,2}/\Delta\lambda_{eff,1} \quad (9\text{-}3)$$

The relationship must be modified when $\Delta\lambda_{instr} \leq 2\ \Delta\lambda_{phy}$, as detailed by Boumans and Vrakking.[30-31] We can now compare the performance of the AGD used here to the performance expected of an ICP using the same spectrometer. We have chosen to use three sets of ICP data for comparison. Detection limits from Winge et al.[33] have been included because they have often been used as standard values,[1-34-40] even though they are less impressive than the other sets of data. Detection limits from Boumans and Vrakking[30] are used because they have been recommended as standard values. For these data, the detection limits had to be standardized to the same k value (changed from $2\sqrt{(2)}$ to 3). Detection limits from the Horiba Jobin-Yvon Activa promotional materials are used to reflect the performance of a modern commercial instrument and are very similar to those of Boumans and Vrakking. Physical line widths needed for the calculations are taken from Boumans and Vrakkers.[41]

Table 9-2 shows the experimentally determined detection limits for the AGD alongside the adjusted detection limits for these three ICPs. For Mn, Mg, and Cu, the detection limits with the AGD are one to two orders of magnitude worse than would be expected

Table 9-2. Comparison of AGD and ICP detection limits. Values not in parentheses are adjusted to match performance expected when using an identical spectrometer (0.1 nm bandpass) as was used in the present study. Values in parentheses are not adjusted for this. Wavelengths are as in Table 9-1 for the AGD and are those with the best reported c_L for the ICPs.

	Adjusted c_L in ppb (unadjusted c_L in ppb)			
Element	AGD	Winge	Boumans	Activa
Cd	7	15 (3)	3 (0.5)	4 (0.3)
Mn	60	8 (1)	0.7 (0.1)	0.7 (0.06)
Mg	12	0.9 (0.2)	0.2 (0.03)	0.2 (0.02)
Cu	111	30 (5)	3 (0.5)	3 (0.4)

from an ICP with a similar spectrometer. For Cd, however, the AGD and ICP detection limits are comparable. The reason for the difference is that the other species are interfered with by molecular species in the AGD (N_2 for Cu and OH for Mn and Mg), but only continuum is present in the region of Cd (see Figure 9-6). The disparity in detection limits points to the severity of the problem caused by background emission, and suggests that future studies should target this interference to improve performance. Better spectral resolution might lessen or remove these interferences, and should improve performance overall by reducing continuum emission. If background and analyte emission have different spatial patterns, spatial resolution would also improved performance. Some degree of isolation from atmosphere should reduce N_2 emission and possibly OH emission (although the latter partly, perhaps even largely, results from water in the sample). Further, changing the electrical, spatial, and flow parameters, which have not been extensively optimized at this point, might yield better results.

The demonstrated performance is already quite good and should be sufficient motivation for further study, including optimization, determination of other elements, coupling to separation techniques, and exploration of the effects of more complex samples (i.e., matrix effects).

9.4 CONCLUSIONS

A new, low-power, low gas consumption, small footprint source for elemental analysis of solution samples has been constructed. Although there is some increase in noise when an aerosol is introduced, the plasma remains stable under significant solvent loads. This

solvent loading does appear to reduce the energy available for excitation; emission-based detection limits, using flow injection, ranged from 7 ppb (0.7 ng) for Cd to 111 ppb (11 ng) for Cu among the metals measured. Linearity of a cadmium calibration is excellent over at least three orders of magnitude. The source shows significant promise as a low-cost alternative to other higher-power discharges.

9.5 REFERENCES

[1] A. Montaser and D. W. Golightly, *Inductively Coupled Plasmas in Analytical Atomic Spectrometry*, 1992,

[2] J. D. Ingle and S. R. Crouch, *Spectrochemical Analysis*, Prentice Hall: Upper Saddle River, NJ, 1988.

[3] G. L. Moore, *Introduction to Inductively Coupled Plasma Atomic Emission Spectrometry*, Elsevier: New York, 1989.

[4] J. A. C. Broekaert and V. Siemens, "Some trends in the development of microplasma for spectrochemical analysis", *Anal. Bioanal. Chem.*, 2004, **380**, 185.

[5] J. Franzke, K. Kunze, M. Miclea and K. Niemax, "Microplasma for analytical spectrometry", *J. Anal. At. Spectrom*, 2003, **18**, 802.

[6] V. Karanassios, "Microplasma for chemical analysis: analytical tools or research toys?" *Spectrochim. Acta, Part B*, 2004, **59**, 909.

[7] W. C. Wetzel, F. J. Andrade, J. A. C. Broekaert and G. M. Hieftje, "Development of a direct current He atmospheric-pressure glow discharge as an ionization source for elemental mass spectrometry via hydride generation", *J. Anal. At. Spectrom.*, 2006, **21**, 750.

[8] T. Ichiki, T. Koidesawa and Y. Horiike, "An atmospheric-pressure microplasma jet source for the optical emission spectroscopic analysis of liquid sample", *Plasma Sources Sci. Technol.*, 2003, **12**, S16.

[9] J. Gubkin, "Elektrolytische Metallabscheidung an der freien Oberfläche einer Salzlösung. " *Ann. Phys. Chem.*, 1887, **32**, 114.

[10] T. Cserfalvi, P. Mezei and P. Apai, "Emission studies on a glow discharge in atmospheric pressure air using water as a cathode", *J. Phys. D-Appl. Phys.*, 1993, **26**, 2184.

[11] T. Cserfalvi and P. Mezei, "Subnanogram sensitive multimetal detector with atmospheric electrolyte cathode glow discharge", *J. Anal. At. Spectrom.*, 2003, **18**, 596.

[12] M. R. Webb, F. J. Andrade, G. Gamez, R. McCrindle and G. M. Hieftje, "Spectroscopic and electrical studies of a solution-cathode glow discharge", *J. Anal. At. Spectrom.*, 2005, **20**, 1218.

[13] R. K. Marcus and W. C. Davis, "An Atmospheric Pressure Glow Discharge Optical Emission Source for the Direct Sampling of Liquid Media", *Anal. Chem.*, 2001, **73**, 2903.

[14] W. C. Davis and R. K. Marcus, "Role of powering geometries and sheath gas composition on operation characteristics and the optical emission in the liquid sampling-atmospheric pressure glow discharge", *Spectrochim. Acta, Part B*, 2002, **57B**, 1473.

[15] F. A. Andrade, W. C. Wetzel, G. C.-Y. Chan, M. R. Webb, G. Gamez, S. J. Ray and G. M. Hieftje, "A New, Versatile Direct-Current Helium Atmospheric-Pressure Glow Discharge." *J. Anal. At. Spec.*, 2006, **21**, 1175.

[16] V. I. Arkhipenko, S. M. Zgirovskii, A. K. Kapanik, L. V. Simonchik and D. A. Solov'yanchik, "Glow discharge in helium at atmospheric pressure as a source of spectrum excitation", *Journal of Applied Spectroscopy* (Translation of Zhurnal Prikladnoi Spektroskopii), 1998, **64**, 721.

[17] Y. P. Raizer, *Gas Discharge Physics*, Springer: New York, 1997.

[18] R. K. Marcus, *Glow Discharge Spectroscopies*, Springer: New York, 1993.

[19] R. K. Marcus and J. A. C. Broekaert, *Glow Discharge Plasmas in Analytical Spectroscopy*, John Wiley & Sons: Chichester, England, 2003.

[20] A. A. Yahya and J. E. Harry, "Factors affecting the glow-to-arc transition at the cathode of an electric discharge at atmospheric pressure", *Int. J. Electronics*, 1999, **86**, 755.

[21] J. L. Todolí, V. Hernandis, A. Canals and J.-M. Mermet, "Comparison of characteristics and limits of detection of pneumatic micronebulizers and a conventional nebulizer operating at low uptake rates in ICP-AES", *J. Anal. At. Spectrom.*, 1999, **14**, 1289.

[22] J. Mora, S. Maestre, V. Hernandis and J. L. Todolí, "Liquid-sample introduction in plasma spectrometry", *TrAC, Trends Anal. Chem.*, 2003, **22**, 123.

[23] K. B. Cull and J. W. Carnahan, "A study of pneumatic nebulization with helium", *Spectrochim. Acta, Part B*, 1987, **42**, 629.

[24] J. W. Novak and R. F. Browner, "Characterization of droplet sprays produced by pneumatic nebulizers", *Anal. Chem.*, 1980, **52**, 792.

[25] J. Park, I. Henins, H. W. Herrmann and G. S. Selwyn, "Gas breakdown in an atmospheric pressues radio-frequency capacitive plasma source", *J. Appl. Phys.*, 2001, **89**, 15.

[26] E. Björn, T. Jonsson and D. Goitom, "Noise characteristics and analytical precision of a direct injection high efficiency and micro concentric nebuliser for sample introduction in inductively coupled plasma mass spectrometry", *J. Anal. At. Spectrom.*, 2002, **10**, 1257.

[27] T. D. Hettipathirana and D. E. Davey, "Analytical performance in flow injection-simultaneous multielement-inductively coupled plasma-optical emission spectrometry employing a cyclonic spreay chamber", *Appl. Spectrosc.*, 1996, **50**, 1015.

[28] R. M. Belchamber and G. Horlick, "Noise-power spectra of optical and acoustic emission signals from an inductively coupled plasma", *Spectrochim. Acta, Part B*, 1982, **37**, 17.

[29] J. W. Olesik, L. J. Smith and E. J. Williams, "Signal fluctuations due to individual droplets in inductively coupled plasma atomic emission spectrometry", *Anal. Chem.*, 1989, **61**, 2002.

[30] P. Boumans and J. Vrakking, "Detection Limits of About 350 Prominent Lines of 65 Elements Observed in 50 and 27 Mhz Inductively Coupled Plasmas (Icp) - Effects of Source Characteristics, Noise and Spectral Bandwidth - Standard Values for the 50 MHz ICP", *Spectrochim. Acta*, Part B, 1987, **42**, 553.

[31] P. Boumans and J. Vrakking, "Inductively Coupled Plasmas - Line Widths and Shapes, Detection Limits and Spectral Interferences - an Integrated Picture - Plenary Lecture", *J. Anal. At. Spectrom.*, 1987, **2**, 513.

[32] J. M. Mermet, M. Carre, A. Fernandez and M. Murillo, "Influence of the Practical Resolution on Limits of Detection Using High Line Number Gratings in Inductively Coupled Plasma Atomic Emission-Spectrometry", *Spectrochim. Acta, Part B*, 1991, **46**, 941.

[33] R. K. Winge, V. J. Peterson and V. A. Fassel, "Inductively Coupled Plasma-Atomic Emission-Spectroscopy - Prominent Lines", *Appl. Spectrosc.*, 1979, **33**, 206.

[34] B. Knauthe and M. Otto, "Nonmetals in the argon-inductively coupled plasma-optical emission spectrometry: I. Phosphorus, sulfur and carbon", *Fresenius' J. Anal. Chem.*, 2001, **371**, 1052.

[35] A. Lopez-Molinero, R. Gimenez, P. Otal, A. Callizo, P. Charmorro and J. R. Castillo, "New sensitive determination of selenium by bromide volatilization inductively coupled plasma atomic emission spectrometry", *J. Anal. At. Spectrom.*, 2002, **17**, 352.

[36] K. Jankowski, "Microdetermination of phosphorus in organic materials from polymer industry by microwave-induced plasma atomic emission spectrometry after microwave digestion", *Microchem. J.*, 2001, **70**, 41.

[37] A. Lopez-Molinero, A. Villareal, D. Andia, C. Velilla and J. R. Castillo, "Volatile germanium tetrachloride for sample introduction and germanium determination by inductively coupled plasma atomic emission spectroscopy", *J. Anal. At. Spectrom.*, 2001, **16**, 744.

[38] A. C. Sahayam, "Determination of Cd, Cu, Pb and Sb in environmental samples by ICP-AES using polyaniline for separation", *Fresenius' J. Anal. Chem.*, 1998, **362**, 285.

[39] A. DeKlerk and R. J. Rademeyer, "Effect of sodium on the determination of some noble metals with inductively coupled plasma optical emission spectrometry", *J. Anal. At. Spectrom.*, 1997, **12**, 1221.

[40] A. L. Molinero, A. Morales, A. Villareal and J. R. Castillo, "Gaseous sample introduction for the determination of silicon by ICP-AES", *Fresenius' J. Anal. Chem.*, 1997, **358**, 599.

[41] P. Boumans and J. Vrakking, "The Widths and Shapes of About 350 Prominent Lines of 65 Elements Emitted by an Inductively Coupled Plasma", *Spectrochim. Acta, Part B*, 1986, **41**, 1235.

Chapter 10

Future and Ongoing Research.

Glow discharge is well recognized as a versatile source.[1-3] In fact, the variety of geometries, powering schemes, and detection methods used with glow discharge have been described as "a source of confusion to the rest of the analytical community," with this confusion being offered as a reason that GD use is not more widespread.[4] At the risk of further muddying the waters, the work described in this thesis has added to the available detection methods (Chapters 2-3) and source designs (Chapters 4-9). In this final chapter, directions for the future are suggested with the hope that, rather than just adding to the turbidity, they may lead to a crystallization of sorts around the seeds described earlier.

10.1 GLOW DISCHARGE IN ELEMENTAL IMAGING

Combining lateral resolution with glow discharge opens a variety of research avenues, both fundamental and applied.

Although trends of resolution with respect to various parameters were explained in Chapter 3 in terms of physical processes, these relationships were largely treated qualitatively. A more quantitative treatment might aid in fundamental understanding of the glow discharge. In particular, transport effects could be better understood. Three complications limited the ability to undertake this treatment with the arrangement

described in Chapter 3: (1) The emission distribution is dependent on both the atom distribution and the excitation distribution. Techniques other than emission might be used to unravel transport and excitation effects; for example, fluorescence or absorption might be used to probe ground-state populations. (2) Some information is lost when the discharge is observed in only two dimensions. Observations of the same discharge from multiple angles would add a layer of information. (3) The images were not time resolved, because the detector could not be gated on the relevant timescale. A detector that could be gated with sub-μs resolution would allow for tracking of transport with time.

On a more practical level, further research is necessary to establish the spatial resolution limits of glow discharge imaging spectrometry. Primarily, improvements are required in the resolution of the imaging system. This could be accomplished by modifying the monochromatic imaging spectrometer so that an image with greater magnification is formed or by using a different sort of imaging system (e.g., a Fabry-Perot interferometer with a two-dimensional detector). Combined with this, features of smaller dimensions could be used in place of the 1-mm diameter copper inclusion. Additionally, greater spatial resolution might be attained through the use of a time-gated detector. In Chapter 3, time resolution was accomplished by gating the excitation. There are, however, some long-lived species in the glow discharge that can excite analytes for some time after the discharge has been terminated. Some improvement in spatial resolution might be achieved by gating the detection, which would eliminate the effects of such "afterpeak" emission.

Spatial resolution could also be expanded into three-dimensions by monitoring the emission as a function of time, thereby adding a depth axis. Such depth profiling is well established in glow discharge spectrometry, but has not yet been combined with surface imaging. Testing the combination would require samples that are heterogeneous in depth as well as laterally. Relatedly, surface spatial resolution could actually be used to improve depth resolution. One limitation of depth resolution in glow discharge spectrometry is that the crater is not completely flat. Specifically, the crater bottom can be somewhat concave or convex, so the depth being probed at the center of the crater is different from that being probed near the crater's edges. Using surface imaging, emission from the crater's edge could be ignored, potentially improving depth resolution at the crater's center.

The glow discharge imaging technique described in Chapter 3 is limited to conductive samples. However, glow discharges can be used to analyze nonconductors if radio frequency powering is used (rather than direct current powering). Combining glow discharge imaging with radio frequency powering greatly broadens the reach of the technique. For example, the use of RF glow discharge imaging for the analysis of gel electrophoresis blotting membranes is now being pursued in the Hieftje laboratory.[5]

10.2 SOLUTION-CATHODE GLOW DISCHARGE

The miniaturized solution-cathode glow discharge (SCGD) has only been characterized from a performance standpoint so far. Fundamental studies similar to those performed on the larger version and described in Chapters 4 and 5 should be undertaken. Comparisons

between the two sources would be particularly fruitful because they could provide further insight into why the miniature SCGD exhibits improved performance. By providing this insight, comparisons could point the way towards further improvements.

The performance of the miniature SCGD should also be further evaluated. For example, the results described in Chapters 8 suggest that the source can be coupled to a separation technique or to preconcentration, but this needs to be demonstrated. Similarly, although matrix effects have already received some attention, it would be worthwhile to test the performance of the miniature SCGD with "real" samples, particularly if some comparison is made between the results and known concentrations and/or concentrations determined for the same sample with a different technique.

10.3 ANNULAR GLOW DISCHARGE

The annular glow discharge (AGD) has received only a preliminary characterization at this point. Given that, a natural path is to perform similar studies to those described in Chapters 4-6. Of particular interest are matrix effect studies; it is not clear what degree of desolvation the AGD accomplishes, and incomplete desolvation can be a factor in matrix effects. In addition, the source design might be improved. A different design might allow the analyte emission to be isolated from the significant background spectrum, which would improve detection limits. Two possibilities were mentioned in Chapter 9: a sheath gas to exclude N_2, and a different viewing geometry. The latter approach would benefit from spatially mapping the emission of different species (both analyte and background). Additionally, a higher resolution spectrometer should improve

detection limits by discriminating against the background.

The AGD also has potential uses not easily feasible with the SCGD. For example, the AGD could atomize and excite the vapor from electrothermal vaporization (ETV). The design of the AGD allows it to be placed very close to the ETV furnace, giving little time for condensation of the vapor into large particles, diffusional spreading, or loss to the walls of transport tubing. All three of these factors should be beneficial. Initial exploration of this possibility found a detection limit of 40 pg for Cd. The AGD might also find use in mass spectrometry, either as an atomization and ionization source, or as an atomization source followed by a separate ionization source.

10.4 OTHER ATMOSPHERIC PRESSURE GLOW DISCHARGES

The majority of this thesis deals with atmospheric pressure glow discharges (APGD), which have (so far) been little-used in analytical chemistry. It's worthwhile to point out that this move to atmospheric pressure opens more uses for glow discharges than have been detailed here. To give one example, the flowing afterglow of an APGD (that is, excited species outside of the APGD's applied electric field) has been used as a soft ionization source for gases[6] and a soft desorption-ionization source for solids.[7] The glow discharge, despite sometimes being described as a "mature" source,[8] continues to find new designs and applications.

10.5 REFERENCES

[1] D. Stuewer, "Glow-Discharge Mass-Spectrometry - a Versatile Tool for Elemental Analysis", *Fresenius Journal of Analytical Chemistry*, 1990, **337**, 737.

[2] W. W. Harrison, "Glow-Discharge - Considerations as a Versatile Analytical Source - Plenary Lecture", *J. Anal. At. Spectrom.*, 1992, **7**, 75.

[3] G. M. Hieftje, I. J. H. Barnes, J. A. C. Broekaert, G. Gamez, O. A. Grøn, V. Hoffmann, M. Huang, S. A. Lehn, S. J. Ray, D. Solyom, M. R. Webb and W. C. Wetzel, "Glow Discharge - The Most Versatile Source", *EC Thematic Network on Glow Discharge Spectroscopy for Spectrochemical Analysis* 2002,

[4] R. K. Marcus, "Glow discharge atomic spectrometries: They're back ... and here to stay", *Spectroscopy*, 1992, **7**, 12.

[5] G. Gamez, S. J. Ray, F. J. Andrade, M. R. Webb and G. M. Hieftje, "Development of a pulsed radio frequency glow discharge for three-dimensional elemental surface imaging. 1. Application to biopolymer analysis", *Anal. Chem.*, 2007, **79**, 1317.

[6] F. J. Andrade, W. C. Wetzel, M. R. Webb, G. Gamez, S. J. Ray and G. M. Hieftje, "A novel atmospheric pressure chemical ionization source. Part I: Ionization of compounds in the gas phase." Submitted to *Anal. Chem.*, 2007.

[7] F. J. Andrade, W. C. Wetzel, M. R. Webb, G. Gamez, S. J. Ray and G. M. Hieftje, "A novel atmospheric pressure chemical ionization source. Part II: Desorption-ionization for the direct analysis of solid compounds." Submitted to *Anal. Chem.,* 2007.

[8] E. Oxley, C. L. Yang and W. W. Harrison, "Quantitative depth analysis using microsecond pulsed glow discharge atomic emission spectrometry", *J. Anal. At. Spectrom.*, 2000, **15**, 1241.

Vita

EDUCATION

Indiana University, Bloomington, IN
PhD, 2007
Major: Analytical Chemistry Minor: Physical Chemistry

Union College, Schenectady, NY
BS, 2001, cum laude
Major: Chemistry Minors: Physics & English

ACADEMIC AND PROFESSIONAL DISTINCTIONS

Indiana University Associate Instructor Award (2007)
E. M. Kratz Fellowship (2006)
Poster award from *Anal. Bioanal. Chem.*, Winter Con. on Plasma Spectrochem. (2006)
Chancellor's Fellowship (2001-2003)
Union College Chemistry Departmental Honors (2001)
ACS Division of Analytical Chemistry Undergraduate Award (2001)
Sigma Xi induction (associate member 2001, full member 2007)
Union College Dean's List (1998-1999, 1999-2000, and 2000-2001)
UNYSSA Scholar-Athlete (1998-1999, 1999-2000, and 2000-2001)
Union Scholar (1997-2001)
ACS High School Chemistry Award (1996)

PROFESSIONAL ORGANIZATIONS AND SERVICE

Society for Applied Spectroscopy, 2002-
Treasurer for the Indiana Section, 2002-2003
Sigma Xi Research Society, 2001-

RESEARCH EXPERIENCE

Graduate Research Assistant, Indiana University, 2001-2007
Principal Investigator: Prof. Gary M. Hieftje
Thesis title: "New designs and detection strategies for glow discharge as an alternative spectrochemical source."
Non-research responsibilities of note: Health & safety officer, webmaster

Undergraduate Research Student, Union College, 2000-2001
Principal Investigator: Prof. Mary K. Carroll
Thesis title: "Interactions between oxazine dyes and sodium dodecyl sulfate studied by molecular spectroscopy."

Intern, New York State Department of Health, Wadsworth Center, 2000
Principal Investigator r: Dr. Katherine T. Alben

Focus: Method development for analysis of chloramines in water and sample collection for analysis of dissolved organic carbons in wetlands.

INSTRUCTIONAL EXPERIENCE

Associate Instructor (AI), Indiana University (9 semesters in total), 2001-2007

C612, Spectrochemical Methods of Analysis, 2007
Head Instructor: Prof. Gary M. Hieftje
Graduate class on analytical spectroscopy.

C501, Chemical Instrumentation (Head Associate Instructor), 2006
Head Instructor: Prof. Gary M. Hieftje
Graduate class on electronics and signal processing.

C501, Chemical Instrumentation Laboratory, 2003-2005
Head Instructor: Prof. Gary M. Hieftje
Graduate class on electronics and signal processing.

C315, Chemical Measurements Laboratory, 2001-2003
Head Instructors: Prof. Milos V. Novotny (2003) & Dr. Lee J. Klein (2001-2002)
Undergraduate (Jr./Sr.) laboratory-focused course on chemical instrumentation.

PEER-REVIEWED PUBLICATIONS (and those undergoing review)

"High-throughput elemental analysis of small aqueous samples using a compact glow discharge." M. R. Webb, F. J. Andrade, and G. M. Hieftje. *Anal. Chem.*, **Submitted.**

"A compact glow discharge for the elemental analysis of aqueous samples." M. R. Webb, F. J. Andrade, and G. M. Hieftje. *Anal. Chem.*, **Submitted.**

"A novel atmospheric pressure chemical ionization source. Part II: Desorption-ionization for the direct analysis of solid compounds." F. J. Andrade, W. C. Wetzel, M. R. Webb, G. Gamez, S. J. Ray, and G. M. Hieftje. *Anal. Chem.*, **Submitted.**

"A novel atmospheric pressure chemical ionization source. Part I: Ionization of compounds in the gas phase." F. J. Andrade, W. C. Wetzel, M. R. Webb, G. Gamez, S. J. Ray, and G. M. Hieftje. *Anal. Chem.*, **Submitted.**

"Use of the electrolyte-cathode glow discharge (ELCAD) for the analysis of complex mixtures." M. R. Webb, F. J. Andrade, and G. M. Hieftje. *J. Anal. At. Spectrom.*, **22**(7), 766-774, (2007).

"The annular glow discharge: a small-scale plasma for solution analysis." M. R. Webb, F. J. Andrade, and G. M. Hieftje. *J. Anal. At. Spectrom.*, **22**(7), 775-782, (2007).

"Development of a pulsed radio-frequency glow discharge for three-dimensional elemental surface imaging. 1. Application to biopolymer analysis." G. Gamez, S. J. Ray, F. J. Andrade, M. R. Webb, and G. M. Hieftje. *Anal. Chem.*, **79**(4), 1317-1326, (2007).

"Surface elemental mapping using glow discharge-optical emission spectroscopy." M. R. Webb, V. Hoffmann, and G. M. Hieftje. *Spectrochim. Acta, Part B*, **61**(12), 1279-1284, (2006).

"A new, versatile, direct-current helium atmospheric-pressure glow discharge." F. J. Andrade, W. C. Wetzel, G. C. Y. Chan, M. R. Webb, G. Gamez, S. J. Ray, and G. M. Hieftje. *J. Anal. At. Spectrom.*, **21**(11), 1175-1184, (2006).

"Spectroscopic characterization of ion and electron populations in a solution-cathode glow discharge." M. R. Webb, G. C. Y. Chan, F. J. Andrade, G. Gamez, and G. M. Hieftje. *J. Anal. At. Spectrom.*, **21**(5), 525-530, (2006).

"An improved monochromatic imaging spectrometer." M. R. Webb and G. M. Hieftje. *Appl. Spectrosc.*, **60**(1), 57-60, (2006).

"Spectroscopic and electrical studies of a solution-cathode glow discharge." M. R. Webb, F. J. Andrade, G. Gamez, R. McCrindle, and G. M. Hieftje. *J. Anal. At. Spectrom.*, **20**(10), 1012-1019, (2005).

PATENT APPLICATIONS

"Glow discharge for determination of elemental concentrations in liquid solutions in a high-throughput or transient fashion." M. R. Webb, G. M. Hieftje, and F. J. Andrade.

"Qualitative, quantitative and elemental analysis of gel electropherograms and blotting membranes via spatially resolved glow discharge optical emission spectrometry." with F. J. Andrade, G. Gamez, G. M. Hieftje, and S. J. Ray.

"Apparatus and methods for ionizing using glow discharge." with F. J. Andrade, G. Gamez, G. M. Hieftje, S. J. Ray, and W. C. Wetzel.

INVITED LECTURE

"The versatile glow discharge." M. R. Webb. *Union College Chemistry Seminar Series*, January 2007, Schenectady, NY.

SUBMITTED CONFERENCE / SYMPOSIUM PRESENTATIONS

"Direct solution sampling with a small-scale glow discharge: pros, cons, understanding, and improvement." M. R. Webb, F. J. Andrade, and G. M. Hieftje. *Pittsburgh Conference on Analytical Chemistry and Applied Spectroscopy*, February-March 2007, Chicago, IL.

"The influence of sample matrix on processes in a glow discharge with direct solution sampling." M. R. Webb, F. J. Andrade, and G. M. Hieftje. *European Winter Conference on Plasma Spectrometry*, February 2007, Taormina, Italy.

"Interferences in the electrolyte-cathode glow discharge: characterization, alleviation, and implications." M. R. Webb, F. J. Andrade, and G. M. Hieftje. *Turkey Run Analytical Conference*, October 2006, Indianapolis, IN.

"Evaluation of the robustness of an electrolyte-cathode glow discharge for the analysis of complex liquid samples." M. R. Webb, F. J. Andrade, and G. M. Hieftje. *Winter Conference on Plasma Spectrochemistry*, January 2006, Tucson, AZ.

"Miniature atmospheric pressure discharge for use with liquid samples." M. R. Webb, F. J. Andrade, and G. M. Hieftje. *Winter Conference on Plasma Spectrochemistry*, January 2006, Tucson, AZ.

"A new miniaturized plasma for liquid analysis." M. R. Webb, F. J. Andrade, G. M. Hieftje. *Turkey Run Analytical Conference*, November 2005, Marshall, IN.

"Characterization of a liquid-cathode glow discharge as an atomic spectroscopy source." M. R. Webb, G. Gamez, F. J. Andrade, and G. M. Hieftje. *Pittsburgh Conference on Analytical Chemistry and Applied Spectroscopy*, February-March 2005, Orlando, FL.

"Characterization of a solution-cathode glow discharge as a source for atomic spectrometry." M. R. Webb, F. J. Andrade, G. Gamez, and G. M. Hieftje. *Turkey Run Analytical Conference*, November 2004, Marshall, IN.

"Three-dimensional spatial resolution in glow discharge emission spectrometry." M. R. Webb, V. Hoffmann, and G. M. Hieftje. *Pittsburgh Conference on Analytical Chemistry and Applied Spectroscopy*, March 2004, Chicago, IL.

"Lateral resolution in glow discharge optical emission spectroscopy." M. R. Webb, V. Hoffmann, S. J. Ray, and G. M. Hieftje. *Turkey Run Analytical Conference*, November 2002, Spencer, IN.

"Interactions between oxazine dyes and SDS studied by molecular spectroscopy." M. R. Webb and M. K. Carroll. *Charles P. Steinmetz Symposium*, May 2001, Schenectady, NY.

"Interactions between oxazine dyes and SDS studied by molecular spectroscopy." M. R. Webb and M. K. Carroll. *National Conference on Undergraduate Research*, March 2001, Lexington, KY.

"Feasibility of HPLC-DAD for analysis of inorganic chloramines." M. R. Webb and K. T. Alben. *Robert A. Laudise Symposium*, September 2000, Schenectady, NY.

COAUTHORED PRESENTATIONS (submitted or invited)

Over 40 coauthored presentations. A selected list follows.

"New sources and spectrometers for chemical and biosciences analysis." G. M. Hieftje, F. J. Andrade, G. Gamez, S. J. Ray, G. D. Schilling, M. R. Webb, J. H. Barnes, IV, M. B. Denton, R. P. Sperline, D. W. Koppenaal, and C. J. Barinaga. *ISRANALYTICA*, January 2007, Tel Aviv, Israel.

"Chemical imaging by glow discharge atomic emission spectroscopy for the analysis of gel electrophoresis separations." S. J. Ray, G. Gamez, M. M. Hedrick, M. R. Webb, F. J. Andrade, and G. M. Hieftje. *Asia-Pacific Winter Conference on Plasma Spectrochemistry*, November-December 2006, Bangkok, Thailand.

"Miniaturizing the glow discharge." S. J. Ray, F. J. Andrade, G. Gamez, M. R. Webb, W. C. Wetzel, and G. M. Hieftje. *Pittsburgh Conference on Analytical Chemistry and Applied Spectroscopy*, March 2006, Orlando, FL.

"New frontiers in the analytical application of an atmospheric-pressure glow discharge: desorption-ionization for the analysis of organic compounds." F. J. Andrade, S. J. Ray, W. C. Wetzel, M. R. Webb, G. Gamez, and G. M. Hieftje. *Winter Conference on Plasma Spectrochemistry*, January 2006, Tucson, AZ.

"Atomic emission imaging of proteins on electrophoresis blotting membranes via radio frequency glow discharge." G. Gamez, S. J. Ray, F. J. Andrade, M. R. Webb, and G. M. Hieftje. *Colloquium Spectroscopicum Internationale XXXIV*, September 2005, University of Antwerp, Belgium.

"Improving plasma spectrometry through fundamental investigations." G. M. Hieftje, G. Gamez, G. C. Y. Chan, F. J. Andrade, S. J. Ray, and M. R. Webb. *8th Asian Conference on Analytical Sciences*, October 2005, Providence University in Taichung Hsien, Taiwan.

"Investigation of optical emission and electrical characteristic of pulsed DC glow discharges." V. Hoffmann, S. J. Ray, M. R. Webb, and G. M. Hieftje. *Colloquium Spectroscopicum Internationale XXXIII*, September 2003, Granada, Spain.

"Glow discharge – the most versatile source." G. M. Hieftje, J. H. Barnes, IV, J. A. C. Broekaert, G. Gamez, O. A. Grøn, V. Hoffmann, M. Huang, S. A. Lehn, S. J. Ray, D. Solyom, M. R. Webb, and W. C. Wetzel. *Glow Discharge Network Meeting*, March 2002, Vienna, Austria.

"Spectral evidence of interaction between oxazine dyes and SDS in aqueous solution." M. K. Carroll, M. R. Webb, J. M. Wright, M. A. Kane, W. E. Gardinier, E. J. Bukowski, and F. V. Bright. *American Chemical Society National Meeting*, April 2002, Orlando, FL.